INVESTIGATING THE ROLE OF ELEVATED FREE FATTY ACIDS IN EPITHELIAL-MESENCHYMAL TRANSITION OF HEPATOCELLULAR CARCINOMA

By

Aritro Nath

A DISSERTATION

Submitted to
Michigan State University
in partial fulfillment of the requirements
for the degree of

Genetics – Doctor of Philosophy

2015

ABSTRACT

INVESTIGATING THE ROLE OF ELEVATED FREE FATTY ACIDS IN EPITHELIAL-MESENCHYMAL TRANSITION OF HEPATOCELLULAR CARCINOMA

By

Aritro Nath

Hepatocellular carcinoma (HCC) is one of the deadliest forms of cancer world-wide with steadily increasing incidence and mortality rates in the United States. Advanced HCC are characterized by increased prevalence of intrahepatic and extrahepatic metastases, and are associated with very poor survival rates. Epidemiological studies indicate elevated free fatty acid (FFA) levels, the physiological manifestation of obesity, may be associated with higher mortality rates in HCC patients. Here, we investigated the effects of elevated FFA uptake on the induction of epithelial to mesenchymal transition (EMT) program – a pathway involved in metastatic progression of human cancers. Our initial studies with saturated FFA palmitate (PA) revealed a significant loss of the obligate desmosomal protein desmoplakin (DSP) in HepG2 cells, indicating a loss of cell adhesion. We next observed enhanced migration and invasiveness in HepG2 and Hep3B cells in response to PA treatment and confirmed loss of cell adhesion in the two cell lines. PA treatment resulted in cytotoxicity and expression of EMT-markers in distinct populations within the treated cells. Additionally, we identified that the Wnt/β-catenin and TGF-β signaling pathways were activated, suggesting a possible mechanism of EMT induction by PA. We further assessed the association between CD36, a FFA uptake gene normally expressed at low levels in hepatocytes but found to be elevated in fatty liver, and the activation of EMT program in human HCC. Our analysis revealed a significant

association between CD36 and expression of EMT markers in the cancer genome anatomy (TCGA) liver cancer mRNA expression dataset, which was confirmed with protein samples from human HCC tumor biopsies. Interestingly, both studies suggested that expression of EMT markers were not correlated with body mass index of the patients. Given the role of exogenous FFA uptake in promoting EMT and metastasis in HCC, we further analyzed somatic mutations, copy number variations, and gene expression profiles of fatty acid uptake and metabolism genes in context of metastatic progression in >8,000 samples from the TCGA database across 12-different cancer types. Our analysis revealed a significant and previously undocumented role of fatty acid uptake and fatty acid metabolism genes in the metastatic progression of multiple human cancers, and demonstrated the utility of genes involved in these pathways as strong prognostic biomarkers with significant influence on survival rates.

Dedicated to my parents, Ashish Kumar Nath and Rita Nath, and my wife, Siddhika.

ACKNOWLEDGEMENTS

I would like to thank Dr. Christina Chan for being a great advisor and research mentor throughout my PhD tenure at MSU, especially for encouraging creative thinking and providing academic freedom. I greatly appreciate Dr. Chan for motivating an interdisciplinary approach towards solving biological problems, combining genetics, cellular and molecular biology with statistics and systems biology, which was crucial in shaping my research profile. In addition, I thank my thesis committee members Dr. Chengfeng Yang, Dr. Eran Andrechek, Dr. Yuehua Cui, and Dr. Cindy Miranti, for providing constant guidance and support during my thesis research.

I thank the Genetics program at MSU, especially Dr. Barb Sears, Dr. Cathy Ernst, and Jeannine Lee, for providing excellent support throughout my PhD career. I thank Dr. Melinda Frame at Center for Advanced Microscopy, and Dr. Louis King at Flow Cytometry Core at MSU for their support and assistance.

I would like to acknowledge the past and present members of Chan and Walton lab for taking the time to discuss my research and providing creative inputs. I specially thank Ms. Irene Li for assistance with experiments and analysis, with constant energy and enthusiasm. I thank all my friends in the MSU and East Lansing community for introducing me to new cultures and cuisine, and for making my stay fun and enjoyable.

Most importantly, I would like to thank my parents and role models, Dr. Ashish Kumar Nath and Mrs. Rita Nath, and my loving wife, Siddhika. None of this would have been possible without their inspiration, love, strength and support. Thank you!

TABLE OF CONTENTS

LIST OF TABLES

LIST OF FIGURES

KEY TO SYMBOLS OR ABBREVIATIONS

ANOVA	analysis of variance
BCLC	Barcelona clinic liver cancer
BFS	breadth-first search
BMI	body mass index
BRCA	breast carcinoma
BSA	bovine serum albumin
CDH	cadherin
ChREBP	carbohydrate responsive element binding protein
CNA	copy number alteration
COADREAD	colorectal adenocarcinoma
COX	cyclo-oxygenase
CPT	carnitine palmitoyltransferase
CRPC	castration resistant prostate cancer
DGAT	diacylglycerol acyltransferase enzymes
DMSO	dimethyl sulfoxide
DSP	desmoplakin
EGFR	epidermal growth factor receptor
EMT	epithelial to mesenchymal transition
ER	endoplasmic reticulum
FABP	fatty acid binding protein
FAO	fatty acid oxidation
FAS	fatty acid synthase
FATP	fatty acid transport protein
FBS	fetal bovine serum

FDA	food and drug administration
FWER	family-wise error rate
FXR	farnesoid X receptor
HCC	hepatocellular carcinoma
HNSC	head and neck squamous cell carcinoma
IGF	insulin like growth factor
IL	interleukin
IRE1	inositol requiring protein
KIRC	kidney renal clear cell carcinoma
LA	linoleic acid
LDH	lactate dehydrogenase
LIHC	liver hepatocellular carcinoma
LIPE	lipase
LUAD	lung adenocarcinoma
LXR	liver X receptor
NAFLD	non-alcoholic fatty liver disease
OL	oleate
OV	ovarian carcinoma
OXPHOS	oxidative phosphorylation
PA	palmitate
PAGE	polyacrylamide gel electrophoresis
PBS	phosphate buffered saline
PMT	photomultiplier tube
PORCN	porcupine
PPAR	peroxisome proliferator-activated protein
PPI	protein protein interaction

PRAD	prostate adenocarcinoma
PXR	pregnane X receptor
qRT-PCR	quantitative real time polymerase chain reaction
ROS	reactive oxygen species
RXR	retinoid X receptor
SDS	sodium dodecyl sulfate
SEM	standard error of the mean
SKCM	skin cutaneous melanoma
SREBP	sterol-regulatory element binding protein
SSO	sulfosuccinimidyl oleate
TBST	tris-buffered saline Tween-20
TCGA	the cancer genome atlas
TGF	transforming growth factor
TNF	tumor necrosis factor
TRED	transcriptional regulatory element database
VIM	vimentin

CHAPTER 1: INTRODUCTION

1.1 The liver and hepatocellular carcinoma

The liver is the largest vital organ in the human body involved in biosynthesis, metabolism and detoxification. The organ receives oxygenated blood from the hepatic artery as well as deoxygenated, nutrient-rich blood from the gastrointestinal tract. Hepatocytes are the basic functional cellular units of the liver that are lined by endothelial cells to form hepatic sinusoids, which facilitates the flow of blood. The sinusoids also contain specialized macrophages known as Kupffer cells, and the bile caniculi are located adjacent to sinusoids. The hepatocytes are involved in the metabolism of nutrients obtained from the gastrointestinal tract including glucose metabolism (gluconeogenesis, glycogenolysis), fatty acid metabolism (lipogenesis and oxidation), cholesterol biosynthesis, ketone body formation (ketogenesis) and production of bile. Additionally, hepatocytes are involved in the production of albumin, insulin-like growth factor (IGF1), clotting factors including fibrinogen and prothrombin, and acute phase proteins such as interleukin 1 (IL-1) and tumor necrosis factor alpha (TNF-α). The liver also processes xenobiotics including toxic substrates and drugs in to less harmful metabolites which can be then removed through the bile or urine. (Silverthorn et al., 2009; Tortora and Anagnostakos, 1976; Tortora and Derrickson, 2008).

Hepatocellular carcinoma (HCC) is a major form of primary hepatic malignancy that results in uncontrolled proliferation of hepatocytes. The process of HCC tumorigenesis takes nearly 3 decades to complete following the establishment of the primary risk factor – cirrhosis (Thorgeirsson and Grisham, 2002). The genomic and transcriptomic investigation of pre-

neoplastic phase of HCC has led to the establishment of key alterations required for HCC pathogenesis. It is well accepted that the molecular pathogenesis of HCC involves somatic mutations in a diverse array of genes that accumulate along the course of the disease progression from primary malignancy to invasive and metastatic HCC. Along with the loss-of-function somatic mutations or loss of heterozygosity in the tumor suppressors *APC* and *TP53*, the Wnt/β-catenin signaling pathway is frequently activated in HCC through activating mutations in the β-catenin gene (*CTNNB1*) or loss-of-function mutations in *AXIN1* and *AXIN2*, which promote stem-cell like properties in the HCC cells (Kan et al., 2013; Taniguchi et al., 2002). Normal adult liver cells exhibit expression of β-catenin primarily at the cell membrane. However, histopathological staining for the nuclear localization of β-catenin in human HCC tumors shows strong association with poorly-differentiated HCC, suggesting a correlation with HCC progression (Tien et al., 2005). Nuclear translocation of β-catenin results in the recruitment of the TCF/LEF complex at the promoter of targets, and activates the transcription of a number of oncogenic genes including matrix metalloproteinase, cyclin D1, c-myc, survivn, fibroblast growth factors and components of the Wnt signaling pathway itself (Nejak-Bowen and Monga, 2011).

Somatic mutations were reported in the phosphatidylinositol 3-kinase (*PIK3CA*) oncogene in HCC tumors (Lee et al., 2005). *PIK3CA* alterations were previously reported in multiple cancer types, with somatic missense mutations increasing the kinase activity of the protein, resulting in the activity of multiple receptor tyrosine kinase and AKT signaling pathways (Karakas et al., 2006). In addition, invasive HCC tumors exhibit elevated production of vascular endothelial growth factor (VEGF) and the pro-inflammatory JAK/STAT pathway which helps promote

angiogenesis and sustain proliferation (Kan et al., 2013; Zhu et al., 2013). More recently, the loss of miR-122 and gain of miR-21 have been found to be strongly associated with the pathogenesis of HCC (Tsai et al., 2012; Wagenaar et al., 2015). Additionally, alterations in the SWI/SNF chromatin remodeling complex due to mutations in *ARID1* and altered expression of *VCAM1* and *CDK14* were found to be associated with invasive HCC (Huang et al., 2012). Gene expression analysis of HCC tumor samples have revealed a significant role of elevated expression levels of hepatocyte growth factor (*HGF*) and its receptor (*MET*) (Ueki et al., 1997), epidermal growth factor receptor (*EGFR*) (Tanabe et al., 2008), oncofetal gene *SAL4* (Yong et al., 2013), osteopontin (*OPN*) (Ye et al., 2003) and the loss of *CDKN1C, SLC22A1L*, and *IGF2* expression (Schwienbacher et al., 2000) in HCC pathogenesis.

1.2 Staging and clinical management

The strategies for clinical management of HCC are dependent on the staging of the tumor. The most commonly used classification methods are the Barcelona Clinic Liver Cancer group (BCLC) staging and Child-Pugh staging. Very early stage (stage 0, Child-Pugh A) patients exhibit in situ lesions ≤ 2cm in diameter, which can be treated with resection with >90% 5-year survival rates (Dai et al., 2014). Early stage (BCLC-A, Child-Pugh A or B) patients with single nodule >2cm or up to three nodules ≤ 3cm in diameter are also candidates for surgical resection or transplantation with >50% 5-year survival rates (Arii et al., 2000). Intermediate stage HCC patients (BCLC-B, Child-Pugh A or B) with large lesions but no vascular invasion and metastases are candidates for treatment with trans-catheter arterial chemoembolization (TACE), but the survival rates are limited to about 16 months (Llovet and Bruix, 2003). Advanced stage patients (BCLC-C, Child-Pugh A or B) with vascular invasion and intra-hepatic

or extra-hepatic metastases are candidates for targeted chemotherapy with the tyrosine kinase inhibitor sorafenib which results in a median increase in survival rates to approximately 11 months (Llovet et al., 2008). Terminal stage (BCLC-D, Child-Pugh C) patient exhibiting severe hepatic dysfunctions receive supportive care and have poor survival rates < 6 months.

1.3 Epidemiology and risk factors

Worldwide, HCC is the fifth-most common form of cancer but is responsible for the second-highest number of cancer related deaths (Ferlay J, 2013). The highest incidence rates of HCC at >20 cases per 100,000 individuals are observed in the sub-Saharan African region and Eastern Asia, with similar patterns of high HCC-associated mortality rates observed in these regions (Ferlay et al., 2013). While the incidence of rates of HCC has steadily declined in the East Asian region, the numbers of HCC cases are steadily increasing in the United States. Between 1975 and 2005, the overall incidence rates of HCC in the United States increased more than three times from 1.6 to 4.9 per 100,000 individuals (age-adjusted rate), with nearly three times higher incidence rates in men than in women (Altekruse et al., 2009).

Nearly 90% of HCC cases develop from cirrhosis of the liver resulting from chronic infection by hepatitis B or hepatitis C viral infection, alcoholic liver disease, exposure of aflatoxins, and hereditary hemochromatosis (El-Serag and Rudolph, 2007). Chronic hepatitis B infection contributes to nearly 50% of all HCC cases globally, however in the United States, only about 10% of the HCC cases are directly attributable to hepatitis B infection (El-Serag, 2012). In contrast, hepatitis C infection is associated with nearly 50% of the HCC cases in the United States (El-Serag and Rudolph, 2007), whereas nearly 35% of the HCC patients are not infected with either hepatitis B or C virus.

Hepatitis B infection mostly occurs through vertical transmission from infected mother to newborn child in high prevalence regions, although, transmission through sexual and parenteral routes are more frequent in regions of low prevalence (El-Serag, 2012). The risk of developing HCC in patients with elevated serum marker levels of hepatitis B viral infection (HBe antigen) is nearly 60 times higher than the baseline levels (Yang et al., 2002). The influence of hepatitis B infection on risk of HCC is dependent on the genotype (A-H) of the virus. For instance, although 90% of hepatitis B infection-associated HCC occur in patients with cirrhosis (Yang et al., 2011), genotype B is associated with HCC development without the occurrence of cirrhosis especially in children (Ni et al., 2004). In the United States, genotypes A and D are most prevalent but genotype D is strongly associated with the risk of HCC development. In addition, specific mutations in the hepatitis B core promoter have been associated with either higher or lower risk of HCC development (Yang et al., 2008a).

Most cases of hepatitis C infection occur through contaminated blood products, unsafe injections or sexual contact. Infection with hepatitis C virus is associated with a 20-fold increase in risk of HCC compared to baseline levels (Hsu et al., 2015). The risk of elevated HCC in hepatitis C virus infected individuals is strongly associate with fibrosis and cirrhosis, where 15-35% of the chronic infections result in cirrhosis (Freeman et al., 2001). A meta-analysis of epidemiological studies suggested that co-infection with both hepatitis B and C viruses has an odds ratio of 165 to develop HCC (Donato et al., 1998). The rates of hepatitis B related HCC have remained constant; however hepatitis C related HCC cases are progressively increasing in the United States, with large proportions of undiagnosed chronic hepatitis infections (Davis et al., 2010).

Excessive alcohol intake is also associated with development of cirrhosis and progression to HCC (Bagnardi et al., 2001). However, the combined synergistic effects of alcoholism and hepatitis infection are associated with a two-fold higher odds ratio for developing HCC (Donato et al., 2002). Hereditary hemochromatosis and iron overload are also linked with cirrhosis and increased risk of development of HCC, with some reports suggesting a 200-fold increase in HCC risk (Kowdley, 2004). In addition, consumption of aflatoxin-contaminated food has been suggested to be associated with up to 28% of all HCC cases worldwide (Liu and Wu, 2010). The predictors of HCC also include the age and gender of the patient with cirrhosis from different etiologies, with a higher risk in patients of older age and male sex (Sangiovanni et al., 2004).

1.4 Obesity and HCC

Epidemiological studies suggest a strong association between obesity with the risk of developing several types of cancer (Bianchini et al., 2002). Mortality rates in men with a body mass index (BMI) greater than 35 were 4.5 times higher, whereas in women the mortality rates were 1.7 times higher than individuals with normal BMI (Calle et al., 2003). Meta-analysis of cohort studies suggest a 1.9 fold increase in risk of developing HCC in overweight individuals (Larsson and Wolk, 2007).

Obesity is strongly associated with type II diabetes and metabolic syndrome, manifested in the form of hyperglycemia, hyperinsulinemia and insulin resistance, and is associated with increased cancer risk (Giovannucci et al., 2010). In the United States, diabetes was found to be linked with a 2-3 fold increase in risk of HCC independent of additional risk factors (Davila et al., 2005). Up to 20% HCC cases arise without an established cirrhosis, and emerging evidence

suggest non-alcoholic fatty liver disease (NAFLD) to be a significant risk factor for non-cirrhotic HCC (Baffy et al., 2012). Retrospective studies in patients with HCC of unknown etiology suggest NAFLD to be the underlying cause in most cases (Bralet et al., 2000). In the United States, NAFLD was reported to be the risk factor for HCC in about 38% of the patients without underling cirrhosis (Sanyal et al., 2010). Given the increasing epidemic of obesity in the United States, the numbers of HCC cases attributed to NAFLD are expected to climb in the coming years.

The molecular pathogenesis of obesity and NAFLD-associated HCC is thought be associated with low-grade, chronic inflammation. Excess accumulation of fats in the liver promotes the release of pro-inflammatory cytokines (Hotamisligil, 2006). TNFα levels are upregulated in NAFLD liver which can activate the oncogenic NFκB, JNK, and mTOR signaling pathways (Stickel and Hellerbrand, 2010). The activation of STAT3 transcription factor downstream of IL-1 and IL-6 activated interleukin signaling pathways is also strongly associated with excess accumulation of fats (Marra and Bertolani, 2009). In addition, insulin resistance and excess levels of insulin like growth factors (IGF) are strongly associated with the pathogenesis of HCC (Chun et al., 2014; Siddique and Kowdley, 2011). Epidemiological studies have shown that diets rich in saturated fats contribute significantly towards elevating risk of NAFLD (Musso et al., 2003; Zelber-Sagi et al., 2007). Diets in which saturated fats were replaced with poly-unsaturated fats resulted in decreased abdominal obesity and improved insulin sensitivity (Summers et al., 2002), whereas substituting unsaturated fats with saturated fats resulted in increased insulin resistance (Vessby et al., 2001), suggesting a potential link between the dietary fat intake and HCC pathogenesis.

1.5 Free fatty acids and cellular signaling

While NAFLD is characterized by increase in stored triglyceride levels in adipocytes, there is a significant increase in the levels of free fatty acids (FFA) in the serum (Cheung and Sanyal, 2008). It is increasingly being recognized that the molecular pathogenesis of NAFLD and obesity associated metabolic syndrome and insulin resistance is associated with elevated FFA levels (Alkhouri et al., 2009). The patients with HCC exhibit a 20-30% decrease in plasma triglyceride levels (Motta et al., 2001), while exhibiting significant increase in levels of mono unsaturated and saturated FFAs (Jiang et al., 2006).

Studies in mice models over-expressing DGAT, the enzyme responsible for triglyceride biosynthesis, show that the increase in levels of triglycerides alone is not sufficient to induce insulin resistance (Monetti et al., 2007). Additionally, inhibition of triglyceride synthesis in obese mice elevated FFA levels and promoted liver damage and fibrosis, while improving steatosis (Yamaguchi et al., 2007). The esterification of FFAs to triglycerides may in fact serve as a protective mechanism, as cells treated with saturated FFAs undergo lipotoxicity (Listenberger et al., 2003). It is also clear that not all types of FFAs have similar effects on the lipotoxic phenotype, as saturated FFAs have been shown to have significant impact on apoptosis, while poly-unsaturated FFAs are in fact protective against the damage caused by saturated FFAs (Alkhouri et al., 2009; Li et al., 2009).

Consequently, a number of studies have focused on the effects of saturated FFAs such as palmitate, the most abundant saturated FFA in the plasma as well as in the diet, on hepatocytes to understand the effects of obesity on pathogenesis and progression of liver diseases (Musso et al., 2009b). Studies with multiple liver cell lines and primary mouse

hepatocytes show that saturated FFAs induce apoptosis in hepatocytes by activating the intrinsic mitochondrial apoptotic pathway, resulting in activation of caspase 3 and 7 following the release of cytochrome C, in a JNK signaling-dependent manner (Malhi et al., 2006a). Our lab has previously established that the saturated FFA palmitate inactivates RNA-dependent protein kinase (PKR) activity, thereby inducing apoptosis via altered expression and activity of Bcl-2 (Yang and Chan, 2009). We further found that PKR regulates the activity and expression of IRS1 and IRS2 proteins respectively, thereby playing a prominent role in palmitate induced insulin-resistance (Yang et al., 2010). In addition, FFAs induce lysosomal apoptosis pathways as well by inducing lysosomal permeabilization, Bax activation and translocation (Feldstein et al., 2006). The FFA-induced lysosomal permeabilization also results in activation of NFκB activation and TNF-alpha dependent apoptosis in human liver (Feldstein et al., 2004a). Another mechanism of FFA induced lipotoxicity involves the activation of endoplasmic reticulum stress (ER-stress) pathway (Ron and Walter, 2007). The ER membrane bound stress sensor inositol requiring protein (IRE1), ATF6 and protein kinase RNA-like ER kinase (PERK) activation leads to downstream splicing and activation of X-box binding protein (XBP1). PERK activation inhibits cellular protein synthesis by inhibiting eukaryotic initiation factor 2 alpha (eIF2α), which leads to selective activation of ATF4 transcription factor. Both ATF4 and XBP transcribe CHOP, which drives apoptosis by inhibiting Bcl-2 expression (McCullough et al., 2001). Palmitate could also activate ER-stress response by promoting ATF4 transcription directly in a CREB1 dependent manner (Cho et al., 2013)

Palmitate is known to activate cell surface receptors belonging to the TNF receptor gene family, also known as death receptors. TNFR1 activation by TNF-α can lead to cellular

apoptosis through the activation of NFκB and JNK pathway (Malhi and Gores, 2008). In addition, palmitate activates Fas and TRAIL, which can lead to direct induction of apoptosis (Malhi et al., 2006b). NAFLD mice models show increased levels of Fas expression as well as elevated levels of TRAIL receptors (Malhi et al., 2007; Siebler et al., 2007). The availability of palmitoyl CoA is the rate limiting step in the synthesis of ceramide, a complex lipid also containing sphingosine. Elevated ceramide levels are linked with insulin resistance (Summers, 2006) and apoptosis (Paumen et al., 1997). Elevated FFA levels are associated with increased expression of mitochondrial cytochrome P450 enzyme 2E1 (*CYP2E1*) and elevated production of reactive oxygen species (ROS) (Chalasani et al., 2003), which leads to increased DNA damage and induction of apoptosis. In addition, palmitate can also activate the toll like receptor 4 (TLR4) which leads to activation of NFκB, TNF-α and IL-6 (Suganami et al., 2005; Szabo et al., 2005).

Studies involving primary liver and HCC cell lines have confirmed that palmitate induces resistance to insulin signaling in hepatocytes (Ruddock et al., 2008). Insulin resistance is associated with release of multiple pro-inflammatory signaling molecules including tumor necrosis factor alpha (TNF-α), interlukin-6 (IL6) and leptin (Bugianesi, 2007). Additionally, resistance to insulin signaling leads to increased activity of insulin-like growth factor 1(IGF1), a hormone that stimulates hepatocyte growth and imparts resistance to apoptosis (Ish-Shalom et al., 1997; Page and Harrison, 2009). Recent studies have also shown that activation of the insulin receptor substrate 1 (IRS1), a key molecule involved in signal transduction downstream of insulin receptor, can suppress the activity of TGF-β and reduce EMT (Shi et al., 2009).

1.6 Regulation of FFA levels

The levels of FFAs in the liver are dependent on the balance between the synthesize of FFAs de novo (lipogenesis), exogenous uptake from the environment and processes that utilize FFAs including oxidation of FFAs and synthesis of triglycerides and other complex lipids (Musso et al., 2009a).

Circulating lipids serve as the largest source for FFAs and the hepatic uptake of FFAs takes place in a controlled, active manner through specialized membrane proteins, instead of passive diffusion across the plasma membrane (Stremmel et al., 2001). The uptake of lipids in the cell is dependent on the integrity of lipid rafts in membranes, which are composed of caveolins (*CAV1-3*) (Pohl et al., 2004). Mice models of *CAV-1* knockout were shown to be resistant against diet-induced obesity and reduced lipid accumulation (Razani et al., 2002). Fatty acid transport proteins, especially FATP2 and FATP5, are liver-specific members of the family responsible for hepatic uptake and metabolism of FFAs. The transcription of FATP is regulated by PPAR-α and PPAR-γ in response to elevated lipid levels or activation of inflammatory cytokine signaling pathways (Doege and Stahl, 2006; Gertow et al., 2006). Mice knockout model of *FATP5* were found to be resistant to diet induced obesity (Hubbard et al., 2006). Another protein, the fatty acid translocase (*CD36*), catalyzes the dissociation of albumin from fatty acids and membrane integration of protonized FFAs, thereby creating a diffusion gradient across the plasma membrane which facilitates a flip-flop of FFAs across the membrane. Interestingly, CD36 is expressed at very low levels in hepatocytes compared to other cell types like muscle, adipose tissues, platelets, heart and endothelial cells (Musso et al., 2009a). However, in conditions of obesity and high fat diet, CD36 expression levels were

found to be significantly higher than normal hepatocytes (Koonen et al., 2007; Luiken et al., 2001). The expression of *CD36* is transcriptionally regulated by liver X receptor (LXR), pregnane X receptor (PXR) and PPAR-γ, while inhibition of *CD36* results in resistance to diet-induced steatosis (Zhou et al., 2008a).

Hepatic de novo lipogenesis in the fatty liver is driven by overexpression of the sterol-regulatory element binding protein SREBP-1c, which was originally described as a master regulator of lipogenesis depending on the availability of cholesterol (Brown and Goldstein, 1997; Shimomura et al., 1999). Studies in rodent models showed that SREBP-1c expression is regulated by the nutritional status of the animals, with higher expression observed in fed state (Horton et al., 1998; Kim et al., 1998). SREBP-1c expression is regulated by LXR, a nuclear transcription factor activated by sensing elevated lipid levels (Kim et al., 2009). The activation of SREBP1-c has also been attributed to elevated levels of oxidative stress and induction of ER-stress pathways in response to elevated FFA levels (Ozcan et al., 2004).

The activation of SREBP-1c is not sufficient to drive lipogenesis, and recent studies have shown that the carbohydrate responsive element binding protein ChREBP, which senses glucose levels and activates transcription of genes involved in de novo lipogenesis in hepatocytes (Uyeda and Repa, 2006b). The expression of ChREBP was shown to be regulated by LXR as well (Cha and Repa, 2007), and the inhibition of ChREBP in the liver of obese mice resulted in alleviation of steatosis and insulin resistance (Dentin et al., 2006).

The LXR and PXR nuclear receptor transcription factors regulate the transcription of a number of lipid metabolism enzymes, including fatty acid synthase (*FASN*), stearoyl-CoA desaturase

(*SCD1*), lipase (*LIPE*), SREBP-1c and ChREBP (Musso et al., 2009a). The peroxisome proliferator-activated receptors (PPARs) are another family of nuclear receptor transcription factors that form heterodimers with retinoid X receptor (RXR) and regulate lipid metabolism in the liver. The activation of PPARα results in elevated uptake of FFAs as well as increased rates of peroxisomal and mitochondrial β-oxidation of FFAs in hepatocytes (Reddy and Hashimoto, 2001). Studies in mice models suggest that PPARα activation is essential for steatosis and pathogenesis of HCC (Tanaka et al., 2008). PPARγ is mostly expressed in adipocytes and regulates FFA uptake in adipocytes for triglyceride synthesis and storage, thus preventing the harmful effects of FFAs on the hepatocytes including metabolic syndrome and insulin resistance (Savage et al., 2003). In vitro and in vivo inhibition of PPARγ was shown to reduce cell proliferation, induce apoptosis and prevent progression of HCC metastases (Shen et al., 2012; Yu et al., 2010). PPARδ is a FFA responsive nuclear receptor which enhances FFA uptake, oxidation and is known to promote hepatic steatosis and insulin resistance (Nagasawa et al., 2006). The activation of PPARδ can promote proliferation of HCC cells via activation of NFκB and cyclooxygenase-2 (COX-2) signaling pathways (Glinghammar et al., 2003).

In terms of metabolic enzymes, the fatty acid synthase (*FASN*) gene is expressed at low levels in most tissues but in several types of cancer cells, overexpression of *FASN* was observed, which resulted in increased de novo lipogenesis and was associated with the progression of cancer (Flavin et al., 2010). FASN catalyzes the synthesis of palmitate from acetyl-CoA and malonyl-CoA. The levels of FFAs including palmitate are regulated by the synthesis of triglycerides from the fatty acids by the diacylglycerol acyltransferase enzyme (DGAT) (Yen et

al., 2008) and lipolysis of the triglycerides by lipase enzyme (LIPE) (Holm et al., 2000). Recent studies suggest elevated LIPE levels may be associated with enhanced proliferation rates of cancer cells (Kuemmerle et al., 2011).

1.7 Epithelial-mesenchymal transition

Intermediate and terminal stage HCC are associated with high rates of vascular invasion and metastases with very high recurrence rates even after surgical resection, and poor survival rates. Most HCC metastases occur as intrahepatic metastases, while common sites of extrahepatic metastases include lung, bone, peritoneum, spleen and lymph nodes (Tung-Ping Poon et al., 2000). The invasiveness of HCC tumors is dependent on infiltration into the portal vein (Toyosaka et al., 1996). Recent evidence suggest that activation of the epithelial to mesenchymal transition or EMT program may be involved in the molecular pathogenesis of metastasis in several cancers, including HCC (Lamouille et al., 2014). For example, the expression of mesenchymal markers vimentin (*VIM*) (Hu et al., 2003) and TWIST (Lee et al., 2006b) were found to be correlated with metastatic ability of HCC cell lines and these were confirmed in histopathological staging of metastatic human HCC samples.

In context of cancer progression, EMT can be described as a set of well-orchestrated series of events that enable changes in cell-cell and cell-matrix interactions, reorganize cytoskeleton, and activate signaling pathways that enable the cells to invade through the extra cellular matrix into the surrounding vasculature (Radisky, 2005). A key feature of epithelial tissues, like the liver, is structural integrity maintained via cell-cell interactions involving tight junctions, gap junctions, adherence junctions and desmosomes. In addition, the intermediate cytoskeletal filament network and cell-matrix interactions maintain the structure and polarity

of the epithelial tissues (Radisky, 2005). The activation of EMT program enables the cells to acquire properties of mesenchymal cells, including loss of adhesion and polarity, and gain of motility, invasiveness, growth signals and plasticity – features that are strongly associated with occurrence of metastases in human cancers and poor prognosis (Tsai and Yang, 2013).

The defining feature of cells undergoing EMT is the loss of E-cadherin (*CDH1*) expression, which acts as tumor suppressor by maintaining cell-cell adhesion via adherence junction and by sequestering and inactivating the Wnt-signaling transcription factor β-catenin (Hajra and Fearon, 2002). The loss of E-cadherin expression has been linked to metastasis and poor-prognosis of several cancer types (Dorudi et al., 1993; Kowalski et al., 2003; Sanders et al., 1999). The mechanism of loss of E-cadherin expression involves transcriptional repression by a number of core EMT transcription factors, including snail (*SNAI1*) (Batlle et al., 2000), slug (*SNAI2*) (Bolos et al., 2003), twist (*TWIST1, TWIST2*) (Yang et al., 2004), and zeb (*ZEB1, ZEB2*) (Comijn et al., 2001; Grooteclaes and Frisch, 2000). In addition, cells undergoing EMT exhibit loss in expression levels of a number of additional epithelial markers, including claudins (*CLDN4, CLDN7*), occluding (*OCLN*), desmoplakin (*DSP*), mucin (*MUC1*) and cytokeratins (*KRT8, KRT18*), along with gain of mesenchymal markers including fibronectin (*FN1*), vimentin (*VIM*) and smooth-muscle actin (*ACTA2*) (Thiery and Sleeman, 2006).

The activation of EMT program requires expression of the core EMT transcription factors that are regulated by a number of different upstream signaling pathways. TGF-β signaling via autocrine or paracrine signaling is known to promote invasiveness and metastasis (Muraoka-Cook et al., 2005) via the induction of EMT program (Xu et al., 2009). Similarly, activation of the Wnt/β-catenin signaling pathway has been investigated as a potent inducer of EMT (Fodde

and Brabletz, 2007). In addition, the activation of oncogenic RAS signaling pathway, PI3K/AKT signaling pathway and receptor tyrosine kinase pathways, including FGF, EGF, TGF and IGF, have been strongly associated with EMT program (Larue and Bellacosa, 2005).

Nearly 60% of HCC patients exhibit loss of E-cadherin and activation of β-catenin, which strongly correlate with intrahepatic metastases and poor survival rates (Zhai et al., 2008). Similarly, *TWIST, SNAIL*, and *SLUG* over expression were found to be associated with EMT induction and poor prognosis of the HCC patients, along with the activation of TGF-β signaling pathway (Battaglia et al., 2009; Giannelli et al., 2005; Lee et al., 2006a).

1.8 Summary and hypotheses

HCC is one of the deadliest forms of cancer with increasing incidence rates in the United States. Advanced-stage HCC is associated with intrahepatic and extrahepatic metastases and has very poor survival rates in response to existing therapeutic regimen. While the molecular mechanism of HCC pathogenesis from various etiologies has been extensively studied, little is known about the mechanism of progression to metastasis. Epidemiological studies suggest elevated FFA levels in HCC patients, which correlate with poor survival rates. Therefore, it is imperative to understand the mechanism by which FFA promote HCC progression, and use this knowledge to identify better, putative, therapeutic targets.

Cancer is a complex disease arising from the combinatorial effect of a number of cellular changes. It is recognized that these events do not arise from mutations to a single gene, but rather from complex interactions between several cellular pathways, which allow a normal cell to transform into a cancerous cell (Fertig et al., 2011; Hornberg et al., 2006). Hanahan and

Weinberg described six "hallmark" capabilities that cells acquire during the course of their development into tumors: sustained proliferation, resistance to growth suppressors, evasion of cell death, unlimited replicative potential, induction of angiogenesis, and capability to invade and metastasize (Hanahan and Weinberg, 2000).

The relationship between genotype and phenotype is complex and not always easily ascribed to changes in a single gene but rather is a composite result of the different components in the biological systems. This coupled with the availability of 'omics' data, have revolutionized the previous view of single gene-phenotype correlation by demonstrating the importance of a "systems" view that captures the inter-relationships between genes. Thus, from a systems biology perspective, a cell can be considered an integrated system of molecular components such as nucleotides, proteins and metabolites that together form a complex network of interacting signaling and regulatory pathways. Cancer can be considered a perturbed state of such networks, and it has been suggested that elucidating the topological and dynamic features of these networks can help generate plausible hypothesis to identify novel markers and therapeutic target. Network modeling approaches can be applied to study the dynamics of signaling and regulatory pathways that may be involved in the progression of cancer. The motivation behind these approaches is to prevent cancer progression by inactivating tumor-specific signaling pathways. However, we still lack suitable strategies to identify ideal candidates from large-scale network models. Potentially, a graph-theoretic solution can be utilized to identify suitable targeted therapeutic candidates from, for instance, an EMT or fatty acid metabolism regulatory network. In **chapter 2** (**section 1**), we investigate the importance of network hierarchy in determining the efficacy of a drug on simulated signaling

networks (Nath and Chan, 2012). We test the utility of this approach on a model drug-target signaling network. This proof-of-concept study establishes a method that could be applied in the future to analyze the drug-response networks of patients with elevated FFA levels.

In recent years, a number of studies have integrated large-scale biological networks with transcriptomic data to identify functional transcriptional regulatory or signaling modules relevant to cancer (Chuang et al., 2007; Ulitsky and Shamir, 2007). The advantage of using such an integrated framework for analysis is that they utilize topological properties of networks along with features contained in the high-throughput data itself. In general, these approaches start with a constraint graph (representing a biological network), consisting of nodes (representing genes or proteins, etc.) and edges (representing biological relationship between nodes). Next, gene expression data is mapped on to the network. Various heuristics then seek sub-networks or modules that share high similarity of expression between connected components. The resultant modules can then be studied further to elucidate regulatory programs or identify network markers that can explain the phenotype. An important class of large scale biological data analysis involves study of similarity relationships between genes from transcriptomic data. These approaches rely on the assumption that genes that exhibit similar expression patterns across different conditions share a common function. For instance, two genes that are co-expressed may be regulated by a common transcription factor or may be involved in a common molecular complex or pathway. In **chapter 2** (**section 2**), we adapt one such approach based on information theory to quantify the synergy or co-operativity between expression levels of two genes in palmitate treated HepG2 cells (Wang et al., 2011). This approach reflects on the contribution of two interacting

genes as whole, instead of the sum of their individual parts, and could reveal new insights into the genetic mechanism by which FFAs could promote HCC progression.

The synergy analysis of HepG2 cells revealed that desmoplakin expression levels were significantly reduced in palmitate treated cells. Given the fact loss of DSP, a cell adhesion protein, is a characteristic feature of cells undergoing EMT. In **chapter 3**, we investigate the role of palmitate on the induction of EMT program by characterizing the in vitro effects of palmitate on migration, invasion, cell adhesion and EMT marker expression in HepG2 and Hep3B cells (Nath et al., 2015). We further identify the upstream signaling pathways that activate EMT program in the palmitate treated cells. We further hypothesize that the CD36-mediated uptake of FFAs is critical for EMT induction in HCC cells. To assess the critical role of elevate FFA uptake via CD36, we analyze the association between CD36 and EMT markers in TCGA liver cancer mRNA dataset and human HCC tumor biopsies.

In the past several years, significant advances have been made in high-throughput sequencing technologies that have permitted the comparison of cancer genomes to reference human genomes across multiple cancer types. The establishments of cancer genome sequencing consortiums like The Cancer Genome Atlas (TCGA) and International Cancer Genome Consortium (ICGC) has provided a platform to integrate data from hundreds of datasets (Wheeler and Wang, 2013). The TCGA project has provided a wealth of knowledge in context of the landscape of somatic mutations and copy number variations that are frequently observed across all human cancers (Beroukhim et al., 2010; Ciriello et al., 2013; Zack et al., 2013). However, a very large proportion of the genetic alterations from the genome-wide studies were found at very low frequencies, and determining the functional

relevance of such alterations remains a fundamental challenge. An alternative, hypothesis-driven, approach to utilize the wealth of TCGA information involves systematic probe of a specific pathway or gene signature in single or multiple cancer types across genomic and transcriptomic datasets. For example, a systematic exploration of components of mammalian SWI/SNF complex revealed a significant role of the chromatin remodeling complex in tumorigenesis (Kadoch et al., 2013). Along similar lines, APOBEC cytidine deaminase mutations were found to be a common feature across several cancer types (Roberts et al., 2013). In addition to establishing statistical association between genetic alterations and the phenotype, the analysis of TCGA data in these studies determined clinical relevance of the alterations by demonstrating their influence on patient prognosis and survival. Thus, analysis of existing, large-scale datasets can provide novel insights into the biology of cancers, help in the discovery of prognostic biomarkers and potential therapeutic targets. As little is known about the role of fatty acid uptake and metabolism in cancer progression, we hypothesize that the alterations in fatty acid uptake and metabolism promote the induction of EMT and metastatic progression of multiple human cancers. In **chapter 4**, we construct a literature-derived network of genes involved in cancer cell metabolism and compare the mutation, copy number variation and gene expression patterns between primary and metastatic tumors across multiple cancer types (Nath and Chan, 2015). We further assess the predictive and prognostic utility of the genes with significant accumulation of alterations in metastatic tumors based on their influence on patient survival rates.

In **chapter 5**, we summarize the findings from the preceding chapters and discuss the future studies that can be derived from this work. We discuss the potential mechanism behind loss

of DSP expression and its influence on the induction of EMT program via the oncogenic activity of junction plakoglobin (JUP). We then discuss the potential role of physical interactions between palmitate and key Wnt signaling and ER-stress pathway proteins as an alternate mechanism of EMT induction. Finally, we discuss the future application of the network modeling approach combined with TCGA omic and clinical data to predict the role of fatty acid uptake and metabolism genes as drug efficacy and resistance biomarkers.

CHAPTER 2: APPLYING SYSTEMS APPROACH TO CANCER RESEARCH

2.1 RELEVANCE OF NETWORK HIERARCHY IN CANCER DRUG-TARGET SELECTION

2.1.1 Introduction

Targeted cancer therapy aims to treat cancer by disrupting the specific pathways that play a key role in the growth and progression of cancer cells. Such an approach contrasts with traditional intervention strategies such as cytotoxic agents (Chabner and Roberts, 2005) and radiotherapy (Bernier et al., 2004), both of which have reached a plateau in management of cancers due to side-effects and drug resistance (Stein et al., 2004). The traditional strategies are non-specific in terms of their mode of action, while targeted therapeutics disable specific proteins of a signaling pathway that are essential for tumor growth with minimal impact on normal tissues (Sawyers, 2004). A key step in developing targeted therapies is the identification and evaluation of suitable targets for rational drug design. However, using conventional target-centric drug discovery approach, i.e. targeting a gene or molecule that is mutated in cancer, it has been difficult to identify suitable targets owing to the abundance of mutated genes associated with a cancer (Futreal et al., 2004) and the vast genetic heterogeneity observed within a tumor (Vogelstein and Kinzler, 2004). Systems biology provides an alternative approach to model cancer pathways from a global perspective instead of focusing on individual components. From a systems biology perspective, a cell can be considered an integrated system of molecular components such as nucleotides, proteins and metabolites that together form a complex network of interacting signaling and regulatory pathways. Cancer can be considered a perturbed state of normal networks, and it

has been suggested that elucidating the topological and dynamic features of these networks could help identify novel drug targets (del Sol et al., 2010; Hood and Friend, 2011).

Cancer networks have been analyzed to identify "hub" proteins (van der Greef and McBurney, 2005), which have been thought to be essential for tumor growth and maintenance owing to their large number of interactions and ability to integrate multiple signaling pathways(Butcher, 2005; Rajasethupathy et al., 2005). Hub proteins are a common feature of scale-free biological networks. In a scale-free network most of the components have very few connections, whereas a small set of component (i.e. hubs) have a large number of connections (Kitano, 2004b). This uneven distribution of connections suggests that in order for any two components to communicate, it is highly probable that they must link through a hub protein (See Figure 1A). Based on this concept, inactivating a hub protein that connects multiple deregulated pathways in cancer could provide potential therapeutic intervention, regardless of the genetic heterogeneity. While this ideology to determine targets based on connectivity appears relevant for an undirected scale-free network, we propose that since cellular signaling and regulatory pathways can be represented as *directed* networks, the significance of a candidate in terms of its therapeutic potential is dependent on its hierarchical properties. Specifically, we hypothesize that nodes at higher levels of the pathway hierarchy can serve as better drug targets than nodes that are at lower levels of the hierarchy. This hypothesis is based on the assumption that directed signaling and regulatory networks are similar in architecture to commonplace pyramidal networks that are oriented towards ordered control (Yu and Gerstein, 2006b). In such chain-of-command networks, information is passed on from a small number of high-level nodes or "master regulators" to

lower-level nodes or "worker nodes" that are present in much larger numbers through mid-level "middle manager" nodes (See Figure 1B). Drawing parallels to common place hierarchies would beg one to question whether the master regulators are more significant than the worker nodes, since the flow of information through the rest of the network is dependent on the master regulators. In order to answer this question, the hierarchical architecture of the yeast and E.*coli* transcriptional regulatory network was determined by Yu and Gerstein (Yu and Gerstein, 2006b). These hierarchical networks were rearranged to assign hierarchical levels to each node and then further analyzed in subsequent studies(Bhardwaj et al., 2010) to determine the relative importance of regulators with respect to their level of hierarchy. These analyses concluded that network rewiring events that affect higher-level nodes had more impact on cell proliferation and survival. In other words, hierarchy played a more significant role in determining the importance of regulators than hubs.

In this section, our goal is to demonstrate the importance of hierarchy in cancer signaling and regulatory networks from the point of view of drug-target selection. First, we construct a model hierarchical network that depicts a regular pyramidal topology. We then apply a Boolean network modeling approach on the model network to test the hypothesis that the nodes at the top level of the hierarchy serve as better drug targets. We evaluate the effectiveness of a drug target in terms of its ability to modulate the output from a signaling network. This criterion is derived from fundamental assumptions of the targeted drug-discovery paradigm (Hellerstein, 2008): targets represent potentially rate-limiting steps in the disease pathway, and the effect on the phenotype will be determined by identification of drugs specific to these targets. We also discuss the effect of targeting nodes at higher vs.

lower levels on this property. Next, we take a closer look at the hierarchy of the targets of FDA-approved drugs as compared to the rejected drugs for treating prostate cancer. Finally, we construct a global transcriptional regulatory network and directional protein-protein interaction network and rearrange them into hierarchical levels to map and discuss the properties of known cancer genes and FDA-approved cancer drug-targets.

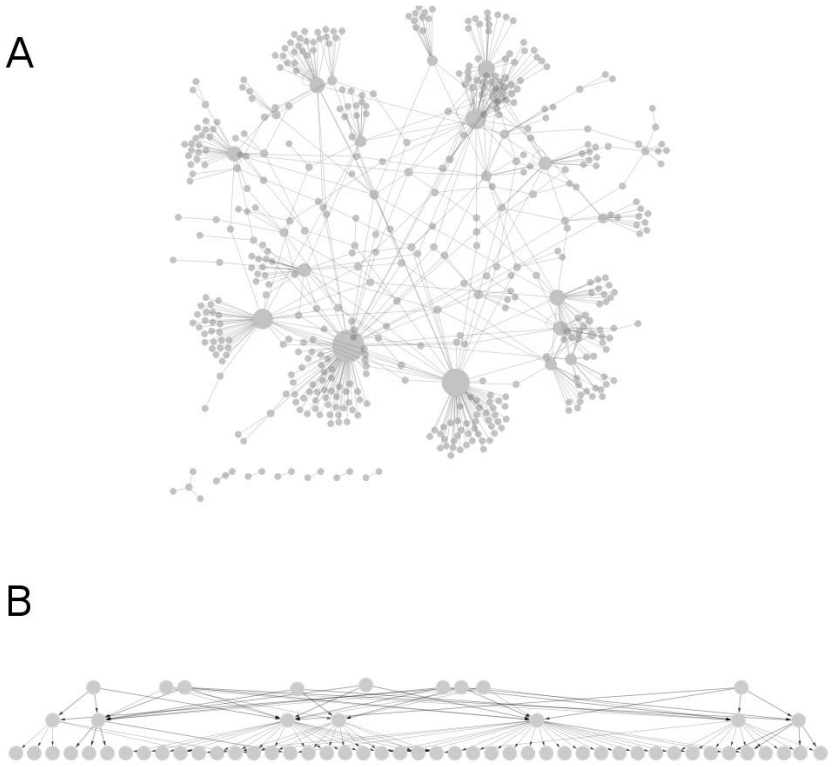

Figure 1: Types of biological network. A. An undirected graph representing the human MAPK signaling network (Bandyopadhyay et al., 2010). The sizes of the nodes in the network are scaled according to degree. This network is an example of a scale-free graph with few hub

Figure 1 (cont'd)

nodes (large circles) containing high degrees while most nodes (small circles) have low degree. Since, a large number of nodes are connected to the rest of the network through hub nodes, any change to the hub nodes can alter the structure of the network dramatically. **B.** A directed graph representing a predicted transcriptional regulatory network of cancer genes obtained from the OMIM morbidity map. The network was constructed using the Promoter Analysis and Interaction Network generation Tool (PAINT)(Vadigepalli et al., 2003) and arranged into hierarchical levels according to the breadth first-search (BFS) algorithm (see methods for details on BFS algorithm). The nodes at the top level of the hierarchy act as the master regulators while the nodes at the bottom act as worker nodes.

2.1.2 Methods

2.1.2.1 Constructing a model hierarchical network

The network topology of our model was adapted from the architecture of *E.coli* and yeast regulatory networks(Yu and Gerstein, 2006b). The pyramidal topology is also observed in human cancer-related signaling networks. For example, the EGFR signaling pathway in the KEGG pathways in cancer (hsa05200) consists of the EGF receptor at the top of the hierarchy. Ligands specific to the EGF receptor initiate multiple signaling cascades in the cell. In order to enhance cell proliferation, multiple pathways are activated downstream of EGFR, including the Ras/Raf signaling cascade and PKB/Akt signaling pathway. Each of these pathways culminates into several effectors that are involved in enhancing proliferation. We attempted to design the model network used in our analysis so that it captured the pattern of flow of information in such signaling networks. The model network was constructed in the form of a regular pyramid featuring three levels of hierarchy. The network consisted of few master regulators at the top level and several worker nodes at the bottom level with intermediate numbers in the middle level. The signaling information was restricted to flow from lower level nodes to upper level nodes, i.e. no upward edges were allowed. The top level of the hierarchy served as receivers of signal input, whereas the bottom level nodes served as effectors of signal output from the network. A comparison between simplified EGFR pathways resulting in proliferation and the model network is shown in Figure 2. Given an input, we analyzed the effects of drugs affecting different nodes in this model network measured in terms of reducing the output.

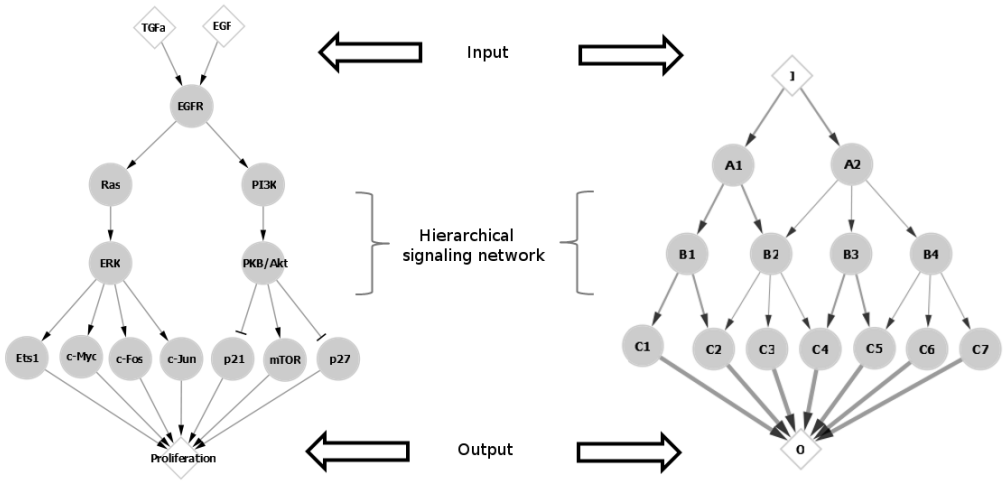

Figure 2: Hierarchy in EGFR pathway. A comparison of simplified model of EGFR induced signaling pathways involved in enhancing proliferation and model network used in our analysis. The model network was designed as a pyramidal hierarchy. The nodes in the top level receive input signal, which is transmitted through the hierarchy down to effecter nodes in the bottom level and that results in a phenotypic output.

2.1.2.2 Boolean modeling approach to select drug-targets from model network

We chose a Boolean approach to model flow of signal information in our model network to capture the dynamic features of information flow through the network. The Boolean model is a logical model that represents the state of the network components in discrete states, with the dynamic progression of the system occurring in discrete time steps. In such a network, components can be present in either of two discrete states: active (1 or on) or inactive (0 or off). A function is then applied to determine the state of a component for each time step. The

method used in our simulation defines the state of a component using an equation derived from De Morgan's law (Zielinski et al., 2009), such that the state of a node *X(t)*, at time *t* is determined by the formula:

$$X(t) = X(t-1) + [1 - \prod (1 - A_i) \times \prod (1 - B_j) \times [1 - X(t-1)]$$

Where, A_i is the product of the signal from the i^{th} incoming acitvating node with edge weight to *X*, B_i is the product of the signal from the j^{th} incoming inactivating node with edge weight to *X* and *Π* is the product of all incoming edges of types *A* and *B* to *X*. This approach was previously applied in a study of 3 pro-survival pathways: Epidermal Growth Factor Receptor, Insulin-like Growth Factor, and Insulin Receptor signaling pathways and the trends obtained from the simulation were confirmed to be similar to the experimental results (Zielinski et al., 2009).

In our simulations, node "I" served as the input node for the network, whereas as node "O" was used to monitor the output from the network. Only the top level nodes were eligible to receive input from node "I", while only the bottom level nodes were eligible to elicit an output to node "O". Weights were assigned according to the outgoing edges of a given node assuming each of its target nodes had equal probability of receiving a signal. The weight was thus calculated by dividing the default edge weight (0.8) by the number of outgoing edges from the node. The simulation was run using an input to node "I" increasing from 0 to 1 in 20 discrete time steps of size 0.05. For drug-targets simulations, a node was chosen at random for complete inhibition by a drug at each of the three levels of hierarchy. The output from the network was measured in the unmodified network, and then compared to the outputs from

various network perturbations that represent the addition of a targeted drug. Multiple pair-wise comparisons were made between the outputs using Student's-test with p-value cut-offs adjusted according to Bonferroni's correction (adjusted p-value cut-off = 0.01/*n*, where *n* = number of comparisons).

2.1.2.3 Constructing a global transcriptional regulatory and directed protein interaction network

A transcriptional or gene regulatory network consists of nodes representing transcription factors and their target genes that are connected by directed edges. The transcriptional regulatory network used in our study was constructed using information from the transcriptional regulatory element database (TRED)(Jiang et al., 2007a). The TRED database is an integrated repository of *cis*- and *trans*- regulatory elements for humans. This database curates transcriptional regulatory information for the target genes of 36 cancer-related transcription factor families from published experimental evidence. We used the cancer-related transcription factor and target information to construct a cancer-specific transcriptional regulatory network (See Table 1).

We also constructed a directed protein-protein interaction (dPPI) network to capture the global signaling. Unlike transcriptional regulatory networks, the edges of a protein interaction networks are undirected, which prevents their direct rearrangement into a hierarchical topology. However, a number of recent studies have provided algorithms to infer the orientation of edges in an undirected protein interaction network (Gitter et al., 2011; Liu et al., 2009; Vinayagam et al., 2011). The dPPI used in our study was constructed using information from the work by Vinayagam et al. (Vinayagam et al., 2011) (See Table 1).

Table 1: Features of the global networks

Network	Type	Nodes	Edges	Interaction
TRED	Transcriptional regulatory network	1840	4512	Protein-DNA
dPPI	Signaling network	6339	34814	Protein-Protein

2.1.2.4 Assigning hierarchical topology to directed networks

To assign hierarchical topology to each global network required an algorithm that achieved the following objectives:

1. All nodes must be assigned to a specific hierarchical level in the network
2. The flow of information should only take place in the decreasing order of hierarchy from the top to the bottom level nodes. In other words, there should be no upward pointing edges
3. Each network should have one unique solution when rearranged using the algorithm
4. The algorithm should be able to deal with loops or feedback, a common feature of complex signaling and regulatory networks

We chose the breadth-first search (BFS) method to rearrange our networks into a hierarchical topology. This approach was used by Yu *et al.* (Yu and Gerstein, 2006a) to assign hierarchical levels to yeast and E.*coli* regulatory networks. In this method, all nodes without any outgoing edges or with only auto-regulatory edges are assigned to the bottom level of the hierarchy, and each direct regulator of a bottom level node is placed on a level directly above the bottom level node. This procedure is repeated for each subsequent level of the hierarchy. To rearrange the TRED and dPPI networks, we first identified all those nodes that had no

outgoing edges in the network and assigned them as the bottom level or level 1 nodes. Then, using a one-level deep BFS search, we identified all the direct regulators of the bottom level nodes, and placed them in level 2. Next, we repeated the search until the subsequent levels of the hierarchy were filled with the remaining nodes. The rearrangement of the two global networks resulted in hierarchies consisting of three levels. The BFS approach allowed for the presence of loops within the network, whilst ensuring that there were no edges that pointed upwards in the hierarchy. The application of the algorithm yielded only one possible solution for each network.

2.1.3 Results and Discussion

2.1.3.1 Modeling approach to select drug-targets from hierarchical network

The aim of targeted therapies is to inhibit specific pathways that are active in cancer. We constructed a model network and evaluated how the signal transduction is perturbed upon disruption of nodes at different levels of the hierarchy. We hypothesized that the nodes at the higher levels of the hierarchy can serve as better drug-targets than nodes at the lower levels. Figure 3A shows a network model that we used to test this hypothesis using the Boolean modeling approach. We first simulated the flow of signal in the unmodified network. The output from this simulation is plotted as control in Figure 3B. Next, we targeted node A1 at the top-level of the hierarchy with drug 1 while leaving the rest of the network intact and plotted the output. Similarly, we targeted nodes B1 and C1 with drugs 2 and 3 respectively and plotted their outputs in Figure 3B. The final outputs from each simulation and their comparison to control are listed in Table 2. The impact of drug 1 targeting the top-level node A1 resulted in a significant decrease of output to 56% of control (p-value << 0.001). Drug 2 targeting the middle level node resulted in a decrease of output to 78% of control, which was also determined to be statistically significant (p-value = 0.002). However, drug 3 targeting the bottom level node C1 resulted in a decrease of output to 89% of control, which was not statistically significant (p-value = 0.135). Assuming that the output represents the influence of the signaling cascade on phenotype, the results from this simulation support our hypothesis that nodes at higher levels of the pyramidal hierarchy have the highest impact.

Cancer tumors have been described as a "robust" system (Kitano, 2004c), where robustness is defined as the ability of the tumor to maintain a stable functioning state despite

perturbations (Kitano, 2004a). The source of these perturbations could be either stochastic changes that modify the dynamics of the cancer signaling network (Huang, 2011), or deterministic genetic mutations that affect tumor suppressor genes and oncogenes (Stratton et al., 2009). A tumor is not only able to survive but gains selective growth advantage as a result of these changes. Ideally, a targeted drug should be able to break-through the robustness of the tumor signaling network. The results from the simulation suggest that targeting the top-level of the hierarchy has the most significant impact on the network output. In other words, targeting the top-level maximizes the deleterious effect on the "robustness" of the network. However, tumors are noted to be robust against several lines of cancer therapies. Tumors achieve robustness through functional redundancy which is derived from cellular heterogeneity (Kitano, 2004c). Tumor cell heterogeneity enables a sub-population of cells to survive after a chemotherapeutic regimen, which can lead to reappearance of the tumor (McClellan and King, 2010). This trait of cellular heterogeneity is achieved by tumors through redundancy. In other words, tumors are able to maintain signal transduction by using alternate pathways. Therefore, it has been suggested that heterogeneity in tumors can be tackled by targeting multiple targets in the signal transduction pathways (Faivre et al., 2006; Petrelli and Giordano, 2008).

In order to simulate the effects of cellular heterogeneity, we modified the weights of two nodes in the bottom level so that they have enhanced impact on the output of the system. In network 2, the edge weights of node C1 and C7 were increased by 25% as compared to the other bottom level nodes (See Figure 4A). This was done to mimic the increase in activity that results from either genetic stochasticity or due to enabling mutations in oncogenes. We

measured the output of the network with the modified edge weights in Figure 4B. Then, we used drug 1 to target node A1 and drug 2 to target node B1 to measure network output. Next, we targeted each of the nodes C1 and C7 with drugs 3 and 4 respectively and plotted their outputs. Additionally, we plotted the output for the combinatorial effect arising from simultaneous use of drugs 3 and 4. The final outputs from each simulation and their comparison to control are listed in Table 3.

Targeting the modified nodes C1 and C7 with drugs 3 and 4 resulted in a decrease in output to 87% and 95% of control respectively, neither of which were statistically significant (p-values = 0.073, 0.424 respectively) individually. Combinatorial use of both drugs 3 and 4 resulted in a decrease in output to 81% of control. However, this decrease was also not statistically significant (p-value = 0.008). Drug 2 targeting the middle level node B1 resulted in a significant decrease in output to 77% of control (p-value = 0.001). Once again, targeting the node A1 with drug 1 resulted in the most significant drop in output to 56% of control (p-value << 0.001). In fact, the output from drug 1 is significantly lower than the combinatorial output from drug 3 and drug 4 (p-value << 0.001). The results from this simulation suggest that targeting a drug at the top of the hierarchy produces a better reduction in network output in the presence of heterogeneity.

A distinct advantage of this modeling approach is that it provides the flexibility to modify the complexity of the simulation by adding or removing components from the network. For example, one can easily expand the model to include additional pathways and study effects of cross-talk on network output. Furthermore, the accuracy of the output from the simulations can be enhanced by including information from experimental evidences. For

example, the initial levels of the nodes in the network can be set according to the expression or activity levels of the individual nodes, whereas the edge weights can be set based on actual kinetic parameters derive from experimental evidence. Thus the overall accuracy would improve with the availability of experimental data. This approach can then be used to model pathways activated in cancer and select suitable targets and for experimental verification.

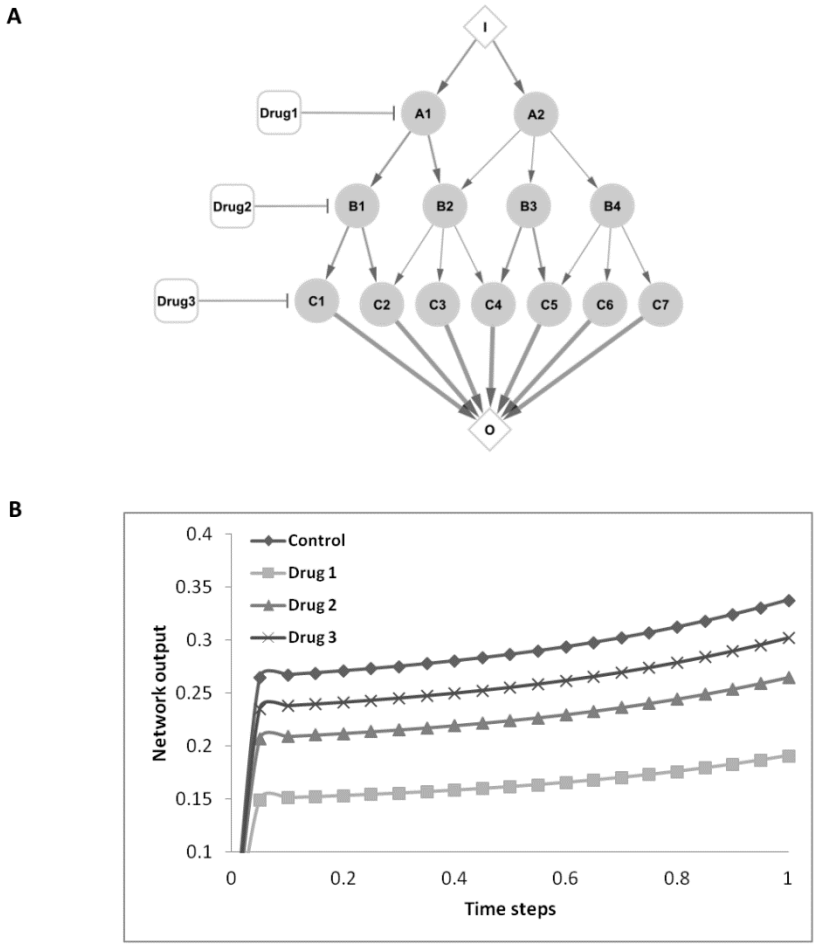

Figure 3: Target inhibition simulation 1. A. Network 1 to test the hypothesis that nodes at the higher level of a pyramidal hierarchy have the highest impact on the network output. The network consists of nodes (circles) in 3 hierarchical levels: nodes A1 and A2 at the top level, nodes B1 to B4 in the middle level and nodes C1 to C7 at the bottom level. A drug-target was random chosen at each level of the hierarchy. Drug 1 targets the node A1, drug 2 targets the node B1 and drug 3 targets the node C1.The drugs are shown as round-rectangles. Diamond-

Figure 3 (cont'd)

shaped nodes I and O represent input and output nodes respectively. The sizes of edges are proportional to their weights and the direction of arrow indicates flow of information in the network. **B.** Output from the simulation of signal flow through the network. Control indicates output levels recorded from the unmodified network. Drugs 1 to drug 3 indicate the output levels from the network when each of the respective targets was inhibited by a drug. The output for control and each drug treatment is plotted against discrete-value time steps on the x-axis.

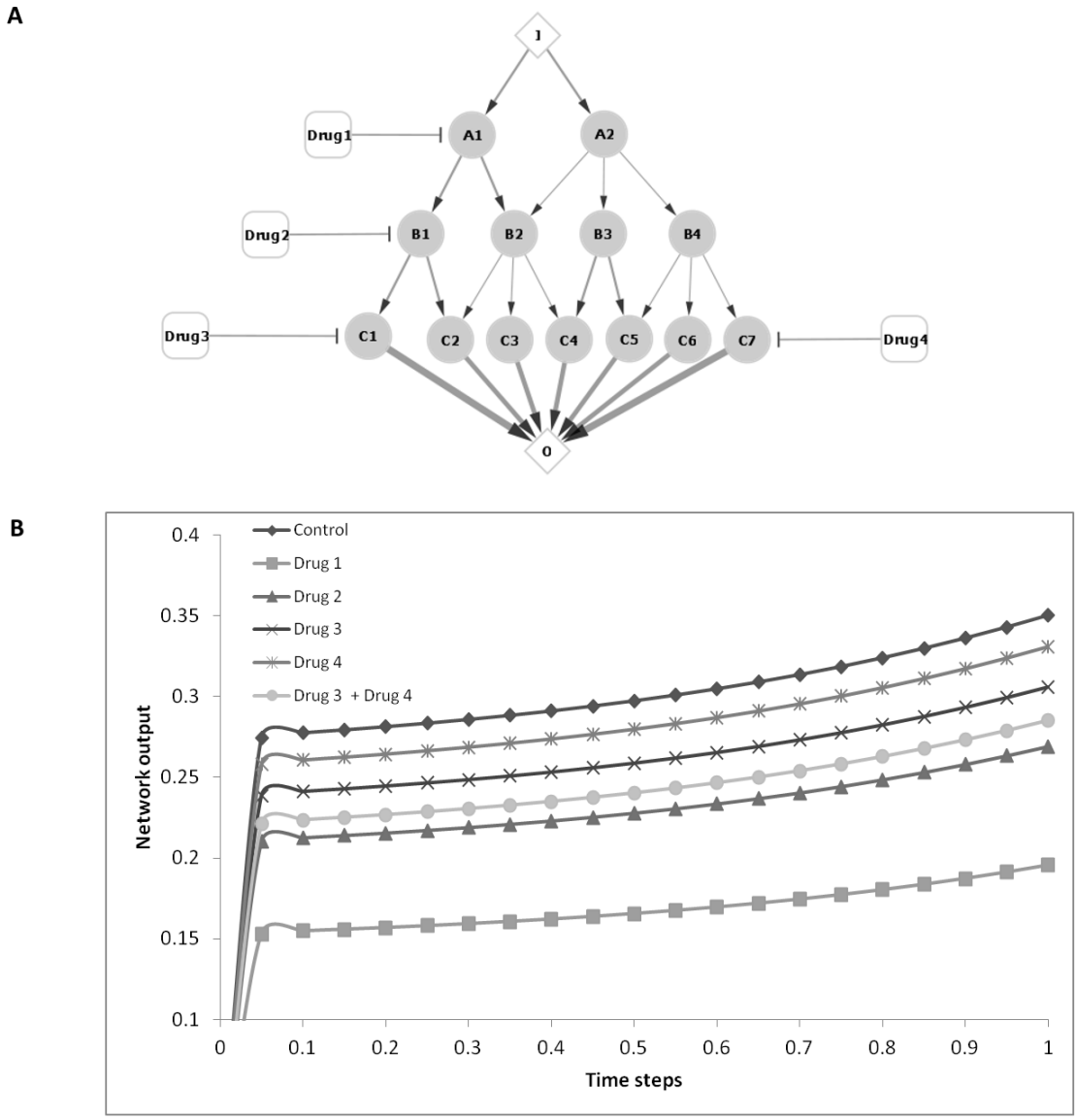

Figure 4: Target inhibition simulation 2. A. Network 2 to test the hypothesis that nodes at higher level of a pyramidal hierarchy serve as better drug targets even with heterogeneity enhancing multiple bottom-nodes in the network. The components of the network used for this simulation are the same as network 1. Edge-weight of nodes C1 and C7 were increased by 25% to 1.0 to represent enhanced activity. In this simulation, drug 1 targets the node A1, drug 2 targets the node B1, drug 3 targets the node C1 and drug 4 targets node C7. The drugs are

Figure 4 (cont'd)

shown as round-rectangles. Diamond-shaped nodes I and O represent input and output nodes respectively. The sizes of edges are proportional to their weights and the direction of arrow indicates flow of information in the network. **B.** Output from simulation for signal flow through the network. Control indicates output levels recorded from the unmodified network. Drugs 1 to drug 4 indicate the output levels from the network when each of the respective targets was inhibited by a drug. The combinatorial effect of using drugs 3 and 4 simultaneously was also recorded. The output for control and each drug treatment is plotted against discrete-value time steps on the x-axis.

Table 2: Results from network 1 simulations

Condition	**Target**	**Output**	**P-value***
Control	-	0.338	-
Drug 1	A1	0.191	**0.000**
Drug 2	B1	0.265	**0.002**
Drug 3	C1	0.302	0.135

(*Bonferroni correction adjusted p-value cut-off = 0.003)

Table 3: Results from network 2 simulations

Condition	Target	Output	P-value*
Control	-	0.350	-
Drug 1	A1	0.195	**0.000**
Drug 2	B1	0.269	**0.001**
Drug 3	C1	0.306	0.073
Drug 4	C7	0.331	0.424
Drug 3 + Drug 4	C1+C7	0.285	0.008

(*Bonferroni correction adjusted p-value cut-off = 0.002)

2.1.3.2 Drugs targeting signaling pathways in prostate cancer and their network properties

The simulations with the model networks emphasized the impact of the nodes that are higher in the pathway hierarchy. To investigate the relevance of hierarchy in drug-target selection with a working example, we examined the drugs approved for targeted therapy in prostate cancer. Prostate cancer is one of the most common forms of cancer in men; an average of 1 in every 6 men in the United States has a lifetime risk of developing prostate cancer (Siegel et al., 2011). When detected at an early stage, prostate cancer is treatable with radiation therapy or through surgical removal of the prostate. However, the treatment of advanced or metastatic prostate cancer is primarily based on castration, or depriving prostate cells of androgen(Shen and Abate-Shen, 2010). We obtained a list of drugs that are approved by the FDA for the treatment of prostate cancer, along with a list of drugs that have been rejected. We then

mapped the targets of these drugs on the androgen receptor pathway (modified from O'donell et al. (O'Donnell et al., 2004)). Additionally, we considered some drugs that have been clinically tested to target various components of the EGFR pathway, which is suggested to play a role in castration resistant prostate cancer (Di Lorenzo et al., 2002). The EGFR pathway (modified from KEGG: hsa05200) showing the relevant components that are targeted by the approved and rejected drugs, combined with the androgen pathway and their respective phenotypic outputs is depicted in Figure 5. The network was organized in a simple hierarchy such that there were no edges present that pointed upwards from the lower to higher level nodes. Then, the drug targets within their respective pathways were ranked from top to bottom according to their relative position in the hierarchy. Next, we examined and compared the efficacy and safety of these approved and rejected drugs. The order of the drugs discussed below follows the ranked order in the hierarchy, and the major features of these drugs are tabulated in Figure 6.

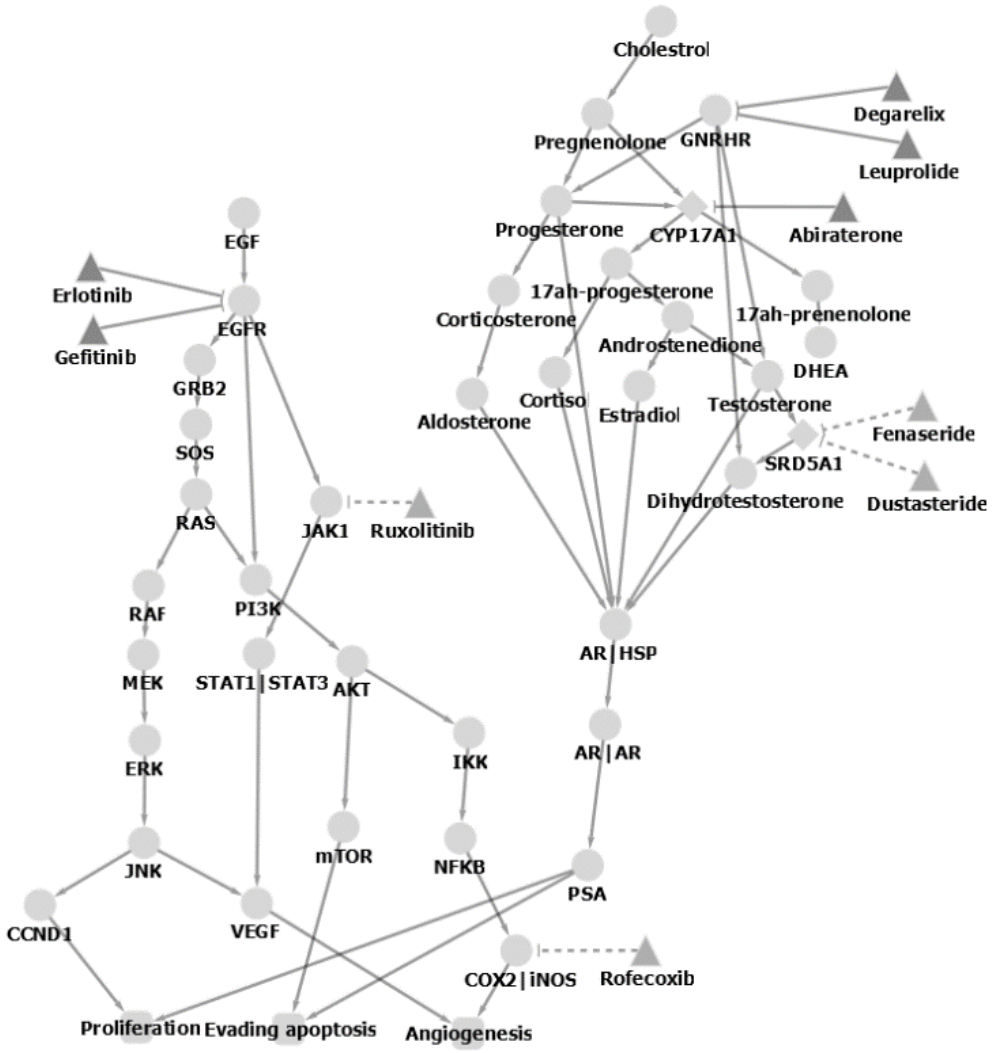

Figure 5: Drugs-targets mapped on signaling pathways in prostate cancer. Different components of the AR network and EGFR network are shown in circles, with arrows indicating direction of regulation. Dark-colored triangles are FDA-approved drugs with T-headed edges indicating the component of the network that is targeted by the drugs.

Figure 5 (cont'd)

Light-colored triangles are drugs that have been rejected by FDA, with dashed T-headed edges indicating the component of the network targeted by the drug. In general, targets of FDA-approved drugs map higher on the hierarchy as compared to targets of rejected drugs.

AR-pathway related drugs

Level*	Drug	Target	Indication	Efficacy	FDA status	Side-effects
1	Degarelix	GnRHR	Advanced PC	90% decrease in testostetone levels, 90% reduction in PSA levels	Approved for PC	
1	Leuprolide	GnRHR	Advanced PC	97% decrease in testosterone levels	Approved for PC	
2	Abiraterone	CYP17A1	CRPC	64% reduction in PSA levels, 42% reduced risk of progression	Approved for PC	
3	Finasteride	5-alpha reductase	PC prevention	25% reduced risk of progression	Rejected	Increased risk of higher grade PC
3	Dutasteride	5-alpha reductase	PC prevention	23% reduced risk of progression	Rejected	Increased risk of higher grade PC, Cardiac failure

EGFR-pathway related drugs

Level*	Drug	Target	Indication	Efficacy	FDA status	Side-effects
1	Erlotinib	EGFR	CRPC	40% clinical benefit, median PSA levels	Approved for other cancers, under trial for PC	
1	Gefitinib	EGFR	CRPC	Median PSA levels	Approved for other cancers, under trial for PC	
2	Ruxolitinib	JAK	CRPC	< 10% response	Trials terminated by manufacturer	Adverse effects in 84% of the patients
3	Rofecoxib	COX	PC Prevention	(efficacy not reported)	Trials terminated by manufacturer	Cardiac events in 36% of the patients

*Level ranks are assigned to according to order of hierarchy in targeted pathway (see figure 5)

Figure 6: Outcome from clinical trials of drugs targeting different components of the AR and EGFR pathways.

2.1.3.3 Drugs targeting androgen receptor pathway

Level 1 drugs. Degarelix is an FDA-approved drug that blocks GnRH receptor to suppress gonadotropin secretion (Broqua et al., 2002). Stage II clinical trials revealed that degarelix treatment achieved decrease in testosterone to castration levels (0.5ng/ml) in approximately 90% of the patients 3 days after treatment (Gittelman et al., 2008). These levels of testosterone were maintained at castration levels after 1 month of treatment. This study also

reported that 90% decrease in PSA levels were achieved after 56 days of treatment. Phase III clinical trials with degarelix measured the efficacy of the drug in terms of reducing testosterone levels to castration levels. These trials reported a decrease in testosterone levels in approximately 97% of the patients over 1 year period of treatment (Klotz et al., 2008). The phase III trials also reported that no systemic allergic reactions were induced as a result of degarelix treatment. **Leuprolide** is another drug approved for prostate cancer treatment that acts as a GnRH agonist and blocks the activation of GnRH receptors. Initial open-label studies with leuprolide acetate showed that testosterone reached castration levels in 100% of the enrolled patients within 42 days (Perez-Marreno et al., 2002). Phase III studies with leuprolide treatment showed approximately 97% of the patients show a decrease in testosterone levels after 57 days (Heyns et al., 2003).

Level 2 drug. Castration resistant prostate cancer (CRPC) tumors remain dependent on hormone driven stimulation for growth and maintenance (Titus, 2005). **Abiraterone** acetate is a selective inhibitor of CYP17A, a key enzyme involved in the biosynthesis of androgen and estrogen. Phase I clinical trials of the drug indicated a decrease of prostate specific antigen by >50% in 64% of the patients (Ryan et al., 2010). In a clinical phase I/II study, the drug was found to decrease PSA levels by >50% in 67% of the CRPC patients, while a decline of >90% was achieved in 19% of the patients (Attard et al., 2009). Phase III clinical trials with metastatic CRPC patients confirmed that PSA reduction following Abiraterone treatment was associated with a 42% decrease in risk of disease progression (de Bono et al., 2011). Furthermore, phase III trials revealed that most common side effects were limited to fatigue, whereas cardiac

events associated with the treatment were not statistically significant when compared to placebo control group (13% in treated vs. 11% in control).

Level 3 drugs. The drug **Finasteride** inhibits one isoform of 5-alpha reductase, whereas **Dutasteride** is a drug that inhibits both isoforms of 5-alpha reductase (Bramson et al., 1997). Long term studies with finasteride for the treatment of benign prostatic hyperplasia indicated a reduction in risk of progression to prostate cancer by 25%(Thompson et al., 2003). However, there was a 27% increase in higher-grade tumors as determined by Gleason score, while surgical intervention was recommended in 23% of the patients due to increase in PSA levels or based on digital prostate examination. Additional concerns due to significantly increased severe side effects were also noted in this study. Long term studies with dutasteride indicated an approximately 23% reduction in risk of progression to prostate cancer (Andriole et al., 2010). The incidence rate of progression to higher-grade tumors based on Gleason score did not improve with the drug treatment, and was found to be statistically similar to placebo treatment group. Additionally, concerns were raised because a significantly higher percentage of the patients receiving dutasteride suffered from cardiac failure compared to placebo group. The FDA issued a warning that the use of both 5-alpha reductase inhibitor drugs increased the risk of higher-grade prostate cancer (FDA, 2011) which led to subsequent suspension of marketing and pursuit for approval of dutasteride for prostate cancer treatment (GlaxoSmithKline, 2011).

2.1.3.4 Drugs targeting the EGFR pathway

Gene expression studies comparing localized androgen-dependent and metastatic androgen-independent prostate cancers against normal prostate epithelial cells and tissues

emphasized a critical role played by the AR and the EGFR pathways (Mimeault, 2005). Multiple studies have reported that overexpression of EGFR and its ligands correlates with advanced grades of prostate cancer(Bartlett et al., 2005; Hernes et al., 2004; Mimeault et al., 2003; Zellweger et al., 2005). Enhanced expression of EGFR and the ensuing signaling cascade may stimulate proliferation and anti-apoptotic pathways, providing an androgen independent mechanism of disease progression.

Level 1 drugs: Monocentric phase II trials with **Erlotinib**, an EGFR inhibitor, show clinical benefit in 40% of the patients (Gravis et al., 2008). Clinical benefit was assessed on the Karnofsky performance status (KPS) and pain based on visual analog scale. Monocentric Phase II trials in HRPC patients with **Gefitinib**, another EGFR inhibitor, indicated stabilization of PSA levels in 14% of the patients, however, no significant decrease in PSA levels (Canil, 2004). Another phase II trial based on combination therapy with docetaxel, a chemotherapeutic agent, and gefitinib showed reasonable tolerance to the therapeutic course. However, this study also suggested no significant decrease in PSA levels in patients receiving the treatment. Similar results were obtained from other combination clinical studies confirming that while gefitinib was well tolerated by patients in combination therapies, it did not induce a significant decrease in PSA levels (Canil, 2004; Small et al., 2007). A caveat of the randomized clinical trials was that the EGFR-expression status of the patients was not taken into account. An investigation on the EGFR expression levels in prostate cancer tissues showed that EGFR overexpression is observed in more than 10% cells of tumor tissues in approximately 37% of the patients (Shuch, 2004). Furthermore, this distribution was shown to be non-uniform for different races within the population, with African-American prostate cancer patients

showing significantly higher association with EGFR overexpression. Studies on efficacy of EGFR inhibitors may benefit in future trials that take EGFR status of the patients into consideration.

Level 2 drugs: Downstream effectors of EGFR pathway have been also clinically tested for targeted therapy. **Ruxolitinib** is a drug that targets the janus kinase proteins (JAKs) which are involved in the JAK-STAT signaling pathway induced downstream of EGFR. Phase II clinical trials of treament with Ruxolitinib produced dismal results with less than 10% of the patients showing response to the drug (ClinicalTrials.gov, 2011). This study was terminated since 70% of the patients showed disease progression along with death or adverse events in an additional 14% of the patients.

Level 3 drugs**:** Nonsteroidal anti-inflammatory drugs (NSAIDs) were suggested to be associated with decreased risks of advanced prostate cancer in multiple epidemiological studies (Langman, 2000; Nelson and Harris, 2000; Norrish et al., 1998). The rationale behind use of NSAIDs is based on the fact that the molecular target of NSAIDs, COX-2, is overexpressed in prostate cancer cells(Gupta et al., 2000; Richardsen et al., 2010). COX-2 together with iNOS (inducible form of NOS-2) are induced downstream of EGFR pathway through the PKB/Akt signaling cascade and can enhance angiogenesis (Chiarugi et al., 1998; Davel et al., 2002). In prostate cancer patients, **Rofecoxib**, a COX-inhibitor drug was evaluated in a long term clinical trial to study its efficacy and safety. However, the trials were terminated before completion because the drug was pulled-off the market by the manufacturer after FDA raised safety concerns (Topol, 2004). The clinical study reported that 36% of the patients

suffered from cardiovascular events during the course of the treatment (van Adelsberg et al., 2007).

From the above discussion, drugs targeting nodes at a higher level in the hierarchy were approved by the FDA for use in prostate cancer treatment, whereas the drugs targeting pathways lower down in the hierarchy were rejected. One of the striking features of the drugs that target the pathways higher in the hierarchy is their relative efficacy in preventing the progression of cancer when compared to drugs at targeting the lower levels of the hierarchy. For instance, in the androgen receptor pathway, the drugs targeting the GnRH receptor and CYP17A1 have much higher success in terms of end-point clinical output when compared to the drugs that target 5-alpha reductase (See Figure 6). These outcomes from the clinical studies in prostate cancer patients lend support to the results of our simulation, and further support the idea that the hierarchical level of the nodes plays an important role in determining their potential relevance as drug targets.

2.1.3.5 Features of cancer genes and drug-targets in global hierarchical networks

We constructed a global transcriptional regulatory network (TRED) and a directional protein interaction network (dPPI) and rearranged the networks into regular hierarchies based on the breadth first search approach (see methods). Next we obtained the list of known cancer genes from the OMIM morbid map (Amberger et al., 2009) and a list of genes that are targeted by approved anti-cancer drugs from the DrugBank (Wishart, 2006). A total of 54 cancer genes were mapped onto the TRED network while 70 cancer genes were mapped onto the dPPI network. Additionally, 16 drug-target genes were mapped onto the TRED network, whereas 13 drug-targets were mapped onto the dPPI network. The frequency distribution of

the cancer genes and the drug-target genes normalized to the number of nodes present in each level of the hierarchy is shown in Figure 7. Note that the architecture of the global dPPI and TRED networks does not make them suitable for direct comparison with the pathway-based networks models used in our simulation or the prostate cancer drug-target network because neither of these two networks directly corresponds to a specific input or a phenotypic output. That said we find that a larger proportion of cancer genes and drug-targets map to the middle and upper levels of the hierarchy than the bottom level of the dPPI network. The distribution of the cancer genes correlates with the distribution of drug-targets in each level (Pearson's correlation coefficient = 0.99). The distribution of cancer genes in the TRED network follows an expected pattern, with low frequency in the lower level as compared to the middle and upper levels. However, the distribution of drug-targets does not correlate with that of the cancer genes in the TRED network (Pearson's correlation coefficient = 0.22). Although, the middle level has a higher frequency of drug-targets than the lower levels, there were no drug-targets that mapped to the top level. We posit that the top level of the TRED hierarchy could be considered in future studies to assess their potential as drug-targets.

Next, we compared the drugs that targeted genes at the higher levels of the hierarchy as compared to drugs that targeted genes at the bottom level of the hierarchy. Target genes with their respective hierarchical levels in the two networks, along with a list of FDA-approved drugs are listed in Table 4. 8 of the 32 listed drugs target a gene in the bottom level of the hierarchy, whereas 24 drugs target a gene that is mapped at a higher hierarchical level in at least one of the networks. This difference is statistically significant (Chi-squared p-value =

0.0047). Although these global networks are not directly applicable to selecting drug-targets, it is noteworthy that a larger proportion of the drugs target genes at the higher levels of these global hierarchies. The findings from the global network map lend further support to our hypothesis that the components at the higher hierarchical levels have more impact and thus could serve as better drug-targets.

Table 4: Hierarchical levels of target genes in TRED and dPPI networks with respective FDA-approved drug.

Target gene name	Entrez GeneID	Number of drugs	TRED level	dPPI level	Names of drugs
ESR1	2099	7	2	2	Chlorotrianisene, conjugated estrogens, Ethinyl Estradiol, Fulvestrant, Megesterol, Tamoxifen, Toremifene
CYP19A1	1588	3	3	-	Exemestane, Letrozole, Testolactone
TOP2A	7153	3	3	1	Epirubicin, Etoposide, Valrubicin
BCL2	596	2	3	1	Docetaxel, Paclitaxel
DHFR	1719	2	-	1	Pemetrexed, Trimetrexate
GNRHR	2798	2	3	-	Abarelix, Leuprolide
TYMS	7298	2	3	-	Capecitabine, Fluorouracil
EGFR	1956	2	3	2	Erlotinib, Gefitinib
ADRA1A	148	1	3	1	Nilutamide
ERBB2	2064	1	3	2	Trastuzumab
FCGR1A	2209	1	3	2	Porfimer
FOLH1	2346	1	3	-	Capromab
LDLR	3949	1	3	1	Porfimer
LHCGR	3973	1	3	1	Goserelin
MTRR	4552	1	3	1	Hydroxocobalamin
PGR	5241	1	2	1	Megestrol
TUBB2C	10383	1	-	1	Vinblastine

A

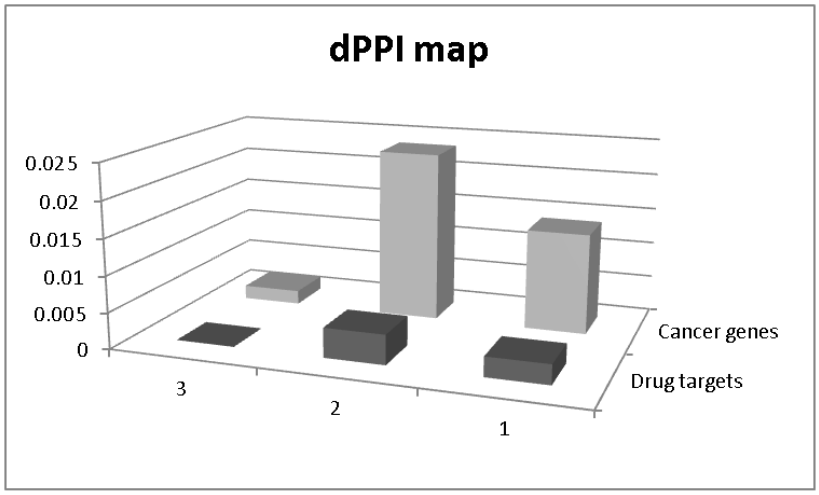

B

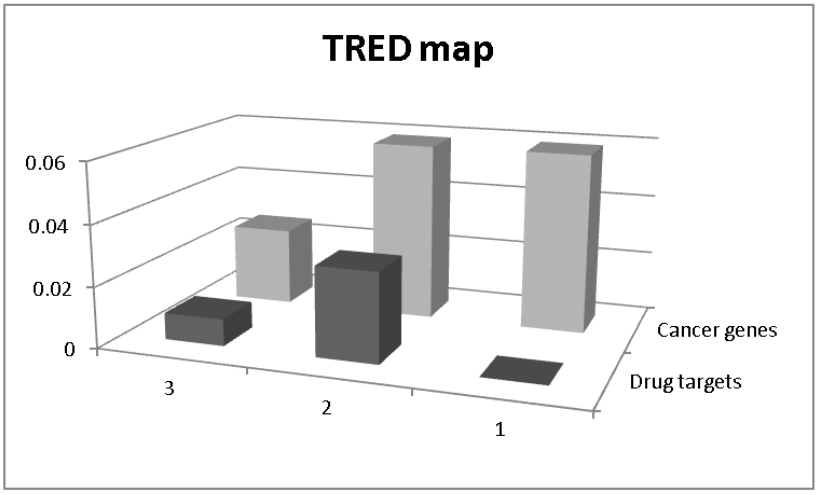

Figure 7: Distribution of cancer genes and drug targets on **A.** the dPPI network **B.** the TRED network. Numbers on the x-axis represent the hierarchical levels in each network, with level 3 corresponding to bottom level, level 2 corresponding to middle level and level 1 corresponding to top level of the hierarchy. The size of the bars indicate frequency of the

Figure 7 (cont'd)

cancer genes (light-colored) and the drug targets (dark-colored) normalized to the number of genes within their respective hierarchical levels.

2.1.4 Summary

In this section, we suggested that the selection of candidates for targeted therapy in cancer signaling networks is influenced by their hierarchal properties. The Boolean modeling approach was able to capture the signaling dynamics of a pyramidal signaling network in the presence or absence of drugs that targeted different components of the network at distinct hierarchical levels and found drugs targeting the higher levels were more influential. The approach used for the simulation can be used as a framework for future studies, with enhanced accuracy imparted with the inclusion of experimental information where available. We provided further support to our hypothesis by analyzing the hierarchical mapping of FDA-approved drugs for prostate cancer treatment, compared to drugs that have been rejected. We found that all FDA-approved drug-targets occupy a higher hierarchical level in their respective signaling pathways as compared to drugs that were rejected. In fact, the higher level drugs had a better overall efficacy than drugs at the lower level. Additionally, we constructed global transcriptional regulatory and PPI networks to analyze the mapping of the cancer genes and FDA-approved drug-targets on these networks. We found that a significantly larger proportion of drugs approved by the FDA targeted genes that occupy higher levels of the hierarchy. Overall, the results from these analyses support our hypothesis that nodes at the higher levels of network hierarchy have more influence and could serve as better drug-targets for cancer therapy.

2.2: SYNERGY ANALYSIS REVEALS ASSOCIATION BETWEEN INSULIN SIGNALING AND DESMOPLAKIN EXPRESSION IN PALMITATE TREATED HEPG2 CELLS

2.2.1 Introduction

Accumulation of lipids (primarily triglycerides) in hepatocytes is considered a hallmark and pre-requisite for development of non-alcoholic fatty liver disease (NAFLD) (Donnelly et al., 2005). With increasing prevalence of obesity among adults and children, NAFLD has become the most common form of chronic liver disease in developed countries (Angulo, 2007). Studies have shown that diets rich in saturated fats contribute significantly towards increasing the risk of NAFLD (Musso et al., 2003; Zelber-Sagi et al., 2007). Consequently, a large number of studies have focused on the effects of free fatty acids (FFA) on hepatocytes to understand the pathogenesis of NAFLD and related liver diseases (reviewed in (Musso et al., 2009b)).

In recent years, systems biology approaches utilizing high-throughput (microarray) measurements have been applied to gain significant insights into the cytotoxic effects of FFAs on hepatocytes using either static (Li et al., 2007a; Li et al., 2007b; Srivastava et al., 2007; Yang et al., 2009b) or dynamic gene expression profiles (Li et al., 2008). While these efforts have focused predominantly on identifying individual target genes, some researchers have suggested a more complex scenario, whereby genes cooperate in regulating cellular events in response to FFA treatment (Remenyi et al., 2004).

In this study, we analyzed the cytotoxic effects of palmitate treatment, the most common FFA in the diet, on HepG2 cells. First, we selected a subset of genes affected by FFA treatment by

mapping their gene expression to metabolite profiles (Srivastava and Chan, 2008; Srivastava et al., 2007) . This allowed the integration of multi-level data and further helped to alleviate the computational burden associated with the analysis of a large set of gene expression data. Next, we used an integrative methodology to reconstruct a gene cooperation network using the concept of "Information Synergy" (Anastassiou, 2007). The underlying principle of information synergy states that if two genes cooperate to affect a phenotype, then the joint expression of these two genes should provide more information on the phenotype than the sum of the information contributed independently by each of the genes. Thus, the gain in information or information synergy could be used to quantitatively asses the cooperative effect of any two genes on a phenotype. To help elucidate the processes that may be altered we analyzed the pathways that were enriched in the network.

Our search for over-represented pathways in the synergy network recovered insulin signaling pathway as the most significantly enriched pathway. This is notable given the fact that almost all patients diagnosed with NAFLD have concomitant insulin resistance (Bugianesi et al., 2005). Ruddock *et al.* confirmed that palmitate treatment induces resistance to insulin signaling in hepatocytes (Ruddock et al., 2008). We further expanded our search to the neighbor genes of the insulin signaling pathway in the synergy network and recovered desmoplakin (DSP), a junction protein, as the top neighbor. The DSP protein is an obligate component of functional desmosomes at intercellular junctions. DSP together with plakoglobin and plakophilin forms the intracellular desmosomal plaque (Getsios et al., 2004), which serves as an anchor for keratin intermediate filament attachment (Rampazzo et al., 2002). In general, junction proteins are known to be inhibited during chronic liver diseases,

including cirrhosis and hepatitis (Vinken et al., 2006). It has also been shown that the loss of expression and abnormal localization of junction proteins, including DSP, is correlated with progression of HCC (Cao et al., 2007). However, the effects of palmitate on DSP protein expression have not been previously reported.

Here, we investigated the effects of palmitate treatment on the expression of DSP in HepG2 cells. Furthermore, since DSP was recovered as a neighbor of insulin signaling pathway, we analyzed the effect of insulin treatment on DSP expression. We found that palmitate treatment leads to the loss of DSP expression and treatment with insulin enhanced the recovery of DSP expression following palmitate treatment. Thus, our study indicates that the junction protein DSP, in synergy with insulin signaling, may be a novel target in the pathology of fatty liver disease.

2.2.2 Materials and Methods

2.2.2.1 Datasets and network analysis

HepG2 cells purchased from American Type Culture Collection (ATCC) were exposed to different FFA treatments for 48 hours. Gene expressions measurements were described in our previous work (Srivastava and Chan, 2008; Srivastava et al., 2007). Gene selection, synergy network construction and pathway analysis were performed as described (Wang et al., 2011)

2.2.2.2 Cell culture and treatment

HepG2 cells were cultured in Dulbecco's Modified Eagle's Medium (DMEM) (Invitrogen) containing 10% fetal bovine serum (Invitrogen) and 2% Penicillin-streptomycin (Invitrogen). Cells were incubated at 37 °C and in 10% CO_2 atmosphere. Confluent cells were treated with 0.7mM palmitate (Sigma) dissolved in DMEM culture medium for 48 hours. Cells were treated with 1nM insulin in culture medium for 24, 48 and 72 hours. DMEM culture medium was used as control for all treatments.

2.2.2.3 Immunofluorescence

Cells were fixed in 3.7% formaldehyde for 20 min. Cells were then washed twice with PBS and treated with 5% Triton-X for 10 min. at room temperature to permeabilize cell membrane. This was followed by washing twice with PBS and incubation with 1% BSA to block non-specific protein interactions. The cells were then incubated with 5µg/ml anti-rabbit DSP primary antibody (Abcam ab71690) overnight at 4°C. After washing twice with PBS, cells were incubated in AlexaFluor-488 (Molecular Probes A11001) conjugated goat anti-rabbit secondary antibody (green) for 1 hour at room temperature. Cells were washed with PBS and

cell nuclei were stained (blue) using DAPI (Molecular Probes D1306) at a concentration of 300nM for 5 min. Coverslips were mounted in ProLong Gold (Molecular Probes P36934) and incubated in the dark for 24 hours.

Confocal imaging was performed on an Olympus FluoView 1000 Inverted IX81 microscope, using a 40X oil objective. Blue and green images were taken sequentially, using a Kalman average of 2X. The intensity graph was constructed by normalizing the total green fluorescence intensity to total blue fluorescence intensity (to account for the number of cells) in 3 separate fields of view for each sample. Multiple comparisons between fluorescence levels across different treatment conditions were performed using one-way ANOVA followed by Tukey's HSD post-hoc analysis with p-value cut-off set at 0.05.

2.2.3 Results

2.2.3.1 Information synergy network

Based upon the concept of information synergy, we reconstructed a gene-cooperation network composed of 570 genes with 4376 connection edges. The reconstructed network suggested potential gene targets and pathways that may play important roles in the induction of the cytotoxic phenotype. We interrogated gene pairs in terms of their ability to jointly distinguish phenotypes. Positive, zero and negative information synergies represent gene pairs that provide synergistic, no and redundant information on the phenotype, respectively. The pathways enriched in the synergy network were explored through KEGG enrichment analysis and the top 10 pathways are listed in Table 5.

As seen in Table 5, cellular activities such as insulin signaling, adherence junction/cytoskeleton regulation, amino acid metabolism, and ubiquitin-mediated proteolysis are highly enriched in the synergy network. Indeed, it has been suggested in the literature that palmitate treatment affects several of these enriched pathways, including insulin signaling inhibited by palmitate in hepatoma cells (Ruddock et al., 2008), ER stress and the ubiquitin mediated protease pathways (Guo et al., 2007; Zhou et al., 2007), as well as adherence junction and cytoskeleton structure (Draghici et al., 2007; Swagell et al., 2005). Palmitate has been also shown to modulate the metabolism of various amino acids (Srivastava and Chan, 2008) which may be important players in palmitate-related cytotoxicity. For example, arginine metabolism provides substrate for nitric oxide synthetase (NOS) and palmitate treatment was found to enhance cell death by increasing NOS activity and NO production (Tsang et al., 2004).

Table 5. Top ten KEGG pathways ranked by their p-values enriched in the synergy network

Pathway names	Genes in network	p-value	Affected by Palmitate
04910: Insulin signaling pathway	15	6.68E-07	Known (Ruddock et al., 2008)
04520: Adherens junction	10	2.10E-05	Known (Draghici et al., 2007; Swagell et al., 2005)
00310: Lysine degradation	7	0.00014	Known (Srivastava and Chan, 2008)
00330: Arginine and proline metabolism	6	0.00053	Known (Srivastava and Chan, 2008)
04916: Melanogenesis	8	0.00556	
04120: Ubiquitin mediated proteolysis	9	0.00644	Known (Smith et al., 2008; Zhou et al., 2007)
04010: MAPK signaling pathway	13	0.00658	Known (Gao et al., 2010)
05210: Colorectal cancer	7	0.00716	
04310: Wnt signaling pathway	9	0.00942	Known (Franch-Marro et al., 2008)
04810: Regulation of actin cytoskeleton	11	0.00981	Known (Borradaile et al., 2006; Swagell et al., 2005)

2.2.3.2 Neighbor genes relevant to insulin signaling pathway

We investigated the associations between the enriched pathways and their neighbors in the synergy network. Neighbors were defined as genes in the network connected to at least one gene of the enriched pathway. The connections in the network represent cooperative relationships between the genes. Therefore, we assumed that the neighbor genes, especially those connected to multiple members of an enriched pathway may function cooperatively with the enriched pathway in the associated phenotype.

We evaluated the biological relevance of insulin signaling, the most significantly enriched pathway, and its neighbor genes. In the synergy network, there are a total of 262 neighbor genes connected to the insulin signaling pathway (Figure 8) and most of these neighbor genes (more than 90%) are connected to one or two insulin signaling genes. We focused on only those neighbor genes that are connected to 3 or more insulin signaling genes in the synergy network. For each of these neighbor genes, the statistical significance of its association with the insulin signaling pathway was evaluated by the hyper-geometric test. The neighbor genes significantly associated with insulin signaling are listed and ranked according to their p-values in Table 6.

Table 6. Neighbors significantly associated with insulin signaling pathway

Gene	Connections to insulin signaling	Degree (overall network)	p-value	Association with insulin signaling
DSP	3	12	4.18E-03	Unknown
ACADSB	3	12	4.18E-03	Unknown [$]
PANK3	3	15	7.50E-03	Known, (Leonardi et al., 2005)
SLC39A3	3	18	9.60E-03	Known, (Huang et al., 2010; Nicolson et al., 2009; Smidt et al., 2009)
ICA1	3	20	1.24E-02	Known, (Buffa et al., 2008)
TTYH1	3	30	2.94E-02	Known, (Anderson et al., 2009)
EP400NL	3	31	2.94E-02	Unknown
EGFR	3	36	3.59E-02	Known, (Chong et al., 2004; Prada et al., 2009)
C6orf150	3	37	3.59E-02	Unknown
FAM69B	3	37	3.59E-02	Unknown
HOMER2	8	180	4.84E-02	Known, (Rong et al., 2003; Shiraishi et al., 2004)

[$] **ACADSB** is involved in the metabolism of fatty acids and branch chained amino acids (Arden et al., 1995). Prolonged treatment with long chain FFAs, including palmitate, increases FA oxidation (Ceddia, 2005; Srivastava and Chan, 2008), which has been proposed to serve as a

Table 6 (cont'd)

protective mechanism against the potential toxic effects of long chain fatty acids (Ceddia, 2005; Kahn et al., 2005). Insulin, on the other hand, down-regulates FA oxidation in various cell types (Dyck et al., 2001; Topping and Mayes, 1972). Since palmitate can impair the insulin signaling pathway (Storz et al., 1999), it is reasonable that ACADSB emerges as a top neighbor of the insulin signaling pathway.

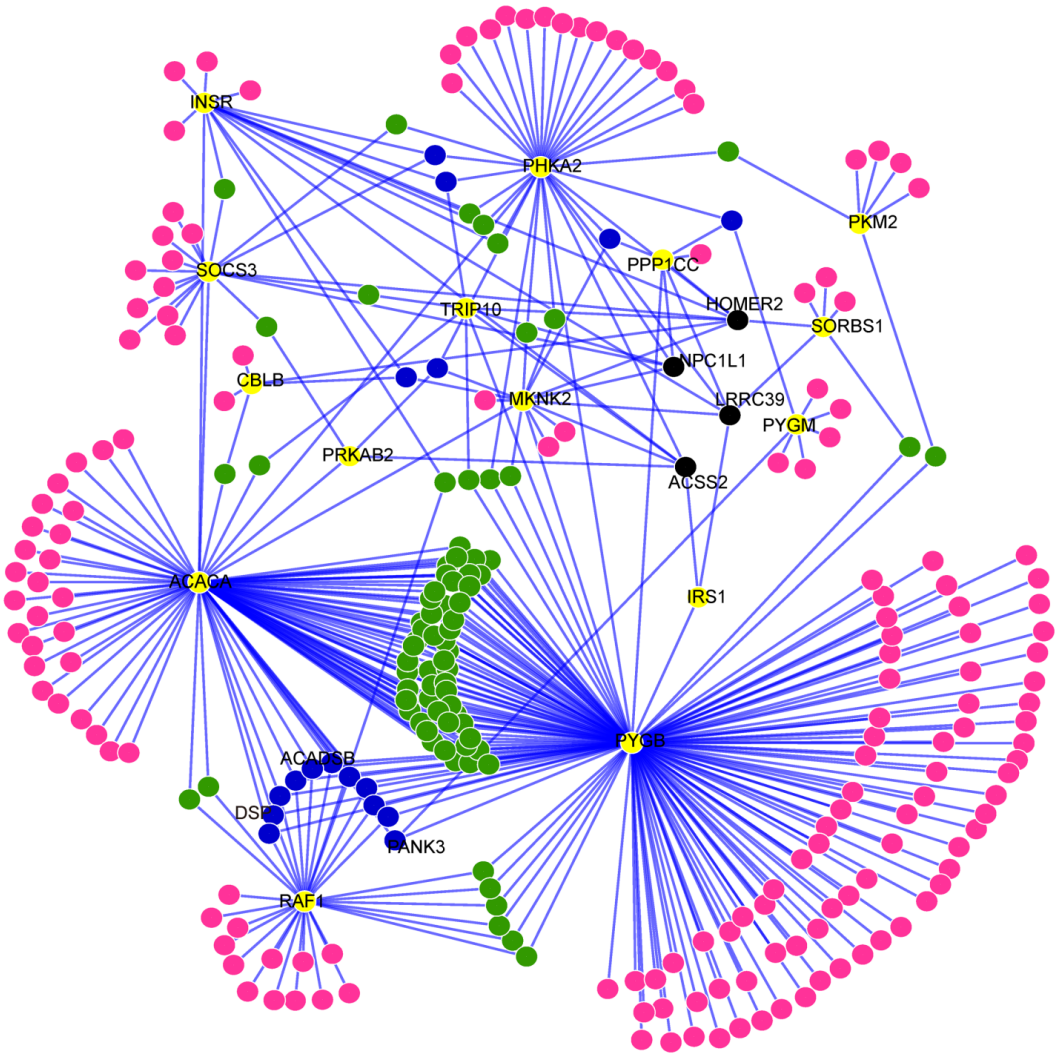

Figure 8. Sub-network for insulin signaling genes and their neighbor genes in the synergy network. Yellow nodes represent insulin signaling genes, and pink, green, blue and black nodes represent the neighbor genes connecting to one, two, three and more insulin signaling genes, respectively. The fifteen insulin genes, the top three neighbor genes (in Table 6) and the four genes connecting to more than three genes were labeled with gene names for reference.

2.2.3.3 DSP: the top neighbor

The junction protein, DSP, was recovered as the top-neighbor of insulin signaling pathway from the synergy network. Loss of DSP expression has been reported in more severe forms of liver disease, i.e. cirrhosis and HCC, but this has not been implicated in the pathology of fatty liver disease. Hence, we investigated the effects of palmitate treatment on the expression of DSP in HepG2 cells. Since, DSP was recovered as a neighbor of the insulin signaling pathway, we also studied the effect of insulin treatment on DSP expression. HepG2 cells were grown to confluency and treated with palmitate containing media. We observed cellular expression of DSP by measuring the fluorescence levels of DSP with immunostaining and confocal microscopy (Figure 9). Relative intensity of DSP against nuclear staining was used to quantify and normalize the amount of DSP under each treatment condition (Figure 10). Finally, we compared changes in relative DSP expression between treatment conditions and determined statistically significant pairs using Tukey's HSD post-hoc analysis (Figure 10).

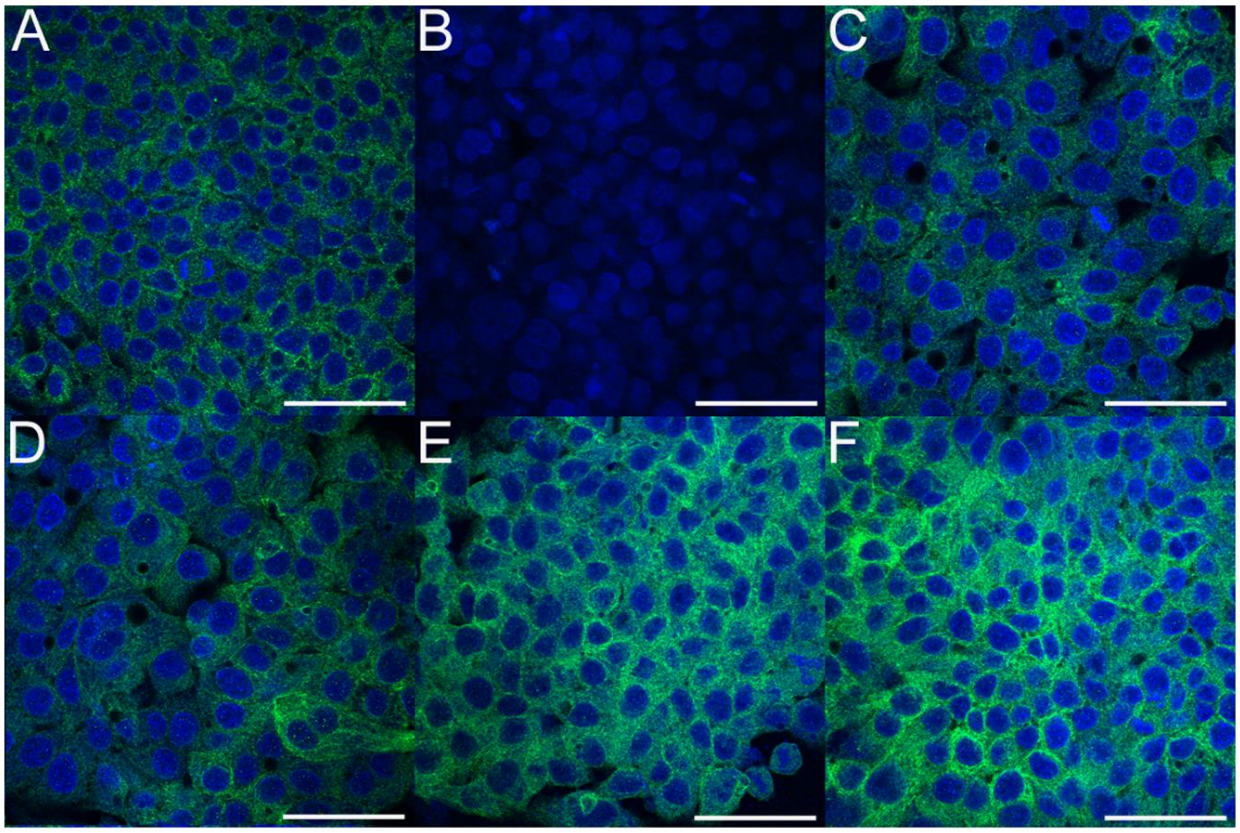

Figure 9. Immuno-fluorescence images of HepG2 cells stained for DSP (green) and cell nuclei (blue) obtained using confocal microscopy (see methods). Scale bars represent 50µm. A) Untreated, control cells grown in regular growth media. B) Cells treated with palmitate for 48 hours show decrease in DSP levels C) Cells treated with palmitate for 48 hours and recovered in normal growth media for 72 hours show partial recovery of DSP expression. Cells treated with palmitate for 48 hours and recovered in growth media with insulin for D) 24 hours and E) 48 hours show partial recovery, whereas for F) 72 hours show complete recovery of DSP expression.

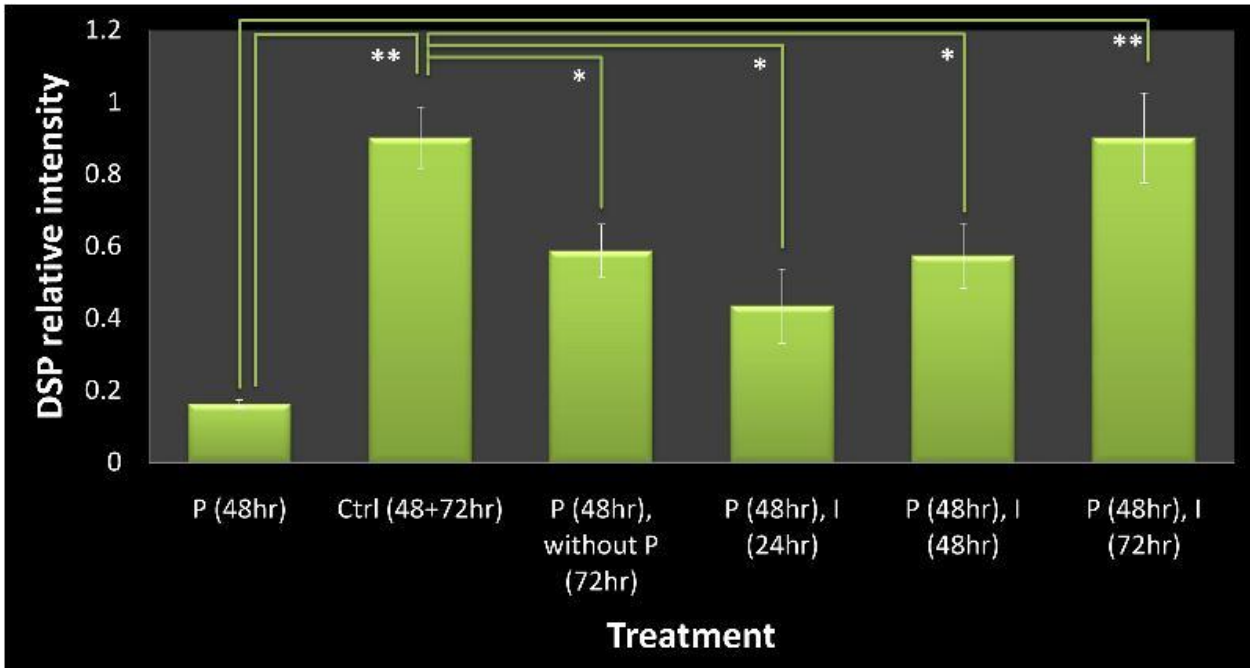

Figure 10. Quantitative effects of palmitate and insulin treatment on DSP expression

Bars indicate relative expression of DSP under various treatment conditions. Palmitate treatment significantly decreases DSP expression whereas subsequent treatment with insulin restores DSP expression. Lines represent pairs of condition where changes in DSP level are significant. * indicates significant difference ($p < 0.05$) from control cells. ** indicates significant difference ($p < 0.05$) from palmitate (48 hours) treated cells.

2.2.3.4 Palmitate reduces DSP expression while insulin enhances recovery of DSP expression

First, we evaluated the effect of palmitate treatment on DSP expression. We treated HepG2 cells with 0.7mM palmitate for 48 hours and observed the fluorescence levels of DSP (Figure 9B). When compared to control (Figure 9A), we found that palmitate treated cells showed a significant decrease in DSP expression levels ($p < 0.05$).

Next, we examined the recovery of DSP expression in palmitate treated cells by removing palmitate after 48 hours of treatment and adding regular growth medium. The cells were allowed to grow for another 72 hours (Figure 9C) and showed some recovery of DSP expression with time, albeit statistically different from control ($p < 0.05$). To assess the effect of insulin on the recovery of DSP expression, we treated HepG2 cells with physiological concentration of insulin (1nM) (Yang et al., 2010) for up to 72 hours, following the removal of palmitate after 48 hours of treatment. Fluorescence levels of DSP in the cells were analyzed every 24 hours. As seen in Figure 9D-E, cells treated with insulin for 24 and 48 hours show partial recovery of DSP levels compared to palmitate treated cells ($p < 0.05$), but cells treated with insulin for 72 hours show a prominent increase in DSP levels ($p < 0.05$) (Figure 9F). In fact, the levels of DSP after 72 hours of insulin treatment are statistically similar to the levels in the control cells ($p > 0.05$). The results suggest the expression of DSP that was lost upon palmitate treatment recovered to basal levels by treating the cells with insulin. Although, cells did recover some expression of DSP after removal of palmitate from the medium, the recovery was not restored to basal levels.

Thus, our experiment supports the association of the palmitate-induced cytotoxic phenotype with the DSP-insulin signaling pathway in our network. Namely, that DSP and insulin signaling act synergistically to ensure the proper function of adherence junctions and the lost or reduction in DSP expression and insulin signaling by palmitate treatment contributes to the cytotoxic effect of palmitate. Thus suggesting that in liver cells DSP may be a novel target of palmitate-induced cytotoxicity.

2.2.4 Discussion

In this section, we applied the information synergy analysis approach to microarray data from palmitate treated HepG2 cells: a condition relevant to NAFLD and HCC. We showed that DSP is a novel target of palmitate treatment. Third, we showed that insulin impacts DSP expression, and palmitate, known to antagonize insulin signaling, also negatively impacts DSP, contributing to the cytotoxic effect of palmitate. Overall, we suggest that a synergy network-based gene and pathway association analysis has the potential to reveal novel targets or mechanisms underlying biological processes, exemplified by the uncovering of DSP as a novel player in palmitate-induced cytoxicity.

The concept of synergy is intuitive and relevant to biological systems. For example, two transcription factors may play a cooperative role in determining the expression of a common gene. Similarly, interactions may occur between signaling proteins, i.e. cross-talk, and such associations may also be seen in receptor mediated transduction. Information synergy aims to capture cooperative effects, and in this study, on the impact of these effects on the induction a particular phenotype. There are several examples of synergistic interactions implicated in the pathology of fatty liver disease. For example, Smith J.J et al. showed that two groups of transcription factors worked in a combinatorial manner to control the transcriptional responses to fatty acids (Smith et al., 2007), thus supporting that cooperativity is important in regulating cellular processes. Similarly, co-expression of HNF4 and GATA transcription factor could synergistically activate the expressions of two genes involved in cholesterol homeostasis, and their binding sites are essential for maximal synergism (Sumi et al., 2007). Peroxisome proliferator activated receptors (PPARs), one of the best characterized

nuclear receptors that mediate transcriptional activities of long-chain unsaturated fatty acids, was found to selectively cooperate with fatty acid binding proteins (FABPs) to regulate transcription (Tan et al., 2002). Sterol receptor element-binding protein (SREBP-1c), a gatekeeper of lipotoxicity (Slawik and Vidal-Puig, 2006), functions together with BETA2, LXRs and SP1, to regulate various cellular processes, such as insulin signaling (Amemiya-Kudo et al., 2005), lipid synthesis (Higuchi et al., 2008), and cholesterol biosynthesis (Reed et al., 2008). It is evident from these examples that identifying genes with cooperative effects (Anastassiou, 2007), instead of limiting efforts to individual genes, has the potential to reveal novel genes or interactions, and ultimately help elucidate the mechanism of progression of complex diseases such as NAFLD. Although synergistic gene pairs have been shown valuable in discriminating phenotypes, interpreting the roles of the individual gene pairs remains a challenge due to the lack of sufficient functional or structural annotations for many of the genes, thereby formulating plausible hypotheses of the gene pairs more difficult. In contrast, organizing the individual gene pairs into a network (synergy network) and then performing gene module level analysis (Wang et al., 2008), i.e. identifying the pathways over-represented in network or pathway-gene associations, could help to hint at potential mechanisms as shown in our study. Nevertheless, investigating individual gene pairs would still be valuable in the future. Since the gene pairs identified from the microarray data do not necessarily interact directly with each other, future investigation of individual gene pairs coupled with physical interaction data (i.e. protein-protein and protein-DNA interaction) should further improve the analysis.

The application of information synergy methodology to microarray data obtained from FFA-treated HepG2 cells revealed insulin signaling as the most significantly enriched biological pathway. Thus, our analysis successfully recovered insulin signaling as a hallmark characteristic pathway involved in fatty liver disease (Mattar et al., 2005). We further examined and confirmed the effects of palmitate treatment on DSP, the top synergistic neighbor of insulin signaling pathway. We found that expression of DSP is reduced by palmitate treatment in HepG2 cells. DSP is a desmosomal protein essential for intercellular attachment by desmosomes. In a study of adhesion molecules in HCC, Cao et al. found that moderately differentiated hepatocytes tend to show a reduction in DSP protein expression, whereas poorly differentiated hepatocytes show complete loss of DSP protein expression (Han et al., 2007). It has been suggested that DSP expression levels are inversely correlated with cell growth and division. As shown in a study with squamous cell carcinoma, inhibition of EGF (epidermal growth factor) using antagonists led to an increase in DSP protein levels (Lorch et al., 2004). Another study has suggested that DSP may play a role in tumor-matrix interaction as it was found to be a major component of exosomes secreted by mesothelioma cells (Hegmans et al., 2004). Other studies have also suggested that loss of desmosomes may be associated with epithelial to mesenchymal transition (EMT) by means which hepatocytes may acquire malignant characteristics (Chidgey and Dawson, 2007). Although, such associations were reported in HCC, our results suggest that the impact on DSP may be an early event in the pathogenesis of fatty liver disease. In other words, reduced expression of DSP may contribute to the progression to more severe forms of liver diseases.

From Table 5, adherens junction was identified as a highly enriched category in our synergy network. Treatment with palmitate has been shown to affect cellular adherence and cytoskeletal structure in hepatocytes (Draghici et al., 2007; Swagell et al., 2005), although the exact mechanism and whether DSP is involved in mediating these processes is unknown. Since, keratins require DSP at the desmosomal plaque for anchoring to the cell membrane (Rampazzo et al., 2002), our results open up the possibility that loss of cytoskeletal structure may be associated with the loss of DSP. Previous studies have shown that inherited mutations in DSP are a characteristic feature of a number diseases of the skin and heart including, skin fragility or wooly hair syndrome (Whittock et al., 2002), arrhythmogenic right ventricular dysplasia (Rampazzo et al., 2002; Yang et al., 2006), lethal acantholytic epidermolysis bullosa (Jonkman et al., 2005), and dilated cardiomyopathy with wooly hair and keratoderma (Uzumcu et al., 2006). It is notable that in recent years some research groups have suggested the risk of cardiovascular disease (CVD) may be elevated in NAFLD patients (Edens et al., 2009; Targher et al., 2010; Targher et al., 2008). Given that alterations in DSP expression are associated with heart disease and since DSP levels are reduced by palmitate treatment, it raises the possibility that DSP may serve as a potential link between fatty liver disease and heart disease.

We also explored the relationship between DSP and insulin signaling and found that insulin treatment enhances the recovery of DSP expression lost due to palmitate treatment. It is known that palmitate can induce resistance to insulin signaling in hepatocytes (Ruddock et al., 2008) and several mechanisms have been proposed to explain this observation. Studies have suggested that PKCA (Protein Kinase C, alpha isoform), known to be activated by lipids

(diacylglycerols) (Ekinci and Shea, 1999), shares an antagonistic relationship with insulin signaling, and that knock-out of PKCA enhances insulin signaling (Leitges et al., 2002). Interestingly, the activation of PKCA also affects the dynamics of desmosomal complex at the plasma membrane (Bass-Zubek et al., 2008; Hobbs et al., 2010). Junction plakoglobin co-localizes with DSP at the desmosomal plaque. It has been shown in a study with mice cardiomyocytes that inhibition of DSP expression leads to a change in localization of plakoglobins from the cytoplasm to the nucleus. This was shown to antagonize Wnt/β-catenin signaling pathway, and trigger the accumulation of fat droplets (Garcia-Gras et al., 2006) due to the role of Wnt signaling in regulating adipogenesis via CREB and protein kinase A (PKA) (Chen et al., 2005; Ross et al., 2000). It is noteworthy that Wnt signaling is a significantly enriched pathway in the synergy network (See Table 1). Wnt signaling is frequently attenuated in HCC patients and is associated with poor prognosis (Polakis, 2000). Furthermore, recent studies have confirmed that activation of Wnt signaling enhances insulin sensitivity (Abiola et al., 2009; Yoon et al., 2010). This suggests that palmitate induced loss of DSP protein can further enhance insulin resistance through the Wnt/β-catenin signaling pathway. Thus, it may not be a coincidence that DSP was recovered as a synergistic pair to the insulin signaling pathway in the network.

CHAPTER 3: ELEVATED FREE FATTY ACID UPTAKE VIA CD36 PROMOTES EPITHELIAL-MESENCHYMAL TRANSITION IN HEPATOCELLULAR CARCINOMA

3.1 Introduction

The incidence rates of HCC have more than tripled in the United States over the past four decades with a steadily increasing mortality rate (Altekruse et al., 2014; Njei et al., 2015). Surgical resection and liver transplantation are potentially curative treatment modalities available for HCC detected at early stages, however, most cases are diagnosed at an advanced stage at which radiotherapy and chemotherapy are either not feasible or are ineffective (Altekruse et al., 2012). Advanced HCC tumors demonstrate high proclivity towards vascular invasion resulting in intrahepatic metastases, which are strongly associated with high post-resection recurrence rates and overall poor prognosis (Tang, 2001; Tung-Ping Poon et al., 2000). Therefore, understanding the mechanisms of HCC progression is important for developing new therapeutic approaches. Evidence from epidemiological studies suggested a link between obesity, manifested in the form of elevated fatty acids, and HCC tumorigenesis and increased mortality (Calle et al., 2003; El–Serag and Rudolph, 2007; Nair, 2002). Surprisingly, the influences of obesity and elevated fatty acid levels have not been evaluated with respect to the molecular pathogenesis of invasive HCC.

Cancer cells frequently exhibit alterations in fatty acid metabolism to sustain growth and proliferation, fulfill energy requirements and provide metabolites for anabolic processes (Currie et al., 2013). It has been observed that FFA levels are significantly elevated in the plasma of HCC patients **(Table 7)**. However, the precise role of elevated FFA levels in

tumorigenesis and cancer progression remains controversial. A number of *in vitro* and animal studies have shown that accumulation of FFAs, especially saturated FFA palmitate, leads to mitochondrial dysfunction and generation of reactive oxidative species (ROS) that contributes to loss of cellular homeostasis and cell death, a phenomenon termed as lipotoxicity (Duncan, 2008). Additionally, elevated saturated FFAs were shown to enhance TNF-α and IL-6 cytokine-induced inflammation (Ajuwon and Spurlock, 2005), aggravate insulin resistance (Kennedy et al., 2009) and enhance endoplasmic reticulum stress (Wei et al., 2006) in hepatocytes. On the other hand, fatty acid synthase, the rate limiting enzyme in the *de novo* lipogenesis pathway was shown to promote proliferation of cancer cells (Menendez and Lupu, 2007). Elevated FFAs were also shown to enhance tumor formation in a mouse model of chemically induced HCC via activation of pro-inflammatory cytokines (Park et al., 2010).

In a previous study exploring the lipotoxic pathways activated by saturated FFAs, we reported a synergistic association between abrogation of insulin signaling and loss of desmoplakin protein (Wang et al., 2011), an obligate component of the desmosomal cell adhesion complex. As desmosomes are lost during epithelial-mesenchymal transition (EMT) (Chidgey and Dawson, 2007), our study suggested a possible role of FFAs in this phenomenon. EMT can be described as a set of well-orchestrated changes, driven by the expression of key transcription factors including *SNAIL*, *ZEB* and *TWIST*, which allow epithelial cells to acquire a mesenchymal phenotype, resulting in enhanced migration, invasiveness, and resistance to apoptosis, thus facilitating progression to a metastatic phenotype (Kalluri and Weinberg, 2009; Thiery, 2002). Several clinical reports described enhanced expression of EMT-genes in advanced stage HCC, correlating with poor prognosis, increased rates of metastases and

elevated mortality rates (Marquardt et al., 2014; Yang et al., 2009a; Zhou et al., 2014). Based on our findings, combined with the epidemiological observations, we hypothesized that elevated FFAs may play a role beyond lipotoxicity or activation of pro-inflammatory pathways, and promote the induction of EMT in HCC.

Evidence shows that fatty acids are actively transported across cell membrane by specialized proteins instead of by passive diffusion (Stremmel et al., 2001). In the liver, the major proteins involved in fatty acid transport and trafficking included the fatty acid transport proteins, FATP2 (SLC27A2) and FATP5 (SLC27A5) and the fatty acid binding proteins (FABP1, FABP4, and FABP5). The CD36 or fatty acid translocase protein mediates the uptake of fatty acids in a variety of cell types but is expressed at very low levels in normal liver cells, however, its expression is increased in hepatocytes from rodent models of diet-induced obesity, which also correlated with elevated fatty acid uptake (Koonen et al., 2007; Luiken et al., 2001). Thus, alterations in CD36 expression could be involved in enhancing the uptake of FFA into the livers of obese HCC patients.

Here we investigated the association between obesity and elevated uptake of FFAs with the induction of EMT program in human HCC. We first probed the association using mRNA expression data derived from the TCGA liver cancer dataset and then confirmed the observations in human HCC tumor samples. Our data suggests that elevated expression of fatty acid uptake proteins including CD36, and not BMI, was associated with EMT progression. We further established that the saturated FFA palmitate induced EMT in HCC cells by activating the Wnt/β-catenin and TGF-β signaling pathways. Additionally, inhibition of CD36

resulted in reduced migration in liver cancer cells, confirming a critical role of the fatty acid uptake protein in the progression of the EMT program.

Table 7: FFA levels in normal liver and HCC			
	Reference FFA values mmol/L (Tavares De Almeida et al., 2002)	**HCC FFA (fold change)** (Zhou et al., 2012a)	**Estimated HCC FFA values** mmol/L
Palmitate (C16:0)	0.097±17	2.49	0.199-0.284
Oleate (C18:1)	0.085±11	3.16	0.234-0.303
Linoleate (C18:2)	0.053±12	1.79	0.055-0.116

3.2 Materials and Methods

3.2.1 Human HCC tumor samples, TCGA data and EMT score calculation

De-identified, IRB-approved frozen samples were obtained from the "International Registry of Patients with or at Risk for Hepatobiliary Cancers, Including Hepatocellular Carcinoma, Cholangiocarcinoma, and Gallbladder Adenocarcinoma, and those Patients with Normal Risk Factors" (Mayo Clinic IRB#: 707-03; PI: Dr. Lewis R. Roberts). Patient clinical information, including body mass index, was provided by Mayo Clinic. Total cellular proteins were extracted from the tumor samples using T-PER protein extraction reagent (Pierce, 78510) supplemented with protease inhibitor cocktail tablets (Roche, 04693159001) according to the manufacturer's protocol.

Liver cancer gene expression data (mRNA, normalized RNAseqV2 RSEM) were retrieved from the TCGA database (Cancer Genome Atlas Research, 2008) using the cBioPortal for cancer genomics (Cerami et al., 2012a; Gao et al., 2013). Expression levels were $\log_2$ transformed and EMT scores were calculated using a previously published metric (Salt et al., 2013). EMT score = Sum of mesenchymal gene expression (*CDH2, FN1, SNAI1, SNAI2, TWIST1, TWIST2, VIM, ZEB1, ZEB2*) – Sum of epithelial gene expression (*CDH1, CLDN4, CLDN7, MUC1, TJP3*). Hierarchical clusters and heatmap visualizations were generated using the GENE-E matrix analysis platform (http://www.broadinstitute.org/cancer/software/GENE-E/index.html) with TCGA gene expression data (mRNA, RNAseq z-scores) retrieved using the cBioPortal. Clusters were obtained using the average linkage method with 1-Pearson's correlation coefficient as the distance metric.

3.2.2 Cell lines, culture medium and treatment

Human liver cancer cell lines (HepG2, Hep3B) were obtained from ATCC, cultured in DMEM (Gibco, 11965), supplemented with 10% FBS (Gibco, 16000) and 1% penicillin/streptomycin (Gibco, 15140), and maintained in a humid, 5% CO_2 environment at 37°C.

FFA preparation media was made by dissolving 2% w/v BSA (US Biologicals, A1311) in serum-free DMEM supplemented with 1% penicillin/streptomycin. Palmitate medium was prepared from a high concentration (40mM) stock solution made by dissolving sodium palmitate (Sigma, P9767) in dH_2O heated to 70°C. An aliquot from the stock was then added drop wise to 2% BSA medium with constant stirring to achieve the desired final palmitate concentration. Oleate (Sigma, O7501) and linoleic acid (Sigma, L8134) media were prepared by directly dissolving the appropriate amounts in BSA media. FFA media with serum was prepared by adding FBS to a final concentration of 10%.

Chemical inhibitors: 0.5mg/ml TGF-β RI Kinase Inhibitor (Calbiochem, 616451), 1mg/ml β-Catenin/Tcf Inhibitor III iCRT3 (Calbiochem, 219332), 5mg/ml LGK-974 (Selleck chemicals, S7143) and 25mg/ml Sulfosuccinimidyl Oleate (SCBT, sc-208404) stocks were prepared in 100% DMSO and diluted to indicated concentrations for *in vitro* experiments.

3.2.3 Dispase-based dissociation assay

Dispase assay was adapted from previous studies (Calkins et al., 2005; Huen, 2002). Cultured monolayers in 6-well plates were washed twice with ice-cold PBS. 2ml of Dispase (1 U/ml) enzyme solution (Stemcell technologies, 07923) was added to each well and incubated at 37°C for 30 min. The released monolayers were then carefully aspirated into a 15ml centrifuge

tube and washed with ice-cold PBS by centrifuging at 1g for 1 min. The monolayers were then disrupted by applying mechanical stress by pipetting 5x with a 1 ml pipette (tube labels were concealed and pipetted in randomized order to avoid bias). The resulting fragments were stained with crystal violet (0.05% w/v in methanol) and transferred to 6-well plates for recording images with a light microscope. Images were analyzed to calculate fragment number and size distribution using ImageJ software (Schneider et al., 2012).

3.2.4 Scratch-wound healing, migration and invasion assays

For scratch-wound healing assays, cells were seeded in 24-well plates with regular media. After a 24-hour acclimatization period, the cells were washed with PBS and cultured for 5 days in FFA or BSA media with serum to encourage EMT induction. Media was refreshed every 48 hours. Following the 5 day incubation, cells were washed with PBS and using the tip of a sterile 10uL pipette tip, a single scratch was made on the cell surface within each well. Perpendicular marks were made to standardize viewing fields. Cells were then cultured in the corresponding serum-free FFA or BSA media and wound healing was monitored over a 48-hour time course. The serum-free media avoided confounding effects of proliferation. Three standardized bright-field images were recorded for each scratch at the 0, 24, and 48-hour time points. The rates of migration were assessed by either quantifying the percentage of open wound area using T-scratch package (Geback et al., 2009) or by counting the number of individual migrating cells in the wound area using automated particle analysis with ImageJ software.

For modified Boyden's chamber assays, following 5 days culture in FFA or BSA media with serum, cells were collected by trypsinization, neutralized with regular media, washed with PBS by centrifugation at 200g for 3 min. and counted using a hemocytometer. The cells were then re-suspended in FFA or BSA medium without serum and seeded on BD Biocoat 8µm membrane inserts (BD Biosciences, 354480) with Matrigel coating (for invasion assay) or without Matrigel coating (for migration assay). The inserts were placed in wells containing regular DMEM media containing 10% FBS as chemoattractant. After 24 hours, the inserts were removed, washed with PBS, fixed in methanol and stained with crystal violet (0.05% w/v in methanol). The bottom surfaces of the stained inserts were then observed under a light microscope, and the numbers of stained cells were counted in 5 fields/insert.

3.2.5 Cytotoxicity/metabolic activity assays and Oil Red O staining

Cytotoxicity and metabolic activity were assessed by microplate assays. Cells were seeded in 96-well plates and treated with PA or BSA with serum over 5 days, followed by serum free treatment. Cytotoxicity was detected using the LDH cytotoxicity detection kit (Roche, 11644793001) following the manufacturer's protocol. Metabolic activity was determined by AlamarBlue assay (Pierce, 88952) following the manufacturer's protocol.

For Oil Red O staining, cells treated in 6-well plates were washed with PBS and fixed with 10% formaldehyde at room temperature for 1 hour. Cells were washed 2x with dH_2O and washed 2x with 60% isopropanol for 5 min. each at room temperature. The cells were then allowed to dry in a fume hood for 30 min. Next, 1 ml of Oil Red O (Sigma, O0625) staining solution (35mg/ml in 60% isopropanol) was added and incubated for 10 min. at room temperature. Cells were washed 4x with dH_2O and bright-field images were recorded at 40X magnification.

For the elution assay, the cells were allowed to air-dry for 30 min and the dye was eluted by adding 1ml 100% isopropanol and incubating on a shaker for 10 min. The eluted dye was mixed by pipetting and aliquoted in a 96-well plate to measure absorbance at 500nm with 100% isopropanol as blank.

3.2.6 qRT-PCR and arrays

Total mRNA for qRT-PCR and PCR array studies was extracted from cells using RNeasy Mini Plus kit (Qiagen, 74134) according to the manufacturer's protocol. cDNA was synthesized from 1µg of total mRNA using High-capacity cDNA reverse transcript kit (Applied Biosystems, 4368814) following the manufacturer's protocol. qRT-PCR experiments were performed in a MyiQ thermal cycler (BioRad) with Sybr-Green mastermix (BioRad, 170-8882) and 200ng of template/reaction using the following sets of primers (Operon) designed using the Primer3/NCBI Primer-BLAST tool (Ye et al., 2012):

Table 8: Primers used in qRT-PCR analysis

Primer	**Sequence (5'->3')**
SNAIL Forward	CACTATGCCGCGCTCTTTC
SNAIL Reverse	GCTGGAAGGTAAACTCTGGATTAGA
SLUG Forward	GGACACATTAGAACTCACACGGG
SLUG Reverse	GCAGTGAGGGCAAGAAAAAGG
ZEB1 Forward	ATGCAGCTGACTGTGAAGGT
ZEB1 Reverse	GAAAATGCATCTGGTGTTCC
ZEB2 Forward	TATGGCCTACACCTACCCAAC
ZEB2 Reverse	AGGCCTGACATGTAGTCTTGTG
TWIST Forward	GCAGGGCCGGAGACCTAG
TWIST Reverse	TGTCCATTTTCTCCTTCTCTGGA
FOXC2 Forward	GCAGGGCTGGCAGAACAG
FOXC2 Reverse	CGCGGCACTTTCACGAA
GAPDH Forward	CAGCCGCATCTTCTTTTGCG
GAPDH Reverse	TGGAATTTGCCATGGGTGGA

The following thermal cycling settings were used: 95°C for 10 min. followed by 40 cycles at 95°C for 30 sec., 62°C for 1 min. and 72°C for 1 min. The fold-change values were calculated as delta-delta Ct (ddCt) values from a minimum of three independent biological replicates.

The PCR array study was performed with an 84-gene EMT pathway-specific array (SABiosciences, PAHS-090Z) according to the manufacturer's protocol. The top 20 genes were ranked by fold change magnitude and analyzed for KEGG pathway enrichment using the DAVID bioinformatics tool (Huang et al., 2007).

3.2.7 Western blots

Cells were washed with ice-cold PBS and incubated with ice-cold RIPA buffer supplemented with protease inhibitor cocktail tablets (Roche, 04693159001) for 30 min. on ice with gentle shaking. The extracts were transferred to pre-chilled tubes and centrifuged for 10min. at 10,000g to separate cell debris from supernatant with proteins. Total protein levels were quantified with micro BCA assay (Pierce, 23235), reduced in Laemmli buffer (NEB, B7703S) and resolved on 10% SDS-PAGE gels by loading 20-40ug of protein per well. The resolved proteins were transferred to 0.45µm nitrocellulose membrane and blocked (5% BSA or milk in TBST) for 1 hour at room temperature. The membranes were incubated with specific primary-antibodies diluted in incubation buffer (2.5% BSA, 0.01% sodium azide in TBST) overnight at 4°C, followed by incubation with isotype-specific secondary antibodies diluted (1:1000) in TBST for 1 hour at room temperature. For reprobing, the membranes were incubated 2x in stripping buffer (0.2M glycine, 0.1% SDS, 1% Tween20, pH=2.2) for 5 min each followed by

two washes with PBS and TBST for 5 min. each. The membranes were then blocked and incubated in antibodies as described above. Chemiluminescence was detected with ECL substrate (Pierce, 34080) in a BioRad gel doc. Band intensities were quantified with ImageJ software and normalized to loading control (GAPDH).

Table 9: List of antibodies

Antibody	Source (catalog)	WB Dil.
ZEB1	Origene (TA802298)	1:2000
ZEB2	Origene (TA802113)	1:2000
PORCN	Millipore (MABS21)	1:2000
CD36	Millipore (CBL168)	1:2000
SNAI1	SantaCruz (sc28199)	1:1000
DSP	Abcam (ab71690)	1:500
CDH1	Cell Signaling (3195)	1:1000
VIM	Cell Signaling (3932)	1:1000
TGFB	Cell Signaling (3711)	1:1000
GAPDH	Cell Signaling (5174)	1:2000
VIM-647	Cell Signaling (9856)	-
CTNNB1	Cell Signaling (8480)	-
SMAD2/3	Cell Signaling (8685)	-

3.2.9 Confocal microscopy

Cells were cultured in glass-bottom 24-well plates (In Vitro Scientific) and treated with FFA or BSA medium. After treatment, cells were washed 2x with ice-cold PBS and fixed with 3.7% formaldehyde for 10 min. at 37°C, washed 2x with PBS, and permeabilized with 0.5% TritonX-100 for 10 min. at room temperature. After 2x washes with PBS, the samples were incubated in blocking buffer (1% BSA in PBS) for 1 hour at 37°C. Next, the cells were incubated with diluted primary antibodies (CDH 1:500, VIM, 1:500, β-catenin 1:1000, SMAD2/3 1:2000) in incubation buffer (0.5% BSA with 0.01% Sodium Azide in PBS) overnight at 4°C. After the overnight incubation, samples were washed 2x with PBS and incubated in respective

secondary antibodies (AlexaFluor 488) diluted in PBS for 1 hour at 37°C in the dark. Cells were washed 2x with PBS and incubated in nuclear counter stain Hoechst 3342 (Invitrogen) for 10 min. at room temperature. After the final incubation, cells were washed twice with PBS and covered with ProLong Gold (Molecular Probes) anti-fade solution for imaging. Images were recorded with an Olympus FluoView 1000 Inverted IX81 microscope, using a 40X oil objective using identical exposure and PMT settings for each primary antibody-fluorophore pair across the different treatment conditions.

3.2.10 Flow cytometry

Cells were washed twice with ice-cold PBS, trypsinized, and counted. Next, the cells were resuspended in PBS to a final concentration of $1x10^6$ cells/ml. A total of 100ul of the cell suspension was aliquoted into microcentrifuge tubes. For live/dead staining, we added 1ul of Zombie Violet stain (BioLegend, 423113) into each tube and incubated for 30 min. at room temperature in the dark (all subsequent steps were performed under minimal light conditions). The cells were then washed with ice-cold incubation buffer (0.5% BSA in PBS with 0.01% Sodium Azide) by centrifugation at 200g for 1min. and fixed with a freshly prepared 4% paraformaldehyde solution in PBS (pH = 6.9) for 10 min. at 37°C. The samples were placed on ice for 1 min., washed with incubation buffer and subsequently permeabilized with 0.5% Triton X-100 in PBS for 20 min. on ice. For primary antibody incubation, cells were washed twice with incubation buffer and resuspended in primary antibodies diluted in incubation buffer (CDH 1:200, DSP 1:200, VIM-647 1:50) for 1 hour at room temperature. For secondary antibody staining (CDH and DSP), cells were washed twice with incubation buffer and incubated in isotype-specific Alexa488 secondary antibody diluted (1:1000) in incubation

buffer for 30 min. at room temperature. After completion of all staining steps, the cells were washed with incubation buffer and resuspended in 500ul incubation buffer. The samples were then analyzed on an LSRII flow cytometer system (BD Biosciences) with $1x10^4$ events recorded per sample.

3.3 Results

3.3.1 CD36 expression, and not BMI, is associated with degree of EMT

We investigated the association between patient BMI, expression levels of hepatic fatty acid uptake proteins and EMT progression in the TCGA liver cancer dataset. The TCGA samples were grouped according to the patient's BMI and an EMT score was assigned to each sample to assess the degree of EMT. We observed that the EMT score was not significantly different between the low and high BMI groups (p=0.99) (Figure 11A), suggesting that BMI did not influence the degree of EMT in HCC patients. Additionally, most genes involved in hepatic FA uptake also did not show a significant difference in expression levels between the two BMI groups. However, *CD36*, a fatty acid uptake protein that is normally expressed at very low levels in hepatocytes, was the exception among the FA uptake genes as it showed increased expression in the high BMI group (p=0.04) (Figure 11A). Furthermore, among the FA uptake genes, *CD36* was the gene for which the expression significantly correlated with BMI (r=0.26, $p=2x10^{-3}$), indicating that altered *CD36* expression could be a major contributor to elevated FA uptake in obese HCC patients (Figure 11B). Although the EMT score was not significantly correlated with the BMI of patients (r=0.05, p=0.55), the expression of the mesenchymal markers *ZEB1* (r=0.17, p=0.04) and *FN1* (r=0.23, $p=6x10^{-3}$) were both correlated with BMI (Figure 11B). Next, we clustered the genes involved in FA uptake, epithelial and mesenchymal genes in the TCGA dataset with samples ordered according to EMT score (Figure 11C). As expected, the epithelial and mesenchymal genes clustered with other members of their respective groups. Intriguingly, the FA uptake genes clustered closer to the mesenchymal genes than the epithelial genes. We further investigated the association between FA uptake

genes and EMT score and found that the expression levels of *CD36* ($r=0.27$, $p=1x10^{-4}$), *FABP4* ($r=0.35$, $p=9.7x10^{-7}$), *FABP5* ($r=0.18$, $p=0.01$), and *SLC27A5* ($r=0.16$, $p=0.03$) were significantly correlated with the EMT score (Figure 11D). These results suggest that while BMI itself did not have an influence, the expression of FA uptake genes was strongly associated with the degree of EMT in HCC patients. Given the lack of expression in normal hepatocytes and exclusive association with both BMI and EMT score, *CD36* emerged as an ideal candidate for subsequent studies.

To verify the association between FA uptake gene expression and EMT observed in TCGA data, we further investigated the protein expression of CD36 and EMT in human HCC tumor samples. The clinical samples were divided into two groups according to the patient's BMI information. Total cellular proteins were resolved and immunoblotted to detect the expression levels of various EMT markers (Figure 12A). Vimentin (VIM), a mesenchymal intermediate filament network protein, was measured along with E-cadherin (CDH) and desmoplakin (DSP), cell-adhesion molecules that served as indicators of epithelial characteristics. Expression levels of the mesenchymal marker VIM ($p=0.02$) were significantly higher in high BMI tumor samples, but levels of epithelial markers CDH ($p=0.32$) or DSP ($p=0.13$) were not significantly altered (Figure 12A and 12B). Next, we measured the expression levels of ZEB1, ZEB2 and SNAIL1 as transcriptional activation markers of EMT. While the expression levels of SNAIL1 ($p=0.05$) were significantly higher in high BMI tumor samples, ZEB1 ($p=0.23$) and ZEB2 ($p=0.43$) did not differ significantly (Fig. 2A and 1B). In addition to the EMT markers, we further measured expression levels of TGFB and PORCN as respective indicators of the activation of TGF-β and Wnt/β-catenin signaling pathways. In the

high BMI patient group, the expression levels of TGFB (p=0.001) were significantly higher, but PORCN (p=0.27) levels did not change (Figure 12A and 12B). While the expression levels of some EMT markers were elevated in the high BMI patients, the disparities in significance levels suggest that BMI alone was not sufficient to predict EMT.

Next, we compared expression levels of the EMT markers with CD36 expression across all the samples, irrespective of BMI. As shown in Figure 12C, the expression of VIM (p=0.01), SNAIL1 (p=0.22), ZEB1 ($p=6x10^{-9}$) and ZEB2 ($p=6x10^{-4}$) were positively correlated with CD36 expression. Additionally, the expression levels of TGFB (p=0.17) and PORCN (p=0.04) also showed positive correlation with CD36 expression. While the comparison of EMT markers between high BMI and low BMI patients was inconclusive, the significant association of CD36 with ZEB1, ZEB2 and VIM corroborate the observations made in the TCGA analysis - that elevated CD36 expression may be indicative of the activation of EMT program. Additionally, the expression levels of TGFB and PORCN also showed positive correlation with CD36 expression, suggesting that the TGF-β and Wnt/β-catenin signaling pathways may be the drivers of EMT program activation in the tumor samples with elevated CD36 levels. These results indicate that the elevated levels of CD36 and the consequently elevated uptake of FFAs may be involved in HCC progression via EMT.

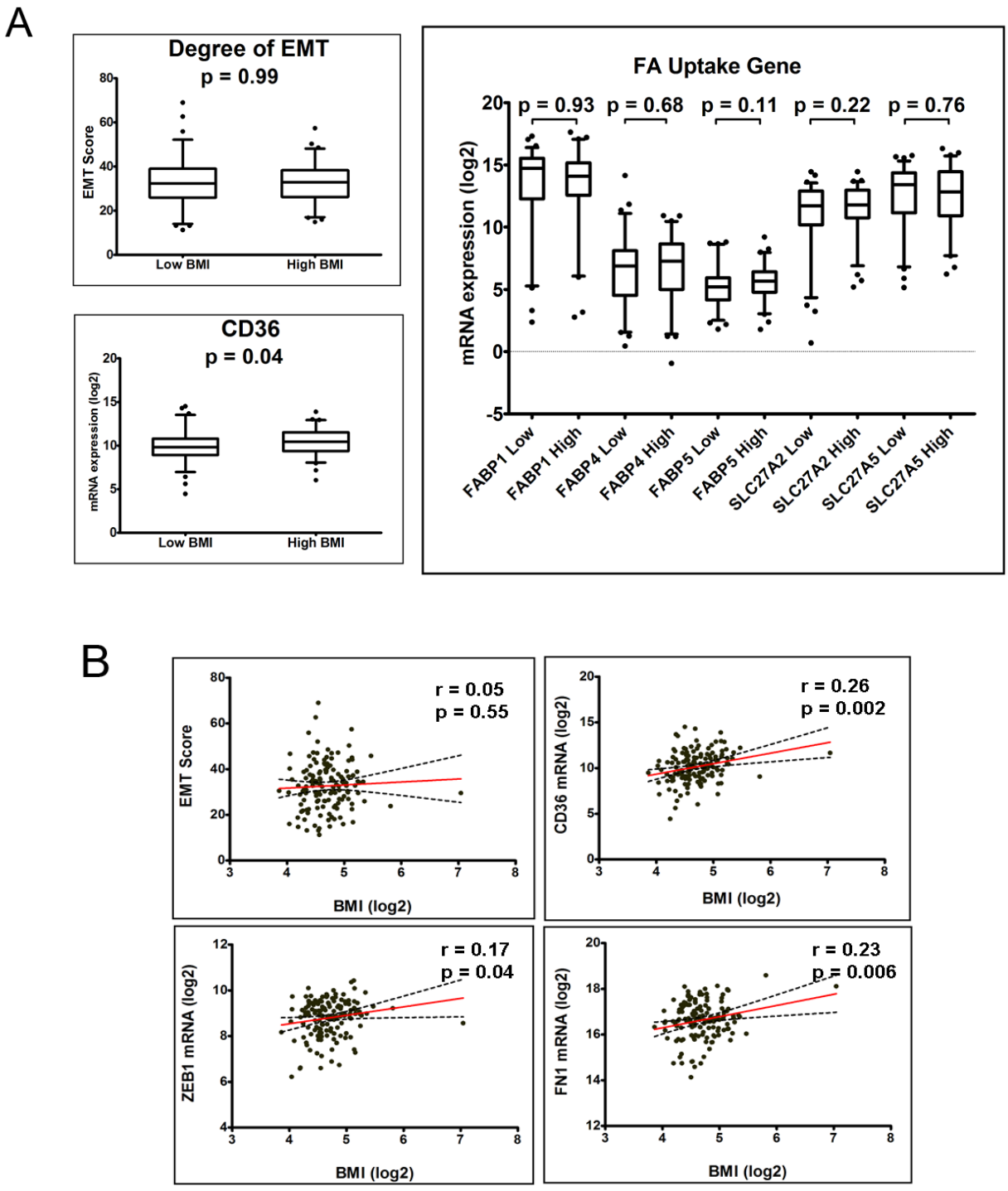

Figure 11: Fatty acid uptake and EMT markers in TCGA liver cancer dataset.

Figure 11 (cont'd)

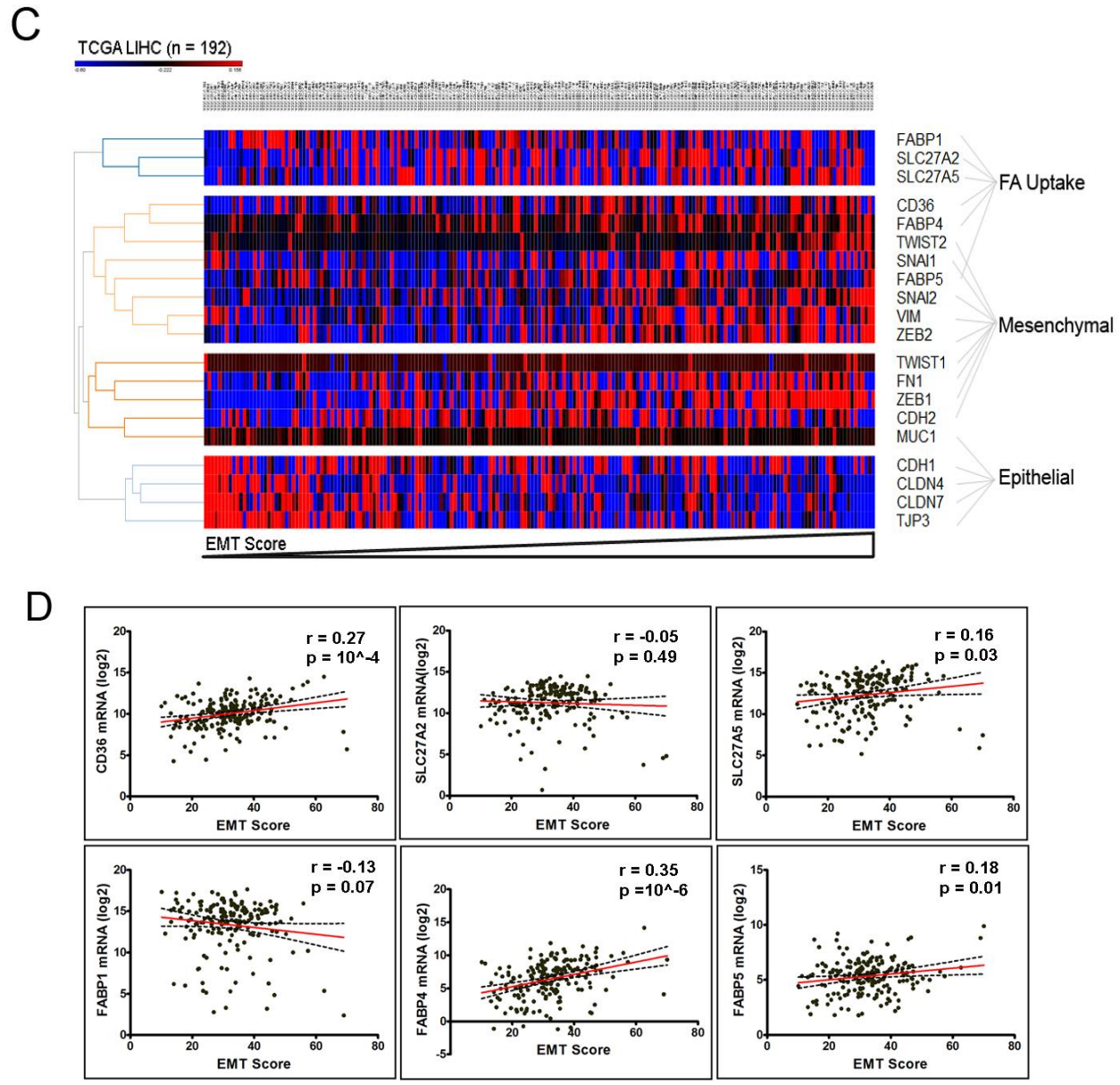

A. Effect of patient's BMI on EMT and FA uptake gene expression. Box plot showing comparison of EMT scores, mRNA expression levels of hepatic FA uptake genes and *CD36* in groups of patients with BMI < 25 (Low BMI) or ≥ 25 (High BMI). P-values indicate significance levels from two-tailed Student's T-test. B. Scatter plots showing correlation between BMI (X-axis) and EMT score, *CD36*, *ZEB1* or *FN1* (Y-axis). The solid red line indicates linear fit, with 95%

Figure 11 (cont'd)

confidence intervals indicated by dotted black lines. r indicates Pearson's correlation coefficient and p-values indicate significance of correlation (two-tailed). Only the EMT or FA uptake genes with significant correlations with BMI are shown here. C. Heatmap showing relative expression levels of hepatic fatty acid uptake genes and EMT genes in the TCGA liver cancer dataset. Gene clusters (vertical axis) were obtained by hierarchical clustering and samples (horizontal axis) were ordered according to the EMT score. D. Scatter plot showing association between the fatty acid uptake genes (Y-axis) and EMT score (X-axis) in the TCGA dataset. The solid red line indicates linear fit, with 95% confidence intervals indicated by dotted black lines. r indicates Pearson's correlation coefficient and p-values indicate significance of correlation (two-tailed).

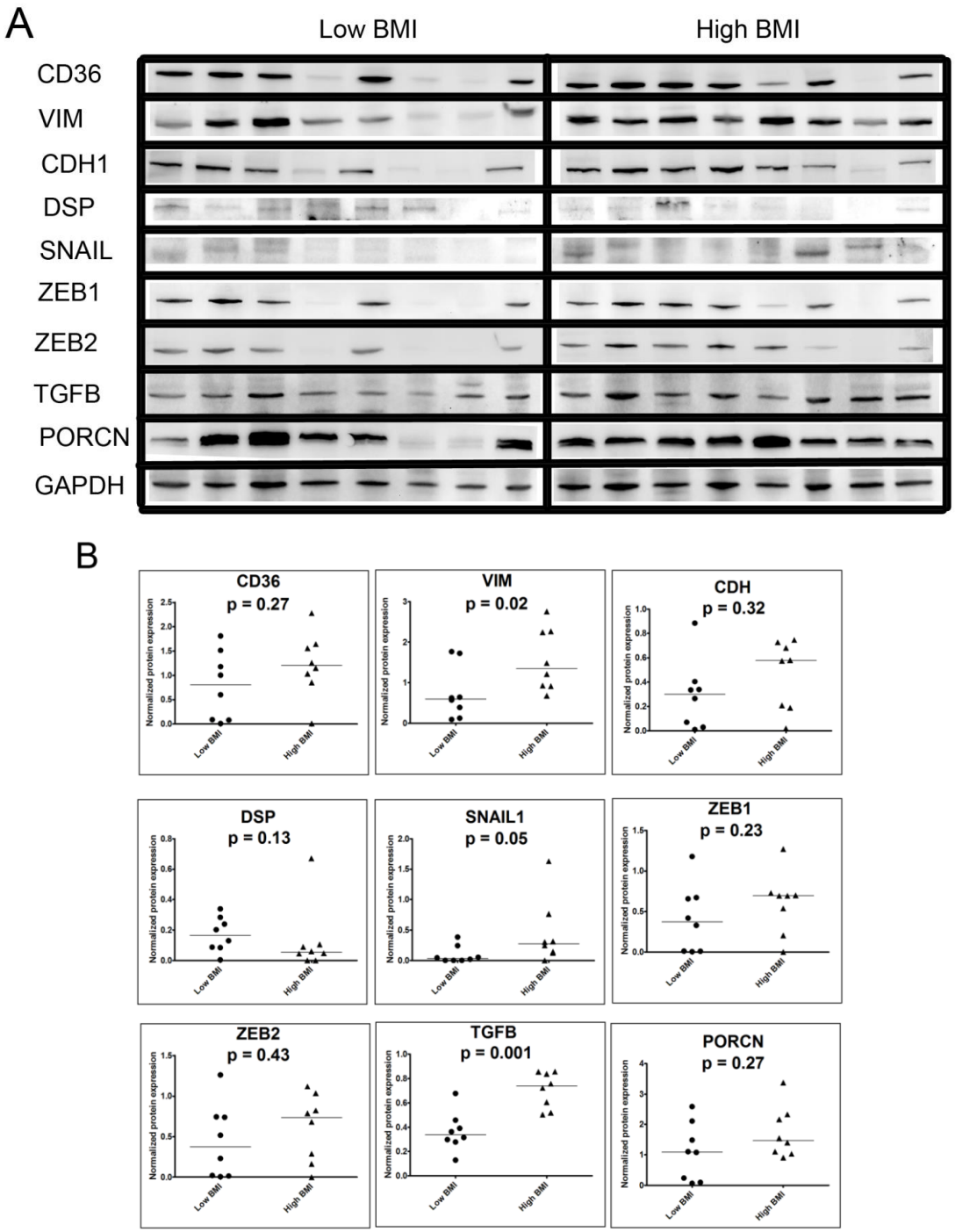

Figure 12: CD36 and EMT marker expression in human HCC tumors

Figure 12 (cont'd)

C

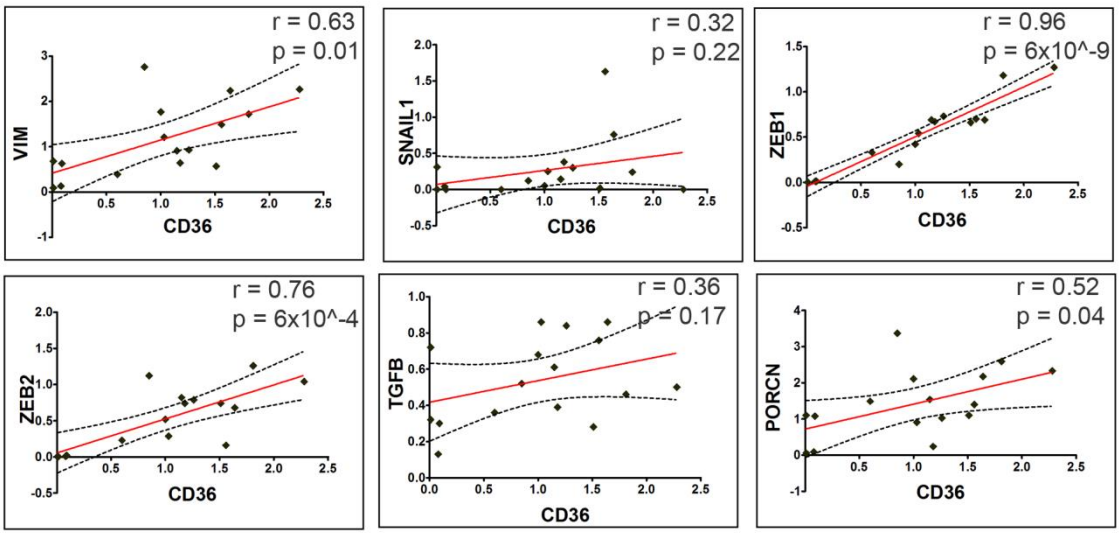

A. Western blots showing expression levels of CD36 and various EMT markers in tumor samples grouped according to BMI. High BMI group (n=8) represents tumor samples obtained from individuals with BMI ≥ 30 and low BMI group (n=8) indicates individuals with BMI ≤ 25. Samples were blotted with specific primary antibodies against the indicated protein with GAPDH used as loading control. B. Expression levels of proteins were determined by quantifying the background-subtracted band intensities normalized to GAPDH. Each dot represents relative expression levels of individual samples, with the horizontal bar indicating the median of the distribution. P-values indicate significance of difference in means between low BMI and high BMI groups determined by Mann-Whitney U test. C. Scatter plot showing association between CD36 (X-axis) and EMT marker (Y-axis) expression. The solid lines indicate linear fit and the dotted lines indicate 95% confidence intervals. r indicates Pearson's correlation coefficient and p-values indicate significance of correlation (two-tailed).

3.3.2 FFA treatment enhances migration and invasion

Having found an association between the fatty acid uptake protein CD36 and EMT regulators, we sought to study the effects of fatty acids themselves on the metastatic behavior of liver cancer cells. We hypothesized that elevated FFAs enhance EMT rates in liver cancer cells. To test this, we first evaluated the rates of migration in human liver cancer cell lines treated with various FFAs. Human HepG2 cells were cultured in media containing carrier control (BSA), the saturated FFA palmitate (PA), monounsaturated FFA oleate (OL), n-6 polyunsaturated FFA linoleic acid (LA), the combinations of PA + LA, or the combination of OL + LA (Fig. 13A and 13B). As shown in Figure 13A and 13C, the percentage wound closure in BSA was not significant (Day 7 $p=0.39$, Day 10 $p=0.16$). In comparison, cells treated with PA and OL exhibited significant wound closure by day 7 (Day7, Day10 $p<0.01$). However, the cells maintained in polyunsaturated LA also did not show a significant reduction in open-wound area (Day 7 $p=0.63$) (Fig. 13B and 13D). We further evaluated the behavior of cells maintained in media containing a combination of different FFAs observing that cells co-treated with PA and LA still showed significant migration (Day 7 $p=0.02$) but this effect was not seen in cells co-treated with OL and LA (Day 7 $p=0.16$) (Figure 13B and 13D), suggesting that while saturated FFAs significantly enhanced migration rates, polyunsaturated FFAs did not enhance migration in liver cancer cells.

The strong effect of PA on cell migration prompted us to further investigate the role of PA in enhancing EMT. We evaluated the dose-dependent effect of PA on migration of liver cancer cells. In this experiment, we treated HepG2 and Hep3B cells, two liver cancer cell lines with different etiologies and inherent metastatic potentials, with different concentrations of PA. In

line with the higher inherent metastatic potential of Hep3B cells, we observed higher overall migration rates in PA treated Hep3B cells as compared to HepG2 cells (Figure 14A and 14B). Both HepG2 and Hep3B cells treated with 0.3mM or 0.4mM PA show significant increases in the number of cells migrating into the open wound area when compared to BSA treated cells (24/48 hours $p<0.05$) (Figure 14A). While lower concentrations of PA did not have a significant effect on the migration of HepG2 cells, 0.2mM PA did have a significant effect on migration of Hep3B cells at 48 hours ($p<0.05$). Since both cell lines showed a significant increase in migration rates at a minimum concentration of 0.3mM, we used this concentration for all further experiments. Note that the level of palmitate in the serum of normal individuals is approximately 0.1mM, whereas in an HCC patient it has an expected range of 0.2-0.3mM **(Table 7)**. Thus, the minimum concentration of PA which was found to enhance HepG2 and Hep3B cell migration rates was very similar to the levels found in HCC patients.

As expected in cells undergoing EMT, we noticed a distinct change in the morphology of PA treated HepG2 cells. The cells were immunostained for the cytoskeletal protein keratin 18 following 5 days of treatment with BSA or PA. Interestingly, while all BSA treated HepG2 cells appeared as round or polygonal shaped, some colonies within PA treated cells exhibited an elongated, spindle-shape, characteristic of mesenchymal cells, along with reduced keratin 18 levels (Figure 14C). This observation further provided evidence that PA treatment may be inducing EMT in the liver cancer cells.

The effects of palmitate on the migration and invasiveness of HepG2 and Hep3B cells were confirmed using the modified Boyden's chamber assay. These experiments were performed by seeding 5-day treated PA or BSA cells in cell culture inserts in the absence of serum. After

24 hours, both HepG2 and Hep3B cells treated with PA exhibited enhanced migration and invasion compared to BSA treated controls (Figure 14D).

EMT induction also decreases cell adhesion. To test if PA treatment resulted in loss of liver cancer cell adhesion, we performed a dispase-based cell dissociation assay. After the 5-day treatment with PA or BSA, cultured monolayers were released using the dispase enzyme and subjected to mechanical stress. We found that applying mechanical stress on PA treated HepG2 and Hep3B cells resulted in fragmentation of the monolayer into a large number of smaller-sized particles. In comparison, control cells resulted in fewer, larger-sized particles or sheets (Figure 14E and 14F). Thus, we inferred that PA treatment promoted loss of cell adhesion in both HepG2 and Hep3B cells, thereby destabilizing the monolayer.

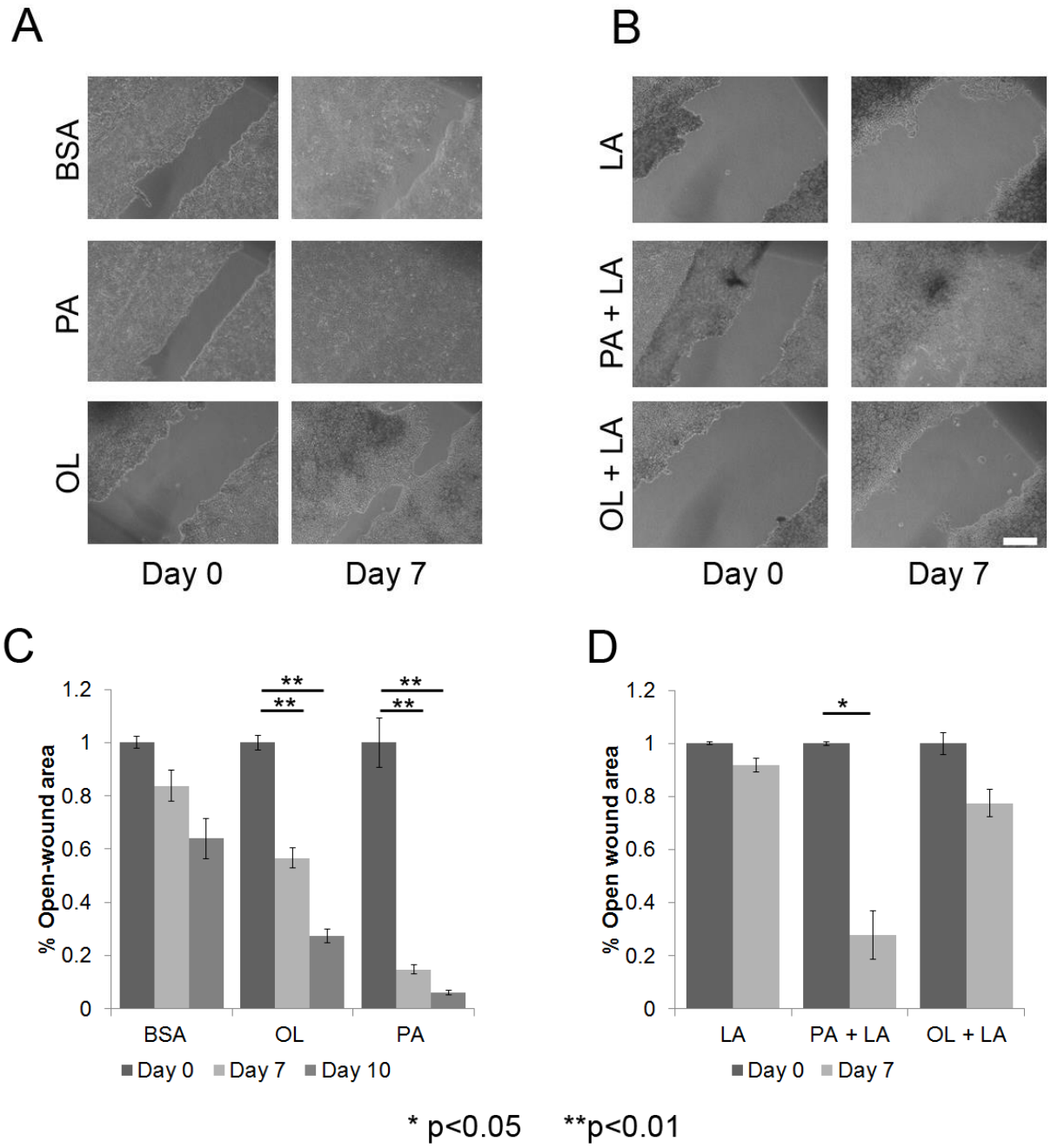

Figure 13: Differential effects of FFA on migration.

A & B. Scratch-wound healing assays. HepG2 cells were grown to 80% confluence in regular medium, and a scratch was introduced on the monolayer. The cells were then cultured in regular media containing either BSA (control), PA (0.4mM), OL (0.4mM), LA (0.4mM), PA

Figure 13 (cont'd)

(0.2mM) + LA (0.2mM) or OL (0.2mM) + LA (0.2mM). The migration of the wound front was monitored over a 10-day period to establish an empirical time-frame within which the cell front acquired the ability to migrate across the wound. Phase contrast images were recorded at 40X magnification (scale bar=50µm) C & D. Bar graph showing the open wound area in treated cells calculated using the T-scratch package at different time points normalized to open wound area at 0 hr. P-values indicate significance levels (n=3) determined by Student's t-test (two tailed).

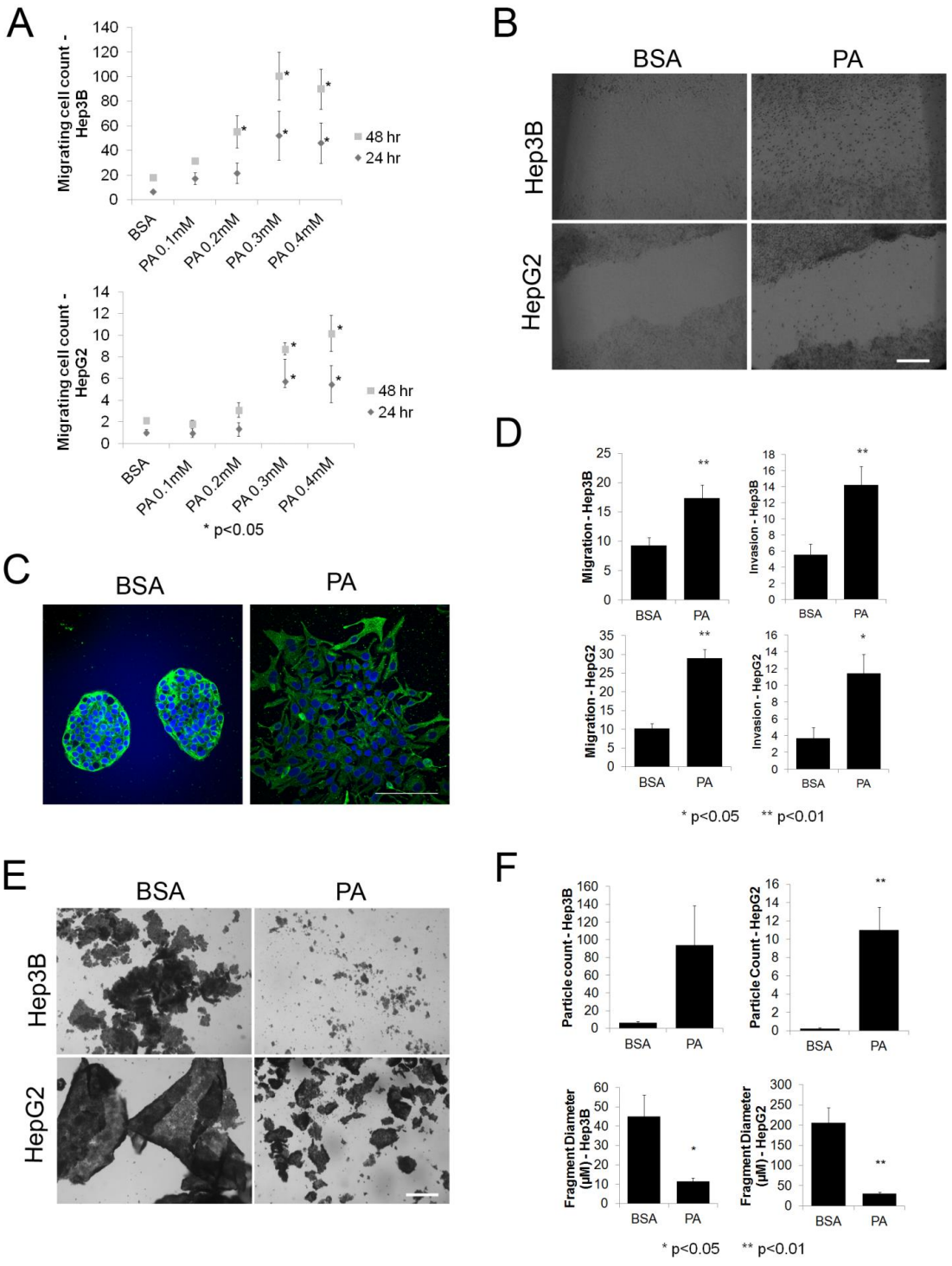

Figure 14: PA mediated EMT induction.

Figure 14 (cont'd) A. Scratch-wound cell migration assays. HepG2 and Hep3B cells were treated with different concentrations of PA (0.1mM to 0.4mM) and BSA (control) for 5 days in presence of serum. A wound was introduced on the cell monolayer on 5th day and imaged after switching to serum-free medium (0 hour time point). The wounds were imaged after 24 and 48 hours in 3 fields of view and the number of cells at each time point were quantified. The plot indicates average number of migrating cells in the wound area at 24 and 48 hours normalized to the number of migrating cells in the wound area at 0 hour time point (n=3). P-values indicate the significance levels compared to BSA at a given time point determined by Tukey's test following one-way ANOVA. B. Phase contrast microscopy images of HepG2 and Hep3B cells treated with BSA or PA (0.3mM) recorded 48 hours after scratching at 40X magnification (scale bar=50µm). C. Changes in morphology upon PA treatment. Confocal images of HepG2 cells were obtained following 5 day treatment with PA (0.3mM) or BSA. Nuclei are indicated with blue fluorescence and keratin 18 with green fluorescence. Images were recorded at 40X magnification (scale bar=100µm). D. Boyden's chamber assays. HepG2 and Hep3B cells were cultured in PA (0.3mM) or BSA for 5 days in presence of serum. The cells were then trypsinized, counted and 1x10^4 cells were re-seeded in the upper compartment of Boyden's chamber inserts (migration/invasion) without serum. The inserts were placed in wells containing regular media supplemented with 10% FBS as a chemoattractant. The bar graph indicates the average number of migrating or invading cells (±SEM, Standard Error of the Mean) counted in 5 fields of view per insert (n=3). P-values indicate significance levels determined by Student's t-test (two-tailed). E. Bright field images at 5X (scale bar=400µm) magnification showing fragmentation in monolayers of BSA or PA treated Hep3B or HepG2

Figure 14 (cont'd)

cells following dispase treatment and application of mechanical stress. F. Particle analysis following dispase assay. Bar graphs showing average particle count and fragment diameter (±SEM) determined from 5 independent images panels obtained after dispase treatment and applying mechanical stress to BSA or PA treated HepG2 and Hep3B cells. P-values indicate significance levels determined by Student's t-test.

3.3.3 Cytotoxicity vs. EMT in FFA treated cells

A number of previous studies have established that PA is in fact cytotoxic to liver cancer cells, and elevated levels may cause lipotoxicity. Indeed, when HepG2 and Hep3B cells were treated with PA at different concentrations, we noticed significant cytotoxicity at the concentrations corresponding to enhanced migration in cell lines (Figure 15A). Note this experiment was performed after the 48-hour serum-free treatment with PA or BSA and serum-starvation can also contribute to cytotoxicity. Next, we assessed the metabolic rates in the PA and BSA treated cells before and after serum starvation. While the metabolic activity rates were reduced in both serum-starved PA (HepG2 66%, Hep3B 71%) and BSA (HepG2 47%, Hep3B 80%) treated cells after 48 hours, the basal metabolic rates were significantly higher in PA treated cells when compared to BSA at both 0 (HepG2 2.2 fold, Hep3B 2.7 fold) and 48 hours (HepG2 3.1 fold, Hep3B 2.4 fold) (Figure 15B). Thus, despite lipotoxicity, the PA treated cells were overall more metabolically active than the BSA treated cells. We further measured metabolic activity by staining for neutral lipids and fatty acids using Oil Red O dye. As shown in Figure 5C, both PA-treated HepG2 and Hep3B cells show enhanced staining with Oil Red O after 48 hours of serum-starvation compared to BSA treated cells. Additionally, we quantified

the relative levels of the dye eluted from stained cells and found significantly higher levels in PA treated cells (Hep3B $p<0.05$, HepG2 $p<0.01$) (Figure 15D).

From these experiments, we hypothesized that while PA induced cell death in a proportion of the liver cancer cells, a distinct surviving population of cells remained metabolically active and acquired the ability to undergo EMT. To further confirm this point, we measured the changes in expression levels of various EMT markers in the PA treated liver cancer cells. We used flow cytometry to analyze the population distribution of cytotoxicity and EMT markers. We stained PA or BSA treated HepG2 cells with a cell death indicator dye (Zombie Violet) followed by formaldehyde fixation. The fixed cells were then permeabilized and immunophenotyped for CDH1, DSP (epithelial markers), and VIM (mesenchymal marker). After background subtraction from unstained cell populations, we analyzed the percentage of cells that were positively stained for each marker. As expected, we found that upon PA treatment a larger percentage of cells stained positive for Zombie Violet as compared to BSA treatment (upper left quadrant, Figure 16A). Moreover, another separate population of cells stained positive for the epithelial and mesenchymal markers (lower right quadrant Fig. 6A). The percentage of cells that stained positive for CDH in BSA (45.42%) was significantly higher than PA (15.63%) ($\chi^2=21.43$, df=1, $p<0.001$). Similarly, a higher percentage of DSP staining was observed in BSA (75.67%) compared to PA (33.13%) ($\chi^2=26.7$, df=1, $p<0.001$). In contrast, a larger number of PA cells (63.57%) showed positive staining for VIM, compared to BSA cells (50.6%) ($\chi^2=3.5$, df=1, $p=0.03$).

The expression of the EMT markers was further confirmed by observing the immunostaining using confocal fluorescence microscopy. HepG2 and Hep3B cells were fixed, permeabilized

and stained to detect CDH and VIM expression (Figure 16B). The PA treated cell population showed reduced CDH expression and increased VIM expression in both HepG2 and Hep3B cells. Within the population of PA treated Hep3B cells, a few cells show very high expression levels of VIM, further corroborating presence of distinct cell populations.

The mRNA expression levels of the EMT transcription factors *SNAIL1* ($p<0.05$), *ZEB2* ($p<0.01$) and *TWIST1* ($p<0.05$) were significantly higher in PA treated HepG2 cells and similarly *ZEB1* and *FOXC2* were expressed at higher levels in the PA treated cells ($p=0.06$) (Figure 16C). The lower fold-change observed in the qRT-PCR experiment reflects population average across all cells, including cytotoxic and EMT cells, within a treatment condition.

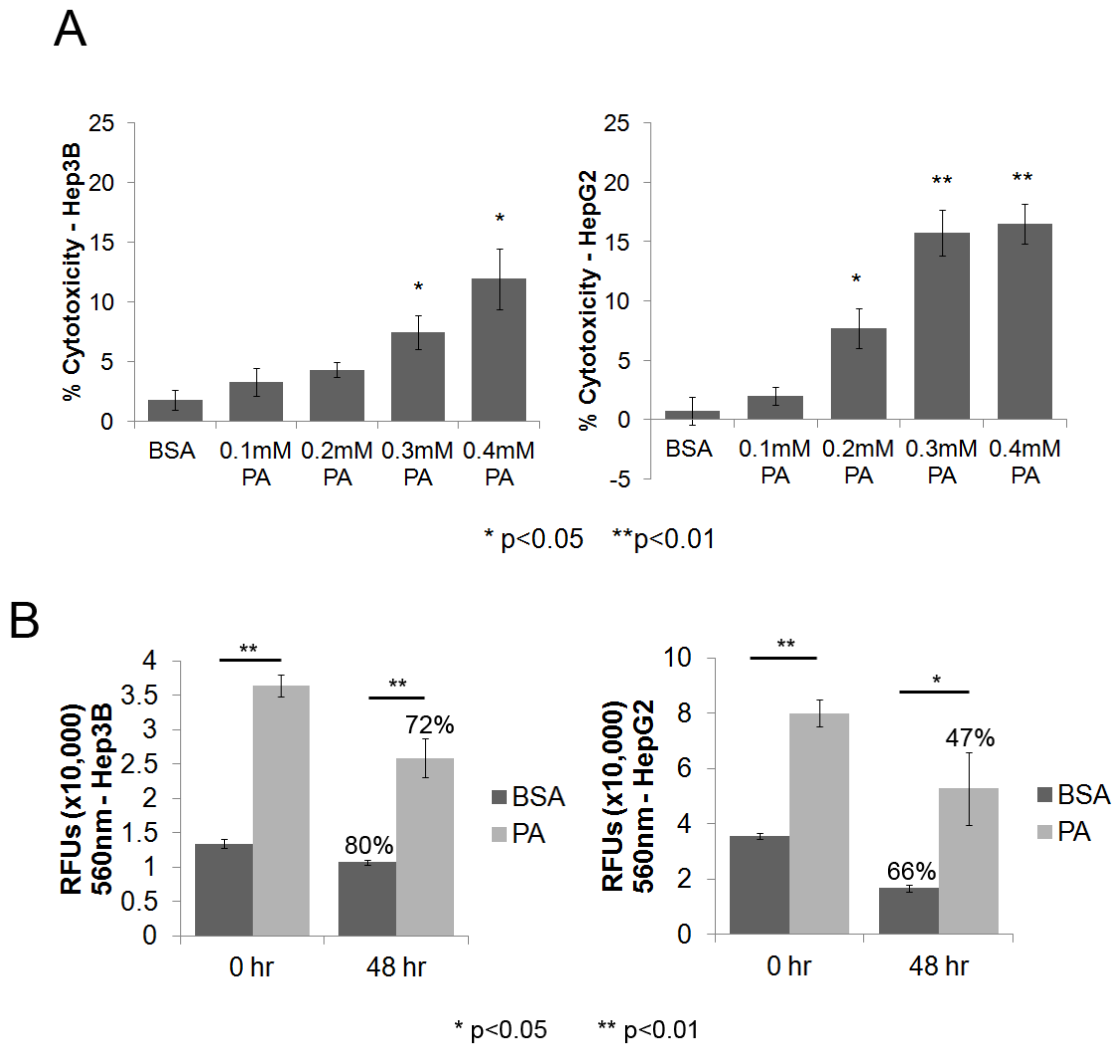

Figure 15: Cytotoxicity vs. metabolic activity.

Figure 15 (cont'd)

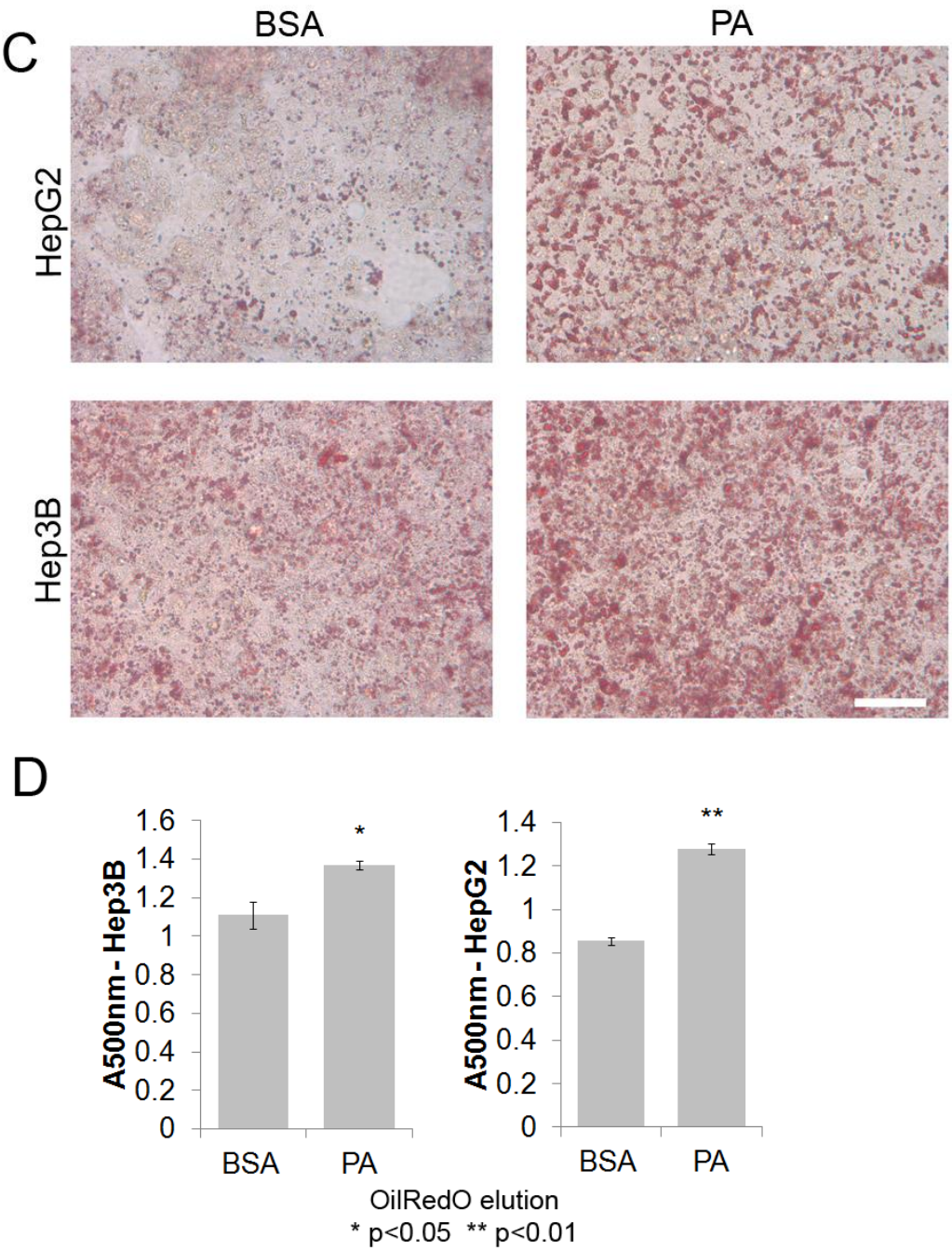

A. LDH cytotoxicity assay. Bar graph showing average cytotoxicity (±SEM) in HepG2 or Hep3B cells following 5 day (with serum) and 2 day (without serum) treatment with BSA or PA at

Figure 15 (cont'd)

different concentrations (n=3). P-values indicate significance levels comparing average LDH release in PA treated cells with BSA treated cells determined by Student's t-test (two tailed). B. AlamarBlue assay. Bar graph showing the relative metabolic activity rates represented by average fluorescence (±SEM) from reduced AlamarBlue reagent (resazurin) in HepG2 or Hep3B cells following 5 day treatment (with serum) and 2 day (without serum) with BSA or PA (n=3). P-values indicate significance levels determined by Student's t-test (two tailed). Numbers above bars indicate the percentage of proliferating cells at 48 hours compared to 0 hours. C. Neutral lipids and fatty acids in HepG2 or Hep3B cells were stained with Oil Red O following 5 day (with serum) and 2 day (without serum) treatment with BSA or PA. Bright-field microscopy images were recorded at 40X magnification (scale bar=50μm). D. Relative levels of lipids and fatty acids in BSA and PA treated cells were quantified by eluting the Oil Red O dye and measuring relative absorbance at 500nm. Bar graph shows average absorbance (±SEM) in BSA and PA treated cells. P-values indicate significance levels comparing average absorbance in BSA or PA treated cells determined by Student's t-test (two tailed).

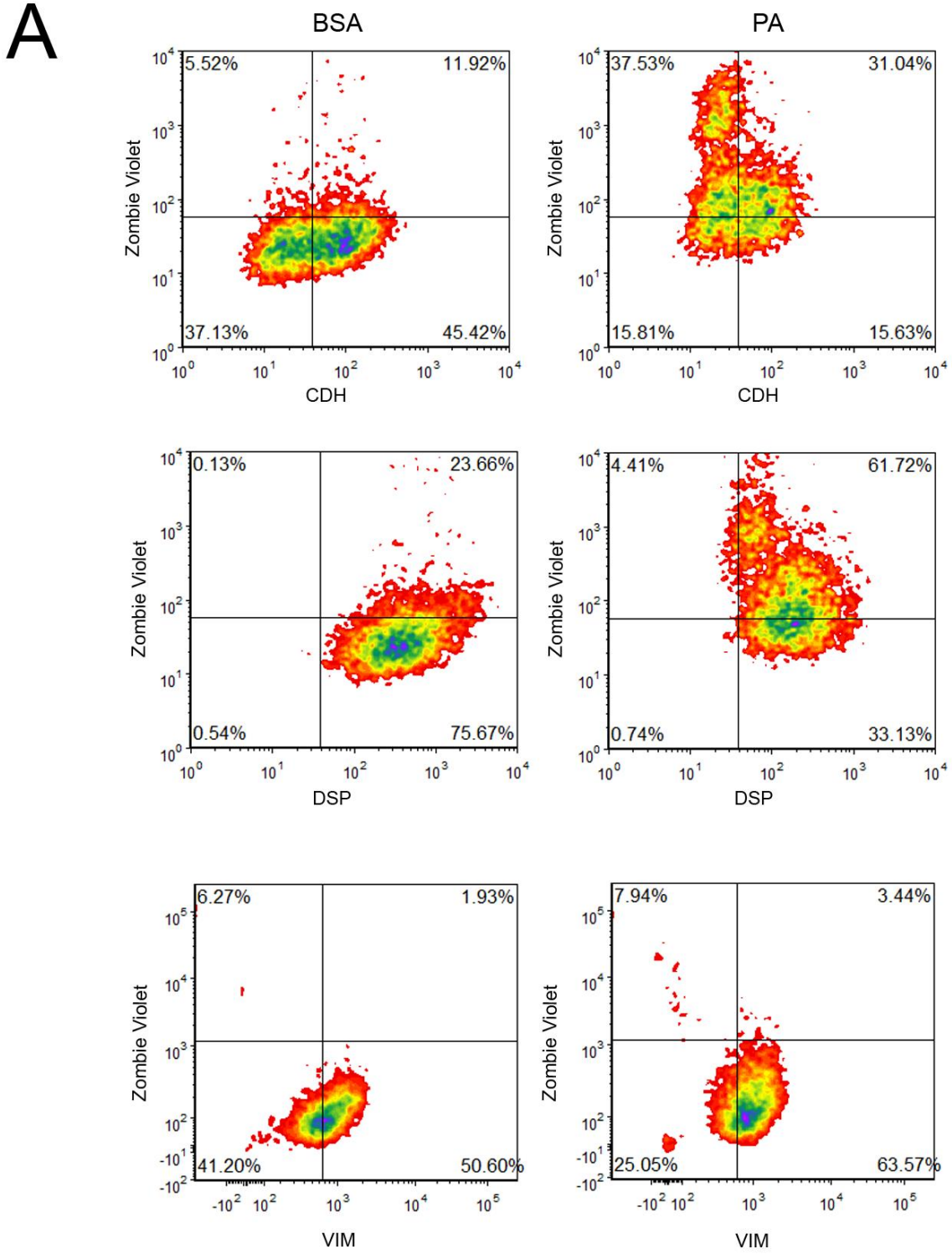

Figure 16: Population effect of PA on EMT marker expression.

Figure 16 (cont'd)

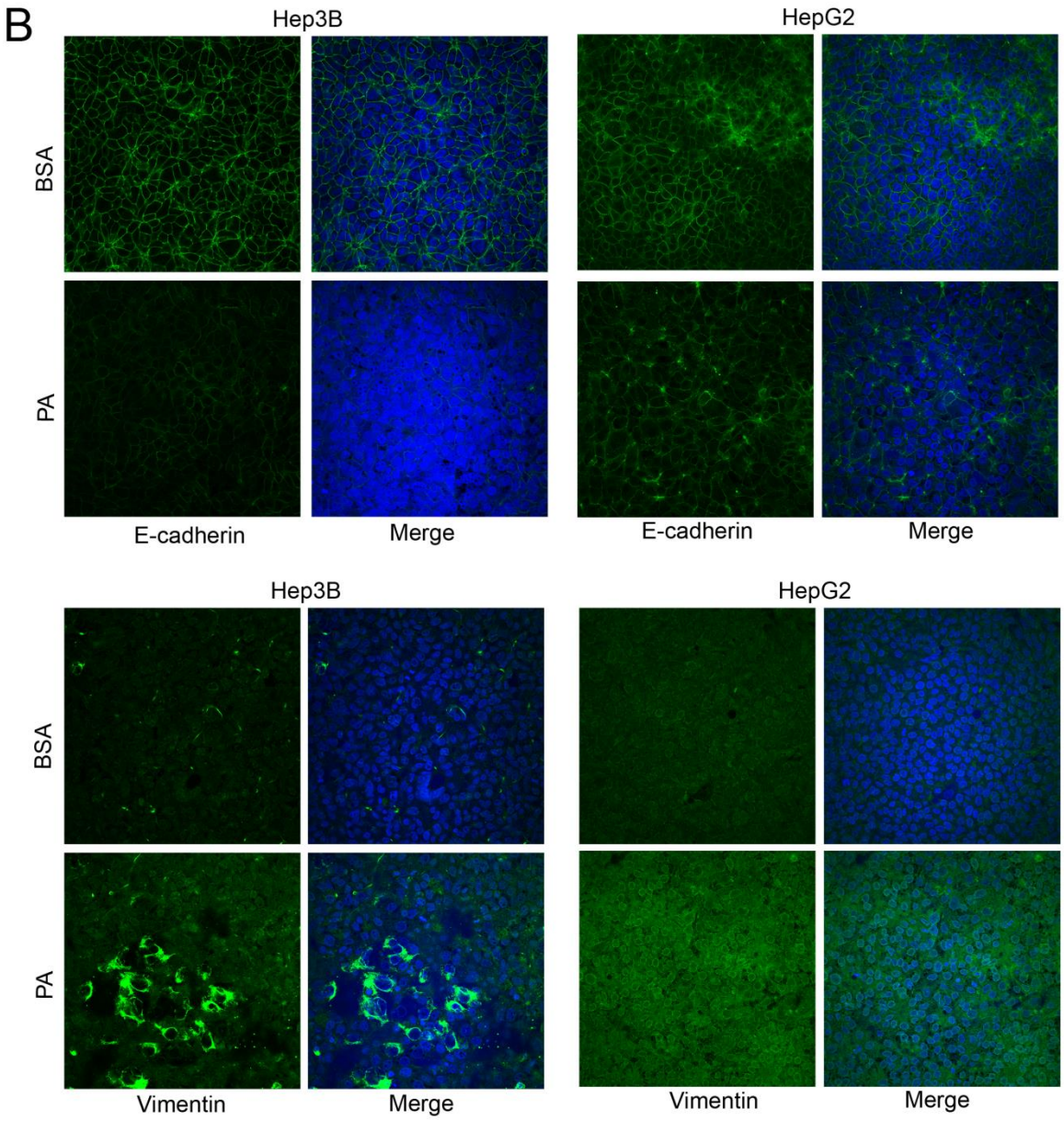

Figure 16 (cont'd)

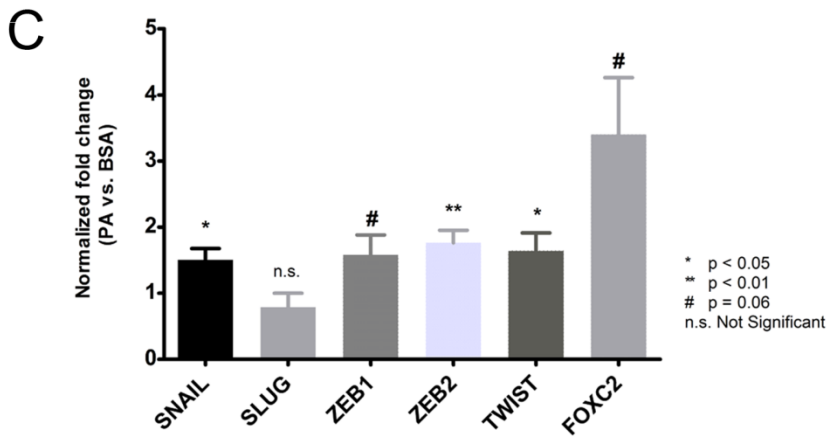

A. Density plots showing distribution of cells co-stained with zombie violet (Y-axis) and either CDH, DSP or VIM (X-axis) in HepG2 cells treated with BSA or PA (0.3mM). The bars represent staining thresholds for zombie violet (horizontal bar) or the protein markers (vertical bar). Lower left quadrant represents background staining, upper left quadrant represents cells stained with only zombie violet, upper right quadrant represent cells co-stained with zombie violet and protein marker and lower right quadrant represent cells stained with protein marker only. The numbers in the plot represent the percentage of total cells within that quadrant. B. Confocal images showing expression levels of CDH and VIM in HepG2 and Hep3B cells. Blue indicates nuclear staining and green indicates CDH or VIM staining. Images were recorded at 40X with identical exposure and PMT settings maintained between BSA and PA treated cells for a given marker (scale bar = 100µm). C Bar graph showing fold-change in mRNA expression levels of various EMT transcription factors determined by qRT-PCR in PA (0.3mM) treated HepG2 cells compared to corresponding expression levels in BSA treated

Figure 16 (cont'd)

cells (*GAPDH* normalized). P-values indicate significance levels compared to BSA determined by Student's t-test (two tailed), n = 3.

3.3.4 FFA treatment activates Wnt and TGF-β signaling

With evidence to support that PA treatment activated the EMT-program, we next sought to understand the driving mechanism behind EMT activation in the PA treated cells. We used the mRNA samples from BSA and PA treated HepG2 and Hep3B cells and profiled the expression levels of genes that were representative of known EMT-inducing signaling pathways using a PCR-based array (Figure 17A). In this study, we ranked the genes obtained from the array according to the PA vs. BSA fold-change and analyzed the enrichment of KEGG-pathways in the top 20 genes (Figure 17B). While the hedgehog signaling pathway was enriched in the HepG2 cells, we did not find a significant increase in the sonic hedgehog ligand (*SHH)* and its downstream transcriptional activator *GLI1* mRNA levels in PA treated HepG2 cells. We found that the TGF-beta and Wnt signaling pathways were significantly enriched in the set of top 20 genes from both HepG2 and Hep3B cells (Figure 17B). Interestingly, a distinct set of genes within these pathways were upregulated in the two cell lines (Figure 17A). Recall that in the human HCC tumor samples in Figure 12C, we found a positive correlation between CD36 with TGFB (TGF-beta signaling ligand) and PORCN (Wnt signaling mediator). These results provide a point of convergence between the correlations observed in the human HCC studies and the experiments with PA treated liver cancer cells – that TGF-beta and Wnt signaling pathways are activated in both cases and may be the drivers behind activation of EMT program.

The activation of TGF-beta and Wnt signaling pathways promote the subsequent activation of EMT transcription factors, driving the expression of several other anti-apoptotic and proliferative oncogenes. This requires the activation and nuclear translocation of downstream transcriptional effectors of TGF-beta and Wnt signaling pathways. Thus, to assess the activation of the two pathways, we investigated the intracellular localization of SMAD2/3 and β-catenin in BSA and PA treated cells. The overall expression levels of β-catenin were higher in both HepG2 and Hep3B cells after PA treatment (Figure 17C-D). Moreover, the expression of β-catenin was restricted to the cell membrane and cytoplasm in BSA treated cells, while in PA treated cells we clearly observed its increased localization to the nucleus, suggesting that the Wnt signaling pathway was activated upon PA treatment of both HepG2 and Hep3B cells. The expression levels of SMAD2/3 were higher in PA treated Hep3B cells (Figure 17E) but did not seem to change in PA treated HepG2 (Figure 17F) cells, corroborating the data from the array (Fig. 7A). Additionally, SMAD2/3 staining showed considerably higher nuclear localization in PA treated Hep3B cells (Figure 17E), but this change was not distinct in the PA treated HepG2 cells (Figure 17F). This indicated differing mechanisms of EMT induction in the two cell lines and a proclivity of the hepatoblastoma-derived HepG2 cells towards activation of the Wnt-signaling pathway.

We further investigated the mRNA expression profiles of the Wnt (Figure 18A) and TGF-beta (Figure 18B) signaling genes in the TCGA dataset in context of *CD36* expression. The components of these two signaling pathways that share a similar expression pattern as *CD36* (marked clusters in dashed box) reveal possible mechanism by which these pathways may be associated with elevated FFA uptake. The BMP family ligands (*GDF5*, *BMP4*), *NODAL*, and the

transcriptional effector (*SMAD3*) of TGF-beta signaling pathway show similar expression pattern as *CD36*. Similarly, the Wnt ligand (*WNT7A)* and the canonical Wnt signaling transcription factors *CTNNB1*, *LEF1* and *TCF7* clustered with *CD36*. Additionally, genes involved in non-canonical Wnt signaling pathways including planar polarity pathway (*DAAM1, ROCK2)* that regulates cytoskeletal rearrangement, and the Wnt/Ca^{2+} pathway (*PPP3R1, NFATC3*) that regulates cell adhesion and migration, also exhibit similar expression patterns as *CD36*. Next, we analyzed the expression patterns of transcription factors that are known to be activated by elevated free fatty acids (Figure 18C). We found that the fatty-acid responsive transcription factors, *PPARA* and *PPARD,* that can transcriptionally upregulate *CD36* (Zhou et al., 2008b), show strong positive correlation with *CD36*. Furthermore, a number of downstream transcriptional effectors of inflammatory pathways (TNF-α, Jak/Stat, IL1-signaling) activated by free fatty acids, including *NFKB1*, *FOS* and *HIF1A* show similar expression pattern as *CD36*. These transcription factors can upregulate the expression of Wnt and TGF-beta signaling pathway components, and also upregulate expression of EMT transcription factors. Figure 8D provides an outline of the influence of elevated uptake of FFA on the various signaling pathways constructed using the results from our in vitro experiments with PA treated HCC cells, and the evidence from TCGA analysis. As shown in the schematic, the uptake of FFA via CD36 is a key event in the induction of EMT program in HCC cells. Therefore, we hypothesized that inhibition of CD36 would result in abrogation of the EMT phenotype.

To verify the critical role of CD36 in mediating the effects of PA on the liver cancer cells, HepG2 cells were cultured in BSA or PA along with Sulfo-N-succinimidyl oleate (SSO) – a chemical that binds irreversibly to the CD36 receptor and inhibits fatty acid uptake (Coort et

al., 2002). After the 5-day treatment period, we measured the protein expression levels of CDH and VIM (Fig. 9A). Note that the PA treatment expression levels reflect the population average across both cytotoxic and EMT cells. We found that inhibiting CD36 activity with SSO resulted in significant upregulation of CDH in not only PA treated cells, but also in BSA treated cells (Fig. 9B). In other words, the inhibition of CD36 was sufficient to recover the mild-EMT phenotype that was observed in BSA treated cells as well. Additionally, the expression levels of VIM were significantly reduced in PA treated cells when CD36 was chemically inhibited (Figure 19C).

To assess the role of TGF-beta and Wnt signaling pathways in mediating the activation of EMT program, we measured the effect of inhibiting these pathways in PA treated HepG2 cells. We found that migration rates were significantly reduced in PA treated cells when they were co-treated with a β-catenin/Tcf inhibitor III inhibitor against the Wnt signaling pathway (Lee et al., 2013) or TGF-β1 RI kinase inhibitor against the TGF-beta signaling pathway (Sawyer et al., 2003) (Figure 19D). Additionally, the inhibition of the PORCN enzyme activity with LGK974 (Liu et al., 2013a) also resulted in significant reduction of migration rates (Figure 19E). Finally, the inhibition of CD36 with SSO reduced migration rates in PA treated cells (Figure 19E), confirming the importance of CD36 in mediating PA induced EMT in the liver cancer cells. These experiments confirm that the induction of EMT by PA is mediated by CD36 and requires activation of TGF-beta and Wnt signaling pathways.

A

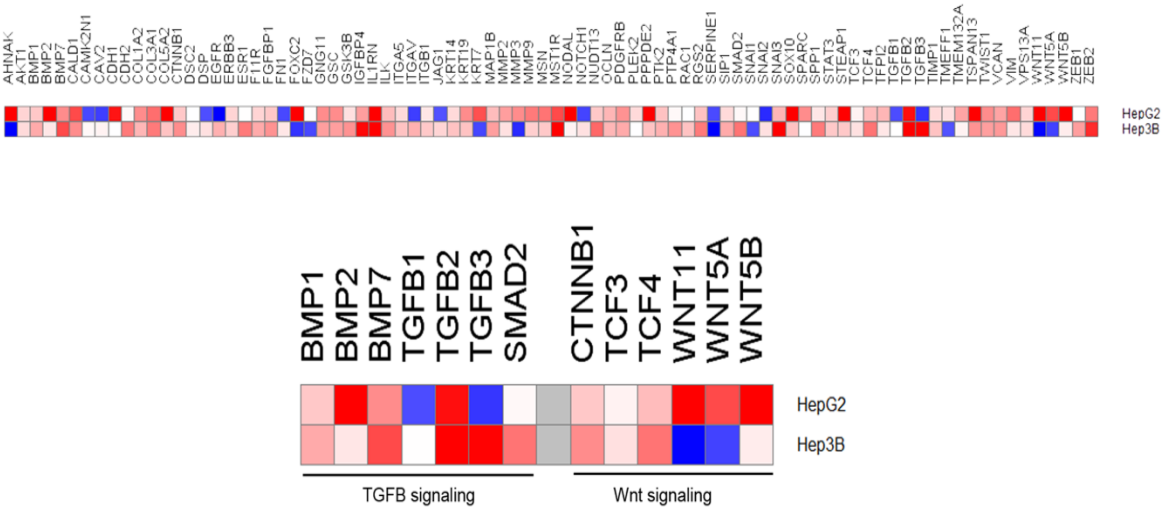

B

KEGG pathway enrichment in top 20 (rank fold-change) HepG2 genes

Term	Count	%	P-Value
Basal cell carcinoma	4	20	0.00
Hedgehog signaling pathway	4	20	0.00
Pathways in cancer	6	30	0.00
TGF-beta signaling pathway	3	15	0.01
Melanogenesis	3	15	0.01
Wnt signaling pathway	3	15	0.03

KEGG pathway enrichment in top 20 (rank fold-change) Hep3B genes

Term	Count	%	P-Value
Colorectal cancer	5	25	0.00
Focal adhesion	5	25	0.00
TGF-beta signaling pathway	4	20	0.00
Cell cycle	4	20	0.00
Pathways in cancer	5	25	0.00
Endometrial cancer	3	15	0.00
Pancreatic cancer	3	15	0.01
Wnt signaling pathway	3	15	0.03
Cytokine-cytokine receptor interaction	3	15	0.09
Intestinal immune network for IgA production	2	10	0.09

Figure 17: EMT pathways induced by PA.

Figure 17 (cont'd)

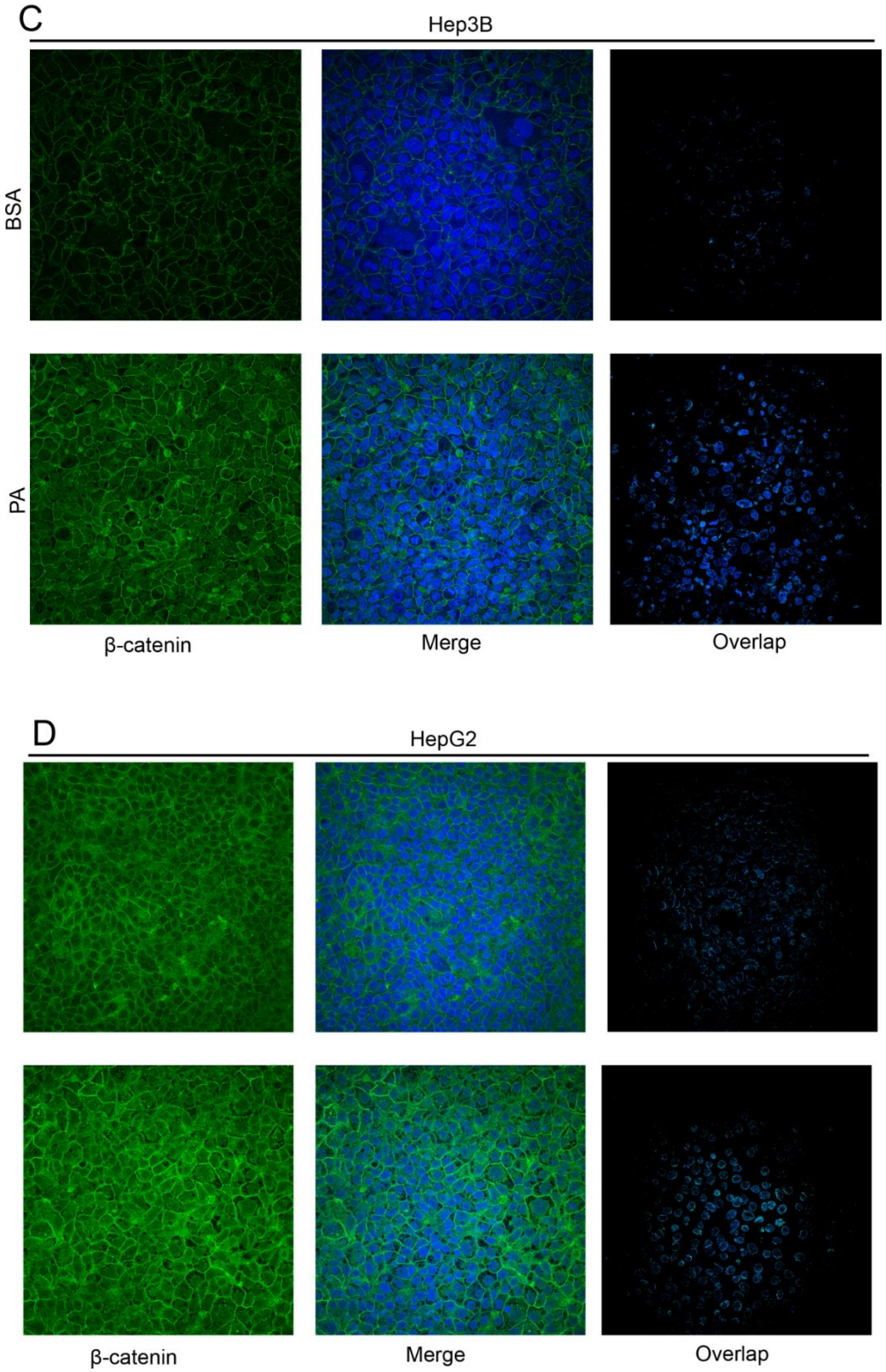

Figure 17 (cont'd)

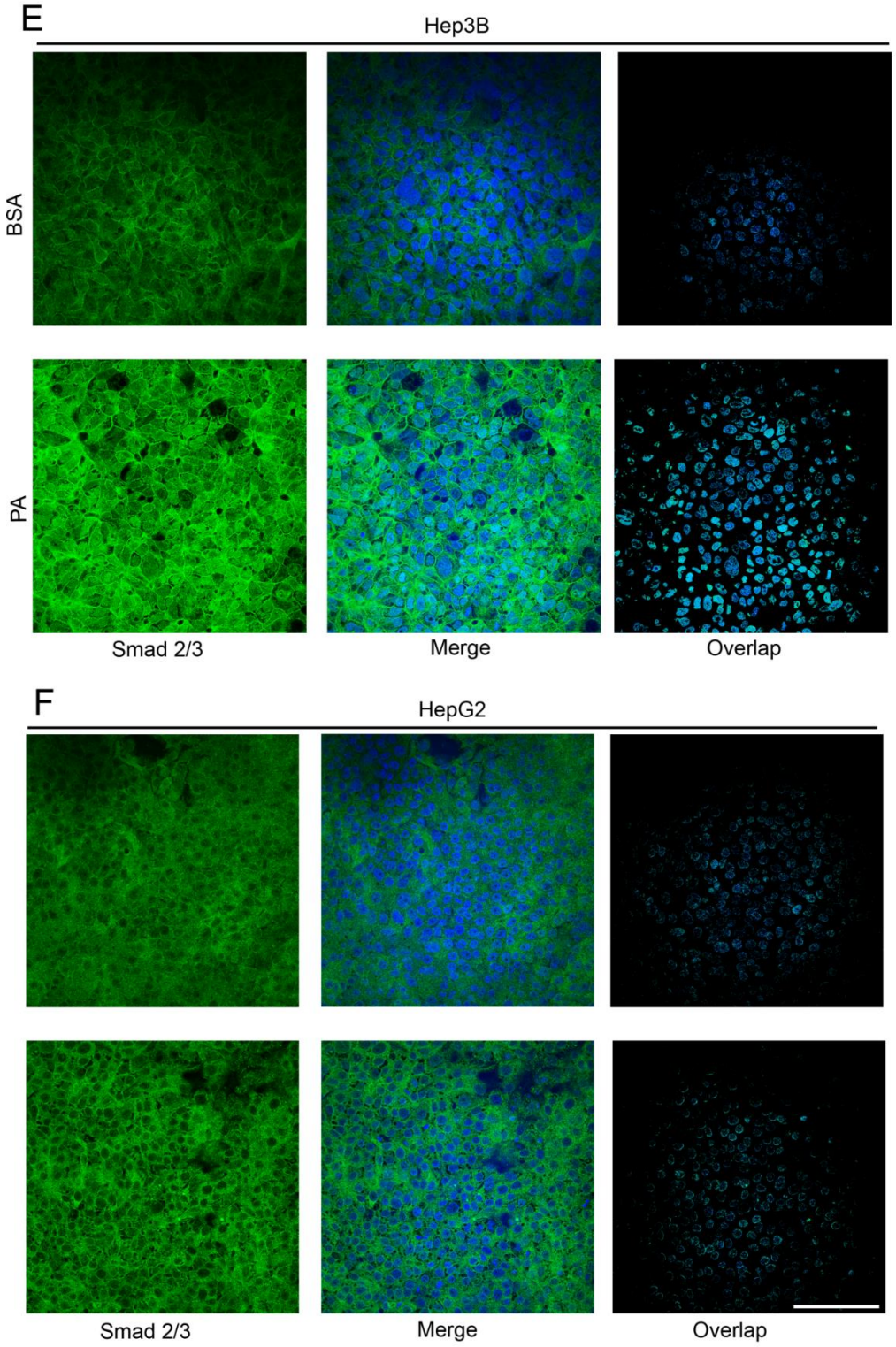

Figure 17 (cont'd)

A. Heatmap showing relative fold-change in mRNA expression levels of various EMT-related genes in PA (0.3mM) vs. BSA treated cells measured by EMT-array. The enlarged heatmap shows fold change in expression levels of the components of TGFB- and Wnt-signaling pathways included in the array. B. The top 20 genes ranked according by fold-change in the array were enriched for KEGG pathways. The table shows the term (KEGG pathway) enriched, number and percentage of genes in the input set belonging to the pathway and significance levels of enrichment. C-F. Confocal images showing expression of β-catenin or SMAD2/3 (green) and nuclei (blue) in HepG2 and Hep3B cells treated with BSA or PA (0.3mM). The overlap panel shows pixels where both green and blue fluorescence co-localize, therefore indicating cells displaying translocation of β-catenin or SMAD2/3 transcription factors to the nucleus. Images were recorded at 40X with identical exposure and PMT settings maintained between BSA and PA treated cells for a given marker (scale bar = 100μm).

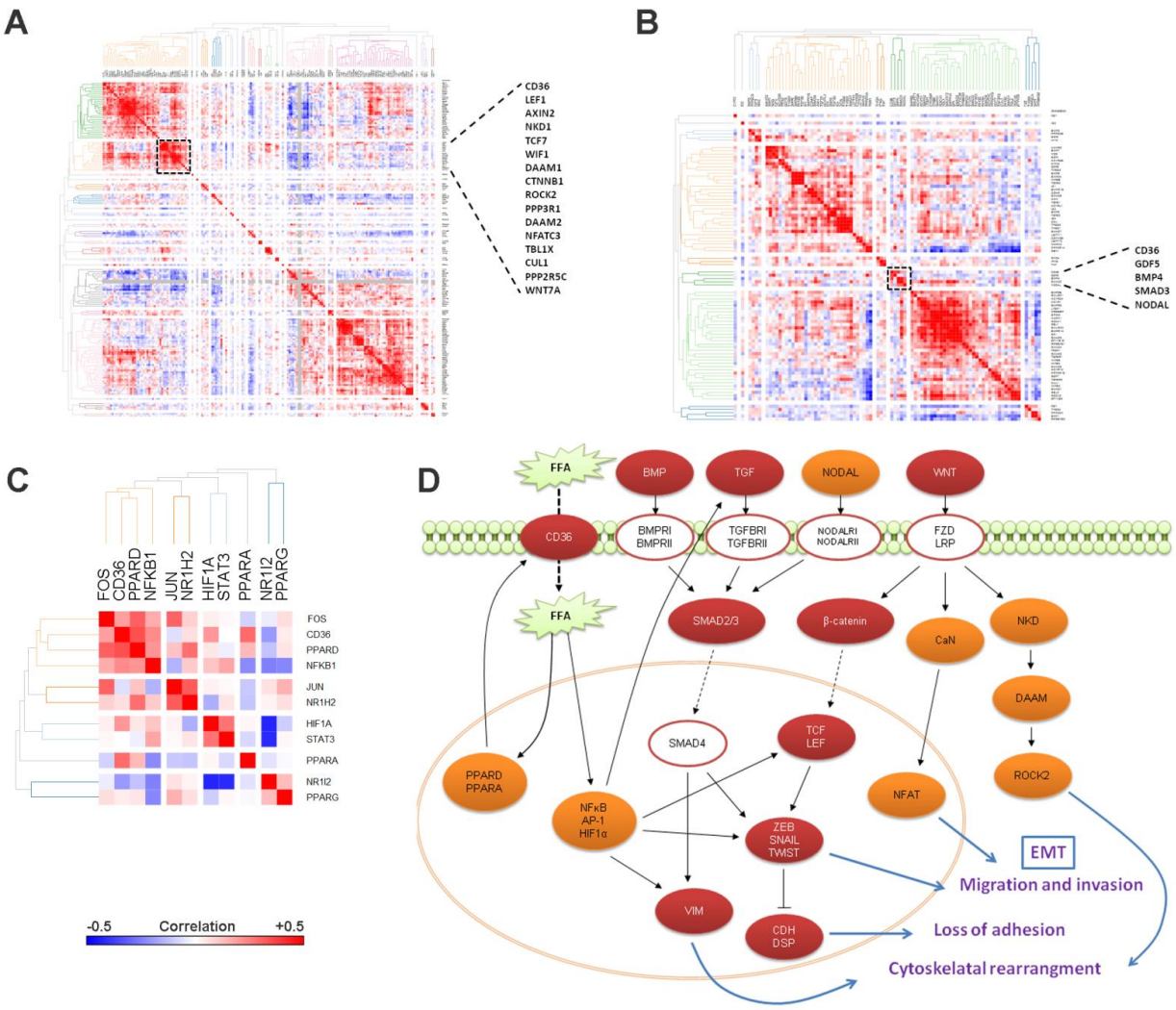

Figure 18: Correlation matrix heatmaps showing the association between mRNA expression z-scores (TCGA) of CD36. A. Wnt signaling pathway genes (KEGG) B. TGF beta signaling pathway (KEGG) C. PPARs and transcriptional mediators of inflammatory pathways known to be induced by free fatty acids. Genes are clustered with average linkage hierarchical clustering using 1-Pearson's correlation as distance metric. Black boxes in A and B show the nearest neighbors of CD36 with strong positive correlation, with enlarged list showing the names of genes in that cluster. D. Overview of the influence of elevated free fatty acid uptake on cell signaling pathways resulting in the induction of EMT program. Red ovals represent

Figure 18 (cont'd)

genes that were upregulated in vitro in PA treated HCC cells; orange ovals represent genes that show positive correlation with *CD36* in the TCGA dataset; white ovals represent genes that did not show a significant correlation with CD36 in the TCGA dataset. Dashed black arrows show transport/translocation, solid black arrows and bar-headed lines indicate positive and negative regulation respectively. Blue arrows indicate consequence of activation of the proteins in context of the EMT program.

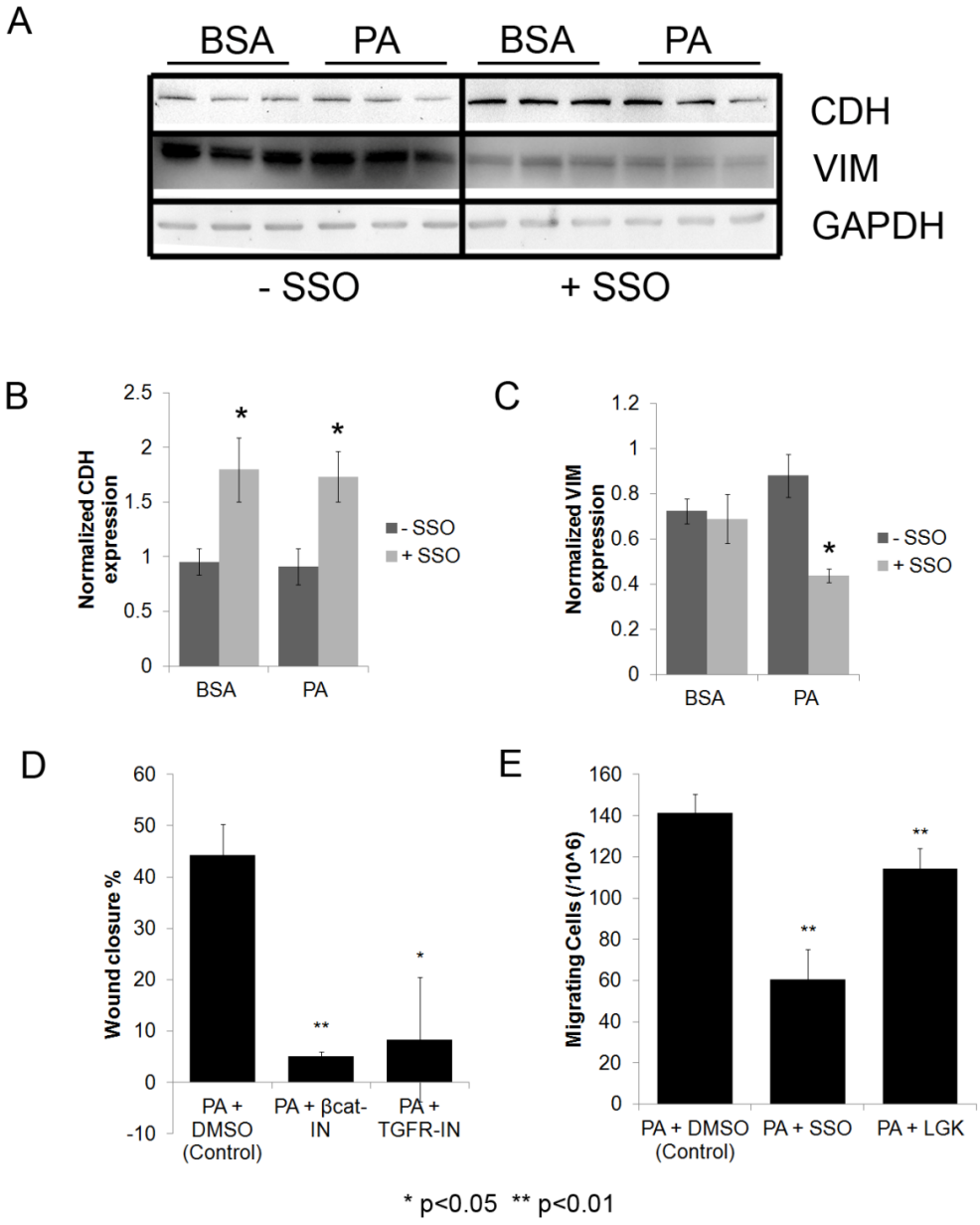

Figure 19: CD36 and TGF-beta/Wnt-signaling mediate PA effects. A. Western blots showing expression of CDH and VIM in HepG2 cells treated with BSA or PA (0.3mM) for 5 days with serum. Additionally, the cells were co-treated with either 100µM SSO (CD36 inhibitor) or DMSO (solvent control). B-C. Bar graphs showing quantification of blots indicating expression levels of CDH and VIM normalized to GAPDH in BSA or PA treated cells (n=3). P-values indicate

Figure 19 (cont'd)

significance levels comparing SSO treated (+SSO) BSA or PA treated cells with DMSO control (-SSO) cells determined by Student's t-test (two tailed). D. HepG2 cells were treated with PA (0.3mM) and DMSO (control), β-catenin/Tcf inhibitor III (100nM) or TGF-β1 RI kinase inhibitor (50nM) in presence of serum for 5-days, followed by wound-healing assay in serum-free media over 48 hours. Bar graph indicates average wound closure (wound closure = 100 - % open wound area) normalized to 0 hour time point (n=3). P-value indicates significance levels comparing the open wound area in inhibitor treated cells with control cells determined by Student's t-test (two tailed). E. HepG2 cells were treated with PA (0.3mM) and DMSO (control), CD36 inhibitor SSO (100μM) or porcupine inhibitor LGK974 (100nM) in presence of serum for 5-days, followed by Boyden's chamber migration assay over 48 hours in serum-free media, with 10% FBS containing regular medium as chemoattractant. Bar graph indicates the average number of migrating cells (n=3). P-value indicates significance levels comparing the number of migrating cells with inhibitor treatment against control, determined by Student's t-test (two tailed).

3.4 Discussion

Although obesity has been strongly associated with progression and high mortality rates in HCC patients (Calle and Kaaks, 2004; Calle et al., 2003), the role of FFAs in HCC progression has remained undefined. Our results provide the first direct evidence that elevated FFA uptake promotes HCC progression by activating the EMT program. By investigating the expression profile of hepatic fatty acid transport proteins in comparison to markers of EMT progression, we showed an association between FFA uptake and EMT. However, we also observed that BMI was not associated with the degree of EMT, highlighting the specific role of FFAs and their cellular uptake in this process. Note that BMI itself may not be an accurate indicator of the level of fatty acids in an individual, as athletic and fit individuals with higher bone density or muscle mass could have high BMI despite low fat levels. Further, BMI at the time of HCC diagnosis may not be fully reflective of the patients BMI during carcinogenesis due to the frequent occurrence of paraneoplastic weight loss once the cancer is established.

Since BMI was not associated with EMT, we speculate that higher *CD36* levels in certain HCC patients could contribute to the accumulation of FFAs in the liver independent of BMI. This notion is supported by evidence from expression analysis of human NAFLD subjects which associated enhanced *CD36* expression with higher liver fat content (Greco et al., 2008). *CD36* knockout studies in mice also showed that loss of CD36 prevented hepatic steatosis in animals fed with high fat diet (Zhou et al., 2008b), confirming the crucial role of CD36 in hepatic fat accumulation independent of other FA uptake proteins. This study also found that the transcription of *CD36* in the liver was regulated by the FA-responsive transcription factors

PPAR-α, PPAR-γ, LXR and PXR, suggesting that a positive feedback loop elevated the hepatic uptake of FFAs.

The fundamental role of the hepatic FFA pool is to produce energy via β-oxidation and provide materials for the biosynthesis of membranes and complex lipids, and other metabolic pathways. Given the increased energy and anabolic demands of rapidly proliferating cancer cells, it is clear why alterations in fatty acid metabolism may be required for tumor progression. Indeed, rewiring of energy metabolism pathways is increasingly being recognized as an emerging hallmark involved in the tumorigenesis of a wide variety of cancers (Currie et al., 2013; Hanahan and Weinberg, 2011). But the role of FFAs in HCC tumorigenesis likely extends beyond cellular sustenance. Our in vitro experiments confirmed that FFAs induced EMT in HCC cells via the activation of Wnt and TGFβ signaling pathways. The Wnt ligands (*WNT5A, WNT5B, WNT11*) were upregulated in PA treated HepG2 cells whereas the downstream transcription factors (*CTNNB1, TCF4*) of Wnt signaling were upregulated in Hep3B cells. Despite different mechanism of activation, both cell lines exhibited nuclear translocation of β-catenin in PA treated cells. The activation of TGFβ signaling was evidenced by the increase in expression of the TGF ligands in both HepG2 (*BMP2*, *BMP7, TGFB2*) and Hep3B (*BMP7, TGFB2, TGFB3*) cells. However, while Hep3B cells showed both increase in expression and nuclear translocation of SMAD2/3 upon PA treatment, we did not observe a similar effect in HepG2 cells.

There are several possible mechanisms by which FFAs could activate Wnt and TGFβ signaling in HCC cells. For instance, an important consequence of elevated hepatic FFA accumulation is the enhanced production of pro-inflammatory cytokines such as TNF-α and IL-6 in the liver

microenvironment (Feldstein et al., 2004b) (Weigert et al., 2004). These cytokines activate oncogenic transcription factors including NF-κB, AP-1 and STAT3 (Grivennikov et al., 2010) which provides a potential link between FFA-induced inflammation, activation of Wnt and TGF-β signaling and progression via EMT. NF-κB was shown to influence Wnt signaling by upregulating the β-catenin associated transcription factor *LEF1* (Yun et al., 2007), and along with AP-1 co-regulated the expression of *WNT10B* ligand (Katoh and Katoh, 2007). Further, studies have shown that expression of NF-κB is essential for EMT induction in multiple carcinomas (Batra et al., 2011; Huber et al., 2004; Li et al., 2012). Along similar lines, AP-1 was shown to influence the induction of the EMT program by regulating the expression of *TGFβ*, *ZEB1* and *ZEB2* (Bakiri et al., 2014). The STAT3 transcription factor was shown to mediate the induction of EMT by regulating *SNAIL* (Yadav et al., 2011), *ZEB1* (Xiong et al., 2011), *TWIST* (Zhang et al., 2012) and the mesenchymal markers *VIM* and *CDH2* (Colomiere et al., 2008). Another potential mechanism of EMT induction could be the activation of the unfolded protein response or ER-stress pathway by FFA (Wei, 2006). A recent study showed that XPB1, the substrate of ER-stress sensor IRE-1, recruits the RNA polymerase complex to several HIF1α targets, thereby regulating the activity of HIF1α (Chen et al., 2014). The involvement of HIF1α in promoting EMT is well documented in multiple cancers via the activation of Wnt signaling (Jiang et al., 2007b) and the direct regulation of *TWIST* (Yang et al., 2008b), *TCF3* and *ZEB* (Krishnamachary, 2006). In addition to fatty acid uptake, CD36 also mediates uptake of HDL (high density lipoproteins) (Brundert et al., 2011) and oxidized LDL (low density lipoproteins) (Park et al., 2012) in hepatocytes. A recent study suggests the uptake of oxidized LDL requires binding of fatty acids to CD36 (Jay et al., 2015). Elevated oxidized LDL accumulation has been

associated with increased ROS accumulation, induction of ER-stress and activation inflammatory pathways in the liver (Bieghs et al., 2010; Musso et al., 2013; Van Rooyen et al., 2011), thereby potentially activating the pro-EMT signaling pathways discussed above.

Thus, the CD36-mediated increase in hepatic FFA accumulation could facilitate the production of EMT-inducing factors. The creation of an environment promoting EMT would not only play a role in progression of HCC, but may also provide a conducive environment for liver metastases arising from other organs, such as colorectal cancers. The majority of colorectal cancer patients (>50%) develop liver metastases (Jemal et al., 2007), and while surgical resection of the liver metastases facilitates long-term survival, only a small fraction of the patients are candidates for resection (Misiakos et al., 2011). Given the need for better chemotherapy options for both advanced colorectal cancers and HCC, future studies investigating the mechanism of EMT induction, and the role of elevated FFAs and FA uptake proteins are warranted to reveal novel therapeutic targets.

CHAPTER 4: GENETIC ALTERATIONS IN FATTY ACID TRANSPORT AND METABOLISM GENES ARE ASSOCIATED WITH METASTATIC PROGRESSION AND POOR PROGNOSIS OF HUMAN CANCERS

4.1 Introduction

Metastases are responsible for the majority of cancer-related mortalities (Mehlen and Puisieux, 2006). While the progression of primary malignancies to metastasis may be driven by linear progression of tumors via accumulation of mutations, or by parallel evolution of metastatic tumors, it is evidently clear that the genetic alterations driving tumorigenesis are distinct from the ones involved in metastatic progression (Klein, 2009; Yokota, 2000). Cancer cells frequently rewire cellular metabolism to increase ATP synthesis, enhance production of macromolecules and maintain redox status, and the acquisition of such alterations is increasingly being recognized as an important hallmark of cancer (Cairns et al., 2011; Hanahan and Weinberg, 2011). However, it is unclear if these genetic alterations in metabolic pathways can provide a selective advantage towards the metastatic progression of cancer cells.

One of the most commonly observed, and widely studied, metabolic rewiring event during cellular transformation is the increased uptake of glucose and the switch to aerobic glycolysis (Warburg effect) (Shaw, 2006). Despite the poor efficiency of ATP generation compared to mitochondrial oxidative phosphorylation (OXPHOS), the switch to aerobic glycolysis increases the availability of intermediate metabolites required for anabolic processes including nucleic acid and amino acid biosynthesis that are essential for the sustenance of rapidly proliferating

cancer cells (Vander Heiden et al., 2009b). Often ignored, another important source of energy and anabolism in cancer cells is fatty acids (FA) metabolism – almost all tumors gain the ability to synthesize long-chain fatty acids *de novo* by upregulating the expression of fatty acid synthase (*FASN*) (Kuhajda, 2006). Besides constituting lipid membranes, FAs serve as a rich source of energy production through mitochondrial fatty acid oxidation (FAO). Tumor cells overexpressing the brain isoform of carnitine palmitoyltransferase (*CPT1C*), the enzyme responsible for mitochondrial uptake of FAs, are more aggressive and resistant to therapeutics (Zaugg et al., 2011a). From a metabolic perspective, adaptations observed during malignant transformation are very similar in nature to those observed in embryonic and adult hematopoetic stem cells, namely, they metabolize glucose through aerobic glycolysis (Simsek et al., 2010; Zhou et al., 2012b). More recently, researchers have established that FA metabolism also plays a major role in the maintenance of stem cells. *De novo* lipogenesis are highly active in adult neural stem cells, and increased *FASN* expression is essential for the proliferation and maintenance of the undifferentiated state of the stem cells (Knobloch et al., 2013). In addition, *PPAR*-regulated mitochondrial FA oxidation are critical for the maintenance of hematopoietic stem cells (Ito et al., 2012). The parallels between characteristics of stem cells and aggressive cancer cells extend beyond metabolic rewiring to proliferative, migratory and self-renewing properties, and the acquisition of stem cell-like features in cancer cells is closely associated with increased invasiveness and metastasis (Brabletz et al., 2005; Pardal et al., 2003). At the functional level, the activation of epithelial-mesenchymal transition (EMT) program enables metastatic dissemination of the cancer cells including the capability for self-renewal (Mani et al., 2008). Hence, the progression of EMT and

cancer stem cell-like features in tumors confer resistance to therapeutics and are associated with poor prognosis (Singh and Settleman, 2010).

The parallels between highly aggressive cancers and stem cells raise the possibility that the genes regulating cellular metabolic pathways, especially fatty acid metabolism, may be altered during metastatic progression of human cancers. Here, we studied the genetic alterations in metabolic genes associated with metastatic progression using the multi-cancer TCGA pan-cancer datasets. We adapted a hypothesis-driven approach, wherein we constructed a literature curated pathway model of genes altered in cancer cells that regulate glycolysis (Warburg effect) or FA metabolism, including FA uptake. Next, we identified the genes exhibiting significant accumulation of mutations or copy number alterations (CNA) in metastatic tumors as compared to primary tumors. We further established a prognostic gene signature by analyzing the gene expression patterns of metabolic genes in context of EMT progression in seven different TCGA datasets. The prognostic value of the alterations and gene signature were validated by stratification of the pan-cancer samples and evaluating the influence on survival rates. Our analysis revealed that the Warburg effect genes with significant prognostic influence (*TP53, STK11*) were uniformly mutated across all tumor types (primary or metastatic). However, genes involved in FA uptake (*CAV1, CD36*) and de novo lipogenesis (*PPARA, PPARD, MLXIPL*) were amplified at higher frequencies in metastatic tumors. In addition, the OXPHOS gene *SCO2*, a transcriptional target of p53 was also amplified in metastatic tumors. Contrary to expectations, the expression levels of *SCO2* were higher in p53 mutation background, with significant influence on prognosis. By analyzing gene expression data, we found that *CAV1*, *CD36*, *MLXIPL*, *CPT1C* and *CYP2E1* were the top ranked

genes associated with EMT phenotype. Stratification of samples based on copy numbers or expression profiles of the genes identified in our analysis revealed significant influence on patient survival rates.

4.2 Methods

4.2.1 Cancer-specific metabolic pathway model

We selected the enzymes and signaling or transcriptional regulators of glucose or fatty acid metabolism based on the criteria that they are altered in cancer cells. For glucose metabolism, we included the genes that are involved in the switch to aerobic glycolysis or Warburg effect in cancer cells. This process is controlled by the oncogenes HIF1α (*HIF1A*), c-MYC (*MYC*) and OCT1 (*POU2F1*) that control the transcription of glycolytic enzymes, in addition to *PDK1* (pyruvate dehydrogenase kinase 1) that prevents entry of pyruvate into TCA cycle by inhibiting pyruvate dehydrogenase. The glycolytic enzymes activated by HIF1α include *PFKFB4* (6-phosphofructo-2-kinase/fructose-2,6-bisphosphatase 4), which diverts glucose towards the pentose phosphate pathway, and *PFKFB3*, which promotes glycolysis. AKT1 activates mTOR, which in turn activates HIF1A, whereas the tumor suppressor liver kinase B1 (*STK11*) activates AMPK (*PRKAA1*) which can inhibit the activity of mTOR. *PKM* (Pyruvate kinase) catalyzes the final step of glycolysis converting phosphoenol pyruvate to pyruvate generating one molecule of ATP. However, the M2 isoform of pyruvate kinase expressed at high levels in cancer cells inhibits the catalytic conversion step, and promotes the utilization of the substrates through the pentose phosphate pathway. The tumor suppressor p53 controls glycolysis by regulating the transcription of TP53-induced glycolysis and apoptosis regulator or TIGAR (*C12ORF5*) and *SCO2* which regulates the assembly of ETC associated cytochrome C oxidase complex.

For fatty acid metabolism, we included genes that may alter the availability of fatty acids to the cancer cells from external sources, in addition to the de novo lipogenesis and fatty acid

oxidation genes altered in cancer cells. ATP-citrate lyase (*ACLY*) controls the synthesis of acetyl-CoA from citrate, thus, linking carbohydrate metabolism to fatty acid synthesis. The conversion of acetyl-CoA to malonly-CoA is catalyzed by acetyl-CoA carboxylase complex (*ACACA, ACACB*). Fatty acid synthase (*FASN*) then catalyzes the condensation of malonyl-CoA and acetyl-CoA into fatty acid. The master regulator of fatty acid synthesis genes, SREBP (*SREBF1*), is in turn transcriptionally regulated by the Liver X Receptor (*NR1H3*) and PPAR-α (*PPARA*) that function as a heterodimer with retinoid X receptor (*RXRA*). ChREBP (*MLXIPL*) regulates the transcription of lipogenic enzymes *FASN, ACACA* and *ACACB* and is activated by elevated glucose levels. The rate limiting step in mitochondrial oxidation is the transport of fatty acids across the membrane through carnitine palmitoyltransferase 1 (CPT1). Among the different isoforms, the brain isoform *CPT1C* is expressed at elevated levels in cancer cells to increase FA oxidation and ATP production. PPAR-α induces expression of *CYP2E1* which is involved in the oxidation of fatty acids and ketolysis as a part of the cytochrome P450 complex. In peroxisomes, acetyl-CoA C-acyltransferase (*ACAA1*) catalyzes final step of β-oxidation yielding acetyl-CoA whereas the CYP4A enzymes (*CYP4A11, CYP4A22*) catalyze microsomal ω-hydroxylation of fatty acids in the endoplasmic reticulum. The dicarboxylic acid generated as a result of ω-oxidation of fatty acids can serve as substrates for β-oxidation or serve as PPAR ligands. The balance between stored lipids and free fatty acids are regulated by DGAT enzymes (*DGAT1, DGAT2*) which catalyze the esterification of fatty acids to triglycerides, whereas lipase enzymes *LIPE* and *MGLL* produce free fatty acids by hydrolyzing triglycerides and mono-acylglycerids, respectively. PPAR-γ (*PPARG*) promotes lipid storage by regulating expression of esterification enzymes and opposes lipid synthesis, whereas PPAR-δ (*PPARD*)

promotes fatty acid transport and oxidation. The poly unsaturated fatty acid activated nuclear receptor FXR (*NR1H4*) inhibits the activity of LXR and regulates *SREBF1*, *PPARA* and *PPARG*, and inhibits lipogenesis. PXR (*NR1I2*)) induces the transcription of fatty acid transport protein CD36 but suppress expression of FA oxidation genes *PPARA* and *ACAA1*. The accumulation of fatty acids in the cells from exogenous sources is mediated by the transport proteins caveolin (*CAV1*), *CD36* and fatty acid trans proteins FATP (*SLC27A1-6*). In addition, the intracellular trafficking of fatty acids and their interactions with nuclear receptors like PPARs and LXR are regulated by fatty acid binding proteins FABP (*FABP1-7, PMP2, FABP9*).

4.2.2 Mutation analysis

Pan-cancer gene-level somatic mutations data was obtained from the Cancer Browser (PANCAN AWG version 2014-08-22). The pan-cancer samples were divided into two groups: primary and metastatic based on sample type information.

We used the Fisher's exact test to identify the mutations with significantly different frequency in metastatic samples compared to primary tumor samples. For each gene, the test was applied to a 2x2 contingency table of expected and observed mutation frequency for metastatic and primary tumor samples. The observed mutation frequency of a gene in each group were calculated as (number of samples with non-synonymous mutations in the group) / (total number of samples in group). Expected mutation frequencies for each gene were calculated as the product of mutation frequency of the gene in the complete dataset (metastatic + primary tumor) and total number of samples in a group. Genes were considered significant with a p-value cut-off set at 0.05 with stringent false discovery rate control (Bonferroni's method). Basal mutation frequencies were calculated as the (cumulative

mutation frequency of all genes in the PANCAN dataset) / (total number of genes x total number of samples).

To evaluate the influence the mutations on survival, we generated Kaplan-Meier survival curves by stratifying the patients in the complete pan-cancer dataset into two groups: no mutation and mutation. The significance of differences in survival rates were calculated using the log-rank (Mantel-Cox) test, with p-value <0.05 considered significant. The combined effects of multiple mutations in a sample were assessed by first obtaining the sum of mutations in all genes within a category. The samples were then stratified into three groups: no mutations, one mutation or multiple mutations, and the significance of differences in survival rates were calculated using the log-rank test, with p-value <0.05 considered significant.

4.2.3 Copy number variation analysis

Pan-cancer gene-level somatic copy number alterations data (GISTIC2 normalized) was obtained from Cancer Browser (PANCAN version 2014-08-22). We discretized the copy number data of each gene in a sample by binning the copy number calls as gain or loss using a threshold of ≥1 to denote samples with copy number gain and ≤-1 to denote samples with copy number loss.

The copy number gain or loss frequencies for each by tumor type were calculated as (number of samples with copy number gain or loss in a group) / (total number of samples in a group). Expected CNA frequencies were calculated as the product of dataset CNA frequency and total number samples in a group. For each gene, a 2x2 contingency table of expected and

observed CNA frequencies for metastatic and primary tumor samples were analyzed with Fisher's exact test, with a p-value cut-off set at 0.05 with stringent false discovery rate control (Bonferroni's method).

To assess the combined influence of the CNAs with significant accumulation in metastatic tumor samples, we stratified the samples in the complete pan-cancer dataset by grouping the samples in to two homogenous subsets based on the CNA profiles of the six significant genes using the K-means clustering algorithm (Euclidean distance metric). The resulting clusters with high copy numbers and low copy numbers of the six genes were then used to generate survival curves using the Kaplan-Meier method and the significance of differences in survival rates were determined using log-rank (Mantel-Cox) test with p-value cut-off set at 0.05. The influence of individual genes were determined by stratifying the samples as copy number gain/loss or no change, and significance of difference in survival rates were obtained with log-rank test with p-value cut-off set at 0.05.

We used the tumorscape database (http://www.broadinstitute.org/tumorscape) to assess if the six significant genes obtained in our analysis overlapped with the known peaks of somatic CNA across all cancers (Beroukhim et al., 2010). The ideograms depicting the loci with known somatic CNA peaks and genomic location of the six significant genes were created using the NCBI genome decoration tool (http://www.ncbi.nlm.nih.gov/genome/tools/gdp).

4.2.4 Gene expression analysis

The TCGA pan-cancer RNAseq dataset (Illumina HiSeqV2, version 2014-08-28, RSEM normalized) and all clinical information files were retrieved using the Cancer Browser

(Goldman et al., 2012; Lopez, 2013). For individual TCGA cancer types, RNAseq datasets (Illumina HiSeqV2, version 2014-08-28, RSEM normalized) were retrieved from cBioPortal for cancer genomics (Cerami et al., 2012b). Next, we log2 transformed all mRNA expression data and merged survival data from the clinical information file matched by sample ID.

We classified the genes based on the metastatic potential of each sample denoted by the EMT score. We first calculated the EMT score for each tumor sample in the pan-cancer or individual cancer datasets using the formula: EMT score = Sum of mesenchymal gene expression (*CDH2, FN1, SNAI1, SNAI2, VIM, TWIST1, TWIST2, ZEB2, ZEB2*) - Sum of epithelial gene expression (*CDH1, CLDN4, CLDN7, MUC1, TJP3*). To demonstrate the utility of EMT score as indicator of metastatic potential, we compared the average EMT scores across different pan-cancer subtypes (normal, primary, blood derived and metastatic) using the Tukey's HSD post-hoc test following one-way ANOVA. We further stratified the pan-cancer samples as "low EMT" if EMT score < Avg. EMT score or "high EMT" if EMT score ≥ Avg. EMT score, and assessed the effect on survival rates using the log-rank test. To identify the genes that were associated with activation of the EMT program in the individual cancers, we classified the genes based on their similarity to the EMT score using the nearest neighbor algorithm. The distances were calculated using Pearson's correlation coefficient (family wise error rate controlled, Bonferroni's method), and the significant positive and negative neighbors were used to assess the overall effect on metabolism in samples in context of EMT.

We further evaluated if the expression levels of the individual genes can predict the stratification of the samples in a given cancer type by EMT score. We classified the samples as low or high EMT based on the average EMT score. Using this binary classification of the

samples as the dependent variable, we analyzed the ability of all model genes to predict the classification using logistic regression analysis. For the logistic regression analysis, we used the likelihood ratio method to obtain the variables with significant association with EMT score indicated by the odds ratio (exponentiation of beta coefficient) and 2-tailed p-values from Wald chi-square test of significance. The –log10 transformed p-values were then used to assign ranks in each cancer type (lowest rank = highest p-value). We then summed ranks across all cancer types to obtain a cumulative rank-sum for each gene. Next, we retrieved the top and bottom 5 genes with the lowest and highest cumulative rank-sum, respectively, and clustered the samples (K-means, k =2) based on the expression profiles of the two gene signatures. The sample stratification based on the gene signatures were used to assessed the survival rates of the patients using Kaplan-Meier curve analysis with the log-rank (Mantel-Cox) test.

4.2.5 Statistical analysis

Hierarchical clustering, nearest neighbor analysis and heatmap visualizations were performed using GENE-E matrix analysis platform (http://www.broadinstitute.org/cancer/software/GENE-E/). All other classification and statistical analysis procedures were performed using SPSS Statistics v20.

4.3 Results

In order to identify the metabolic genes that are significantly altered in metastatic cancer cells, we first constructed a literature-derived pathway model of genes that regulate FA metabolism and glycolysis in cancer cells and analyzed for changes in mutations, copy number alterations and mRNA expression patterns that altered significantly in metastatic tumors (Figure 20a). We further validated the clinical relevance of these alterations by their ability to predict patient survival rates. The list of candidate genes in the literature-based model (herein denoted as model genes) was restricted to genes previously reported to be significantly altered between normal and cancer cells, and included enzymes, signaling or transcriptional regulators of glucose metabolism (Warburg effect), FA oxidation, and lipogenesis (including lipolysis and esterifaction) (Figure 20b) (Cairns et al., 2011; Carracedo et al., 2013; Currie et al., 2013; Dang, 2012; Musso et al., 2009a) . Additionally, we included the FA transport genes since elevated uptake of exogenous FFAs contributes to the cellular FA pool (Musso et al., 2009a). To investigate the influence of genetic alterations in the model genes, we compared the mutation, CNA and gene expression profiles of the model genes between tumors classified as primary or metastatic in the TCGA pan-cancer datasets, or against a composite EMT-score in the TCGA datasets of individual cancers. The mRNA expression-based EMT score, consisting of relative expression levels of mesenchymal and epithelial genes, served as a proxy for metastatic status(Salt et al., 2013). Using analysis of variance (ANOVA) test followed by Tukey's post-hoc test, the EMT score was significantly higher in the pan-cancer metastatic tumors than the primary tumors ($p=2.1x10^{-13}$) (Figure 21a). In addition, we evaluated the influence of the EMT score on the patient's prognosis by classifying the samples

by their mean EMT score (Figure 21b), and found significant reduction in survival rates in the high EMT subset ($p=1.6x10^{-20}$).

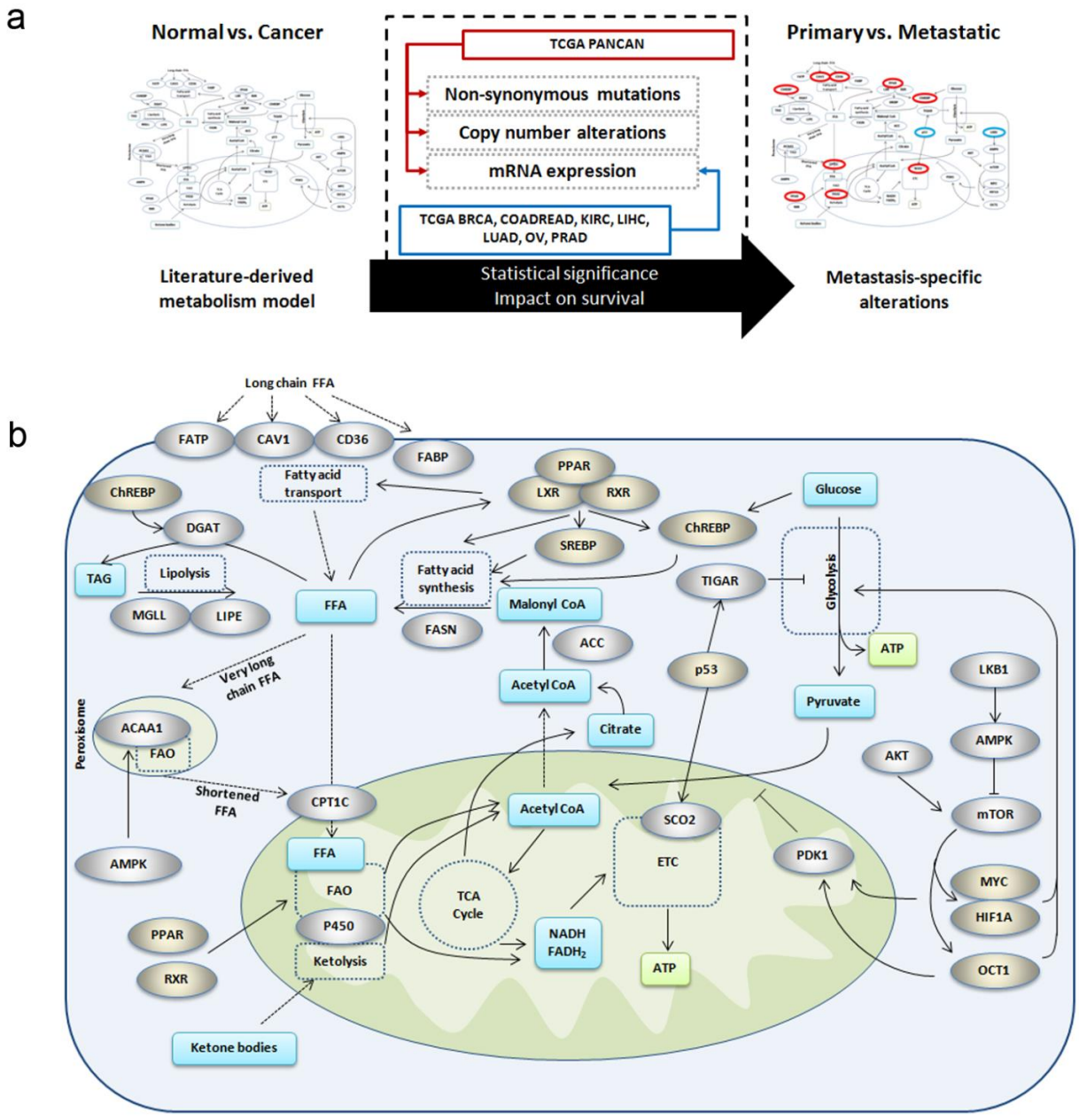

Figure 20: Overview of approach and metabolic alterations in cancer cells.

Figure 20 (cont'd)

A. Schematic showing the approach and datasets used in the study to identify metabolic alterations that are relevant to metastatic progression of cancer cells. Mutation, CNA and mRNA expression data of the genes in the literature-derived model were analyzed for statistical significance in samples stratified by metastatic status. **B.** Literature-derived metabolic pathway model showing the genetic alterations that control glucose and fatty acid metabolism in cancer cells. The genes affecting FA transport were included in the pathway as potential contributors to the FFA pool. Silver ovals = proteins/enzymes, gold ovals = transcription factors, blue box = metabolites, dashed lines = transport, yellow box = ATP.

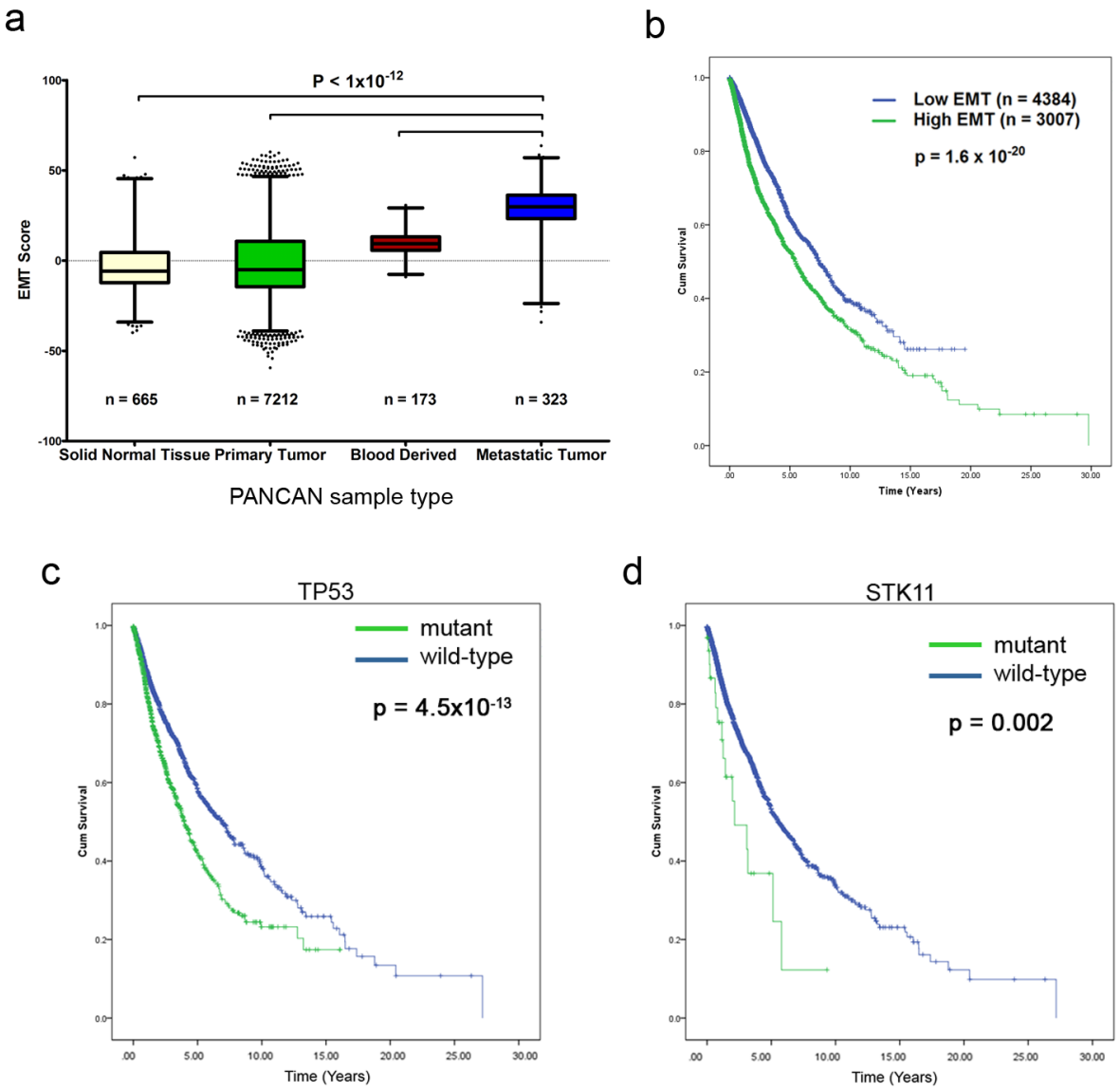

Figure 21. EMT scores and influence of mutations on survival

A. Distribution of EMT scores in different tumor types in the pan-cancer gene expression dataset. Boxplots show mean and SEM with whiskers indicating 1-99th percentile. P-values indicate significance of difference in means from Tukey's HSD post-hoc analysis (following one-way ANOVA). **B.** EMT score as a metric for metastatic potential and impact on patient

Figure 21 (cont'd)

survival rates. Kaplan-Meier survival curve for the pan-cancer patient tumors stratified according to Low EMT (< Avg. EMT score) or High EMT (≥ Avg. EMT score). Kaplan-Meier survival curve for pan-cancer tumors stratified by the mutation status of **C.** *TP53* and **D.** *STK11*. **(B-D).** P-value indicates significance levels from the comparison of survival curves using the Log-rank (Mantel-Cox) test.

4.3.1 Accumulation of FA metabolism gene mutations in metastatic tumors

We evaluated the influence of non-synonymous mutations in the FA metabolism and Warburg effect genes from the pan-cancer dataset. We found that mutations in the tumor suppressors *TP53* ($p=4.5x10^{-13}$) and *STK11* (LKB1, p=0.002) resulted in significant reduction in survival rates (Figure 21c,d). Both *TP53* and *STK11* are among the 127 significantly mutated genes identified in the mutation landscape study of the pan-cancer cohort (Kandoth et al., 2013). In addition, we evaluated the role of cumulative mutations within each model category and found the most frequently mutated genes in the Warburg effect category, however *TP53* alone contributed nearly 97% of the mutations in this group. Thus in the Warburg effect group, mutations in *TP53* and *STK11* contribute significantly to reduced survival rates ($p=2.7x10^{-7}$), whereas mutations in the FA transport and metabolism group of genes did not influence survival. However, when compared to primary tumors, 83% of the FA oxidation, 65% of the lipogenesis and 41% of FA uptake genes exhibited significantly higher mutation frequency in metastatic tumors, whereas only 15% of the Warburg effect genes showed this trend.

We next evaluated the accumulation of CNAs in metastatic tumors. For this analysis, we used the GISTIC2 calls from the pan-cancer CNA dataset to calculate the frequency of patients with either a copy number gain or copy number loss, defined as a GISTIC call ≥1 or ≤1, respectively. We used the Fisher's exact test to compare if the gain or loss frequencies were significantly different between metastatic and primary tumors (Figure 22a). We did not observe significant difference in copy number loss frequencies of any gene between primary and metastatic tumors. However, 6 genes were amplified at significantly higher frequencies in metastatic tumors: *SCO2* ($p=1.1x10^{-9}$), *MLXIPL* ($p=2.1x10^{-4}$), *PPARA* ($p=1.2x10^{-10}$), *PPARD* ($p=4x10^{-15}$), *CAV1* ($p=3.4x10^{-4}$) and *CD36* ($p=3.5x10^{-4}$). To further assess the prognostic role of these genes, we classified the pan-cancer tumors into two clusters using their CNA profiles (Figure 22b). The samples were classified as low copy number (Cluster 1) or high copy number (Cluster 2) based on the 6-genes, identified in the previous step. A Kaplan-Meier curve analysis of the two clusters indicates a reduction in survival rates in the high copy number cluster ($p=3.2x10^{-29}$) (Figure 22c). When compared to the known regions of focal somatic copy number alterations, none of the six genes overlapped with focal peak regions of amplification (Beroukhim et al., 2010) (Figure 22d). However, *CAV1* ($p=8.3x10^{-6}$) and *CD36* ($p=0.01$) were both significantly amplified across all cancers according to the genome-wide GISTIC analysis (http://www.broadinstitute.org/tumorscape).

The carbohydrate response element binding protein ChREBP encoded by *MLXIPL* transcribes lipogenic enzymes *LPK*, *ACC1* and *FASN* and gluconeogenesis enabling enzyme *G6Pase* in response to increased levels of carbohydrates (Iizuka et al., 2004; Uyeda and Repa, 2006a). While the fatty acid synthesis reaction requires NADPH, the switch to aerobic glycolysis in

cancer cells promotes pentose phosphate pathway, which serves as the major source of cellular NADPH (Vander Heiden et al., 2009a). The PPAR transcription factors (*PPARA, PPARD*) transcribe genes that regulate a number of lipid metabolism pathways including lipolysis, fatty acid uptake, oxidation and lipogenesis, and together with the amplification of the fatty acid transporters, *CAV1* and *CD36,* would result in elevated synthesis and accumulation of fatty acids. The expression of *CAV1* has been previously discussed in the context of tumor growth (Sotgia et al., 2012), and has been found to be associated with metastasis and poor prognosis of prostate (Ayala et al., 2013), pancreatic metastasis (Huang et al., 2011) and gastric cancer (Nam et al., 2013). While not as extensively studied, the fatty acid translocase encoding *CD36* has been recently reported to be associated with the progression of breast cancer (DeFilippis et al., 2012), glioblastoma (Hale et al., 2014) and the *in vitro* proliferation of sarcoma and breast cancer cells (Kuemmerle et al., 2011). The p53-regulated *SCO2* gene, encodes a protein that, together with SCO1, regulates the assembly of electron transport chain-associated cytochrome C oxidase complex (Matoba et al., 2006). Mutations in *TP53* downregulate the transcription of *SCO2*, thereby preventing the assembly of this critical OXPHOS complex and increase the cell's reliance on glycolysis for ATP. However, we found that the *SCO2* gene was frequently amplified in metastatic tumors and these alterations corresponded to the mRNA levels of *SCO2* (Figure 23a). Contrary to expectations, *SCO2* mRNA levels were significantly higher in tumors bearing *TP53* mutations (Figure 23b) and higher *SCO2* expression was associated with poorer prognosis (Figure 23c). Additionally, the combined impact of p53 mutation and high *SCO2* expression resulted in the lowest survival rates compared to unaltered state of both genes or altered state of one of the two genes

(Figure 23d). It was reported that both mutations and overexpression of *SCO2* gene can delay the assembly of cytochrome C oxidase on the mitochondrial membrane (Leary et al., 2009). However, it remains to be identified whether SCO2 amplification serves as a mechanism to bypass the influence of p53 mutation on OXPHOS, or whether *SCO2* amplification further disrupts OXPHOS thereby driving the cell towards glycolysis.

In addition to the literature-curated model genes, we also analyzed the influence of the lipid and carbohydrate metabolism gene sets obtained from the REACTOME database. We found that copy number gains in only 2 out of the 471 lipid (*CYP27B1, SUMF2*) and 1 out 235 carbohydrate (*PHKG1*) metabolism genes had a significant impact on survival rates. Further, mutations in only 3 lipid (*NEU3, PIK3CA, PRKD1*) metabolism genes influenced survival rates while none of the carbohydrate metabolism gene mutations had a significant impact. Of the significant CNA and mutation genes, only *PIK3CA* mutations frequency varied significantly between primary and metastatic tumors.

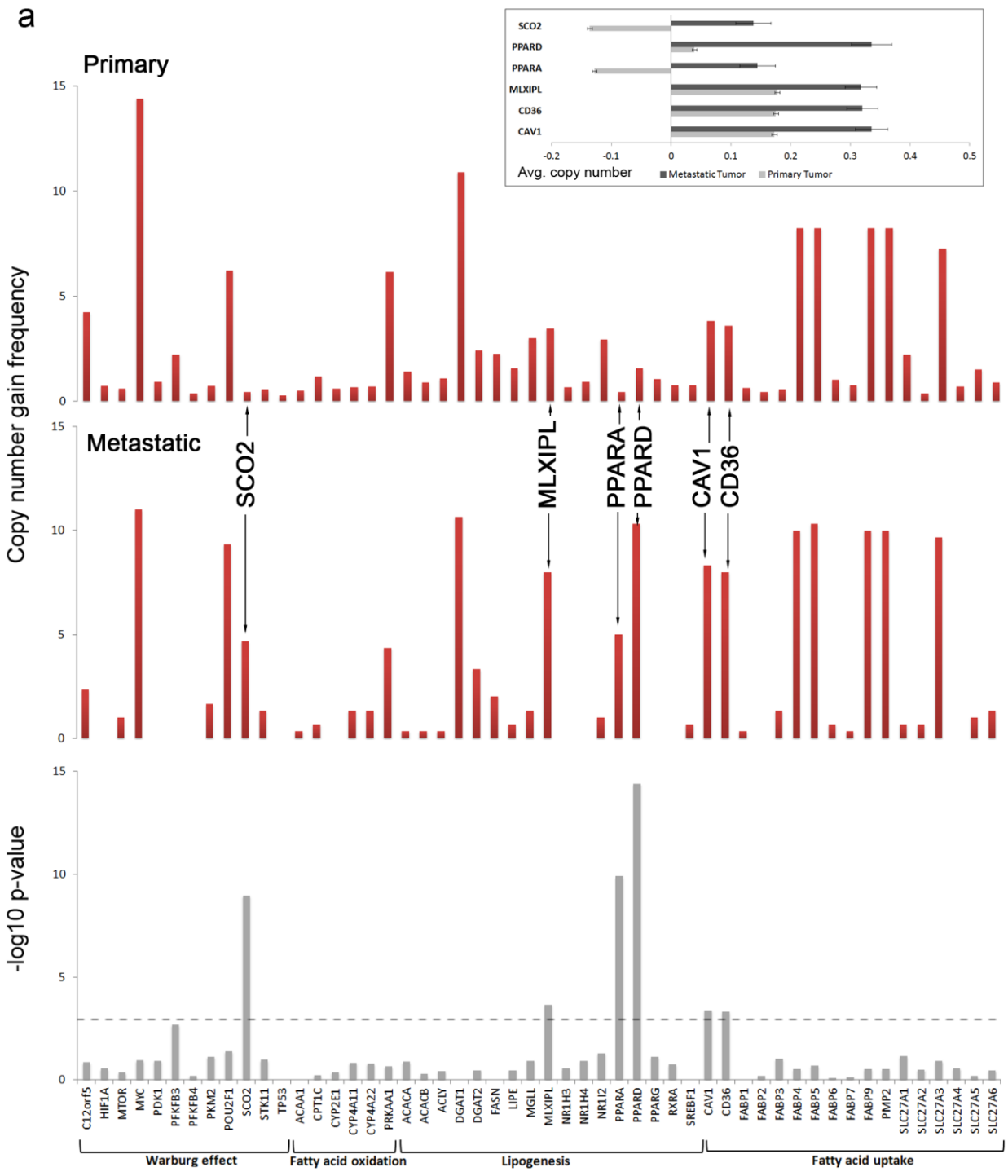

Figure 22. Metabolic gene CNA accumulations in metastatic tumors

Figure 22 (cont'd)

b

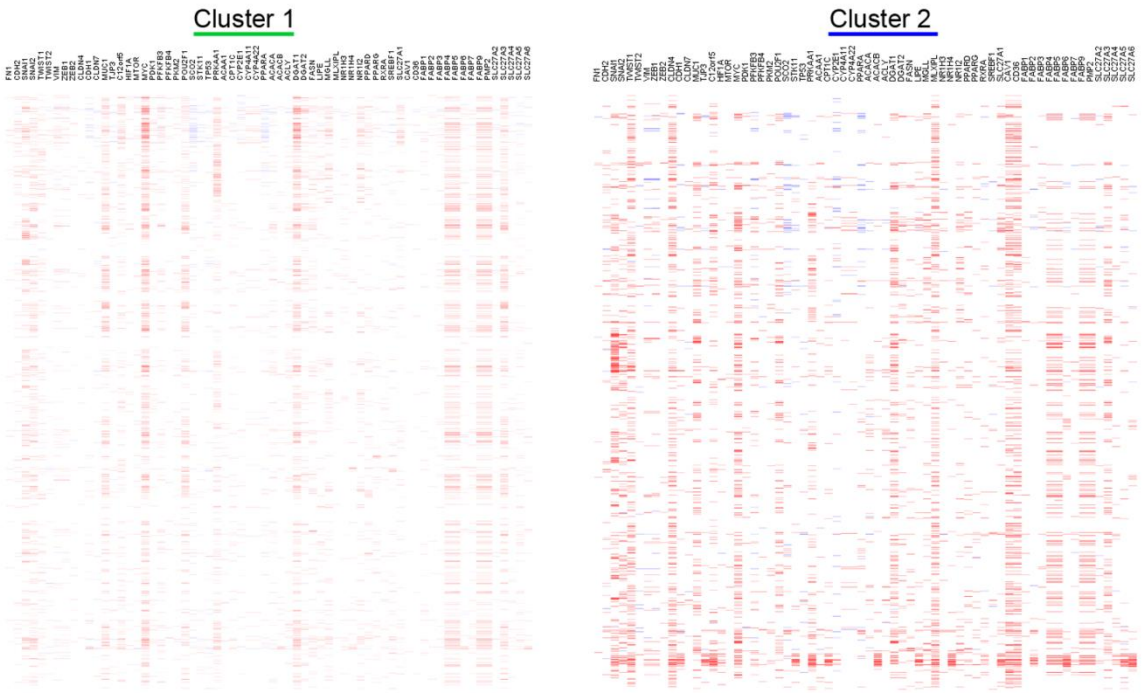

c

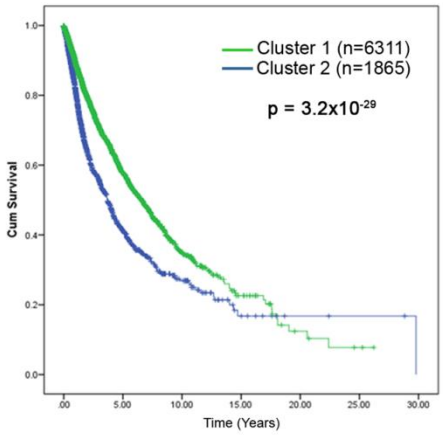

d

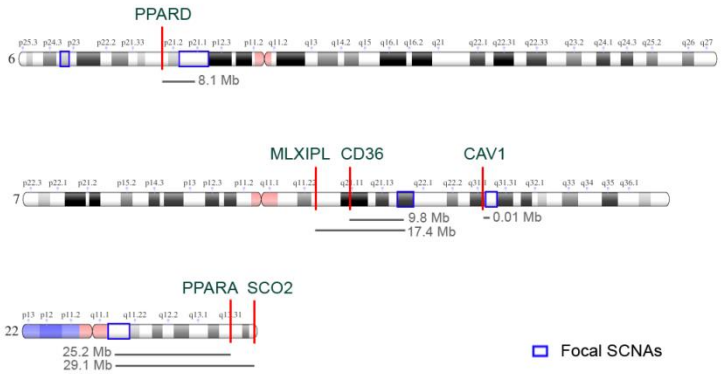

Figure 22 (cont'd)

A. Comparison between primary and metastatic tumors for frequency of tumors with copy number gains in metabolic genes. Red bars indicate the frequency of tumors that show a copy number gain (defined as GISTIC2 normalized copy number gain > 1), grey bars indicate – log10 of the p-value from Fischer's exact test (two-tailed) comparing copy number gain frequency of each gene between primary and metastatic tumors. Inset bar graph shows average copy numbers of the six significant genes in primary and metastatic tumors. **B.** Heatmaps showing copy number alterations in pan-cancer tumors split into clusters. The tumors were clustered (K-means, *k*=2) according to the copy number profiles of the 6 genes with significant accumulation of copy number gains in metastatic tumors (*SCO2, MLXIPL, PPARA, PPARD, CAV1 and CD36*). **C.** Kaplan-Meier survival curve for pan-cancer tumors stratified by the two copy number distribution clusters. P-value indicates significance levels from the comparison of survival curves using the Log-rank (Mantel-Cox) test. **D.** Ideograms depicting the genomic location of the six significant copy number gains. Blue boxes indicate the cytogenetic bands that were identified as focal somatic number alterations gain peaks in the GISTIC analysis of TCGA data across all cancers, and the gray bars show the distance between the six genes to the nearest gain peak.

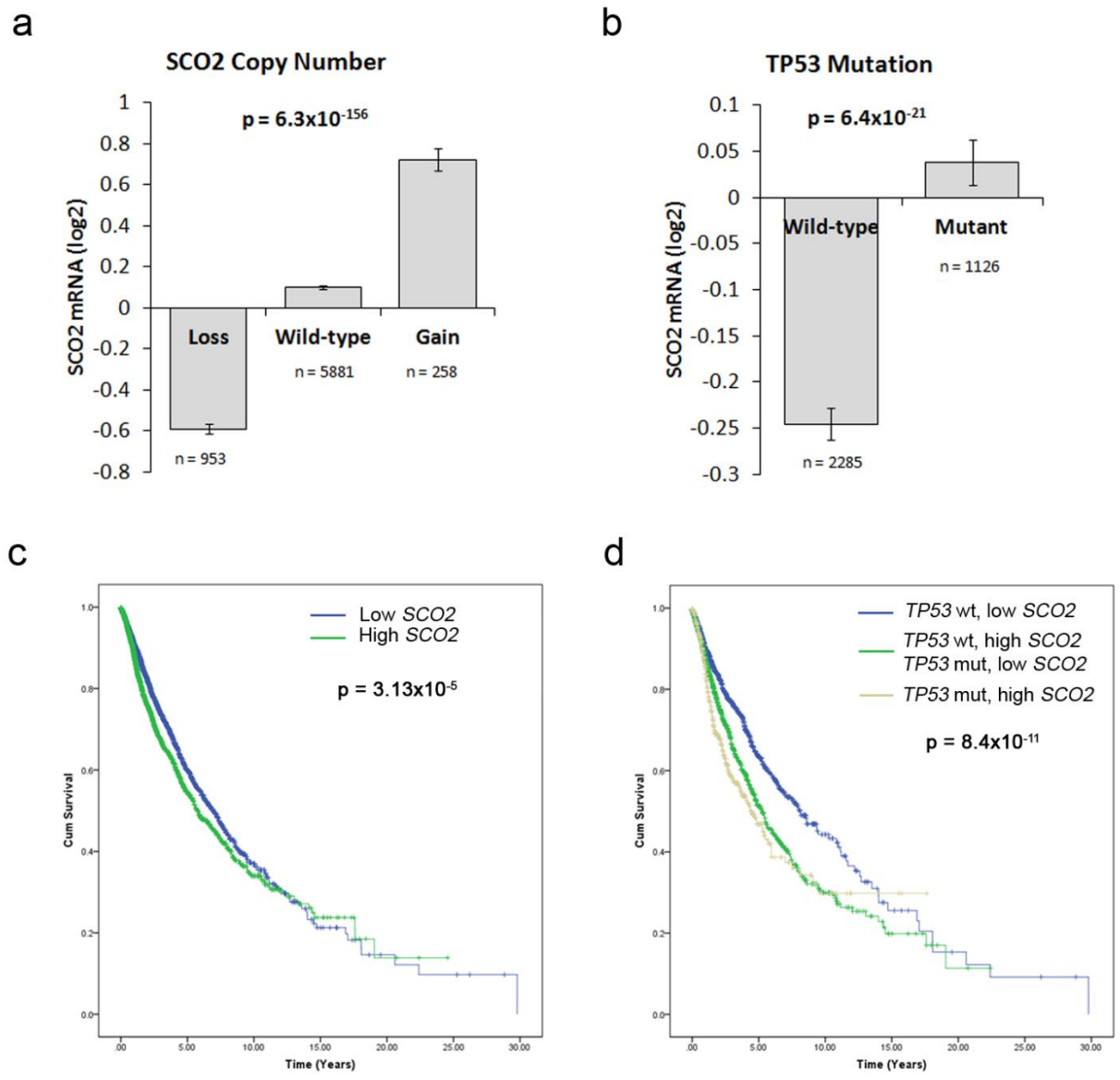

Figure 23. *SCO2* overexpression in *TP53* mutation background

A. Bar graph showing average *SCO2* expression levels in tumors loss or gain in copy number compared to somatic levels in the pan-cancer dataset. **B.** Bar graph showing average expression of *SCO2* in context of p53 mutation background. P-values in **A** and **B** indicate significance level from one-way ANOVA. **C.** Kaplan-Meier survival curves indicating the influence of tumor stratification on the basis of low (n=4366) or high (n=3025) *SCO2*

Figure 23 (cont'd)

expression in the pan-cancer dataset. **D.** Kaplan-Meier survival curves showing the influence of wild-type p53 and low *SCO2* expression (n=1561), wild-type p53 with high *SCO2* expression or mutant p53 with low *SCO2* expression (n=1269), and mutant p53 with high *SCO2* expression (n=495) on the survival rates in the pan-cancer dataset. P-values in **c** and **d** indicate significance levels from the comparison of survival curves using the Log-rank (Mantel-Cox) test.

4.3.2 Establishing a metabolic gene expression signature associated with metastatic progression

We performed an association analysis between the mRNA expression profiles of the model genes and the EMT score for several epithelial cancers from the TCGA database: breast cancer (BRCA), colorectal adenocarcinoma (COADREAD), kidney renal clear cell cancer (KIRC), liver hepatocellular carcinoma (LIHC), lung adenocarcinoma (LUAD), ovarian cancer (OV) and prostate adenocarcinoma (PRAD). Using the nearest neighbor algorithm based on Pearson's correlation with stringent family-wise error rate control (Bonferroni's FWER), we identified the model genes with either significant positive or negative association with EMT score.

An intriguing generalized pattern emerged from this analysis. We found that elevated expression of fatty acid uptake genes, *CAV1* and *CD36,* were consistently associated with a high EMT score across all cancers. We also observed cancer type-specific alterations in the pathways. For instance, in ovarian cancer, the Warburg effect genes typically altered in all other cancer types were not associated with the EMT score. Similarly, the expression levels of

FA oxidation and lipogenesis genes were not associated with the EMT score in lung cancer. One possible explanation may be that the alterations related to Warburg effect in ovarian cancer and FA oxidation/lipogenesis in lung cancer might be early events in the tumorigenesis of these cancer types. These patterns are reflected in the simplified schematics in Figure 24a-g**,** showing the expected influence of the genes significantly associated with EMT score in each cancer type. Here, we note that the processes that could elevate the FFA pool were strongly associated with EMT score. For instance, we observe reduced expression of esterification genes in 4 cancer types, and increased lipolysis in 3 cancer types. Furthermore, the appearance of *CAV1* and *CD36* across the cancer types in this study clearly supports the role of elevated FA uptake and accumulation in the progression and maintenance of metastatic tumors. Overall, we observed that the genes in fatty acid uptake pathway constituted the largest percentage of significant genes associated with EMT score among the four categories analyzed (Figure 24h). Additionally, the largest fractions of significant Warburg effect genes were contributed by the breast cancer dataset, whereas the colorectal cancer contributed the largest fraction of significant FA uptake genes. The breast and colorectal cancer datasets together contributed nearly half of all the significant genes in this analysis.

We next derived a gene signature using a logistic regression based approach to calculate the odds ratio for the influence of each gene on EMT and patient prognosis in individual cancer types (Figure 25a). The genes were ranked based on their influence on EMT score across all the cancer types using a cumulative rank-sum metric obtained from the odds ration p-values (Figure 25b). Based on the cumulative ranks, the top 5 genes identified were *CPT1C, CAV1,*

CD36, MLXIPL, and *CYP2E1*. The fatty acid uptake genes *CAV1* and *CD36,* as well as the carbohydrate response element binding protein encoding *MLXIPL*, also exhibited significant accumulation of copy number gain in the pan-cancer metastatic tumors (Figure 22a). *CPT1C* mediates the uptake of long-chain fatty acid across the mitochondrial membrane to activate β-oxidation, and promotes tumor adaptation under metabolic stress conditions (Zaugg et al., 2011b). *CYP2E1* encodes the mitochondrial cytochrome P450 2E1 protein that is involved in fatty acid, ketone body, ethanol and xenobiotic metabolism. Mutations and over expression of this gene elevates oxidative stress and inflammation (Abdelmegeed et al., 2012), and *CYP2E1* alterations correlated with the development of malignant tumors (Leung et al., 2013; Trafalis et al., 2010). Using the 5-gene signature to classify the pan-cancer samples based on mRNA levels found the high expression cluster (Cluster 2) resulted in dramatic decrease in the survival rates of the patients ($p=1.2x10^{-12}$) (Figure 25c). In contrast, the clusters based on the bottom ranked genes did not influence the survival rates (p=0.421) (Figure 25d). For validation, the prognostic value of the 5-gene signature were used to clustered two independent TCGA datasets that were not used to generate the gene signature – head and neck squamous cell carcinoma (HNSC) and skin cutaneous melanoma (SKCM). The clusters with high expression of the signature genes resulted in significant decrease in survival rates of both head & neck cancer (p=0.003) and melanoma (p=0.006) patients. Thus, the metabolic gene signature identified in the analysis successfully predicted poor prognosis in unrelated cancer dataset, further supporting the role of fatty acid uptake and metabolism in metastatic progression of cancers.

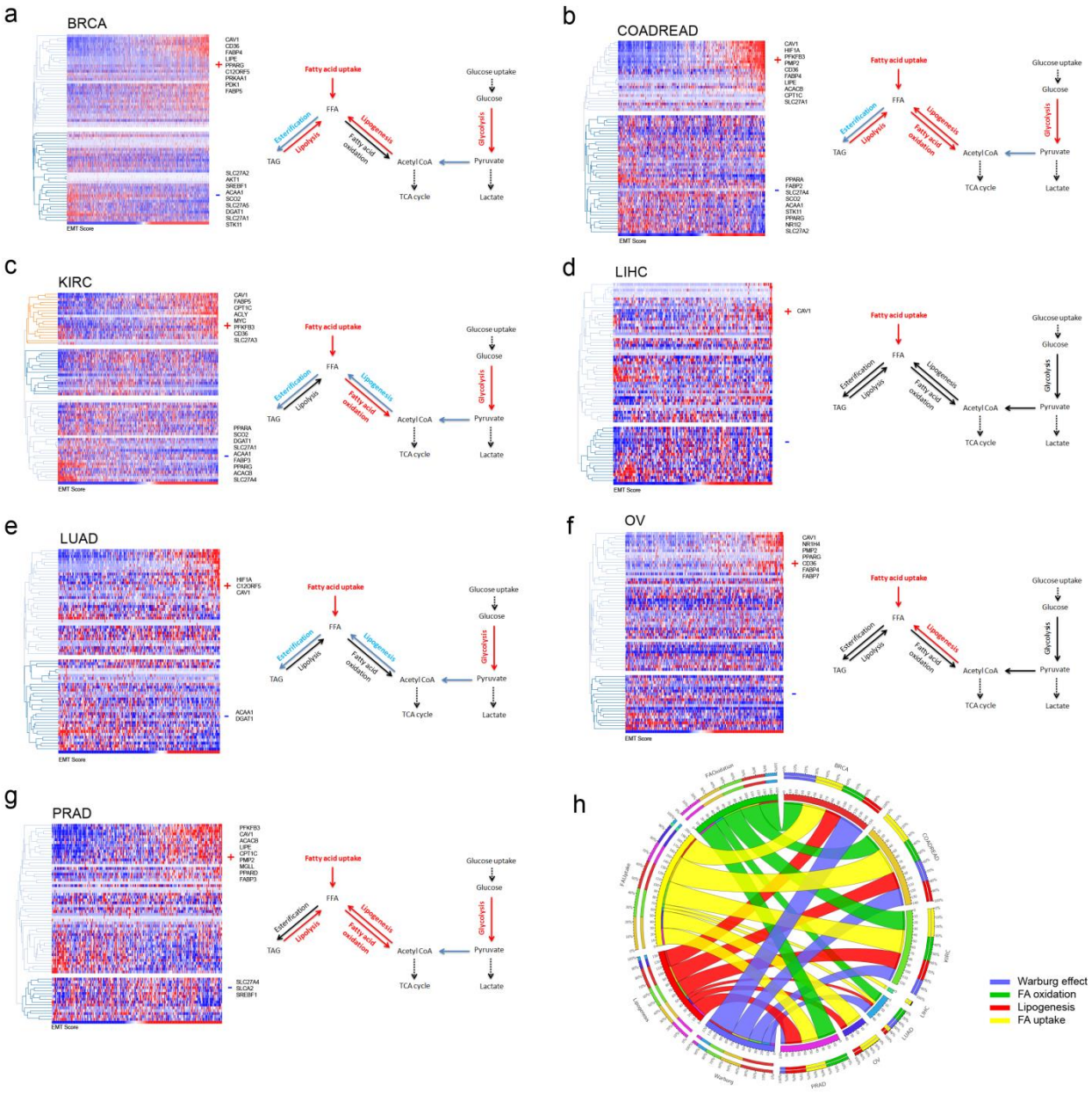

Figure 24. Association between metabolic gene expression and metastatic potential in multiple cancers

Figure 24 (cont'd)

Heatmaps showing expression profiles of EMT and metabolic genes in **A.** Breast invasive carcinoma, BRCA (n=1037) **B.** Colorectal adenocarcinoma, COADREAD (n=352) **C.** KIRC (n=518) **D.** Liver hepatocellular carcinoma LIHC (n=191) **E.** LUAD (n=230) **F.** Ovarian serous cystadenocarcinoma, OV (n=261) **G.** Prostate adenocarcinoma, PRAD (n=236). The tumor samples (X-axis) are ordered according to EMT score shown in bottom row of each heatmap and genes (Y-axis) are arranged in hierarchical clusters (average linkage method, Pearson's correlation distance metric). Genes with significant positive (+) or negative (-) correlation with EMT score are listed next to the heatmap, along with a schematic of the metabolic processes predicted to be altered on the basis of significant correlation in each cancer type. **H.** Circos diagram showing the relationship between the percentage of significant EMT-associated genes within each cancer type and the percent contribution to the total number of significant EMT-associated genes within each model category.

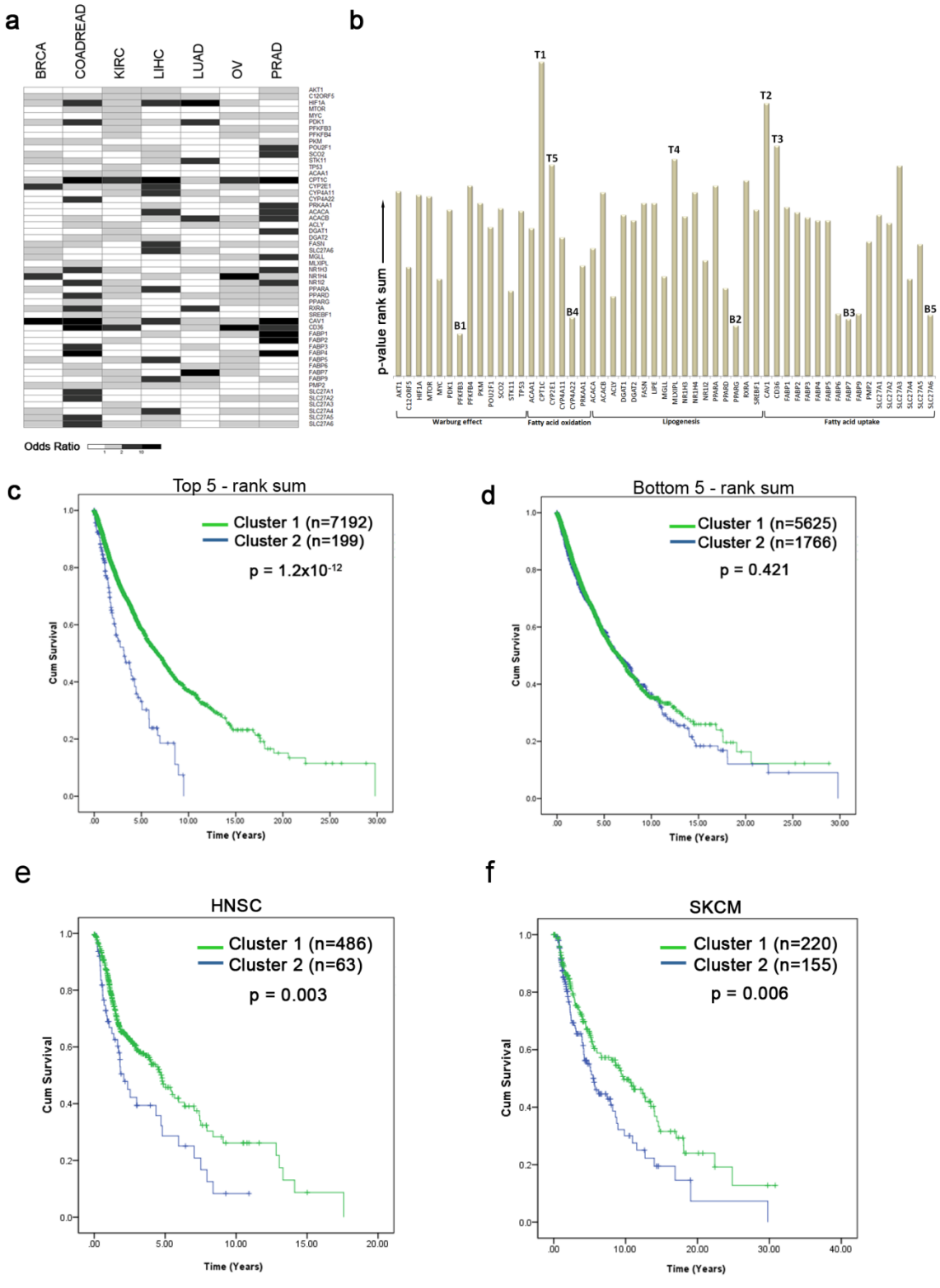

Figure 25. Influence of fatty acid metabolism gene signature on patient survival

Figure 25 (cont'd)

A. Odds ratio obtained from logistic regression analysis demonstrating association between individual metabolism genes and EMT (low or high) across the seven cancer types, with shades of grey indicating increasing odds ratio. **B**. Bar graphs showing cumulative rank sum of odds-ratio –log10 p-value of individual genes across all seven cancer types. T1-5 and B1-5 indicate the five top and bottom ranked genes respectively. **C-D.** Kaplan-Meier survival curve for pan-cancer tumors stratified by two mRNA expression clusters. The sample clusters were obtained by K-means (*k*=2) using (**C**) top 5 genes (*CPT1C, CAV1, CD36, MLXIPL, CYP2E1*) or (**D**) bottom 5 genes (*PFKFB3, PPARG, FABP7, CYP4A22, SLC27A6*) from the rank-sum analysis. P-value indicates significance levels from the comparison of survival curves using the Log-rank (Mantel-Cox) test. **E-F** Kaplan-Meier survival curves for (**E**) head & neck cancer (HNSC) or (**F**) melanoma (SKCM) tumors stratified by the mRNA expression profiles of the top-ranked genes identified in the previous analysis.

4.4 Discussion

In recent years, deregulated glycolysis and fatty acid metabolism has been linked with resistance to chemotherapeutics in multiple cancer types (Zhao et al., 2013). Consequently, the regulators of cancer cell metabolism have emerged as attractive therapeutic targets and primarily include genes that are significantly altered between normal and cancer cells, such as glucose transporters (*GLUT1*, *GLUT4*), hexokinase (*HK1*), pyruvate kinase (*PKM2*) and fatty acid synthase (*FASN*) (Tennant et al., 2010; Vander Heiden, 2011). Given the prognostic impact of the activation of EMT program and metastasis, the objective of this study was to identify the metabolic alterations that are not only relevant to carcinogenesis, but are acquired during metastatic progression of cancer cells. Figure 26 provides a summary of the genes with prognostic consequences that are significantly altered between primary and metastatic tumors (highlighted in red).

One of the prime requirements of rapidly replicating malignant cells is fulfilling increased energy demands. We found that mutations in the tumor suppressor genes that control Warburg effect, *TP53* and *STK11,* uniformly influenced survival rates across all tumors. However, the mutation frequencies were not elevated in metastatic tumors, suggesting that the switch to glycolysis may occur during early stages of cancer progression. Glycolysis produces ATP at greatly reduced efficiency as compared to mitochondrial OXPHOS and in vitro studies with malignant cancer cells have reported that OXPHOS may still contribute to the bulk of ATP produced by cancer cells depending on the availability of oxygen(Guppy et al., 2002; Rodríguez-Enríquez et al., 2008). In such a scenario, alternate pathways must provide the acetyl CoA that is metabolized in the TCA cycle to produce NADH and $FADH_2$ for

ATP synthesis through OXPHOS. β-oxidation of fatty acids could be advantageous to cancer cells by providing a supply of acetyl CoA, NADH and $FADH_2$ during aerobic glycolysis but would require a steady supply of the substrate, free fatty acids. The intracellular pool of free fatty acids can be positively influenced by lipolysis of stored triglycerides, elevated uptake of fatty acids from the environment, or lipogenesis using carbon from carbohydrates, amino acids or oxidized fatty acids. While the upregulation of *FASN* is well documented in cancer cells, we did not observe a significant change in metastatic cells. Instead, we observed significant amplification of *PPARA* and *MXIPL* in metastatic tumors which could upregulate the transcription of lipogenesis genes. Moreover, we found amplifications in the FA uptake genes *CAV1* and *CD36*. While recent studies showed that cancer cells activate lipid scavenging pathways during nutrient starvation (Kamphorst et al., 2013; Young et al., 2013), our results suggest that metastatic cancer cells might increase the cellular FA pool by elevating the uptake of exogenous FAs. Furthermore, we observed gain of *CPT1C* and *CYP2E1* expression which may be indicative of increased mitochondrial FA oxidation in metastatic tumors. Additionally, *CYP2E1* could also contribute to elevated ATP production by facilitating the breakdown of ketone bodies (Bonuccelli et al., 2010). Elevated utilization of ketone bodies in a MDA-MB-231 breast cancer xenograft model (Martinez-Outschoorn et al., 2012) was shown to promote their metastatic potential. These results indicate that alterations in regulators of FA metabolism could be a key adaptation in highly aggressive metastatic cancer cells.

In addition to providing energy, the elevated mitochondrial oxidation of FAs also affect cellular redox status by elevating the levels of reactive oxygen species (ROS) and by reducing the NAD^+/NADH ratio (Furukawa et al., 2004). ROS are well known as potent DNA-damage

inducing agents that not only increase genomic instability to drive malignant transformation, but also influence signaling pathways that increase proliferation and confer resistance to apoptosis (Fruehauf and Meyskens, 2007; Ishikawa et al., 2008; Schumacker, 2006). Elevated NADH levels induce proliferation and migration by repressing transcription of E-cadherin by regulating the activity of CtBP co-repressor (Zhang et al., 2002; Zhang et al., 2006). Recently, reduced NAD^+/NADH ratios were shown to drive the metastatic progression of MDA-MB-435 and MDA-MB-231 breast cancer xenografts by activating AKT/mTOR and autophagy signaling pathways while increasing the NAD^+/NADH ratio inhibited tumor growth (Santidrian et al., 2013).

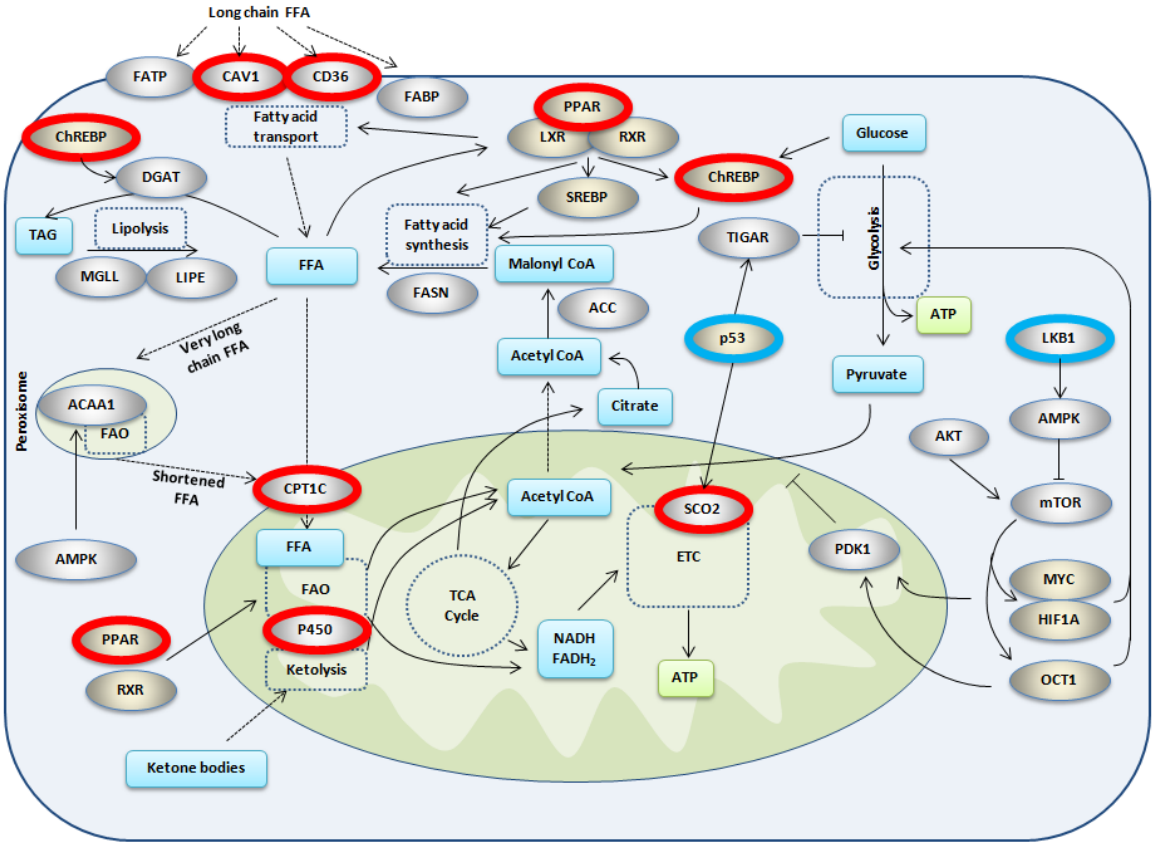

Figure 26. Summary of alterations in metastatic tumors

A. Metabolic pathway model modified to indicate the genes that were identified as significantly altered in metastatic tumors with significant impact on patient prognosis. The red-highlighted ovals show genes with metastasis-associated gain-of-function alterations with prognostic significance. The blue-highlighted ovals show the genes with loss-of-function alterations with prognostic significance in cancer but did not differ between primary and metastatic samples **B.** Distribution of average mRNA expression levels of *SCO2* grouped by CNAs in the pan-cancer dataset. P-value indicates significance level from one-way ANOVA analysis.

Figure 26 (cont'd)

C. Expression levels of *SCO2* in the pan-cancer dataset according to *TP53* mutation background. P-value indicates significance level from one-way ANOVA analysis.

CHAPTER 5: SUMMARY AND FUTURE PERSPECTIVES

5.1 Summary

The objective of this study was to establish the role of elevated free fatty acid uptake in the metastatic progression of hepatocellular carcinoma. In the first part of this study, we applied a network analysis approach as a proof-of-concept to demonstrate the utility of network approaches to identify suitable targets from biological data. We then applied a synergy-based approach to identify insulin signaling and its top-neighbor, DSP, as the top targets in palmitate treated HepG2 cells. By showing that palmitate treatment resulted in loss of DSP, a marker of cells undergoing EMT, we rationalized that elevated FFA levels can potentially activate the EMT program in HCC cells.

In the second part of this study, we studied the relationship between the expression levels of hepatic fatty acid uptake proteins and EMT markers in the publicly available TCGA gene expression dataset, and confirmed our results in human HCC tumor biopsy protein samples. We found that the expression levels of CD36 were significantly associated with the EMT marker expression, while obesity, as indicated by BMI, did not influence EMT score. We further tested the role of elevated FFA levels on the induction of EMT program by assessing the physical and molecular profiles of HepG2 and Hep3B cells treated with palmitate. Our results further demonstrated a population-based expression pattern of EMT marker expression independent of cells undergoing lipotoxicity. We further established that WNT and TGFB signaling pathways mediated palmitate induced EMT, and inhibition of CD36, WNT or TGFB signaling abrogated the migratory effects of palmitate.

In the third part of this study, we extended the hypothesis of altered fatty acid uptake and metabolism promoting EMT and metastasis to multiple cancer types. We first constructed a literature-curated model of metabolic genes altered in cancer cells, including genes regulating glycolysis (Warburg effect), fatty acid oxidation and lipogenesis (including lipolysis and esterification) and fatty acid uptake. We then performed association analysis with the somatic gene-level mutations and CNA data from the 12-tumor type TCGA pan-cancer dataset to identify the metabolic genes significantly enriched in metastatic tumors and demonstrated the functional relevance by analyzing the effect of these alterations on patient survival rates. Additionally, using a logistic regression approach, we established a metabolic gene signature that was correlated with the epithelial to mesenchymal (EMT) gene expression pattern in 7 tumor types and strongly influenced patient survival rates in the pan-cancer as well as in 2 independent tumor types.

Mutations in genes regulating the Warburg effect, *STK11* (LKB1) and *TP53,* uniformly influenced survival rates across all tumor types, but were not specifically enriched in metastatic tumors. Further, *SCO2* – a mitochondrial oxidative phosphorylation gene transcriptionally regulated by *TP53* – was significantly amplified in metastatic tumors and the expression levels of *SCO2* were significantly higher in tumors with TP53 mutation background, contradictory to the expected reduction in transcription. Moreover, the net influence of high *SCO2* expression and *TP53* mutation resulted in the worst prognosis in terms of survival rates, whereas low SCO2 expression and wild-type *TP53* were associated with the highest survival rates.

Amplifications in the fatty acid uptake genes *CAV1* and *CD36* were significantly enriched in metastatic tumors. In addition, genes regulating lipogenesis: *PPARA, PPARD* and *MLXIPL* were also significantly amplified in metastatic tumors. Stratification of the pan-cancer tumors based on the copy number profiles of these 6 genes (including *SCO2*) revealed significant reductions in survival rates. While elevated lipogenesis has been documented in malignant transformation, our results show a strong influence of exogenous fatty acid uptake in metastatic progression.

The mRNA expression levels of fatty acid uptake genes *CAV1* and *CD36*, lipogenesis regulator *MLXIPL*, mitochondrial fatty acid uptake gene *CPT1C,* and the fatty acid oxidation and ketolysis enzyme *CYP2E1,* were identified as the top genes significantly associated with EMT across 7 individual cancer types (breast, colorectal, kidney, lung, liver, ovarian, and prostate). Stratification of the pan-cancer samples based on the mRNA expression profiles of these 5 genes significantly influences survival rates. The prognostic utility of this gene-signature was further verified in two independent cancer types (head and neck, and melanoma).

5.2 Future Perspectives

5.2.1 Regulation of DSP expression and the role of JUP dynamics in EMT program

In this study, we found that palmitate treatment resulted in the significant loss of desmoplakin protein, which served as a rationale for further studying the role of palmitate in inducing EMT in HCC cells. However, the precise role of DSP in the EMT program is not currently known. We profiled the *DSP* expression levels in the TCGA pan-cancer dataset and stratified patients based on low, basal or high *DSP* mRNA expression levels, and observed a

significant reduction in the survival rates of the patients with low *DSP* expression (Figure 27A). The analysis of *DSP* promoter revealed ZEB binding sites, which further led us to speculate that ZEB1 or ZEB2 may be responsible for the repression of *DSP* transcription in HCC and other cancers. By analyzing the mRNA expression data from TCGA pan-cancer, we observed a significant negative correlation between the expression levels of *DSP* and *ZEB1* or *ZEB2* (Figure 27B), a pattern reflected across the pan-cancer datasets (Figure 27C). Furthermore, the mRNA levels of *ZEB1* or *ZEB2* were significantly correlated with the methylation of *DSP* gene (Figure 27D), suggesting that the ZEB transcription factors may be responsible for the transcriptional repression. The loss of DSP could potential lead to the induction of the EMT program itself (Figure 28). One possible mechanism of EMT induction could involve the oncogenic translocation of JUP protein from the desmosomal plaque to the cytoplasm or the nucleus. As DSP function as an obligate component of the desmosomes, the loss of DSP could lead to the disruption of inner plaque thereby releasing JUP into the cytosol. The JUP protein is very similar in structure to β-catenin bearing conserved armadillo repeats involved in the physical interactions with E-cadherin and the GSK3B-AXIN-APC repression complex (Zhurinsky et al., 2000). Thus, the presence of excess free JUP in the cytosol cold possibly outcompete β-catenin from sequestration at the cell junctions or by the repression complex. Furthermore, JUP could also function as transcriptional activator of the Wnt signaling target genes, as the DNA-binding domains of both JUP and β-catenin are similar, and both proteins can interact with the TCF/LEF complex (Maeda et al., 2004). Thus, loss of DSP and translocation of JUP to either the cytoplasm or the nucleus could facilitate the activation of Wnt target genes. Preliminary results indicate that siRNA-mediated *DSP* knockdown indeed

results in nuclear translocation of JUP (Figure 27E). This hypothesis could be further validated using ZEB1 and ZEB2 chromatin immunoprecipations (ChIP) or promoter bash studies with DSP-promoter luciferase reporters. In addition, the translocation of JUP in response to DSP knockdown and correlation with induction of the EMT program could be characterized. The role of DSP loss in promoting tumor growth and metastasis could be further studied in vivo using an HCC model. A liver-specific inducible DSP knockdown (cre-lox) rodent model could be subjected to N-nitrosodiethylamine (DEN) induced hepatocarcinogenesis (Heindryckx et al., 2009). Once the adult animals subjected to DEN treatment develop primary tumors, DSP expression can be disrupted in the liver to study the effect of loss of DSP expression on HCC progression and metastasis.

5.2.2 EMT-promoting molecular pathways induced by PA via direct physical interactions

Alongside the potential influence of DSP loss on EMT induction, palmitate could potentially induce EMT via direct physical interactions with cellular proteins. The transport of WNT ligands across the cell membrane for autocrine or paracrine signaling requires covalent attachment of a palmitate molecule to the WNT ligand by a process known as palmitoylation (Gao et al., 2011). This process is catalyzed by the WNT pathway-specific palmitoyl acetyl-transferase enzyme porcupine (PORCN), which itself requires palmitoylation for activation (Gao and Hannoush, 2013). We have previously found increased activity of serine palmitoyl acetyl-transferase (SPT), an enzyme that catalyzes the covalent attachment of palmitate to L-serine in the ceramide biosynthesis pathway, in animals fed with a high saturated fat diet as well as in response to palmitate treatment in vitro (Geekiyanage and Chan, 2011; Liu et al., 2013b). Thus, the induction of the WNT pathway could be contingent upon palmitoylation of

PORCN and WNT ligands in response to elevated levels of palmitate. Another potential mechanism of EMT induction may involve physical interaction between palmitate and IRE1 to directly induce the ER-stress pathway. Recent studies from our group suggest that palmitate can physically interact with the luminal domain of IRE1 and could result in dimerization and activation of the IRE1 protein (Cho et al., 2012). Thus, the activation of XBP1 and HIF1α downstream of palmitate-induced IRE1 activation could be an alternate mechanism of EMT induction.

5.2.3 Identifying novel drug-targets by applying hierarchical modeling on TCGA data

The role of exogenous FA uptake in malignancies has received less attention compared to alterations in glycolytic pathways and de novo lipogenesis. The revelation from our analysis of the TCGA datasets suggests that association between FA uptake and EMT or metastatic progression is not just restricted to HCC but extends to multiple cancers. Future studies could focus on evaluating the role of alterations in FA uptake genes in conferring drug resistance in retrospective clinical analysis. In addition, the patient-serum levels of FFAs could be included as variables in drug response studies. Further, understanding the precise role of *SCO2* in regulating OXPHOS could reveal new mechanisms by which glycolytic switch is regulated in cancer cells. Importantly, the significant alterations identified from the analysis, including *CAV1*, *CD36*, *MLXIPL*, *CYP2E1*, *CPT1C*, *PPARA* and *PPARD* could be further validated in vitro or in vivo to understand their mechanism in promoting metastasis.

The next phase of TCGA project data release will include clinical information, including the details of chemotherapeutic regimen, duration of treatment and patient response, in multiple cancer types. This data, combined with the existing genomic and transcriptomic data could

be used to predict the role of the fatty acid uptake and metabolism genes in determining drug response and efficacy. In this direction, a hierarchical network of metabolism and EMT genes could be constructed and modeled using TCGA data for all cancers or individual cancer types. This hierarchical model, similar to the one discussed in chapter 2, could be used to simulate the effects of targeting different pathway components which can be validated using actual clinical data. Additionally, the pharmacogenomic analysis of genetic variations in the fatty acid uptake and metabolism genes in context of drug-resistance and efficacy could further establish the clinical utility of these genes as important prognostic biomarkers and as putative drug targets.

One of the biggest challenges that emerged in the post-next generation sequencing era is the identification of new clinically actionable genetic alterations. Apart from a limited number of mutations with large effect-sizes, it remains a major challenge to generate new testable hypotheses from the existing omic data. Thus, an integrated systems biology approach that utilizes domain knowledge and large-scale omic datasets would be useful to understand the complex interactions that influence progression of cancer.

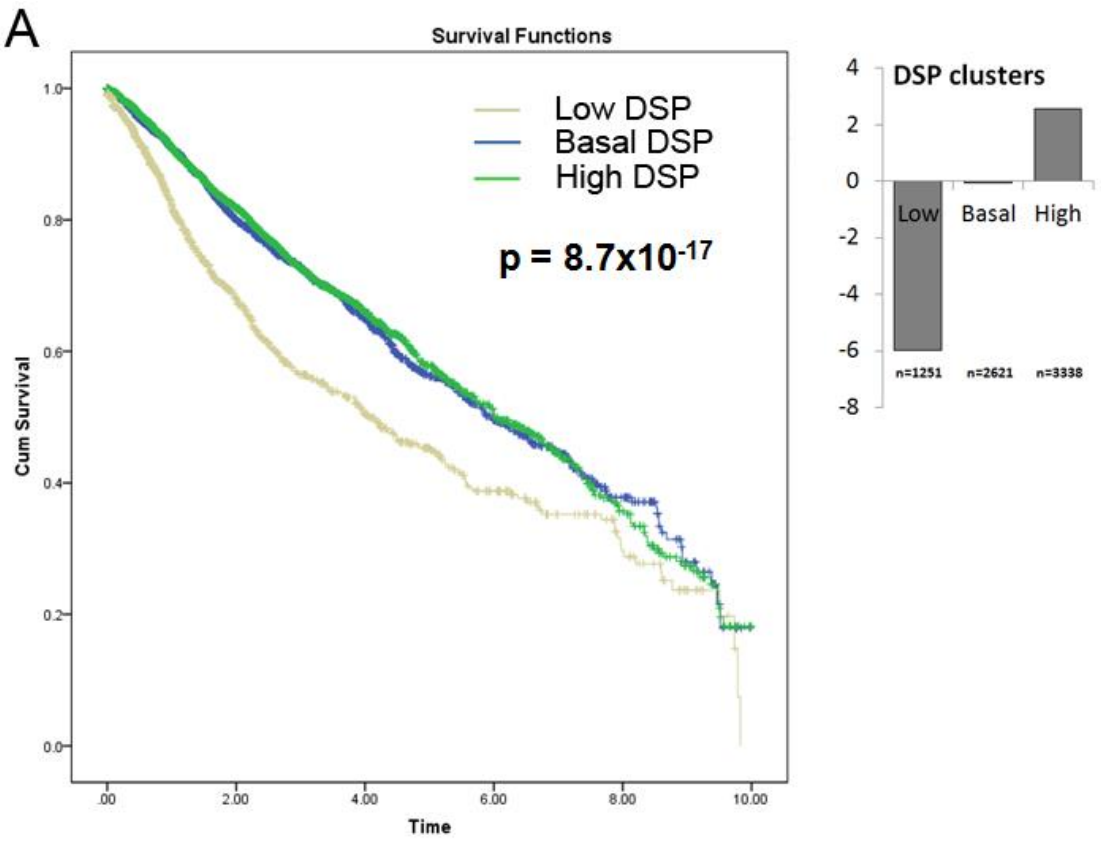

Figure 27. Analysis of DSP in TCGA datasets and effect on DSP knockdown on JUP.

Figure 27 (cont'd)

Figure 27 (cont'd)

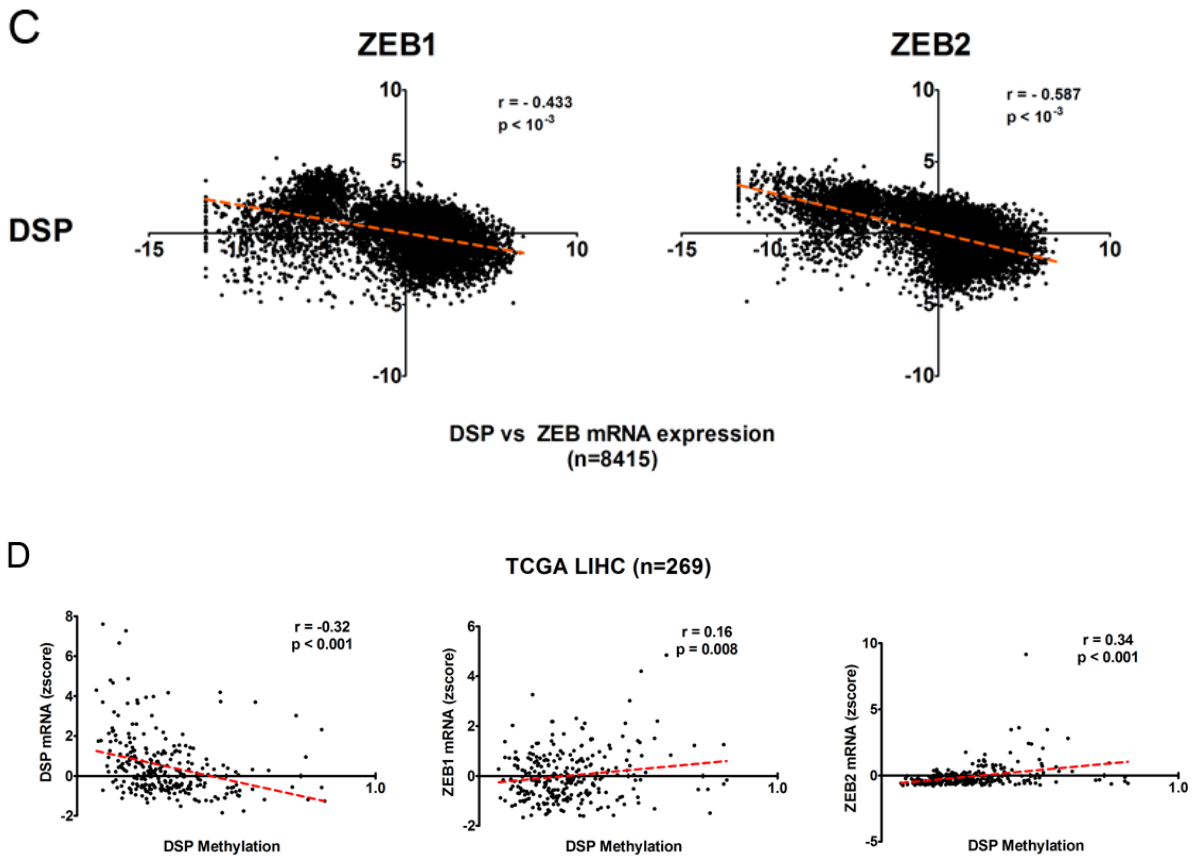

Figure 27 (cont'd)

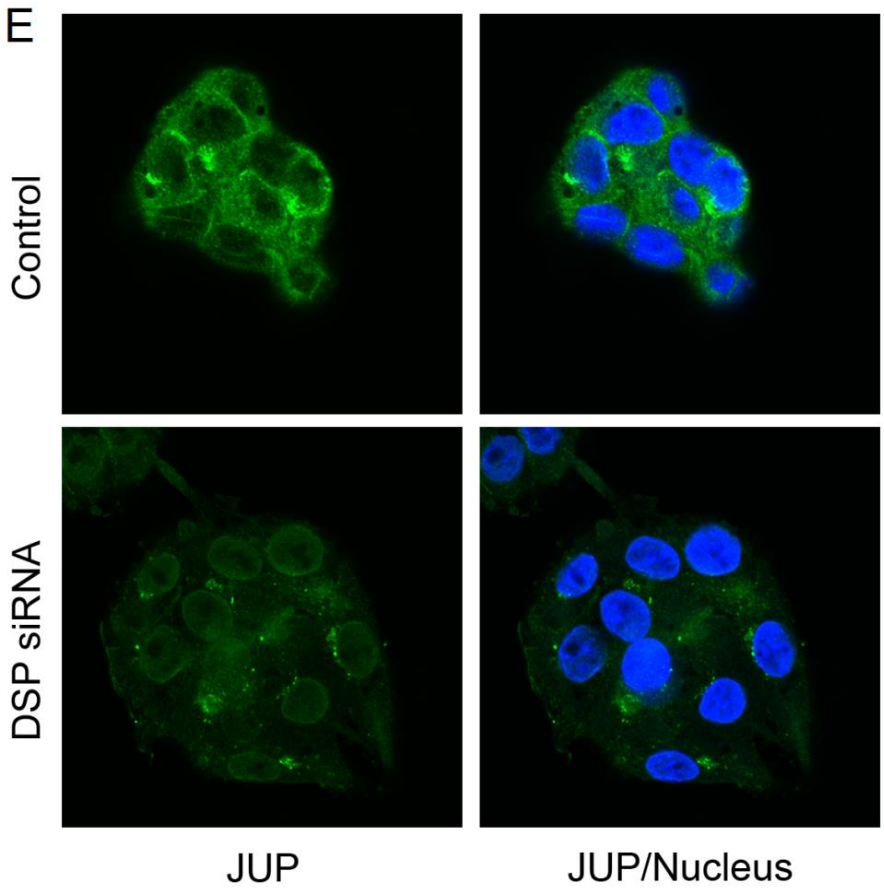

A. Kaplan-Meier survival curves showing the influence of stratification of patients by DSP expression levels. Inset bar graph shows mean DSP mRNA expression in the three groups (low, basal, high). B. The expression profiles of DSP, ZEB1 and ZEB2 (X-axis) across the pan-cancer database grouped by cancer type (Y-axis). Red indicates high expression levels, while blue indicates low expression levels, with inverse patterns observed between DSP and ZEB1 or ZEB2 in almost all cancer types. C-D. Scatter-plots showing correlation between (C) DSP and ZEB1 or ZEB2 expression in pan-cancer dataset or (D) DSP methylation and ZEB1 or ZEB2 expression in TCGA LIHC dataset. Red line indicates linear fit, with r indicating Pearson's correlation coefficient and p-value showing significance of correlation. E. Confocal images

Figure 27 (cont'd)

showing the expression and localization of JUP (green) in control or DSP siRNA knockdown (25mM) HepG2 cells, with blue indicating nucleus.

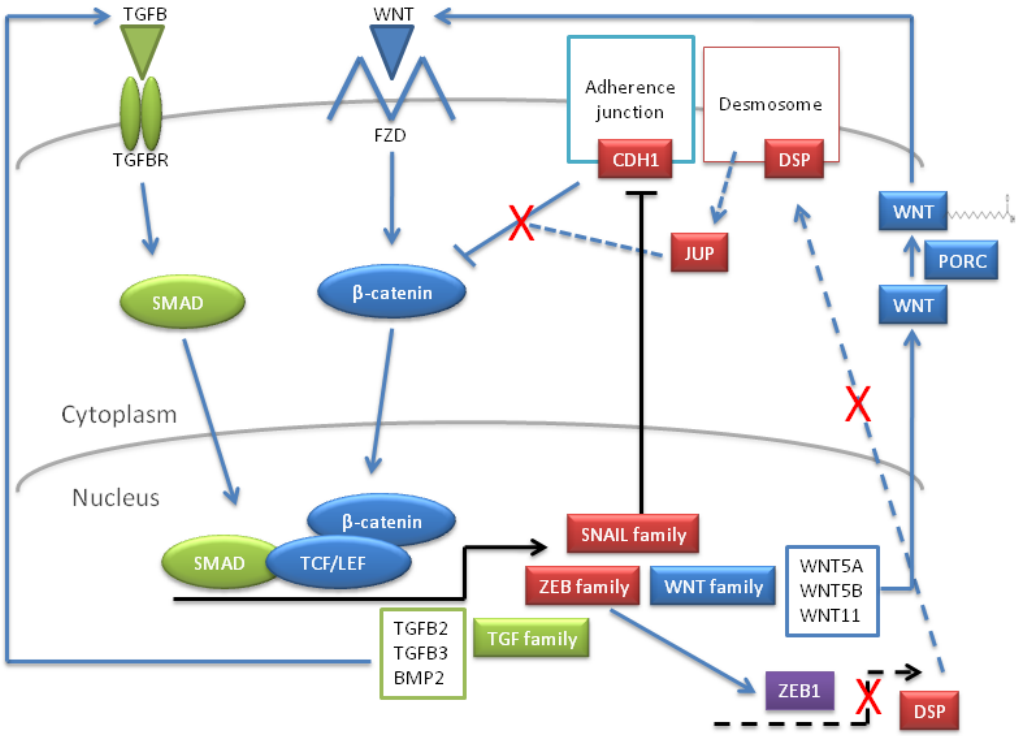

Figure 28. Summary of future studies on mechanism of PA induced EMT.

REFERENCES

REFERENCES

Abdelmegeed, M.A., Banerjee, A., Yoo, S.-H., Jang, S., Gonzalez, F.J., and Song, B.-J. (2012). Critical role of cytochrome P450 2E1 (CYP2E1) in the development of high fat-induced non-alcoholic steatohepatitis. Journal of Hepatology *57*, 860-866.

Abiola, M., Favier, M., Christodoulou-Vafeiadou, E., Pichard, A.L., Martelly, I., and Guillet-Deniau, I. (2009). Activation of Wnt/beta-catenin signaling increases insulin sensitivity through a reciprocal regulation of Wnt10b and SREBP-1c in skeletal muscle cells. PLoS One *4*, e8509.

Ajuwon, K.M., and Spurlock, M.E. (2005). Palmitate activates the NF-kappaB transcription factor and induces IL-6 and TNFalpha expression in 3T3-L1 adipocytes. The Journal of nutrition *135*, 1841-1846.

Alkhouri, N., Dixon, L.J., and Feldstein, A.E. (2009). Lipotoxicity in nonalcoholic fatty liver disease: not all lipids are created equal. Expert Review of Gastroenterology & Hepatology *3*, 445-451.

Altekruse, S.F., Henley, S.J., Cucinelli, J.E., and McGlynn, K.A. (2014). Changing Hepatocellular Carcinoma Incidence and Liver Cancer Mortality Rates in the United States. The American Journal of Gastroenterology *109*, 542-553.

Altekruse, S.F., McGlynn, K.A., Dickie, L.A., and Kleiner, D.E. (2012). Hepatocellular carcinoma confirmation, treatment, and survival in surveillance, epidemiology, and end results registries, 1992-2008. Hepatology *55*, 476-482.

Altekruse, S.F., McGlynn, K.A., and Reichman, M.E. (2009). Hepatocellular carcinoma incidence, mortality, and survival trends in the United States from 1975 to 2005. Journal of clinical oncology : official journal of the American Society of Clinical Oncology *27*, 1485-1491.

Amberger, J., Bocchini, C.A., Scott, A.F., and Hamosh, A. (2009). McKusick's Online Mendelian Inheritance in Man (OMIM(R)). Nucleic Acids Research *37*, D793-D796.

Amemiya-Kudo, M., Oka, J., Ide, T., Matsuzaka, T., Sone, H., Yoshikawa, T., Yahagi, N., Ishibashi, S., Osuga, J., Yamada, N., *et al.* (2005). Sterol regulatory element-binding proteins activate insulin gene promoter directly and indirectly through synergy with BETA2/E47. J Biol Chem *280*, 34577-34589.

Anastassiou, D. (2007). Computational analysis of the synergy among multiple interacting genes. Molecular systems biology *3*, 83.

Anderson, A.A., Helmering, J., Juan, T., Li, C.M., McCormick, J., Graham, M., Baker, D.M., Damore, M.A., Veniant, M.M., and Lloyd, D.J. (2009). Pancreatic islet expression profiling in diabetes-prone C57BLKS/J mice reveals transcriptional differences contributed by DBA loci, including Plagl1 and Nnt. Pathogenetics *2*, 1.

Andriole, G.L., Bostwick, D.G., Brawley, O.W., Gomella, L.G., Marberger, M., Montorsi, F., Pettaway, C.A., Tammela, T.L., Teloken, C., Tindall, D.J., *et al.* (2010). Effect of dutasteride on the risk of prostate cancer. N Engl J Med *362*, 1192-1202.

Angulo, P. (2007). Obesity and nonalcoholic fatty liver disease. Nutr Rev *65*, S57-63.

Arden, K.C., Viars, C.S., Fu, K., and Rozen, R. (1995). Localization of short/branched chain acyl-CoA dehydrogenase (ACADSB) to human chromosome 10. Genomics *25*, 743-745.

Arii, S., Yamaoka, Y., Futagawa, S., Inoue, K., Kobayashi, K., Kojiro, M., Makuuchi, M., Nakamura, Y., Okita, K., and Yamada, R. (2000). Results of surgical and nonsurgical treatment for small-sized hepatocellular carcinomas: a retrospective and nationwide survey in Japan. The Liver Cancer Study Group of Japan. Hepatology *32*, 1224-1229.

Attard, G., Reid, A.H.M., A'Hern, R., Parker, C., Oommen, N.B., Folkerd, E., Messiou, C., Molife, L.R., Maier, G., Thompson, E., *et al.* (2009). Selective Inhibition of CYP17 With Abiraterone Acetate Is Highly Active in the Treatment of Castration-Resistant Prostate Cancer. Journal of Clinical Oncology *27*, 3742-3748.

Ayala, G., Morello, M., Frolov, A., You, S., Li, R., Rosati, F., Bartolucci, G., Danza, G., Adam, R.M., Thompson, T.C., *et al.* (2013). Loss of caveolin-1 in prostate cancer stroma correlates with reduced relapse-free survival and is functionally relevant to tumour progression. The Journal of Pathology *231*, 77-87.

Baffy, G., Brunt, E.M., and Caldwell, S.H. (2012). Hepatocellular carcinoma in non-alcoholic fatty liver disease: An emerging menace. Journal of Hepatology *56*, 1384-1391.

Bagnardi, V., Blangiardo, M., La Vecchia, C., and Corrao, G. (2001). A meta-analysis of alcohol drinking and cancer risk. British journal of cancer *85*, 1700-1705.

Bakiri, L., Macho-Maschler, S., Custic, I., Niemiec, J., Guío-Carrión, A., Hasenfuss, S.C., Eger, A., Müller, M., Beug, H., and Wagner, E.F. (2014). Fra-1/AP-1 induces EMT in mammary epithelial cells by modulating Zeb1/2 and TGFβ expression. Cell Death and Differentiation.

Bandyopadhyay, S., Chiang, C.Y., Srivastava, J., Gersten, M., White, S., Bell, R., Kurschner, C., Martin, C.H., Smoot, M., Sahasrabudhe, S., *et al.* (2010). A human MAP kinase interactome. Nat Methods *7*, 801-805.

Bartlett, J.M.S., Brawley, D., Grigor, K., Munro, A.F., Dunne, B., and Edwards, J. (2005). Type I receptor tyrosine kinases are associated with hormone escape in prostate cancer. The Journal of Pathology *205*, 522-529.

Bass-Zubek, A.E., Hobbs, R.P., Amargo, E.V., Garcia, N.J., Hsieh, S.N., Chen, X., Wahl, J.K., 3rd, Denning, M.F., and Green, K.J. (2008). Plakophilin 2: a critical scaffold for PKC alpha that regulates intercellular junction assembly. J Cell Biol *181*, 605-613.

Batlle, E., Sancho, E., Franci, C., Dominguez, D., Monfar, M., Baulida, J., and Garcia De Herreros, A. (2000). The transcription factor snail is a repressor of E-cadherin gene expression in epithelial tumour cells. Nature cell biology *2*, 84-89.

Batra, S.K., Cheng, Z.-X., Sun, B., Wang, S.-J., Gao, Y., Zhang, Y.-M., Zhou, H.-X., Jia, G., Wang, Y.-W., Kong, R., *et al.* (2011). Nuclear Factor-κB–Dependent Epithelial to Mesenchymal Transition Induced by HIF-1α Activation in Pancreatic Cancer Cells under Hypoxic Conditions. PloS one *6*, e23752.

Battaglia, S., Benzoubir, N., Nobilet, S., Charneau, P., Samuel, D., Zignego, A.L., Atfi, A., Brechot, C., and Bourgeade, M.F. (2009). Liver cancer-derived hepatitis C virus core proteins shift TGF-beta responses from tumor suppression to epithelial-mesenchymal transition. PLoS One *4*, e4355.

Bernier, J., Hall, E.J., and Giaccia, A. (2004). Radiation oncology: a century of achievements. Nat Rev Cancer *4*, 737-747.

Beroukhim, R., Mermel, C.H., Porter, D., Wei, G., Raychaudhuri, S., Donovan, J., Barretina, J., Boehm, J.S., Dobson, J., Urashima, M., *et al.* (2010). The landscape of somatic copy-number alteration across human cancers. Nature *463*, 899-905.

Bhardwaj, N., Kim, P.M., and Gerstein, M.B. (2010). Rewiring of transcriptional regulatory networks: hierarchy, rather than connectivity, better reflects the importance of regulators. Sci Signal *3*, ra79.

Bianchini, F., Kaaks, R., and Vainio, H. (2002). Overweight, obesity, and cancer risk. The Lancet Oncology *3*, 565-574.

Bieghs, V., Wouters, K., van Gorp, P.J., Gijbels, M.J.J., de Winther, M.P.J., Binder, C.J., Lütjohann, D., Febbraio, M., Moore, K.J., van Bilsen, M., *et al.* (2010). Role of Scavenger Receptor A and CD36 in Diet-Induced Nonalcoholic Steatohepatitis in Hyperlipidemic Mice. Gastroenterology *138*, 2477-2486.e2473.

Bolos, V., Peinado, H., Perez-Moreno, M.A., Fraga, M.F., Esteller, M., and Cano, A. (2003). The transcription factor Slug represses E-cadherin expression and induces epithelial to mesenchymal transitions: a comparison with Snail and E47 repressors. J Cell Sci *116*, 499-511.

Bonuccelli, G., Tsirigos, A., Whitaker-Menezes, D., Pavlides, S., Pestell, R.G., Chiavarina, B., Frank, P.G., Flomenberg, N., Howell, A., Martinez-Outschoorn, U.E., *et al.* (2010). Ketones and lactate "fuel" tumor growth and metastasis: Evidence that epithelial cancer cells use oxidative mitochondrial metabolism. Cell cycle *9*, 3506-3514.

Borradaile, N.M., Buhman, K.K., Listenberger, L.L., Magee, C.J., Morimoto, E.T., Ory, D.S., and Schaffer, J.E. (2006). A critical role for eukaryotic elongation factor 1A-1 in lipotoxic cell death. Mol Biol Cell *17*, 770-778.

Brabletz, T., Jung, A., Spaderna, S., Hlubek, F., and Kirchner, T. (2005). Opinion: migrating cancer stem cells - an integrated concept of malignant tumour progression. Nature reviews Cancer *5*, 744-749.

Bralet, M.P., Regimbeau, J.M., Pineau, P., Dubois, S., Loas, G., Degos, F., Valla, D., Belghiti, J., Degott, C., and Terris, B. (2000). Hepatocellular carcinoma occurring in nonfibrotic liver: epidemiologic and histopathologic analysis of 80 French cases. Hepatology *32*, 200-204.

Bramson, H.N., Hermann, D., Batchelor, K.W., Lee, F.W., James, M.K., and Frye, S.V. (1997). Unique preclinical characteristics of GG745, a potent dual inhibitor of 5AR. J Pharmacol Exp Ther *282*, 1496-1502.

Broqua, P., Riviere, P.J., Conn, P.M., Rivier, J.E., Aubert, M.L., and Junien, J.L. (2002). Pharmacological profile of a new, potent, and long-acting gonadotropin-releasing hormone antagonist: degarelix. J Pharmacol Exp Ther *301*, 95-102.

Brown, M.S., and Goldstein, J.L. (1997). The SREBP pathway: regulation of cholesterol metabolism by proteolysis of a membrane-bound transcription factor. Cell *89*, 331-340.

Brundert, M., Heeren, J., Merkel, M., Carambia, A., Herkel, J., Groitl, P., Dobner, T., Ramakrishnan, R., Moore, K.J., and Rinninger, F. (2011). Scavenger receptor CD36 mediates uptake of high density lipoproteins in mice and by cultured cells. The Journal of Lipid Research *52*, 745-758.

Buffa, L., Fuchs, E., Pietropaolo, M., Barr, F., and Solimena, M. (2008). ICA69 is a novel Rab2 effector regulating ER-Golgi trafficking in insulinoma cells. Eur J Cell Biol *87*, 197-209.

Bugianesi, E. (2007). Non-alcoholic Steatohepatitis and Cancer. Clinics in Liver Disease *11*, 191-207.

Bugianesi, E., McCullough, A.J., and Marchesini, G. (2005). Insulin resistance: a metabolic pathway to chronic liver disease. Hepatology *42*, 987-1000.

Butcher, E.C. (2005). Can cell systems biology rescue drug discovery? Nat Rev Drug Discov *4*, 461-467.

Cairns, R.A., Harris, I.S., and Mak, T.W. (2011). Regulation of cancer cell metabolism. Nature Reviews Cancer *11*, 85-95.

Calkins, C.C., Setzer, S.V., Jennings, J.M., Summers, S., Tsunoda, K., Amagai, M., and Kowalczyk, A.P. (2005). Desmoglein Endocytosis and Desmosome Disassembly Are Coordinated Responses to Pemphigus Autoantibodies. Journal of Biological Chemistry *281*, 7623-7634.

Calle, E.E., and Kaaks, R. (2004). Overweight, obesity and cancer: epidemiological evidence and proposed mechanisms. Nature Reviews Cancer *4*, 579-591.

Calle, E.E., Rodriguez, C., Walker-Thurmond, K., and Thun, M.J. (2003). Overweight, Obesity, and Mortality from Cancer in a Prospectively Studied Cohort of U.S. Adults. New England Journal of Medicine *348*, 1625-1638.

Cancer Genome Atlas Research, N. (2008). Comprehensive genomic characterization defines human glioblastoma genes and core pathways. Nature *455*, 1061-1068.

Canil, C.M. (2004). Randomized Phase II Study of Two Doses of Gefitinib in Hormone-Refractory Prostate Cancer: A Trial of the National Cancer Institute of Canada-Clinical Trials Group. Journal of Clinical Oncology *23*, 455-460.

Cao, Y., Chang, H., Li, L., Cheng, R.C., and Fan, X.N. (2007). Alteration of adhesion molecule expression and cellular polarity in hepatocellular carcinoma. Histopathology *51*, 528-538.

Carracedo, A., Cantley, L.C., and Pandolfi, P.P. (2013). Cancer metabolism: fatty acid oxidation in the limelight. Nature Reviews Cancer *13*, 227-232.

Ceddia, R.B. (2005). Direct metabolic regulation in skeletal muscle and fat tissue by leptin: implications for glucose and fatty acids homeostasis. Int J Obes (Lond) *29*, 1175-1183.

Cerami, E., Gao, J., Dogrusoz, U., Gross, B.E., Sumer, S.O., Aksoy, B.A., Jacobsen, A., Byrne, C.J., Heuer, M.L., Larsson, E., *et al.* (2012a). The cBio cancer genomics portal: an open platform for exploring multidimensional cancer genomics data. Cancer discovery *2*, 401-404.

Cerami, E., Gao, J., Dogrusoz, U., Gross, B.E., Sumer, S.O., Aksoy, B.A., Jacobsen, A., Byrne, C.J., Heuer, M.L., Larsson, E., *et al.* (2012b). The cBio Cancer Genomics Portal: An Open Platform for Exploring Multidimensional Cancer Genomics Data. Cancer discovery *2*, 401-404.

Cha, J.Y., and Repa, J.J. (2007). The liver X receptor (LXR) and hepatic lipogenesis. The carbohydrate-response element-binding protein is a target gene of LXR. The Journal of biological chemistry *282*, 743-751.

Chabner, B.A., and Roberts, T.G., Jr. (2005). Timeline: Chemotherapy and the war on cancer. Nat Rev Cancer *5*, 65-72.

Chalasani, N., Gorski, J.C., Asghar, M.S., Asghar, A., Foresman, B., Hall, S.D., and Crabb, D.W. (2003). Hepatic cytochrome P450 2E1 activity in nondiabetic patients with nonalcoholic steatohepatitis. Hepatology *37*, 544-550.

Chen, A.E., Ginty, D.D., and Fan, C.M. (2005). Protein kinase A signalling via CREB controls myogenesis induced by Wnt proteins. Nature *433*, 317-322.

Chen, X., Iliopoulos, D., Zhang, Q., Tang, Q., Greenblatt, M.B., Hatziapostolou, M., Lim, E., Tam, W.L., Ni, M., Chen, Y., *et al.* (2014). XBP1 promotes triple-negative breast cancer by controlling the HIF1α pathway. Nature *508*, 103-107.

Cheung, O., and Sanyal, A.J. (2008). Abnormalities of lipid metabolism in nonalcoholic fatty liver disease. Seminars in liver disease *28*, 351-359.

Chiarugi, V., Magnelli, L., and Gallo, O. (1998). Cox-2, iNOS and p53 as play-makers of tumor angiogenesis (review). Int J Mol Med *2*, 715-719.

Chidgey, M., and Dawson, C. (2007). Desmosomes: a role in cancer? British journal of cancer *96*, 1783-1787.

Cho, H., Fang, L., Feig, M., and Chan, C. (2012). Molecular Mechanism of Activation of IRE1α Cytosolic Domain by Palmitate. Biophysical Journal *102*, 627a-628a.

Cho, H., Wu, M., Zhang, L., Thompson, R., Nath, A., and Chan, C. (2013). Signaling dynamics of palmitate-induced ER stress responses mediated by ATF4 in HepG2 cells. BMC systems biology *7*, 9.

Chong, M.P., Barritt, G.J., and Crouch, M.F. (2004). Insulin potentiates EGFR activation and signaling in fibroblasts. Biochem Biophys Res Commun *322*, 535-541.

Chuang, H.Y., Lee, E., Liu, Y.T., Lee, D., and Ideker, T. (2007). Network-based classification of breast cancer metastasis. Mol Syst Biol *3*, 140.

Chun, Y.S., Huang, M., Rink, L., and Von Mehren, M. (2014). Expression levels of insulin-like growth factors and receptors in hepatocellular carcinoma: a retrospective study. World journal of surgical oncology *12*, 231.

Ciriello, G., Miller, M.L., Aksoy, B.A., Senbabaoglu, Y., Schultz, N., and Sander, C. (2013). Emerging landscape of oncogenic signatures across human cancers. Nature Genetics *45*, 1127-1133.

ClinicalTrials.gov (2011). Study of Ruxolitinib (INCB018424) Administered Orally to Patients With Androgen Independent Metastatic Prostate Cancer. http://clinicaltrialsgov/ct2/show/results/NCT00638378.

Colomiere, M., Ward, A.C., Riley, C., Trenerry, M.K., Cameron-Smith, D., Findlay, J., Ackland, L., and Ahmed, N. (2008). Cross talk of signals between EGFR and IL-6R through JAK2/STAT3 mediate epithelial–mesenchymal transition in ovarian carcinomas. British journal of cancer *100*, 134-144.

Comijn, J., Berx, G., Vermassen, P., Verschueren, K., van Grunsven, L., Bruyneel, E., Mareel, M., Huylebroeck, D., and van Roy, F. (2001). The two-handed E box binding zinc finger protein SIP1 downregulates E-cadherin and induces invasion. Molecular cell *7*, 1267-1278.

Coort, S.L., Willems, J., Coumans, W.A., van der Vusse, G.J., Bonen, A., Glatz, J.F., and Luiken, J.J. (2002). Sulfo-N-succinimidyl esters of long chain fatty acids specifically inhibit fatty acid translocase (FAT/CD36)-mediated cellular fatty acid uptake. Molecular and cellular biochemistry *239*, 213-219.

Currie, E., Schulze, A., Zechner, R., Walther, Tobias C., and Farese, Robert V. (2013). Cellular Fatty Acid Metabolism and Cancer. Cell Metabolism *18*, 153-161.

Dai, Y., Li, C., Wen, T.F., and Yan, L.N. (2014). Comparison of liver resection and transplantation for Child-pugh A cirrhotic patient with very early hepatocellular carcinoma and portal hypertension. Pakistan journal of medical sciences *30*, 996-1000.

Dang, C.V. (2012). Links between metabolism and cancer. Genes & Development *26*, 877-890.

Davel, L., D'Agostino, A., Espanol, A., Jasnis, M.A., Lauria de Cidre, L., de Lustig, E.S., and Sales, M.E. (2002). Nitric oxide synthase-cyclooxygenase interactions are involved in tumor cell angiogenesis and migration. J Biol Regul Homeost Agents *16*, 181-189.

Davila, J.A., Morgan, R.O., Shaib, Y., McGlynn, K.A., and El-Serag, H.B. (2005). Diabetes increases the risk of hepatocellular carcinoma in the United States: a population based case control study. Gut *54*, 533-539.

Davis, G.L., Alter, M.J., El–Serag, H., Poynard, T., and Jennings, L.W. (2010). Aging of Hepatitis C Virus (HCV)-Infected Persons in the United States: A Multiple Cohort Model of HCV Prevalence and Disease Progression. Gastroenterology *138*, 513-521.e516.

de Bono, J.S., Logothetis, C.J., Molina, A., Fizazi, K., North, S., Chu, L., Chi, K.N., Jones, R.J., Goodman, O.B., Saad, F., *et al.* (2011). Abiraterone and Increased Survival in Metastatic Prostate Cancer. New England Journal of Medicine *364*, 1995-2005.

DeFilippis, R.A., Chang, H., Dumont, N., Rabban, J.T., Chen, Y.Y., Fontenay, G.V., Berman, H.K., Gauthier, M.L., Zhao, J., Hu, D., *et al.* (2012). CD36 Repression Activates a Multicellular Stromal Program Shared by High Mammographic Density and Tumor Tissues. Cancer discovery *2*, 826-839.

del Sol, A., Balling, R., Hood, L., and Galas, D. (2010). Diseases as network perturbations. Current Opinion in Biotechnology *21*, 566-571.

Dentin, R., Benhamed, F., Hainault, I., Fauveau, V., Foufelle, F., Dyck, J.R., Girard, J., and Postic, C. (2006). Liver-specific inhibition of ChREBP improves hepatic steatosis and insulin resistance in ob/ob mice. Diabetes *55*, 2159-2170.

Di Lorenzo, G., Tortora, G., D'Armiento, F.P., De Rosa, G., Staibano, S., Autorino, R., D'Armiento, M., De Laurentiis, M., De Placido, S., Catalano, G., *et al.* (2002). Expression of epidermal growth factor receptor correlates with disease relapse and progression to androgen-independence in human prostate cancer. Clin Cancer Res *8*, 3438-3444.

Doege, H., and Stahl, A. (2006). Protein-mediated fatty acid uptake: novel insights from in vivo models. Physiology *21*, 259-268.

Donato, F., Boffetta, P., and Puoti, M. (1998). A meta-analysis of epidemiological studies on the combined effect of hepatitis B and C virus infections in causing hepatocellular carcinoma. International journal of cancer Journal international du cancer *75*, 347-354.

Donato, F., Tagger, A., Gelatti, U., Parrinello, G., Boffetta, P., Albertini, A., Decarli, A., Trevisi, P., Ribero, M.L., Martelli, C., *et al.* (2002). Alcohol and hepatocellular carcinoma: the effect of lifetime intake and hepatitis virus infections in men and women. American journal of epidemiology *155*, 323-331.

Donnelly, K.L., Smith, C.I., Schwarzenberg, S.J., Jessurun, J., Boldt, M.D., and Parks, E.J. (2005). Sources of fatty acids stored in liver and secreted via lipoproteins in patients with nonalcoholic fatty liver disease. J Clin Invest *115*, 1343-1351.

Dorudi, S., Sheffield, J.P., Poulsom, R., Northover, J.M., and Hart, I.R. (1993). E-cadherin expression in colorectal cancer. An immunocytochemical and in situ hybridization study. The American journal of pathology *142*, 981-986.

Draghici, S., Khatri, P., Tarca, A.L., Amin, K., Done, A., Voichita, C., Georgescu, C., and Romero, R. (2007). A systems biology approach for pathway level analysis. Genome Res *17*, 1537-1545.

Duncan, J.G. (2008). Lipotoxicity: what is the fate of fatty acids? The Journal of Lipid Research *49*, 1375-1376.

Dyck, D.J., Steinberg, G., and Bonen, A. (2001). Insulin increases FA uptake and esterification but reduces lipid utilization in isolated contracting muscle. Am J Physiol Endocrinol Metab *281*, E600-607.

Edens, M.A., Kuipers, F., and Stolk, R.P. (2009). Non-alcoholic fatty liver disease is associated with cardiovascular disease risk markers. Obes Rev *10*, 412-419.

Ekinci, F.J., and Shea, T.B. (1999). Free PKC catalytic subunits (PKM) phosphorylate tau via a pathway distinct from that utilized by intact PKC. Brain Res *850*, 207-216.

El-Serag, H.B. (2012). Epidemiology of viral hepatitis and hepatocellular carcinoma. Gastroenterology *142*, 1264-1273 e1261.

El-Serag, H.B., and Rudolph, K.L. (2007). Hepatocellular carcinoma: epidemiology and molecular carcinogenesis. Gastroenterology *132*, 2557-2576.

El–Serag, H.B., and Rudolph, K.L. (2007). Hepatocellular Carcinoma: Epidemiology and Molecular Carcinogenesis. Gastroenterology *132*, 2557-2576.

Faivre, S., Djelloul, S., and Raymond, E. (2006). New paradigms in anticancer therapy: targeting multiple signaling pathways with kinase inhibitors. Semin Oncol *33*, 407-420.

FDA (2011). FDA drug safety communication: 5-ARIs may increase the risk of a more serious form of prostate cancer. http://wwwfdagov/Drugs/DrugSafety/ucm258314htm.

Feldstein, A.E., Werneburg, N.W., Canbay, A., Guicciardi, M.E., Bronk, S.F., Rydzewski, R., Burgart, L.J., and Gores, G.J. (2004a). Free fatty acids promote hepatic lipotoxicity by stimulating TNF-alpha expression via a lysosomal pathway. Hepatology *40*, 185-194.

Feldstein, A.E., Werneburg, N.W., Canbay, A., Guicciardi, M.E., Bronk, S.F., Rydzewski, R., Burgart, L.J., and Gores, G.J. (2004b). Free fatty acids promote hepatic lipotoxicity by stimulating TNF-α expression via a lysosomal pathway. Hepatology *40*, 185-194.

Feldstein, A.E., Werneburg, N.W., Li, Z., Bronk, S.F., and Gores, G.J. (2006). Bax inhibition protects against free fatty acid-induced lysosomal permeabilization. American journal of physiology Gastrointestinal and liver physiology *290*, G1339-1346.

Ferlay J, S.I., Ervik M, Dikshit R, Eser S, Mathers C, et al. (2013). GLOBOCAN 2012: Estimated Cancer Incidence, Mortality, and Prevalence Worldwide in 2012. International Agency for Research on Cancer *http://globocan.iarc.fr. Accessed April 2014*.

Ferlay, J., Soerjomataram, I., Ervik, M., Dikshit, R., Eser, S., Mathers, C., Rebelo, M., Parkin, D., Forman, D., and Bray, F. (2013). GLOBOCAN 2012 v1. 0. Cancer incidence and mortality worldwide: IARC CancerBase.

Fertig, E.J., Danilova, L.V., and Ochs, M.F. (2011). Cancer Systems Biology. In Handbook of Statistical Bioinformatics, H.H.-S. Lu, B. Schölkopf, and H. Zhao, eds. (Springer Berlin Heidelberg), pp. 533-565.

Flavin, R., Peluso, S., Nguyen, P.L., and Loda, M. (2010). Fatty acid synthase as a potential therapeutic target in cancer. Future Oncology *6*, 551-562.

Fodde, R., and Brabletz, T. (2007). Wnt/β-catenin signaling in cancer stemness and malignant behavior. Current Opinion in Cell Biology *19*, 150-158.

Franch-Marro, X., Wendler, F., Griffith, J., Maurice, M.M., and Vincent, J.P. (2008). In vivo role of lipid adducts on Wingless. J Cell Sci *121*, 1587-1592.

Freeman, A.J., Dore, G.J., Law, M.G., Thorpe, M., Von Overbeck, J., Lloyd, A.R., Marinos, G., and Kaldor, J.M. (2001). Estimating progression to cirrhosis in chronic hepatitis C virus infection. Hepatology *34*, 809-816.

Fruehauf, J.P., and Meyskens, F.L., Jr. (2007). Reactive oxygen species: a breath of life or death? Clinical cancer research : an official journal of the American Association for Cancer Research *13*, 789-794.

Furukawa, S., Fujita, T., Shimabukuro, M., Iwaki, M., Yamada, Y., Nakajima, Y., Nakayama, O., Makishima, M., Matsuda, M., and Shimomura, I. (2004). Increased oxidative stress in obesity and its impact on metabolic syndrome. Journal of Clinical Investigation *114*, 1752-1761.

Futreal, P.A., Coin, L., Marshall, M., Down, T., Hubbard, T., Wooster, R., Rahman, N., and Stratton, M.R. (2004). A census of human cancer genes. Nat Rev Cancer *4*, 177-183.

Gao, D., Nong, S., Huang, X., Lu, Y., Zhao, H., Lin, Y., Man, Y., Wang, S., Yang, J., and Li, J. (2010). The effects of palmitate on hepatic insulin resistance are mediated by NADPH Oxidase 3-derived reactive oxygen species through JNK and p38MAPK pathways. J Biol Chem *285*, 29965-29973.

Gao, J., Aksoy, B.A., Dogrusoz, U., Dresdner, G., Gross, B., Sumer, S.O., Sun, Y., Jacobsen, A., Sinha, R., Larsson, E., *et al.* (2013). Integrative analysis of complex cancer genomics and clinical profiles using the cBioPortal. Science signaling *6*, pl1.

Gao, X., Arenas-Ramirez, N., Scales, S.J., and Hannoush, R.N. (2011). Membrane targeting of palmitoylated Wnt and Hedgehog revealed by chemical probes. FEBS Letters *585*, 2501-2506.

Gao, X., and Hannoush, R.N. (2013). Single-cell imaging of Wnt palmitoylation by the acyltransferase porcupine. Nature Chemical Biology *10*, 61-68.

Garcia-Gras, E., Lombardi, R., Giocondo, M.J., Willerson, J.T., Schneider, M.D., Khoury, D.S., and Marian, A.J. (2006). Suppression of canonical Wnt/beta-catenin signaling by nuclear plakoglobin recapitulates phenotype of arrhythmogenic right ventricular cardiomyopathy. The Journal of clinical investigation *116*, 2012-2021.

Geback, T., Schulz, M.M., Koumoutsakos, P., and Detmar, M. (2009). TScratch: a novel and simple software tool for automated analysis of monolayer wound healing assays. BioTechniques *46*, 265-274.

Geekiyanage, H., and Chan, C. (2011). MicroRNA-137/181c Regulates Serine Palmitoyltransferase and In Turn Amyloid , Novel Targets in Sporadic Alzheimer's Disease. Journal of Neuroscience *31*, 14820-14830.

Gertow, K., Rosell, M., Sjogren, P., Eriksson, P., Vessby, B., de Faire, U., Hamsten, A., Hellenius, M.L., and Fisher, R.M. (2006). Fatty acid handling protein expression in adipose tissue, fatty acid composition of adipose tissue and serum, and markers of insulin resistance. European journal of clinical nutrition *60*, 1406-1413.

Getsios, S., Huen, A.C., and Green, K.J. (2004). Working out the strength and flexibility of desmosomes. Nat Rev Mol Cell Biol *5*, 271-281.

Giannelli, G., Bergamini, C., Fransvea, E., Sgarra, C., and Antonaci, S. (2005). Laminin-5 with transforming growth factor-beta1 induces epithelial to mesenchymal transition in hepatocellular carcinoma. Gastroenterology *129*, 1375-1383.

Giovannucci, E., Harlan, D.M., Archer, M.C., Bergenstal, R.M., Gapstur, S.M., Habel, L.A., Pollak, M., Regensteiner, J.G., and Yee, D. (2010). Diabetes and cancer: a consensus report. CA: a cancer journal for clinicians *60*, 207-221.

Gittelman, M., Pommerville, P.J., Persson, B.-E., Jensen, J.-K., and Olesen, T.K. (2008). A 1-Year, Open Label, Randomized Phase II Dose Finding Study of Degarelix for the Treatment of Prostate Cancer in North America. The Journal of Urology *180*, 1986-1992.

Gitter, A., Klein-Seetharaman, J., Gupta, A., and Bar-Joseph, Z. (2011). Discovering pathways by orienting edges in protein interaction networks. Nucleic Acids Res *39*, e22.

GlaxoSmithKline (2011). GSK statement on Avodart (dutasteride) for prostate cancer risk reduction. http://wwwgskcom/media/pressreleases/2011/2011_pressrelease_10043htm.

Glinghammar, B., Skogsberg, J., Hamsten, A., and Ehrenborg, E. (2003). PPARdelta activation induces COX-2 gene expression and cell proliferation in human hepatocellular carcinoma cells. Biochemical and biophysical research communications *308*, 361-368.

Goldman, M., Craft, B., Swatloski, T., Ellrott, K., Cline, M., Diekhans, M., Ma, S., Wilks, C., Stuart, J., Haussler, D., *et al.* (2012). The UCSC Cancer Genomics Browser: update 2013. Nucleic Acids Research *41*, D949-D954.

Gravis, G., Bladou, F., Salem, N., Goncalves, A., Esterni, B., Walz, J., Bagattini, S., Marcy, M., Brunelle, S., and Viens, P. (2008). Results from a monocentric phase II trial of erlotinib in patients with metastatic prostate cancer. Annals of Oncology *19*, 1624-1628.

Greco, D., Kotronen, A., Westerbacka, J., Puig, O., Arkkila, P., Kiviluoto, T., Laitinen, S., Kolak, M., Fisher, R.M., Hamsten, A., *et al.* (2008). Gene expression in human NAFLD. AJP: Gastrointestinal and Liver Physiology *294*, G1281-G1287.

Grivennikov, S.I., Greten, F.R., and Karin, M. (2010). Immunity, Inflammation, and Cancer. Cell *140*, 883-899.

Grooteclaes, M.L., and Frisch, S.M. (2000). Evidence for a function of CtBP in epithelial gene regulation and anoikis. Oncogene *19*, 3823-3828.

Guo, W., Wong, S., Xie, W., Lei, T., and Luo, Z. (2007). Palmitate modulates intracellular signaling, induces endoplasmic reticulum stress, and causes apoptosis in mouse 3T3-L1 and rat primary preadipocytes. Am J Physiol Endocrinol Metab *293*, E576-586.

Guppy, M., Leedman, P., Zu, X., and Russell, V. (2002). Contribution by different fuels and metabolic pathways to the total ATP turnover of proliferating MCF-7 breast cancer cells. The Biochemical journal *364*, 309-315.

Gupta, S., Srivastava, M., Ahmad, N., Bostwick, D.G., and Mukhtar, H. (2000). Over-expression of cyclooxygenase-2 in human prostate adenocarcinoma. The Prostate *42*, 73-78.

Hajra, K.M., and Fearon, E.R. (2002). Cadherin and catenin alterations in human cancer. Genes, chromosomes & cancer *34*, 255-268.

Hale, J.S., Otvos, B., Sinyuk, M., Alvarado, A.G., Hitomi, M., Stoltz, K., Wu, Q., Flavahan, W., Levison, B., Johansen, M.L., *et al.* (2014). Cancer Stem Cell-Specific Scavenger Receptor CD36 Drives Glioblastoma Progression. Stem Cells *32*, 1746-1758.

Han, S.F., Deng, R.L., Xu, H.R., Cao, Y.F., Wang, X.Y., and Xiao, K. (2007). [Photosynthesis and active-oxygen-scavenging enzyme activities in rice varieties with different phosphorus efficiency under phosphorus stress]. Ying Yong Sheng Tai Xue Bao *18*, 2462-2467.

Hanahan, D., and Weinberg, R.A. (2000). The hallmarks of cancer. Cell *100*, 57-70.

Hanahan, D., and Weinberg, Robert A. (2011). Hallmarks of Cancer: The Next Generation. Cell *144*, 646-674.

Hegmans, J.P., Bard, M.P., Hemmes, A., Luider, T.M., Kleijmeer, M.J., Prins, J.B., Zitvogel, L., Burgers, S.A., Hoogsteden, H.C., and Lambrecht, B.N. (2004). Proteomic analysis of exosomes secreted by human mesothelioma cells. Am J Pathol *164*, 1807-1815.

Heindryckx, F., Colle, I., and Van Vlierberghe, H. (2009). Experimental mouse models for hepatocellular carcinoma research. International Journal of Experimental Pathology *90*, 367-386.

Hellerstein, M.K. (2008). A critique of the molecular target-based drug discovery paradigm based on principles of metabolic control: advantages of pathway-based discovery. Metab Eng *10*, 1-9.

Hernes, E., Fosså, S.D., Berner, A., Otnes, B., and Nesland, J.M. (2004). Expression of the epidermal growth factor receptor family in prostate carcinoma before and during androgen-independence. British Journal of Cancer *90*, 449-454.

Heyns, C.F., Simonin, M.P., Grosgurin, P., Schall, R., and Porchet, H.C. (2003). Comparative efficacy of triptorelin pamoate and leuprolide acetate in men with advanced prostate cancer. BJU International *92*, 226-231.

Higuchi, N., Kato, M., Shundo, Y., Tajiri, H., Tanaka, M., Yamashita, N., Kohjima, M., Kotoh, K., Nakamuta, M., Takayanagi, R., *et al.* (2008). Liver X receptor in cooperation with SREBP-1c is a major lipid synthesis regulator in nonalcoholic fatty liver disease. Hepatol Res *38*, 1122-1129.

Hobbs, R.P., Amargo, E.V., Somasundaram, A., Simpson, C.L., Prakriya, M., Denning, M.F., and Green, K.J. (2010). The calcium ATPase SERCA2 regulates desmoplakin dynamics and intercellular adhesive strength through modulation of PKC{alpha} signaling. FASEB J.

Holm, C., Østerlund, T., Laurell, H., and Contreras, J.A. (2000). Molecularmechanismsregulatinghormone-Sensitivelipaseandlipolysis. Annual review of nutrition *20*, 365-393.

Hood, L., and Friend, S.H. (2011). Predictive, personalized, preventive, participatory (P4) cancer medicine. Nat Rev Clin Oncol *8*, 184-187.

Hornberg, J.J., Bruggeman, F.J., Westerhoff, H.V., and Lankelma, J. (2006). Cancer: a Systems Biology disease. Biosystems *83*, 81-90.

Horton, J.D., Bashmakov, Y., Shimomura, I., and Shimano, H. (1998). Regulation of sterol regulatory element binding proteins in livers of fasted and refed mice. Proceedings of the National Academy of Sciences of the United States of America *95*, 5987-5992.

Hotamisligil, G.S. (2006). Inflammation and metabolic disorders. Nature *444*, 860-867.

Hsu, Y.-C., Wu, C.-Y., and Lin, J.-T. (2015). Hepatitis C Virus Infection, Antiviral Therapy, and Risk of Hepatocellular Carcinoma. Seminars in Oncology *42*, 329-338.

Hu, L., Lau, S.H., Tzang, C.-H., Wen, J.-M., Wang, W., Xie, D., Huang, M., Wang, Y., Wu, M.-C., Huang, J.-F., *et al.* (2003). Association of Vimentin overexpression and hepatocellular carcinoma metastasis. Oncogene.

Huang, C., Qiu, Z., Wang, L., Peng, Z., Jia, Z., Logsdon, C.D., Le, X., Wei, D., Huang, S., and Xie, K. (2011). A Novel FoxM1-Caveolin Signaling Pathway Promotes Pancreatic Cancer Invasion and Metastasis. Cancer Research *72*, 655-665.

Huang, D.W., Sherman, B.T., Tan, Q., Kir, J., Liu, D., Bryant, D., Guo, Y., Stephens, R., Baseler, M.W., Lane, H.C., *et al.* (2007). DAVID Bioinformatics Resources: expanded annotation database and novel algorithms to better extract biology from large gene lists. Nucleic Acids Research *35*, W169-W175.

Huang, J., Deng, Q., Wang, Q., Li, K.Y., Dai, J.H., Li, N., Zhu, Z.D., Zhou, B., Liu, X.Y., Liu, R.F., *et al.* (2012). Exome sequencing of hepatitis B virus-associated hepatocellular carcinoma. Nat Genet *44*, 1117-1121.

Huang, L., Yan, M., and Kirschke, C.P. (2010). Over-expression of ZnT7 increases insulin synthesis and secretion in pancreatic beta-cells by promoting insulin gene transcription. Exp Cell Res.

Huang, S. (2011). On the intrinsic inevitability of cancer: from foetal to fatal attraction. Semin Cancer Biol *21*, 183-199.

Hubbard, B., Doege, H., Punreddy, S., Wu, H., Huang, X., Kaushik, V.K., Mozell, R.L., Byrnes, J.J., Stricker-Krongrad, A., Chou, C.J., *et al.* (2006). Mice deleted for fatty acid transport protein 5

have defective bile acid conjugation and are protected from obesity. Gastroenterology *130*, 1259-1269.

Huber, M.A., Azoitei, N., Baumann, B., Grünert, S., Sommer, A., Pehamberger, H., Kraut, N., Beug, H., and Wirth, T. (2004). NF-κB is essential for epithelial-mesenchymal transition and metastasis in a model of breast cancer progression. Journal of Clinical Investigation *114*, 569-581.

Huen, A.C. (2002). Intermediate filament-membrane attachments function synergistically with actin-dependent contacts to regulate intercellular adhesive strength. The Journal of Cell Biology *159*, 1005-1017.

Iizuka, K., Bruick, R.K., Liang, G., Horton, J.D., and Uyeda, K. (2004). From The Cover: Deficiency of carbohydrate response element-binding protein (ChREBP) reduces lipogenesis as well as glycolysis. Proceedings of the National Academy of Sciences *101*, 7281-7286.

Ish-Shalom, D., Christoffersen, C.T., Vorwerk, P., Sacerdoti-Sierra, N., Shymko, R.M., Naor, D., and Meyts, P.D. (1997). Mitogenic properties of insulin and insulin analogues mediated by the insulin receptor. Diabetologia *40*, S25-S31.

Ishikawa, K., Takenaga, K., Akimoto, M., Koshikawa, N., Yamaguchi, A., Imanishi, H., Nakada, K., Honma, Y., and Hayashi, J. (2008). ROS-generating mitochondrial DNA mutations can regulate tumor cell metastasis. Science *320*, 661-664.

Ito, K., Carracedo, A., Weiss, D., Arai, F., Ala, U., Avigan, D.E., Schafer, Z.T., Evans, R.M., Suda, T., Lee, C.H., *et al.* (2012). A PML-PPAR-delta pathway for fatty acid oxidation regulates hematopoietic stem cell maintenance. Nature medicine *18*, 1350-1358.

Jay, A.G., Chen, A.N., Paz, M.A., Hung, J.P., and Hamilton, J.A. (2015). CD36 binds oxidized LDL in a mechanism dependent upon fatty acid binding. Journal of Biological Chemistry.

Jemal, A., Siegel, R., Ward, E., Murray, T., Xu, J., and Thun, M.J. (2007). Cancer statistics, 2007. CA: a cancer journal for clinicians *57*, 43-66.

Jiang, C., Xuan, Z., Zhao, F., and Zhang, M.Q. (2007a). TRED: a transcriptional regulatory element database, new entries and other development. Nucleic Acids Res *35*, D137-140.

Jiang, J., Nilsson-Ehle, P., and Xu, N. (2006). Lipids in Health and Disease *5*, 4.

Jiang, Y.-G., Luo, Y., He, D.-l., Li, X., Zhang, L.-l., Peng, T., Li, M.-C., and Lin, Y.-H. (2007b). Role of Wnt/β-catenin signaling pathway in epithelial-mesenchymal transition of human prostate cancer induced by hypoxia-inducible factor-1α. International Journal of Urology *14*, 1034-1039.

Jonkman, M.F., Pasmooij, A.M., Pasmans, S.G., van den Berg, M.P., Ter Horst, H.J., Timmer, A., and Pas, H.H. (2005). Loss of desmoplakin tail causes lethal acantholytic epidermolysis bullosa. Am J Hum Genet *77*, 653-660.

Kadoch, C., Hargreaves, D.C., Hodges, C., Elias, L., Ho, L., Ranish, J., and Crabtree, G.R. (2013). Proteomic and bioinformatic analysis of mammalian SWI/SNF complexes identifies extensive roles in human malignancy. Nature Genetics *45*, 592-601.

Kahn, B.B., Alquier, T., Carling, D., and Hardie, D.G. (2005). AMP-activated protein kinase: ancient energy gauge provides clues to modern understanding of metabolism. Cell Metab *1*, 15-25.

Kalluri, R., and Weinberg, R.A. (2009). The basics of epithelial-mesenchymal transition. Journal of Clinical Investigation *119*, 1420-1428.

Kamphorst, J.J., Cross, J.R., Fan, J., de Stanchina, E., Mathew, R., White, E.P., Thompson, C.B., and Rabinowitz, J.D. (2013). Hypoxic and Ras-transformed cells support growth by scavenging unsaturated fatty acids from lysophospholipids. Proceedings of the National Academy of Sciences of the United States of America *110*, 8882-8887.

Kan, Z., Zheng, H., Liu, X., Li, S., Barber, T.D., Gong, Z., Gao, H., Hao, K., Willard, M.D., Xu, J., *et al.* (2013). Whole-genome sequencing identifies recurrent mutations in hepatocellular carcinoma. Genome research *23*, 1422-1433.

Kandoth, C., McLellan, M.D., Vandin, F., Ye, K., Niu, B., Lu, C., Xie, M., Zhang, Q., McMichael, J.F., Wyczalkowski, M.A., *et al.* (2013). Mutational landscape and significance across 12 major cancer types. Nature *502*, 333-339.

Karakas, B., Bachman, K.E., and Park, B.H. (2006). Mutation of the PIK3CA oncogene in human cancers. British journal of cancer *94*, 455-459.

Katoh, M., and Katoh, M. (2007). AP1- and NF-kappaB-binding sites conserved among mammalian WNT10B orthologs elucidate the TNFalpha-WNT10B signaling loop implicated in carcinogenesis and adipogenesis. International journal of molecular medicine *19*, 699-703.

Kennedy, A., Martinez, K., Chuang, C.C., LaPoint, K., and McIntosh, M. (2009). Saturated fatty acid-mediated inflammation and insulin resistance in adipose tissue: mechanisms of action and implications. The Journal of nutrition *139*, 1-4.

Kim, J.B., Sarraf, P., Wright, M., Yao, K.M., Mueller, E., Solanes, G., Lowell, B.B., and Spiegelman, B.M. (1998). Nutritional and insulin regulation of fatty acid synthetase and leptin gene expression through ADD1/SREBP1. The Journal of clinical investigation *101*, 1-9.

Kim, T.H., Kim, H., Park, J.M., Im, S.S., Bae, J.S., Kim, M.Y., Yoon, H.G., Cha, J.Y., Kim, K.S., and Ahn, Y.H. (2009). Interrelationship between Liver X Receptor , Sterol Regulatory Element-binding Protein-1c, Peroxisome Proliferator-activated Receptor , and Small Heterodimer Partner in the

Transcriptional Regulation of Glucokinase Gene Expression in Liver. Journal of Biological Chemistry *284*, 15071-15083.

Kitano, H. (2004a). Biological robustness. Nature Reviews Genetics *5*, 826-837.

Kitano, H. (2004b). Biological robustness. Nat Rev Genet *5*, 826-837.

Kitano, H. (2004c). Opinion: Cancer as a robust system: implications for anticancer therapy. Nature Reviews Cancer *4*, 227-235.

Klein, C.A. (2009). Parallel progression of primary tumours and metastases. Nature Reviews Cancer *9*, 302-312.

Klotz, L., Boccon-Gibod, L., Shore, N.D., Andreou, C., Persson, B.-E., Cantor, P., Jensen, J.-K., Olesen, T.K., and Schröder, F.H. (2008). The efficacy and safety of degarelix: a 12-month, comparative, randomized, open-label, parallel-group phase III study in patients with prostate cancer. BJU International *102*, 1531-1538.

Knobloch, M., Braun, S.M., Zurkirchen, L., von Schoultz, C., Zamboni, N., Arauzo-Bravo, M.J., Kovacs, W.J., Karalay, O., Suter, U., Machado, R.A., *et al.* (2013). Metabolic control of adult neural stem cell activity by Fasn-dependent lipogenesis. Nature *493*, 226-230.

Koonen, D.P., Jacobs, R.L., Febbraio, M., Young, M.E., Soltys, C.L., Ong, H., Vance, D.E., and Dyck, J.R. (2007). Increased hepatic CD36 expression contributes to dyslipidemia associated with diet-induced obesity. Diabetes *56*, 2863-2871.

Kowalski, P.J., Rubin, M.A., and Kleer, C.G. (2003). Breast Cancer Research *5*, R217.

Kowdley, K.V. (2004). Iron, hemochromatosis, and hepatocellular carcinoma. Gastroenterology *127*, S79-86.

Krishnamachary, B. (2006). Hypoxia-Inducible Factor-1-Dependent Repression of E-cadherin in von Hippel-Lindau Tumor Suppressor-Null Renal Cell Carcinoma Mediated by TCF3, ZFHX1A, and ZFHX1B. Cancer Research *66*, 2725-2731.

Kuemmerle, N.B., Rysman, E., Lombardo, P.S., Flanagan, A.J., Lipe, B.C., Wells, W.A., Pettus, J.R., Froehlich, H.M., Memoli, V.A., Morganelli, P.M., *et al.* (2011). Lipoprotein Lipase Links Dietary Fat to Solid Tumor Cell Proliferation. Molecular Cancer Therapeutics *10*, 427-436.

Kuhajda, F.P. (2006). Fatty Acid Synthase and Cancer: New Application of an Old Pathway. Cancer Research *66*, 5977-5980.

Lamouille, S., Xu, J., and Derynck, R. (2014). Molecular mechanisms of epithelial–mesenchymal transition. Nature Reviews Molecular Cell Biology *15*, 178-196.

Langman, M.J.S. (2000). Effect of anti-inflammatory drugs on overall risk of common cancer: case-control study in general practice research database. BMJ *320*, 1642-1646.

Larsson, S.C., and Wolk, A. (2007). Overweight, obesity and risk of liver cancer: a meta-analysis of cohort studies. British journal of cancer.

Larue, L., and Bellacosa, A. (2005). Epithelial–mesenchymal transition in development and cancer: role of phosphatidylinositol 3′ kinase/AKT pathways. Oncogene *24*, 7443-7454.

Leary, S.C., Sasarman, F., Nishimura, T., and Shoubridge, E.A. (2009). Human SCO2 is required for the synthesis of CO II and as a thiol-disulphide oxidoreductase for SCO1. Hum Mol Genet *18*, 2230-2240.

Lee, E., Madar, A., David, G., Garabedian, M.J., DasGupta, R., and Logan, S.K. (2013). Inhibition of androgen receptor and -catenin activity in prostate cancer. Proceedings of the National Academy of Sciences *110*, 15710-15715.

Lee, J.W., Soung, Y.H., Kim, S.Y., Lee, H.W., Park, W.S., Nam, S.W., Kim, S.H., Lee, J.Y., Yoo, N.J., and Lee, S.H. (2005). PIK3CA gene is frequently mutated in breast carcinomas and hepatocellular carcinomas. Oncogene *24*, 1477-1480.

Lee, T.K., Poon, R.T., Yuen, A.P., Ling, M.T., Kwok, W.K., Wang, X.H., Wong, Y.C., Guan, X.Y., Man, K., Chau, K.L., *et al.* (2006a). Twist overexpression correlates with hepatocellular carcinoma metastasis through induction of epithelial-mesenchymal transition. Clinical cancer research : an official journal of the American Association for Cancer Research *12*, 5369-5376.

Lee, T.K., Poon, R.T.P., Yuen, A.P., Ling, M.T., Kwok, W.K., Wang, X.H., Wong, Y.C., Guan, X.Y., Man, K., Chau, K.L., *et al.* (2006b). Twist Overexpression Correlates with Hepatocellular Carcinoma Metastasis through Induction of Epithelial-Mesenchymal Transition. Clinical Cancer Research *12*, 5369-5376.

Leitges, M., Plomann, M., Standaert, M.L., Bandyopadhyay, G., Sajan, M.P., Kanoh, Y., and Farese, R.V. (2002). Knockout of PKC alpha enhances insulin signaling through PI3K. Mol Endocrinol *16*, 847-858.

Leonardi, R., Zhang, Y.M., Rock, C.O., and Jackowski, S. (2005). Coenzyme A: back in action. Prog Lipid Res *44*, 125-153.

Leung, T., Rajendran, R., Singh, S., Garva, R., Krstic-Demonacos, M., and Demonacos, C. (2013). Cytochrome P450 2E1 (CYP2E1) regulates the response to oxidative stress and migration of breast cancer cells. Breast Cancer Research *15*, R107.

Li, C.W., Xia, W., Huo, L., Lim, S.O., Wu, Y., Hsu, J.L., Chao, C.H., Yamaguchi, H., Yang, N.K., Ding, Q., *et al.* (2012). Epithelial-mesenchymal transition induced by TNF-alpha requires NF-kappaB-mediated transcriptional upregulation of Twist1. Cancer Res *72*, 1290-1300.

Li, Z., Srivastava, S., Findlan, R., and Chan, C. (2008). Using dynamic gene module map analysis to identify targets that modulate free fatty acid induced cytotoxicity. Biotechnol Prog *24*, 29-37.

Li, Z., Srivastava, S., Mittal, S., Yang, X., Sheng, L., and Chan, C. (2007a). A Three Stage Integrative Pathway Search (TIPS) framework to identify toxicity relevant genes and pathways. BMC Bioinformatics *8*, 202.

Li, Z., Srivastava, S., Yang, X., Mittal, S., Norton, P., Resau, J., Haab, B., and Chan, C. (2007b). A hierarchical approach employing metabolic and gene expression profiles to identify the pathways that confer cytotoxicity in HepG2 cells. BMC systems biology *1*, 21.

Li, Z.Z., Berk, M., McIntyre, T.M., and Feldstein, A.E. (2009). Hepatic lipid partitioning and liver damage in nonalcoholic fatty liver disease: role of stearoyl-CoA desaturase. The Journal of biological chemistry *284*, 5637-5644.

Listenberger, L.L., Han, X., Lewis, S.E., Cases, S., Farese, R.V., Jr., Ory, D.S., and Schaffer, J.E. (2003). Triglyceride accumulation protects against fatty acid-induced lipotoxicity. Proceedings of the National Academy of Sciences of the United States of America *100*, 3077-3082.

Liu, J., Pan, S., Hsieh, M.H., Ng, N., Sun, F., Wang, T., Kasibhatla, S., Schuller, A.G., Li, A.G., Cheng, D., *et al.* (2013a). Targeting Wnt-driven cancer through the inhibition of Porcupine by LGK974. Proceedings of the National Academy of Sciences *110*, 20224-20229.

Liu, L., Martin, R., and Chan, C. (2013b). Palmitate-activated astrocytes via serine palmitoyltransferase increase BACE1 in primary neurons by sphingomyelinases. Neurobiology of Aging *34*, 540-550.

Liu, W., Li, D., Wang, J., Xie, H., Zhu, Y., and He, F. (2009). Proteome-wide Prediction of Signal Flow Direction in Protein Interaction Networks Based on Interacting Domains. Molecular & Cellular Proteomics *8*, 2063-2070.

Liu, Y., and Wu, F. (2010). Global Burden of Aflatoxin-Induced Hepatocellular Carcinoma: A Risk Assessment. Environmental Health Perspectives *118*, 818-824.

Llovet, J.M., and Bruix, J. (2003). Systematic review of randomized trials for unresectable hepatocellular carcinoma: Chemoembolization improves survival. Hepatology *37*, 429-442.

Llovet, J.M., Ricci, S., Mazzaferro, V., Hilgard, P., Gane, E., Blanc, J.F., de Oliveira, A.C., Santoro, A., Raoul, J.L., Forner, A., *et al.* (2008). Sorafenib in advanced hepatocellular carcinoma. The New England journal of medicine *359*, 378-390.

Lopez, B. (2013). Thread 4: Data discovery, transparency and visualization. Nature Genetics.

Lorch, J.H., Klessner, J., Park, J.K., Getsios, S., Wu, Y.L., Stack, M.S., and Green, K.J. (2004). Epidermal growth factor receptor inhibition promotes desmosome assembly and strengthens intercellular adhesion in squamous cell carcinoma cells. J Biol Chem *279*, 37191-37200.

Luiken, J.J., Arumugam, Y., Dyck, D.J., Bell, R.C., Pelsers, M.M., Turcotte, L.P., Tandon, N.N., Glatz, J.F., and Bonen, A. (2001). Increased rates of fatty acid uptake and plasmalemmal fatty acid transporters in obese Zucker rats. The Journal of biological chemistry *276*, 40567-40573.

Maeda, O., Usami, N., Kondo, M., Takahashi, M., Goto, H., Shimokata, K., Kusugami, K., and Sekido, Y. (2004). Plakoglobin (gamma-catenin) has TCF/LEF family-dependent transcriptional activity in beta-catenin-deficient cell line. Oncogene *23*, 964-972.

Malhi, H., Barreyro, F.J., Isomoto, H., Bronk, S.F., and Gores, G.J. (2007). Free fatty acids sensitise hepatocytes to TRAIL mediated cytotoxicity. Gut *56*, 1124-1131.

Malhi, H., Bronk, S.F., Werneburg, N.W., and Gores, G.J. (2006a). Free fatty acids induce JNK-dependent hepatocyte lipoapoptosis. The Journal of biological chemistry *281*, 12093-12101.

Malhi, H., and Gores, G. (2008). Molecular Mechanisms of Lipotoxicity in Nonalcoholic Fatty Liver Disease. Seminars in Liver Disease *28*, 360-369.

Malhi, H., Gores, G.J., and Lemasters, J.J. (2006b). Apoptosis and necrosis in the liver: a tale of two deaths? Hepatology *43*, S31-44.

Mani, S.A., Guo, W., Liao, M.-J., Eaton, E.N., Ayyanan, A., Zhou, A.Y., Brooks, M., Reinhard, F., Zhang, C.C., Shipitsin, M., *et al.* (2008). The Epithelial-Mesenchymal Transition Generates Cells with Properties of Stem Cells. Cell *133*, 704-715.

Marquardt, J.U., Seo, D., Andersen, J.B., Gillen, M.C., Kim, M.S., Conner, E.A., Galle, P.R., Factor, V.M., Park, Y.N., and Thorgeirsson, S.S. (2014). Sequential transcriptome analysis of human liver cancer indicates late stage acquisition of malignant traits. J Hepatol *60*, 346-353.

Marra, F., and Bertolani, C. (2009). Adipokines in liver diseases. Hepatology *50*, 957-969.

Martinez-Outschoorn, U.E., Lin, Z., Whitaker-Menezes, D., Howell, A., Sotgia, F., and Lisanti, M.P. (2012). Ketone body utilization drives tumor growth and metastasis. Cell cycle *11*, 3964-3971.

Matoba, S., Kang, J.G., Patino, W.D., Wragg, A., Boehm, M., Gavrilova, O., Hurley, P.J., Bunz, F., and Hwang, P.M. (2006). p53 regulates mitochondrial respiration. Science *312*, 1650-1653.

Mattar, S.G., Velcu, L.M., Rabinovitz, M., Demetris, A.J., Krasinskas, A.M., Barinas-Mitchell, E., Eid, G.M., Ramanathan, R., Taylor, D.S., and Schauer, P.R. (2005). Surgically-induced weight loss significantly improves nonalcoholic fatty liver disease and the metabolic syndrome. Ann Surg *242*, 610-617; discussion 618-620.

McClellan, J., and King, M.-C. (2010). Genetic Heterogeneity in Human Disease. Cell *141*, 210-217.

McCullough, K.D., Martindale, J.L., Klotz, L.O., Aw, T.Y., and Holbrook, N.J. (2001). Gadd153 Sensitizes Cells to Endoplasmic Reticulum Stress by Down-Regulating Bcl2 and Perturbing the Cellular Redox State. Molecular and cellular biology *21*, 1249-1259.

Mehlen, P., and Puisieux, A. (2006). Metastasis: a question of life or death. Nature Reviews Cancer *6*, 449-458.

Menendez, J.A., and Lupu, R. (2007). Fatty acid synthase and the lipogenic phenotype in cancer pathogenesis. Nature Reviews Cancer *7*, 763-777.

Mimeault, M. (2005). Recent advances on multiple tumorigenic cascades involved in prostatic cancer progression and targeting therapies. Carcinogenesis *27*, 1-22.

Mimeault, M., Pommery, N., and Hénichart, J.-P. (2003). New Advances on Prostate Carcinogenesis and Therapies: Involvement of EGF-EGFR Transduction System. Growth Factors *21*, 1-14.

Misiakos, E.P., Karidis, N.P., and Kouraklis, G. (2011). Current treatment for colorectal liver metastases. World journal of gastroenterology : WJG *17*, 4067-4075.

Monetti, M., Levin, M.C., Watt, M.J., Sajan, M.P., Marmor, S., Hubbard, B.K., Stevens, R.D., Bain, J.R., Newgard, C.B., Farese, R.V., Sr., *et al.* (2007). Dissociation of hepatic steatosis and insulin resistance in mice overexpressing DGAT in the liver. Cell Metab *6*, 69-78.

Motta, M., Giugno, I., Ruello, P., Pistone, G., Di Fazio, I., and Malaguarnera, M. (2001). Lipoprotein (a) behaviour in patients with hepatocellular carcinoma. Minerva medica *92*, 301-305.

Muraoka-Cook, R.S., Dumont, N., and Arteaga, C.L. (2005). Dual role of transforming growth factor beta in mammary tumorigenesis and metastatic progression. Clinical cancer research : an official journal of the American Association for Cancer Research *11*, 937s-943s.

Musso, G., Gambino, R., and Cassader, M. (2009a). Recent insights into hepatic lipid metabolism in non-alcoholic fatty liver disease (NAFLD). Progress in Lipid Research *48*, 1-26.

Musso, G., Gambino, R., and Cassader, M. (2009b). Recent insights into hepatic lipid metabolism in non-alcoholic fatty liver disease (NAFLD). Prog Lipid Res *48*, 1-26.

Musso, G., Gambino, R., and Cassader, M. (2013). Cholesterol metabolism and the pathogenesis of non-alcoholic steatohepatitis. Progress in Lipid Research *52*, 175-191.

Musso, G., Gambino, R., De Michieli, F., Cassader, M., Rizzetto, M., Durazzo, M., Faga, E., Silli, B., and Pagano, G. (2003). Dietary habits and their relations to insulin resistance and postprandial lipemia in nonalcoholic steatohepatitis. Hepatology *37*, 909-916.

Nagasawa, T., Inada, Y., Nakano, S., Tamura, T., Takahashi, T., Maruyama, K., Yamazaki, Y., Kuroda, J., and Shibata, N. (2006). Effects of bezafibrate, PPAR pan-agonist, and GW501516,

PPARdelta agonist, on development of steatohepatitis in mice fed a methionine- and choline-deficient diet. European journal of pharmacology *536*, 182-191.

Nair, S. (2002). Is obesity an independent risk factor for hepatocellular carcinoma in cirrhosis? Hepatology *36*, 150-155.

Nam, K.H., Lee, B.L., Park, J.H., Kim, J., Han, N., Lee, H.E., Kim, M.A., Lee, H.S., and Kim, W.H. (2013). Caveolin 1 Expression Correlates with Poor Prognosis and Focal Adhesion Kinase Expression in Gastric Cancer. Pathobiology *80*, 87-94.

Nath, A., and Chan, C. (2012). Relevance of Network Hierarchy in Cancer Drug-Target Selection. In Systems Biology in Cancer Research and Drug Discovery (Springer), pp. 339-362.

Nath, A., and Chan, C. (2015). Genetic alterations in fatty acid transport and metabolism genes are associated with metastatic progression and poor prognosis of human cancers.

Nath, A., Li, I., Roberts, L.R., and Chan, C. (2015). Elevated free fatty acid uptake via CD36 promotes epithelial to mesenchymal transition in hepatocellular carcinoma.

Nejak-Bowen, K.N., and Monga, S.P.S. (2011). Beta-catenin signaling, liver regeneration and hepatocellular cancer: Sorting the good from the bad. Seminars in Cancer Biology *21*, 44-58.

Nelson, J.E., and Harris, R.E. (2000). Inverse association of prostate cancer and non-steroidal anti-inflammatory drugs (NSAIDs): results of a case-control study. Oncol Rep *7*, 169-170.

Ni, Y.H., Chang, M.H., Wang, K.J., Hsu, H.Y., Chen, H.L., Kao, J.H., Yeh, S.H., Jeng, Y.M., Tsai, K.S., and Chen, D.S. (2004). Clinical relevance of hepatitis B virus genotype in children with chronic infection and hepatocellular carcinoma. Gastroenterology *127*, 1733-1738.

Nicolson, T.J., Bellomo, E.A., Wijesekara, N., Loder, M.K., Baldwin, J.M., Gyulkhandanyan, A.V., Koshkin, V., Tarasov, A.I., Carzaniga, R., Kronenberger, K., *et al.* (2009). Insulin storage and glucose homeostasis in mice null for the granule zinc transporter ZnT8 and studies of the type 2 diabetes-associated variants. Diabetes *58*, 2070-2083.

Njei, B., Rotman, Y., Ditah, I., and Lim, J.K. (2015). Emerging trends in hepatocellular carcinoma incidence and mortality. Hepatology *61*, 191-199.

Norrish, A.E., Jackson, R.T., and McRae, C.U. (1998). Non-steroidal anti-inflammatory drugs and prostate cancer progression. Int J Cancer *77*, 511-515.

O'Donnell, A., Judson, I., Dowsett, M., Raynaud, F., Dearnaley, D., Mason, M., Harland, S., Robbins, A., Halbert, G., Nutley, B., *et al.* (2004). Hormonal impact of the 17α-hydroxylase/C17,20-lyase inhibitor abiraterone acetate (CB7630) in patients with prostate cancer. British Journal of Cancer.

Ozcan, U., Cao, Q., Yilmaz, E., Lee, A.H., Iwakoshi, N.N., Ozdelen, E., Tuncman, G., Gorgun, C., Glimcher, L.H., and Hotamisligil, G.S. (2004). Endoplasmic reticulum stress links obesity, insulin action, and type 2 diabetes. Science *306*, 457-461.

Page, J.M., and Harrison, S.A. (2009). NASH and HCC. Clinics in Liver Disease *13*, 631-647.

Pardal, R., Clarke, M.F., and Morrison, S.J. (2003). Applying the principles of stem-cell biology to cancer. Nature reviews Cancer *3*, 895-902.

Park, E.J., Lee, J.H., Yu, G.-Y., He, G., Ali, S.R., Holzer, R.G., Österreicher, C.H., Takahashi, H., and Karin, M. (2010). Dietary and Genetic Obesity Promote Liver Inflammation and Tumorigenesis by Enhancing IL-6 and TNF Expression. Cell *140*, 197-208.

Park, Y.M., Drazba, J.A., Vasanji, A., Egelhoff, T., Febbraio, M., and Silverstein, R.L. (2012). Oxidized LDL/CD36 interaction induces loss of cell polarity and inhibits macrophage locomotion. Molecular biology of the cell *23*, 3057-3068.

Paumen, M.B., Ishida, Y., Muramatsu, M., Yamamoto, M., and Honjo, T. (1997). Inhibition of carnitine palmitoyltransferase I augments sphingolipid synthesis and palmitate-induced apoptosis. The Journal of biological chemistry *272*, 3324-3329.

Perez-Marreno, R., Chu, F.M., Gleason, D., Loizides, E., Wachs, B., and Tyler, R.C. (2002). A six-month, open-label study assessing a new formulation of leuprolide 7.5 mg for suppression of testosterone in patients with prostate cancer. Clinical Therapeutics *24*, 1902-1914.

Petrelli, A., and Giordano, S. (2008). From single- to multi-target drugs in cancer therapy: when aspecificity becomes an advantage. Curr Med Chem *15*, 422-432.

Pohl, J., Ring, A., Ehehalt, R., Herrmann, T., and Stremmel, W. (2004). New concepts of cellular fatty acid uptake: role of fatty acid transport proteins and of caveolae. The Proceedings of the Nutrition Society *63*, 259-262.

Polakis, P. (2000). Wnt signaling and cancer. Genes Dev *14*, 1837-1851.

Prada, P.O., Ropelle, E.R., Mourao, R.H., de Souza, C.T., Pauli, J.R., Cintra, D.E., Schenka, A., Rocco, S.A., Rittner, R., Franchini, K.G., *et al.* (2009). EGFR tyrosine kinase inhibitor (PD153035) improves glucose tolerance and insulin action in high-fat diet-fed mice. Diabetes *58*, 2910-2919.

Radisky, D.C. (2005). Epithelial-mesenchymal transition. Journal of Cell Science *118*, 4325-4326.

Rajasethupathy, P., Vayttaden, S.J., and Bhalla, U.S. (2005). Systems modeling: a pathway to drug discovery. Curr Opin Chem Biol *9*, 400-406.

Rampazzo, A., Nava, A., Malacrida, S., Beffagna, G., Bauce, B., Rossi, V., Zimbello, R., Simionati, B., Basso, C., Thiene, G., *et al.* (2002). Mutation in human desmoplakin domain binding to

plakoglobin causes a dominant form of arrhythmogenic right ventricular cardiomyopathy. Am J Hum Genet *71*, 1200-1206.

Razani, B., Combs, T.P., Wang, X.B., Frank, P.G., Park, D.S., Russell, R.G., Li, M., Tang, B., Jelicks, L.A., Scherer, P.E., *et al.* (2002). Caveolin-1-deficient mice are lean, resistant to diet-induced obesity, and show hypertriglyceridemia with adipocyte abnormalities. The Journal of biological chemistry *277*, 8635-8647.

Reddy, J.K., and Hashimoto, T. (2001). Peroxisomal beta-oxidation and peroxisome proliferator-activated receptor alpha: an adaptive metabolic system. Annual review of nutrition *21*, 193-230.

Reed, B.D., Charos, A.E., Szekely, A.M., Weissman, S.M., and Snyder, M. (2008). Genome-wide occupancy of SREBP1 and its partners NFY and SP1 reveals novel functional roles and combinatorial regulation of distinct classes of genes. PLoS genetics *4*, e1000133.

Remenyi, A., Scholer, H.R., and Wilmanns, M. (2004). Combinatorial control of gene expression. Nat Struct Mol Biol *11*, 812-815.

Richardsen, E., Uglehus, R.D., Due, J., Busch, C., and Busund, L.T. (2010). COX-2 is overexpressed in primary prostate cancer with metastatic potential and may predict survival. A comparison study between COX-2, TGF-beta, IL-10 and Ki67. Cancer Epidemiol *34*, 316-322.

Roberts, S.A., Lawrence, M.S., Klimczak, L.J., Grimm, S.A., Fargo, D., Stojanov, P., Kiezun, A., Kryukov, G.V., Carter, S.L., Saksena, G., *et al.* (2013). An APOBEC cytidine deaminase mutagenesis pattern is widespread in human cancers. Nature Genetics *45*, 970-976.

Rodríguez-Enríquez, S., Gallardo-Pérez, J.C., Avilés-Salas, A., Marín-Hernández, A., Carreño-Fuentes, L., Maldonado-Lagunas, V., and Moreno-Sánchez, R. (2008). Energy metabolism transition in multi-cellular human tumor spheroids. Journal of Cellular Physiology *216*, 189-197.

Ron, D., and Walter, P. (2007). Signal integration in the endoplasmic reticulum unfolded protein response. Nature reviews Molecular cell biology *8*, 519-529.

Rong, R., Ahn, J.Y., Huang, H., Nagata, E., Kalman, D., Kapp, J.A., Tu, J., Worley, P.F., Snyder, S.H., and Ye, K. (2003). PI3 kinase enhancer-Homer complex couples mGluRI to PI3 kinase, preventing neuronal apoptosis. Nat Neurosci *6*, 1153-1161.

Ross, S.E., Hemati, N., Longo, K.A., Bennett, C.N., Lucas, P.C., Erickson, R.L., and MacDougald, O.A. (2000). Inhibition of adipogenesis by Wnt signaling. Science *289*, 950-953.

Ruddock, M.W., Stein, A., Landaker, E., Park, J., Cooksey, R.C., McClain, D., and Patti, M.E. (2008). Saturated fatty acids inhibit hepatic insulin action by modulating insulin receptor expression and post-receptor signalling. J Biochem *144*, 599-607.

Ryan, C.J., Smith, M.R., Fong, L., Rosenberg, J.E., Kantoff, P., Raynaud, F., Martins, V., Lee, G., Kheoh, T., Kim, J., *et al.* (2010). Phase I Clinical Trial of the CYP17 Inhibitor Abiraterone Acetate Demonstrating Clinical Activity in Patients With Castration-Resistant Prostate Cancer Who Received Prior Ketoconazole Therapy. Journal of Clinical Oncology *28*, 1481-1488.

Salt, M.B., Bandyopadhyay, S., and McCormick, F. (2013). Epithelial-to-Mesenchymal Transition Rewires the Molecular Path to PI3K-Dependent Proliferation. Cancer discovery *4*, 186-199.

Sanders, D.S., Blessing, K., Hassan, G.A., Bruton, R., Marsden, J.R., and Jankowski, J. (1999). Alterations in cadherin and catenin expression during the biological progression of melanocytic tumours. Molecular pathology : MP *52*, 151-157.

Sangiovanni, A., Del Ninno, E., Fasani, P., De Fazio, C., Ronchi, G., Romeo, R., Morabito, A., De Franchis, R., and Colombo, M. (2004). Increased survival of cirrhotic patients with a hepatocellular carcinoma detected during surveillance. Gastroenterology *126*, 1005-1014.

Santidrian, A.F., Matsuno-Yagi, A., Ritland, M., Seo, B.B., LeBoeuf, S.E., Gay, L.J., Yagi, T., and Felding-Habermann, B. (2013). Mitochondrial complex I activity and NAD+/NADH balance regulate breast cancer progression. The Journal of clinical investigation *123*, 1068-1081.

Sanyal, A., Poklepovic, A., Moyneur, E., and Barghout, V. (2010). Population-based risk factors and resource utilization for HCC: US perspective. Current medical research and opinion *26*, 2183-2191.

Savage, D.B., Tan, G.D., Acerini, C.L., Jebb, S.A., Agostini, M., Gurnell, M., Williams, R.L., Umpleby, A.M., Thomas, E.L., Bell, J.D., *et al.* (2003). Human metabolic syndrome resulting from dominant-negative mutations in the nuclear receptor peroxisome proliferator-activated receptor-gamma. Diabetes *52*, 910-917.

Sawyer, J.S., Anderson, B.D., Beight, D.W., Campbell, R.M., Jones, M.L., Herron, D.K., Lampe, J.W., McCowan, J.R., McMillen, W.T., Mort, N., *et al.* (2003). Synthesis and activity of new aryl- and heteroaryl-substituted pyrazole inhibitors of the transforming growth factor-beta type I receptor kinase domain. Journal of medicinal chemistry *46*, 3953-3956.

Sawyers, C. (2004). Targeted cancer therapy. Nature *432*, 294-297.

Schneider, C.A., Rasband, W.S., and Eliceiri, K.W. (2012). NIH Image to ImageJ: 25 years of image analysis. Nature Methods *9*, 671-675.

Schumacker, P.T. (2006). Reactive oxygen species in cancer cells: live by the sword, die by the sword. Cancer cell *10*, 175-176.

Schwienbacher, C., Gramantieri, L., Scelfo, R., Veronese, A., Calin, G.A., Bolondi, L., Croce, C.M., Barbanti-Brodano, G., and Negrini, M. (2000). Gain of imprinting at chromosome 11p15: A pathogenetic mechanism identified in human hepatocarcinomas. Proceedings of the National Academy of Sciences of the United States of America *97*, 5445-5449.

Shaw, R.J. (2006). Glucose metabolism and cancer. Current opinion in cell biology *18*, 598-608.

Shen, B., Chu, E.S.H., Zhao, G., Man, K., Wu, C.W., Cheng, J.T.Y., Li, G., Nie, Y., Lo, C.M., Teoh, N., *et al.* (2012). PPARgamma inhibits hepatocellular carcinoma metastases in vitro and in mice. British journal of cancer *106*, 1486-1494.

Shen, M.M., and Abate-Shen, C. (2010). Molecular genetics of prostate cancer: new prospects for old challenges. Genes Dev *24*, 1967-2000.

Shi, J., Wang, D.M., Wang, C.M., Hu, Y., Liu, A.H., Zhang, Y.L., Sun, B., and Song, J.G. (2009). Insulin Receptor Substrate-1 Suppresses Transforming Growth Factor- 1-Mediated Epithelial-Mesenchymal Transition. Cancer Research *69*, 7180-7187.

Shimomura, I., Bashmakov, Y., and Horton, J.D. (1999). Increased levels of nuclear SREBP-1c associated with fatty livers in two mouse models of diabetes mellitus. The Journal of biological chemistry *274*, 30028-30032.

Shiraishi, Y., Mizutani, A., Yuasa, S., Mikoshiba, K., and Furuichi, T. (2004). Differential expression of Homer family proteins in the developing mouse brain. J Comp Neurol *473*, 582-599.

Shuch, B. (2004). Racial Disparity of Epidermal Growth Factor Receptor Expression in Prostate Cancer. Journal of Clinical Oncology *22*, 4725-4729.

Siddique, A., and Kowdley, K.V. (2011). Insulin resistance and other metabolic risk factors in the pathogenesis of hepatocellular carcinoma. Clinics in liver disease *15*, 281-296, vii-x.

Siebler, J., Schuchmann, M., Strand, S., Lehr, H.A., Neurath, M.F., and Galle, P.R. (2007). Enhanced sensitivity to CD95-induced apoptosis in ob/ob mice. Digestive diseases and sciences *52*, 2396-2402.

Siegel, R., Ward, E., Brawley, O., and Jemal, A. (2011). Cancer statistics, 2011: the impact of eliminating socioeconomic and racial disparities on premature cancer deaths. CA Cancer J Clin *61*, 212-236.

Silverthorn, D.U., Ober, W.C., Garrison, C.W., Silverthorn, A.C., and Johnson, B.R. (2009). Human physiology: an integrated approach (Pearson/Benjamin Cummings).

Simsek, T., Kocabas, F., Zheng, J., Deberardinis, R.J., Mahmoud, A.I., Olson, E.N., Schneider, J.W., Zhang, C.C., and Sadek, H.A. (2010). The distinct metabolic profile of hematopoietic stem cells reflects their location in a hypoxic niche. Cell stem cell *7*, 380-390.

Singh, A., and Settleman, J. (2010). EMT, cancer stem cells and drug resistance: an emerging axis of evil in the war on cancer. Oncogene *29*, 4741-4751.

Slawik, M., and Vidal-Puig, A.J. (2006). Lipotoxicity, overnutrition and energy metabolism in aging. Ageing research reviews *5*, 144-164.

Small, E.J., Fontana, J., Tannir, N., DiPaola, R.S., Wilding, G., Rubin, M., Iacona, R.B., and Kabbinavar, F.F. (2007). A phase II trial of gefitinib in patients with non-metastatic hormone-refractory prostate cancer. BJU International *100*, 765-769.

Smidt, K., Jessen, N., Petersen, A.B., Larsen, A., Magnusson, N., Jeppesen, J.B., Stoltenberg, M., Culvenor, J.G., Tsatsanis, A., Brock, B., *et al.* (2009). SLC30A3 responds to glucose- and zinc variations in beta-cells and is critical for insulin production and in vivo glucose-metabolism during beta-cell stress. PLoS One *4*, e5684.

Smith, J., Su, X., El-Maghrabi, R., Stahl, P.D., and Abumrad, N.A. (2008). Opposite regulation of CD36 ubiquitination by fatty acids and insulin: effects on fatty acid uptake. J Biol Chem *283*, 13578-13585.

Smith, J.J., Ramsey, S.A., Marelli, M., Marzolf, B., Hwang, D., Saleem, R.A., Rachubinski, R.A., and Aitchison, J.D. (2007). Transcriptional responses to fatty acid are coordinated by combinatorial control. Molecular systems biology *3*, 115.

Sotgia, F., Martinez-Outschoorn, U.E., Howell, A., Pestell, R.G., Pavlides, S., and Lisanti, M.P. (2012). Caveolin-1 and Cancer Metabolism in the Tumor Microenvironment: Markers, Models, and Mechanisms. Annual Review of Pathology: Mechanisms of Disease *7*, 423-467.

Srivastava, S., and Chan, C. (2008). Application of metabolic flux analysis to identify the mechanisms of free fatty acid toxicity to human hepatoma cell line. Biotechnol Bioeng *99*, 399-410.

Srivastava, S., Li, Z., Yang, X., Yedwabnick, M., Shaw, S., and Chan, C. (2007). Identification of genes that regulate multiple cellular processes/responses in the context of lipotoxicity to hepatoma cells. BMC Genomics *8*, 364.

Stein, W.D., Bates, S.E., and Fojo, T. (2004). Intractable cancers: the many faces of multidrug resistance and the many targets it presents for therapeutic attack. Curr Drug Targets *5*, 333-346.

Stickel, F., and Hellerbrand, C. (2010). Non-alcoholic fatty liver disease as a risk factor for hepatocellular carcinoma: mechanisms and implications. Gut *59*, 1303-1307.

Storz, P., Doppler, H., Wernig, A., Pfizenmaier, K., and Muller, G. (1999). Cross-talk mechanisms in the development of insulin resistance of skeletal muscle cells palmitate rather than tumour necrosis factor inhibits insulin-dependent protein kinase B (PKB)/Akt stimulation and glucose uptake. Eur J Biochem *266*, 17-25.

Stratton, M.R., Campbell, P.J., and Futreal, P.A. (2009). The cancer genome. Nature *458*, 719-724.

Stremmel, W., Pohl, L., Ring, A., and Herrmann, T. (2001). A new concept of cellular uptake and intracellular trafficking of long-chain fatty acids. Lipids *36*, 981-989.

Suganami, T., Nishida, J., and Ogawa, Y. (2005). A paracrine loop between adipocytes and macrophages aggravates inflammatory changes: role of free fatty acids and tumor necrosis factor alpha. Arteriosclerosis, thrombosis, and vascular biology *25*, 2062-2068.

Sumi, K., Tanaka, T., Uchida, A., Magoori, K., Urashima, Y., Ohashi, R., Ohguchi, H., Okamura, M., Kudo, H., Daigo, K., *et al.* (2007). Cooperative interaction between hepatocyte nuclear factor 4 alpha and GATA transcription factors regulates ATP-binding cassette sterol transporters ABCG5 and ABCG8. Mol Cell Biol *27*, 4248-4260.

Summers, L.K., Fielding, B.A., Bradshaw, H.A., Ilic, V., Beysen, C., Clark, M.L., Moore, N.R., and Frayn, K.N. (2002). Substituting dietary saturated fat with polyunsaturated fat changes abdominal fat distribution and improves insulin sensitivity. Diabetologia *45*, 369-377.

Summers, S.A. (2006). Ceramides in insulin resistance and lipotoxicity. Prog Lipid Res *45*, 42-72.

Swagell, C.D., Henly, D.C., and Morris, C.P. (2005). Expression analysis of a human hepatic cell line in response to palmitate. Biochem Biophys Res Commun *328*, 432-441.

Szabo, G., Velayudham, A., Romics, L., Jr., and Mandrekar, P. (2005). Modulation of non-alcoholic steatohepatitis by pattern recognition receptors in mice: the role of toll-like receptors 2 and 4. Alcoholism, clinical and experimental research *29*, 140S-145S.

Tan, N.S., Shaw, N.S., Vinckenbosch, N., Liu, P., Yasmin, R., Desvergne, B., Wahli, W., and Noy, N. (2002). Selective cooperation between fatty acid binding proteins and peroxisome proliferator-activated receptors in regulating transcription. Mol Cell Biol *22*, 5114-5127.

Tanabe, K.K., Lemoine, A., Finkelstein, D.M., Kawasaki, H., Fujii, T., Chung, R.T., Lauwers, G.Y., Kulu, Y., Muzikansky, A., Kuruppu, D., *et al.* (2008). Epidermal growth factor gene functional polymorphism and the risk of hepatocellular carcinoma in patients with cirrhosis. Jama *299*, 53-60.

Tanaka, N., Moriya, K., Kiyosawa, K., Koike, K., Gonzalez, F.J., and Aoyama, T. (2008). PPARalpha activation is essential for HCV core protein-induced hepatic steatosis and hepatocellular carcinoma in mice. The Journal of clinical investigation *118*, 683-694.

Tang, Z.Y. (2001). Hepatocellular carcinoma--cause, treatment and metastasis. World journal of gastroenterology : WJG *7*, 445-454.

Taniguchi, K., Roberts, L.R., Aderca, I.N., Dong, X., Qian, C., Murphy, L.M., Nagorney, D.M., Burgart, L.J., Roche, P.C., Smith, D.I., *et al.* (2002). Mutational spectrum of beta-catenin, AXIN1, and AXIN2 in hepatocellular carcinomas and hepatoblastomas. Oncogene *21*, 4863-4871.

Targher, G., Bertolini, L., Padovani, R., Rodella, S., Zoppini, G., Pichiri, I., Sorgato, C., Zenari, L., and Bonora, E. (2010). Prevalence of non-alcoholic fatty liver disease and its association with cardiovascular disease in patients with type 1 diabetes. J Hepatol *53*, 713-718.

Targher, G., Marra, F., and Marchesini, G. (2008). Increased risk of cardiovascular disease in non-alcoholic fatty liver disease: causal effect or epiphenomenon? Diabetologia *51*, 1947-1953.

Tavares De Almeida, I., Cortez-Pinto, H., Fidalgo, G., Rodrigues, D., and Camilo, M.E. (2002). Plasma total and free fatty acids composition in human non-alcoholic steatohepatitis. Clinical Nutrition *21*, 219-223.

Tennant, D.A., Duran, R.V., and Gottlieb, E. (2010). Targeting metabolic transformation for cancer therapy. Nature reviews Cancer *10*, 267-277.

Thiery, J.P. (2002). Epithelial–mesenchymal transitions in tumour progression. Nature Reviews Cancer *2*, 442-454.

Thiery, J.P., and Sleeman, J.P. (2006). Complex networks orchestrate epithelial–mesenchymal transitions. Nature Reviews Molecular Cell Biology *7*, 131-142.

Thompson, I.M., Goodman, P.J., Tangen, C.M., Lucia, M.S., Miller, G.J., Ford, L.G., Lieber, M.M., Cespedes, R.D., Atkins, J.N., Lippman, S.M., *et al.* (2003). The influence of finasteride on the development of prostate cancer. N Engl J Med *349*, 215-224.

Thorgeirsson, S.S., and Grisham, J.W. (2002). Molecular pathogenesis of human hepatocellular carcinoma. Nat Genet *31*, 339-346.

Tien, L.T., Ito, M., Nakao, M., Niino, D., Serik, M., Nakashima, M., Wen, C.Y., Yatsuhashi, H., and Ishibashi, H. (2005). Expression of beta-catenin in hepatocellular carcinoma. World journal of gastroenterology : WJG *11*, 2398-2401.

Titus, M.A. (2005). Testosterone and Dihydrotestosterone Tissue Levels in Recurrent Prostate Cancer. Clinical Cancer Research *11*, 4653-4657.

Topol, E.J. (2004). Failing the public health--rofecoxib, Merck, and the FDA. N Engl J Med *351*, 1707-1709.

Topping, D.L., and Mayes, P.A. (1972). The immediate effects of insulin and fructose on the metabolism of the perfused liver. Changes in lipoprotein secretion, fatty acid oxidation and esterification, lipogenesis and carbohydrate metabolism. Biochem J *126*, 295-311.

Tortora, G.J., and Anagnostakos, N.P. (1976). Principles of anatomy and physiology.

Tortora, G.J., and Derrickson, B.H. (2008). Principles of anatomy and physiology (John Wiley & Sons).

Toyosaka, A., Okamoto, E., Mitsunobu, M., Oriyama, T., Nakao, N., and Miura, K. (1996). Intrahepatic metastases in hepatocellular carcinoma: evidence for spread via the portal vein as an efferent vessel. Am J Gastroenterol *91*, 1610-1615.

Trafalis, D.T., Panteli, E.S., Grivas, A., Tsigris, C., and Karamanakos, P.N. (2010). CYP2E1 and risk of chemically mediated cancers. Expert Opinion on Drug Metabolism & Toxicology *6*, 307-319.

Tsai, J.H., and Yang, J. (2013). Epithelial-mesenchymal plasticity in carcinoma metastasis. Genes & Development *27*, 2192-2206.

Tsai, W.C., Hsu, S.D., Hsu, C.S., Lai, T.C., Chen, S.J., Shen, R., Huang, Y., Chen, H.C., Lee, C.H., Tsai, T.F., *et al.* (2012). MicroRNA-122 plays a critical role in liver homeostasis and hepatocarcinogenesis. The Journal of clinical investigation *122*, 2884-2897.

Tsang, M.Y., Cowie, S.E., and Rabkin, S.W. (2004). Palmitate increases nitric oxide synthase activity that is involved in palmitate-induced cell death in cardiomyocytes. Nitric Oxide *10*, 11-19.

Tung-Ping Poon, R., Fan, S.T., and Wong, J. (2000). Risk factors, prevention, and management of postoperative recurrence after resection of hepatocellular carcinoma. Annals of surgery *232*, 10-24.

Ueki, T., Fujimoto, J., Suzuki, T., Yamamoto, H., and Okamoto, E. (1997). Expression of hepatocyte growth factor and its receptor c-met proto-oncogene in hepatocellular carcinoma. Hepatology *25*, 862-866.

Ulitsky, I., and Shamir, R. (2007). Identification of functional modules using network topology and high-throughput data. BMC Syst Biol *1*, 8.

Uyeda, K., and Repa, J.J. (2006a). Carbohydrate response element binding protein, ChREBP, a transcription factor coupling hepatic glucose utilization and lipid synthesis. Cell Metabolism *4*, 107-110.

Uyeda, K., and Repa, J.J. (2006b). Carbohydrate response element binding protein, ChREBP, a transcription factor coupling hepatic glucose utilization and lipid synthesis. Cell Metab *4*, 107-110.

Uzumcu, A., Norgett, E.E., Dindar, A., Uyguner, O., Nisli, K., Kayserili, H., Sahin, S.E., Dupont, E., Severs, N.J., Leigh, I.M., *et al.* (2006). Loss of desmoplakin isoform I causes early onset cardiomyopathy and heart failure in a Naxos-like syndrome. J Med Genet *43*, e5.

Vadigepalli, R., Chakravarthula, P., Zak, D.E., Schwaber, J.S., and Gonye, G.E. (2003). PAINT: a promoter analysis and interaction network generation tool for gene regulatory network identification. OMICS *7*, 235-252.

van Adelsberg, J., Gann, P., Ko, A.T., Damber, J.E., Logothetis, C., Marberger, M., Schmitz-Drager, B.J., Tubaro, A., Harms, C.J., and Roehrborn, C. (2007). The VIOXX in Prostate Cancer Prevention study: cardiovascular events observed in the rofecoxib 25 mg and placebo treatment groups. Curr Med Res Opin *23*, 2063-2070.

van der Greef, J., and McBurney, R.N. (2005). Innovation: Rescuing drug discovery: in vivo systems pathology and systems pharmacology. Nat Rev Drug Discov *4*, 961-967.

Van Rooyen, D.M., Larter, C.Z., Haigh, W.G., Yeh, M.M., Ioannou, G., Kuver, R., Lee, S.P., Teoh, N.C., and Farrell, G.C. (2011). Hepatic Free Cholesterol Accumulates in Obese, Diabetic Mice and Causes Nonalcoholic Steatohepatitis. Gastroenterology *141*, 1393-1403.e1395.

Vander Heiden, M.G. (2011). Targeting cancer metabolism: a therapeutic window opens. Nature reviews Drug discovery *10*, 671-684.

Vander Heiden, M.G., Cantley, L.C., and Thompson, C.B. (2009a). Understanding the Warburg effect: the metabolic requirements of cell proliferation. Science *324*, 1029-1033.

Vander Heiden, M.G., Cantley, L.C., and Thompson, C.B. (2009b). Understanding the Warburg Effect: The Metabolic Requirements of Cell Proliferation. Science *324*, 1029-1033.

Vessby, B., Uusitupa, M., Hermansen, K., Riccardi, G., Rivellese, A.A., Tapsell, L.C., Nalsen, C., Berglund, L., Louheranta, A., Rasmussen, B.M., *et al.* (2001). Substituting dietary saturated for monounsaturated fat impairs insulin sensitivity in healthy men and women: The KANWU Study. Diabetologia *44*, 312-319.

Vinayagam, A., Stelzl, U., Foulle, R., Plassmann, S., Zenkner, M., Timm, J., Assmus, H.E., Andrade-Navarro, M.A., and Wanker, E.E. (2011). A directed protein interaction network for investigating intracellular signal transduction. Sci Signal *4*, rs8.

Vinken, M., Papeleu, P., Snykers, S., De Rop, E., Henkens, T., Chipman, J.K., Rogiers, V., and Vanhaecke, T. (2006). Involvement of cell junctions in hepatocyte culture functionality. Crit Rev Toxicol *36*, 299-318.

Vogelstein, B., and Kinzler, K.W. (2004). Cancer genes and the pathways they control. Nature Medicine *10*, 789-799.

Wagenaar, T.R., Zabludoff, S., Ahn, S.M., Allerson, C., Arlt, H., Baffa, R., Cao, H., Davis, S., Garcia-Echeverria, C., Gaur, R., *et al.* (2015). Anti-miR-21 Suppresses Hepatocellular Carcinoma Growth via Broad Transcriptional Network De-regulation. Molecular cancer research : MCR.

Wang, X., Dalkic, E., Wu, M., and Chan, C. (2008). Gene module level analysis: identification to networks and dynamics. Curr Opin Biotechnol *19*, 482-491.

Wang, X., Nath, A., Yang, X., Portis, A., Walton, S.P., and Chan, C. (2011). Synergy analysis reveals association between insulin signaling and desmoplakin expression in palmitate treated HepG2 cells. PloS one *6*, e28138.

Wei, Y. (2006). Saturated fatty acids induce endoplasmic reticulum stress and apoptosis independently of ceramide in liver cells. AJP: Endocrinology and Metabolism *291*, E275-E281.

Wei, Y., Wang, D., Topczewski, F., and Pagliassotti, M.J. (2006). Saturated fatty acids induce endoplasmic reticulum stress and apoptosis independently of ceramide in liver cells. American journal of physiology Endocrinology and metabolism *291*, E275-281.

Weigert, C., Brodbeck, K., Staiger, H., Kausch, C., Machicao, F., Haring, H.U., and Schleicher, E.D. (2004). Palmitate, but Not Unsaturated Fatty Acids, Induces the Expression of Interleukin-6 in Human Myotubes through Proteasome-dependent Activation of Nuclear Factor- B. Journal of Biological Chemistry *279*, 23942-23952.

Wheeler, D.A., and Wang, L. (2013). From human genome to cancer genome: The first decade. Genome research *23*, 1054-1062.

Whittock, N.V., Wan, H., Morley, S.M., Garzon, M.C., Kristal, L., Hyde, P., McLean, W.H., Pulkkinen, L., Uitto, J., Christiano, A.M., *et al.* (2002). Compound heterozygosity for non-sense and mis-sense mutations in desmoplakin underlies skin fragility/woolly hair syndrome. J Invest Dermatol *118*, 232-238.

Wishart, D.S. (2006). DrugBank: a comprehensive resource for in silico drug discovery and exploration. Nucleic Acids Research *34*, D668-D672.

Xiong, H., Hong, J., Du, W., Lin, Y.w., Ren, L.l., Wang, Y.c., Su, W.y., Wang, J.l., Cui, Y., Wang, Z.h., *et al.* (2011). Roles of STAT3 and ZEB1 Proteins in E-cadherin Down-regulation and Human Colorectal Cancer Epithelial-Mesenchymal Transition. Journal of Biological Chemistry *287*, 5819-5832.

Xu, J., Lamouille, S., and Derynck, R. (2009). TGF-beta-induced epithelial to mesenchymal transition. Cell Res *19*, 156-172.

Yadav, A., Kumar, B., Datta, J., Teknos, T.N., and Kumar, P. (2011). IL-6 Promotes Head and Neck Tumor Metastasis by Inducing Epithelial-Mesenchymal Transition via the JAK-STAT3-SNAIL Signaling Pathway. Molecular Cancer Research *9*, 1658-1667.

Yamaguchi, K., Yang, L., McCall, S., Huang, J., Yu, X.X., Pandey, S.K., Bhanot, S., Monia, B.P., Li, Y.X., and Diehl, A.M. (2007). Inhibiting triglyceride synthesis improves hepatic steatosis but exacerbates liver damage and fibrosis in obese mice with nonalcoholic steatohepatitis. Hepatology *45*, 1366-1374.

Yang, H.I., Lu, S.N., Liaw, Y.F., You, S.L., Sun, C.A., Wang, L.Y., Hsiao, C.K., Chen, P.J., Chen, D.S., Chen, C.J., *et al.* (2002). Hepatitis B e antigen and the risk of hepatocellular carcinoma. The New England journal of medicine *347*, 168-174.

Yang, H.I., Yeh, S.H., Chen, P.J., Iloeje, U.H., Jen, C.L., Su, J., Wang, L.Y., Lu, S.N., You, S.L., Chen, D.S., *et al.* (2008a). Associations between hepatitis B virus genotype and mutants and the risk of hepatocellular carcinoma. Journal of the National Cancer Institute *100*, 1134-1143.

Yang, J., Mani, S.A., Donaher, J.L., Ramaswamy, S., Itzykson, R.A., Come, C., Savagner, P., Gitelman, I., Richardson, A., and Weinberg, R.A. (2004). Twist, a master regulator of morphogenesis, plays an essential role in tumor metastasis. Cell *117*, 927-939.

Yang, J.D., Kim, W.R., Coelho, R., Mettler, T.A., Benson, J.T., Sanderson, S.O., Therneau, T.M., Kim, B., and Roberts, L.R. (2011). Cirrhosis is present in most patients with hepatitis B and hepatocellular carcinoma. Clinical gastroenterology and hepatology : the official clinical practice journal of the American Gastroenterological Association *9*, 64-70.

Yang, M.-H., Wu, M.-Z., Chiou, S.-H., Chen, P.-M., Chang, S.-Y., Liu, C.-J., Teng, S.-C., and Wu, K.-J. (2008b). Direct regulation of TWIST by HIF-1α promotes metastasis. Nature cell biology *10*, 295-305.

Yang, M.H., Chen, C.L., Chau, G.Y., Chiou, S.H., Su, C.W., Chou, T.Y., Peng, W.L., and Wu, J.C. (2009a). Comprehensive analysis of the independent effect of twist and snail in promoting metastasis of hepatocellular carcinoma. Hepatology *50*, 1464-1474.

Yang, X., and Chan, C. (2009). Repression of PKR mediates palmitate-induced apoptosis in HepG2 cells through regulation of Bcl-2. Cell Res *19*, 469-486.

Yang, X., Nath, A., Opperman, M.J., and Chan, C. (2010). The double-stranded RNA-dependent protein kinase differentially regulates insulin receptor substrates 1 and 2 in HepG2 cells. Molecular biology of the cell *21*, 3449-3458.

Yang, X., Zhou, Y., Jin, R., and Chan, C. (2009b). Reconstruct modular phenotype-specific gene networks by knowledge-driven matrix factorization. Bioinformatics (Oxford, England) *25*, 2236-2243.

Yang, Z., Bowles, N.E., Scherer, S.E., Taylor, M.D., Kearney, D.L., Ge, S., Nadvoretskiy, V.V., DeFreitas, G., Carabello, B., Brandon, L.I., *et al.* (2006). Desmosomal dysfunction due to mutations in desmoplakin causes arrhythmogenic right ventricular dysplasia/cardiomyopathy. Circ Res *99*, 646-655.

Ye, J., Coulouris, G., Zaretskaya, I., Cutcutache, I., Rozen, S., and Madden, T.L. (2012). Primer-BLAST: A tool to design target-specific primers for polymerase chain reaction. BMC Bioinformatics *13*, 134.

Ye, Q.H., Qin, L.X., Forgues, M., He, P., Kim, J.W., Peng, A.C., Simon, R., Li, Y., Robles, A.I., Chen, Y., *et al.* (2003). Predicting hepatitis B virus-positive metastatic hepatocellular carcinomas using gene expression profiling and supervised machine learning. Nature medicine *9*, 416-423.

Yen, C.L.E., Stone, S.J., Koliwad, S., Harris, C., and Farese, R.V. (2008). Thematic Review Series: Glycerolipids. DGAT enzymes and triacylglycerol biosynthesis. The Journal of Lipid Research *49*, 2283-2301.

Yokota, J. (2000). Tumor progression and metastasis. Carcinogenesis *21*, 497-503.

Yong, K.J., Gao, C., Lim, J.S., Yan, B., Yang, H., Dimitrov, T., Kawasaki, A., Ong, C.W., Wong, K.F., Lee, S., *et al.* (2013). Oncofetal gene SALL4 in aggressive hepatocellular carcinoma. The New England journal of medicine *368*, 2266-2276.

Yoon, J.C., Ng, A., Kim, B.H., Bianco, A., Xavier, R.J., and Elledge, S.J. (2010). Wnt signaling regulates mitochondrial physiology and insulin sensitivity. Genes Dev *24*, 1507-1518.

Young, R.M., Ackerman, D., Quinn, Z.L., Mancuso, A., Gruber, M., Liu, L., Giannoukos, D.N., Bobrovnikova-Marjon, E., Diehl, J.A., Keith, B., *et al.* (2013). Dysregulated mTORC1 renders cells critically dependent on desaturated lipids for survival under tumor-like stress. Genes Dev *27*, 1115-1131.

Yu, H., and Gerstein, M. (2006a). Colloquium Papers: Genomic analysis of the hierarchical structure of regulatory networks. Proceedings of the National Academy of Sciences *103*, 14724-14731.

Yu, H., and Gerstein, M. (2006b). Genomic analysis of the hierarchical structure of regulatory networks. Proc Natl Acad Sci U S A *103*, 14724-14731.

Yu, J., Shen, B., Chu, E.S., Teoh, N., Cheung, K.F., Wu, C.W., Wang, S., Lam, C.N., Feng, H., Zhao, J., *et al.* (2010). Inhibitory role of peroxisome proliferator-activated receptor gamma in hepatocarcinogenesis in mice and in vitro. Hepatology *51*, 2008-2019.

Yun, K., Choi, Y.D., Nam, J.H., Park, Z., and Im, S.H. (2007). NF-kappaB regulates Lef1 gene expression in chondrocytes. Biochemical and biophysical research communications *357*, 589-595.

Zack, T.I., Schumacher, S.E., Carter, S.L., Cherniack, A.D., Saksena, G., Tabak, B., Lawrence, M.S., Zhang, C.-Z., Wala, J., Mermel, C.H., *et al.* (2013). Pan-cancer patterns of somatic copy number alteration. Nature Genetics *45*, 1134-1140.

Zaugg, K., Yao, Y., Reilly, P.T., Kannan, K., Kiarash, R., Mason, J., Huang, P., Sawyer, S.K., Fuerth, B., Faubert, B., *et al.* (2011a). Carnitine palmitoyltransferase 1C promotes cell survival and tumor growth under conditions of metabolic stress. Genes Dev *25*, 1041-1051.

Zaugg, K., Yao, Y., Reilly, P.T., Kannan, K., Kiarash, R., Mason, J., Huang, P., Sawyer, S.K., Fuerth, B., Faubert, B., *et al.* (2011b). Carnitine palmitoyltransferase 1C promotes cell survival and tumor growth under conditions of metabolic stress. Genes & Development *25*, 1041-1051.

Zelber-Sagi, S., Nitzan-Kaluski, D., Goldsmith, R., Webb, M., Blendis, L., Halpern, Z., and Oren, R. (2007). Long term nutritional intake and the risk for non-alcoholic fatty liver disease (NAFLD): a population based study. J Hepatol *47*, 711-717.

Zellweger, T., Ninck, C., Bloch, M., Mirlacher, M., Koivisto, P.A., Helin, H.J., Mihatsch, M.J., Gasser, T.C., and Bubendorf, L. (2005). Expression patterns of potential therapeutic targets in prostate cancer. International Journal of Cancer *113*, 619-628.

Zhai, B., Yan, H.X., Liu, S.Q., Chen, L., Wu, M.C., and Wang, H.Y. (2008). Reduced expression of E-cadherin/catenin complex in hepatocellular carcinomas. World journal of gastroenterology : WJG *14*, 5665-5673.

Zhang, C.-H., Xu, G.-L., Jia, W.-D., Li, J.-S., Ma, J.-L., Ren, W.-H., Ge, Y.-S., Yu, J.-H., Liu, W.-B., and Wang, W. (2012). Activation of STAT3 Signal Pathway Correlates with Twist and E-Cadherin Expression in Hepatocellular Carcinoma and Their Clinical Significance. Journal of Surgical Research *174*, 120-129.

Zhang, Q., Piston, D.W., and Goodman, R.H. (2002). Regulation of corepressor function by nuclear NADH. Science *295*, 1895-1897.

Zhang, Q., Wang, S.Y., Nottke, A.C., Rocheleau, J.V., Piston, D.W., and Goodman, R.H. (2006). Redox sensor CtBP mediates hypoxia-induced tumor cell migration. Proceedings of the National Academy of Sciences *103*, 9029-9033.

Zhao, Y., Butler, E.B., and Tan, M. (2013). Targeting cellular metabolism to improve cancer therapeutics. Cell death & disease *4*, e532.

Zhou, J., Febbraio, M., Wada, T., Zhai, Y., Kuruba, R., He, J., Lee, J.H., Khadem, S., Ren, S., Li, S., *et al.* (2008a). Hepatic fatty acid transporter Cd36 is a common target of LXR, PXR, and PPARgamma in promoting steatosis. Gastroenterology *134*, 556-567.

Zhou, J., Febbraio, M., Wada, T., Zhai, Y., Kuruba, R., He, J., Lee, J.H., Khadem, S., Ren, S., Li, S., *et al.* (2008b). Hepatic Fatty Acid Transporter Cd36 Is a Common Target of LXR, PXR, and PPARγ in Promoting Steatosis. Gastroenterology *134*, 556-567.e551.

Zhou, L., Wang, Q., Yin, P., Xing, W., Wu, Z., Chen, S., Lu, X., Zhang, Y., Lin, X., and Xu, G. (2012a). Serum metabolomics reveals the deregulation of fatty acids metabolism in hepatocellular carcinoma and chronic liver diseases. Analytical and Bioanalytical Chemistry *403*, 203-213.

Zhou, Q., Du, J., Hu, Z., Walsh, K., and Wang, X.H. (2007). Evidence for adipose-muscle cross talk: opposing regulation of muscle proteolysis by adiponectin and Fatty acids. Endocrinology *148*, 5696-5705.

Zhou, W., Choi, M., Margineantu, D., Margaretha, L., Hesson, J., Cavanaugh, C., Blau, C.A., Horwitz, M.S., Hockenbery, D., Ware, C., *et al.* (2012b). HIF1alpha induced switch from bivalent to exclusively glycolytic metabolism during ESC-to-EpiSC/hESC transition. EMBO J *31*, 2103-2116.

Zhou, Z.J., Dai, Z., Zhou, S.L., Hu, Z.Q., Chen, Q., Zhao, Y.M., Shi, Y.H., Gao, Q., Wu, W.Z., Qiu, S.J., *et al.* (2014). HNRNPAB induces epithelial-mesenchymal transition and promotes metastasis of hepatocellular carcinoma by transcriptionally activating SNAIL. Cancer Res *74*, 2750-2762.

Zhu, A.X., Finn, R.S., Mulcahy, M., Gurtler, J., Sun, W., Schwartz, J.D., Dalal, R.P., Joshi, A., Hozak, R.R., Xu, Y., *et al.* (2013). A phase II and biomarker study of ramucirumab, a human monoclonal antibody targeting the VEGF receptor-2, as first-line monotherapy in patients with advanced hepatocellular cancer. Clinical cancer research : an official journal of the American Association for Cancer Research *19*, 6614-6623.

Zhurinsky, J., Shtutman, M., and Ben-Ze'ev, A. (2000). Plakoglobin and beta-catenin: protein interactions, regulation and biological roles. J Cell Sci *113 (Pt 18)*, 3127-3139.

Zielinski, R., Przytycki, P.F., Zheng, J., Zhang, D., Przytycka, T.M., and Capala, J. (2009). The crosstalk between EGF, IGF, and Insulin cell signaling pathways - computational and experimental analysis. BMC Systems Biology *3*, 88.